frontiers | Research Topics

The role of post-translational modifications in cancer biology

Edited by
Arun Kumar Trivedi, Swati Srivastava and Anurag Tripathi

Published in
Frontiers in Oncology

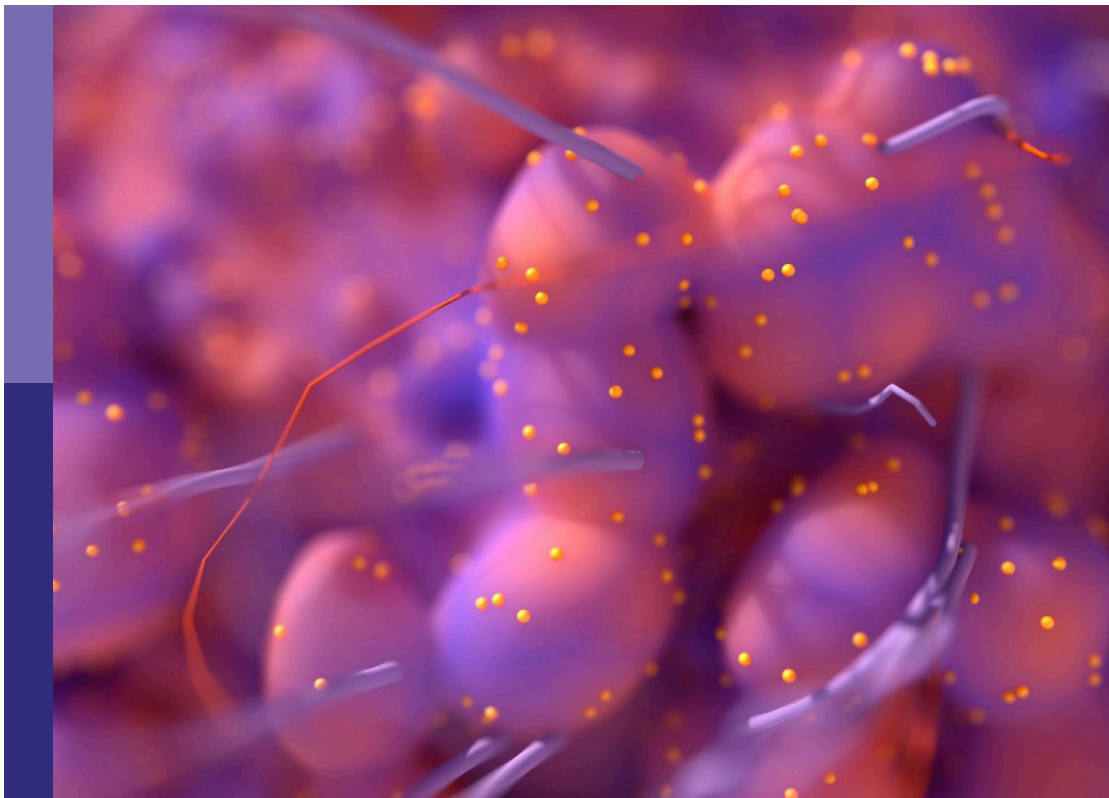

ISSN 1664-8714
ISBN 978-2-8325-6473-8
DOI 10.3389/978-2-8325-6473-8

About Frontiers

Frontiers is more than just an open access publisher of scholarly articles: it is a pioneering approach to the world of academia, radically improving the way scholarly research is managed. The grand vision of Frontiers is a world where all people have an equal opportunity to seek, share and generate knowledge. Frontiers provides immediate and permanent online open access to all its publications, but this alone is not enough to realize our grand goals.

Frontiers journal series

The Frontiers journal series is a multi-tier and interdisciplinary set of open-access, online journals, promising a paradigm shift from the current review, selection and dissemination processes in academic publishing. All Frontiers journals are driven by researchers for researchers; therefore, they constitute a service to the scholarly community. At the same time, the *Frontiers journal series* operates on a revolutionary invention, the tiered publishing system, initially addressing specific communities of scholars, and gradually climbing up to broader public understanding, thus serving the interests of the lay society, too.

Dedication to quality

Each Frontiers article is a landmark of the highest quality, thanks to genuinely collaborative interactions between authors and review editors, who include some of the world's best academicians. Research must be certified by peers before entering a stream of knowledge that may eventually reach the public - and shape society; therefore, Frontiers only applies the most rigorous and unbiased reviews. Frontiers revolutionizes research publishing by freely delivering the most outstanding research, evaluated with no bias from both the academic and social point of view. By applying the most advanced information technologies, Frontiers is catapulting scholarly publishing into a new generation.

What are Frontiers Research Topics?

Frontiers Research Topics are very popular trademarks of the *Frontiers journals series*: they are collections of at least ten articles, all centered on a particular subject. With their unique mix of varied contributions from Original Research to Review Articles, Frontiers Research Topics unify the most influential researchers, the latest key findings and historical advances in a hot research area.

Find out more on how to host your own Frontiers Research Topic or contribute to one as an author by contacting the Frontiers editorial office: frontiersin.org/about/contact

The role of post-translational modifications in cancer biology

Topic editors

Arun Kumar Trivedi — Central Drug Research Institute (CSIR), India
Swati Srivastava — Central Drug Research Institute (CSIR), India
Anurag Tripathi — Indian Institute of Toxicology Research (CSIR), India

Citation

Trivedi, A. K., Srivastava, S., Tripathi, A., eds. (2025). *The role of post-translational modifications in cancer biology*. Lausanne: Frontiers Media SA.
doi: 10.3389/978-2-8325-6473-8

Table of contents

04 Editorial: The role of post-translational modifications in cancer biology
Swati Srivastava, Anurag Tripathi and Arun Kumar Trivedi

07 Tip110/SART3-Mediated Regulation of NF-κB Activity by Targeting IκBα Stability Through USP15
Khalid Amine Timani, Sahar Rezaei, Amanda Whitmill, Ying Liu and Johnny J. He

21 SIRT4-Catalyzed Deacetylation of Axin1 Modulates the Wnt/β-Catenin Signaling Pathway
Yuting Wang, Jicheng Yue, Mingzhe Xiao, Xiaomei Lu and Yuen Eugene Chin

32 Stabilization of CCDC102B by Loss of RACK1 Through the CMA Pathway Promotes Breast Cancer Metastasis *via* Activation of the NF-κB Pathway
Jing Si, Rong Guo, Bingqiu Xiu, Weiru Chi, Qi Zhang, Jianjing Hou, Yonghui Su, Jiajian Chen, Jingyan Xue, Zhi-Ming Shao, Jiong Wu and Yayun Chi

49 DEPDC1B promotes development of cholangiocarcinoma through enhancing the stability of CDK1 and regulating malignant phenotypes
Zhenhai Zhang, Xinxing Wang, Peihua Nie, Yejun Qin, Junping Shi and Shifeng Xu

63 Inhibition of RNF182 mediated by Bap promotes non-small cell lung cancer progression
Yating Liu, Lianlian Ouyang, Chao Mao, Yuanbing Chen, Na Liu, Ling Chen, Ying Shi, Desheng Xiao, Shuang Liu and Yongguang Tao

76 UBE2S and UBE2C confer a poor prognosis to breast cancer *via* downregulation of Numb
Yanjing Guo, Xinyu Chen, Xiaowei Zhang and Xichun Hu

88 UCHL3 promotes hepatocellular carcinoma cell migration by de-ubiquitinating and stabilizing Vimentin
Qiancheng Ma, Qiliang Lu, Xiangxiang Lei, Jie Zhao, Wen Sun, Jun Wang, Qing Zhu and Dongsheng Huang

97 The deubiquitinating enzyme MINDY2 promotes pancreatic cancer proliferation and metastasis by stabilizing ACTN4 expression and activating the PI3K/AKT/mTOR signaling pathway
Peng Liu, Songbai Liu, Changhao Zhu, Yongning Li, Ying Li, Xiaobin Fei, Junyi Hou, Xing Wang and Yaozhen Pan

112 Post-translational modifications and their implications in cancer
Hashnu Dutta and Nishant Jain

125 Focal adhesion kinase promotes ribosome biogenesis to drive advanced thyroid cancer cell growth and survival
Meghan D. Kellett, Vibha Sharma, Madeline E. Sherlock, Umarani Pugazhenthi, Madison M. Rose, Molishree U. Joshi, Monika Dzieciatkowska, Vu Nguyen, Philip Reigan, Kirk C. Hansen, Jeffrey S. Kieft and Rebecca E. Schweppe

frontiers | Frontiers in Oncology

TYPE Editorial
PUBLISHED 28 August 2024
DOI 10.3389/fonc.2024.1470173

OPEN ACCESS

EDITED AND REVIEWED BY
Luisa Lanfrancone,
European Institute of Oncology (IEO), Italy

*CORRESPONDENCE
Arun Kumar Trivedi
arun3vedi@cdri.res.in

RECEIVED 25 July 2024
ACCEPTED 12 August 2024
PUBLISHED 28 August 2024

CITATION
Srivastava S, Tripathi A and Trivedi AK (2024) Editorial: The role of post-translational modifications in cancer biology.
Front. Oncol. 14:1470173.
doi: 10.3389/fonc.2024.1470173

Editorial: The role of post-translational modifications in cancer biology

Swati Srivastava[1], Anurag Tripathi[2,3] and Arun Kumar Trivedi[1,3]*

[1]Division of Cancer Biology, CSIR-Central Drug Research Institute, Lucknow, Uttar Pradesh, India, [2]Food Toxicology Group, CSIR- Indian Institute of Toxicology Research, Lucknow, India, [3]Academy of Scientific and Innovative Research (AcSIR), Ghaziabad, India

KEYWORDS

post translational modification (PTM), ubiquitination, phosphorylation, cancer, acetylation

Editorial on the Research Topic
The role of post-translational modifications in cancer biology

Introduction

This editorial presents articles published on the Research Topic "The role of post-translational modifications in cancer biology" in the journal "Frontiers in Oncology". It aimed to explore post-translational modifications (PTMs) of key proteins and their association with cancer pathogenesis. Various articles in this Research Topic highlight PTMs of key oncogenic factors and provide a deeper insight into the basic, translational, and clinical implications of protein modifications.

The article by Kellete et al. demonstrated the most frequently reported PTM, phosphorylation, which is often involved in multiple cellular signaling pathways. They showed that the phosphorylation of focal adhesion kinase (FAK) protein at pY397 is responsible for its nucleolar translocation, activation, and accumulation in thyroid cancers. In addition, phosphorylated FAK (pY397) also regulates 60S ribosomal subunit biogenesis by co-localizing with other nucleolar proteins.

Ubiquitination, another PTM that plays a key role in maintaining protein homeostasis, has also been implicated in tumorigenesis. Ubiquitin–proteasome system (UPS) is a multistep process involving the sequential action of various enzymes, leading to proteasome-mediated protein degradation. This biological process is mediated by E1, E2, and E3 enzymes that work sequentially and carry out ubiquitin activation, conjugation, and ligation, respectively. Abnormalities in any of these enzymes may lead to dysregulated protein turnover resulting in disease pathology. E1 enzymes activate the ubiquitin molecules followed by the conjugation of activated ubiquitins by E2 enzymes. E3 enzymes, also known as E3 ubiquitin ligases, add the ubiquitin molecules to the target proteins leading to their polyubiquitination and subsequent degradation by the proteasome machinery (1, 2). Deubiquitinases (DUBs), another class of enzymes, are also an essential component of the UPS that removes the ubiquitin chains from protein substrates, thus reversing the ubiquitination process.

Several articles in this Research Topic addressed the involvement of various enzymes in the ubiquitination process. Guo et al. showed that the ubiquitin-conjugating enzymes E2S (UBE2S) and E2C (UBE2C) are upregulated in breast cancer patients and are associated with poor survival. Interestingly, UBE2S and UBE2C target a key tumor suppressor, Numb,

which is also lowly expressed in patients with breast cancer. They argue that the combination of UBE2S/UBE2C and Numb could potentially serve as novel biomarkers for breast cancer. The report by Liu et al. highlighted the role of E3 enzymes in cancer progression. Through gene expression omnibus (GEO) analysis, they identified the potential really interesting new gene (RING) finger protein family (RNF) members that form the majority of ubiquitin ligases in case of non-small cell lung cancer (NSCLC). They showed that Benzo[a]pyrene (BaP), an environmental carcinogen, suppresses the expression of RNF182 in NSCLC. Mechanistically, BaP promotes abnormal methylation of RNF182 gene, leading to its suppression resulting in the progression of lung cancer. It is intriguing to see the epigenetic regulation of E3 enzymes and its consequences in tumor progression.

Other reports highlighted the role of DUBs in cancer progression. Timani et al. showed that Tip110 activates NF-κB signaling by targeting IκBα stability through ubiquitin-specific peptidase (USP15). With various intricate assays, they showed that Tip110 potentiates IκBα phosphorylation, leading to its degradation and hence, increase in NF-κB activity. On the other hand, authors also showed that IκBα is a substrate of USP15 that stabilizes IκBα and thus inhibits NF-κB activation. They demonstrated that Tip110 also interacts with USP15 and affects its nuclear localization. It seems that fine-tuning in the triad of Tip110-USP15-IκBα is crucial for the NF-κB signaling. Another oncogenic deubiquitinase in pancreatic cancer was highlighted by Liu et al. They discovered a novel deubiquitinase MINDY2 (a member of the motif interacting with Ub-containing novel DUB family). Pancreatic cancer is one of the deadliest cancers since patients with pancreatic cancer usually present with advanced-stage cancer at the time of diagnosis. They showed that MINDY2 expression is elevated in cancer tissues as compared to their adjacent normal and correlates with poor prognosis, distant metastasis, and angiogenesis of cancer cells. They further showed that MINDY2 interacts with ACTN4 and stabilizes it through deubiquitination. This stabilized ACTN4 stimulates the PI3K/AKT/mTOR pathway leading to the proliferation and invasive metastasis of pancreatic cancers. Similarly, Ma et al. showed that levels of UCHL3, yet another deubiquitinase, is significantly elevated in hepatocellular carcinoma and is associated with poor prognosis. Interestingly, similar to MINDY2-ACTN4 crosstalk, UCHL3 stabilizes another structural protein Vimentin, leading to metastasis.

Moreover, Zhang et al. identified Dishevelled, Egl-10 and Pleckstrin (DEP) domain-containing protein 1B (DEPDC1B) to have an oncogenic role in cholangiocarcinoma. Unlike the above studies, DEPDC1B was shown to stabilize CDK1 by inhibiting SMURF1-mediated CDK1 ubiquitination. DEPDC1B was shown to interfere in the protein–protein interaction between Smurf1 and CDK1. Notably, Smurf1 is an E3 ubiquitin ligase of CDK1. Other than proteasome-mediated degradation, lysosomal degradation pathway is also one of the key mechanisms to regulate protein turnover. Si et al. demonstrated that coiled-coil domain containing 102B (CCDC102B) was significantly upregulated in metastatic lesions in lymph nodes compared to matched primary breast tumors. RACK1 promoted CCDC102B lysosomal degradation through chaperone-mediated autophagy. The aggressive behavior of CCDC102B in breast cancer cells could be reversed by the expression of RACK1. The article by Wang et al. discussed yet another important PTM, acetylation. It is intriguing to see the role of protein acetylation not only in subcellular translocation but also in the activation of a key oncogenic signaling pathway. They showed that Wnt ligand stimulation leads to SIRT4 translocation from the mitochondria to the cytoplasm where it deacetylates Axin1-K147, resulting in the reduced assembly of β-TrCP to the destruction complex and thus, leading to β-catenin nuclear translocation and accumulation. Finally, Dutta and Jain summarized glimpses of different PTMs in cancer pathology in a minireview where they not only highlighted the conventional PTMs but also discussed several less-reported PTMs such as monoaminylation, crotonylation, propionylation, butyrylation, and lactylation. Summarily, the findings of the collective articles presented in this editorial highlight the role of distinct PTMs of various key proteins that impact their functionality and contribute to cancer pathogenesis.

Author contributions

SS: Writing – original draft, Writing – review & editing. AT: Writing – review & editing. AKT: Writing – original draft, Writing – review & editing.

Conflict of interest

The authors declare that the research was conducted in the absence of any commercial or financial relationships that could be construed as a potential conflict of interest.

Publisher's note

References

1. Chowdhury S, Trivedi AK. Origin, production and molecular determinants of macrophages for their therapeutic targeting. *Cell Biol Int*. (2023) 47:15–29. doi: 10.1002/cbin.11914

2. Thacker G, Mishra M, Sharma A, Singh AK, Sanyal S, Trivedi. AK. E3 ligase SCF (SKP2) ubiquitinates and degrades tumor suppressor C/EBPalpha in acute myeloid leukemia. *Life Sci*. (2020) 257:118041. doi: 10.1016/j.lfs.2020.118041

frontiers | Frontiers in Oncology

ORIGINAL RESEARCH
published: 21 April 2022
doi: 10.3389/fonc.2022.843157

Tip110/SART3-Mediated Regulation of NF-κB Activity by Targeting IκBα Stability Through USP15

Khalid Amine Timani[1,2,3]*, *Sahar Rezaei*[1,2,3], *Amanda Whitmill*[4], *Ying Liu*[1,2,3] *and Johnny J. He*[1,2,3]

[1] Department of Microbiology and Immunology, Rosalind Franklin University, Chicago Medical School, North Chicago, IL, United States, [2] Center for Cancer Cell Biology, Immunology and Infection, Rosalind Franklin University, North Chicago, IL, United States, [3] School of Graduate and Postdoctoral Studies, Rosalind Franklin University, North Chicago, IL, United States, [4] Department of Microbiology, Immunology, and Genetics, University of North Texas Health Science Center, Fort Worth, TX, United States

To date, there are a small number of nuclear-restricted proteins that have been reported to play a role in NF-κB signaling. However, the exact molecular mechanisms are not fully understood. Tip110 is a nuclear protein that has been implicated in multiple biological processes. In a previous study, we have shown that Tip110 interacts with oncogenic ubiquitin specific peptidase 15 (USP15) and that ectopic expression of Tip110 leads to re-distribution of USP15 from the cytoplasm to the nucleus. USP15 is known to regulate NF-κB activity through several mechanisms including modulation of IκBα ubiquitination. These findings prompted us to investigate the role of Tip110 in the NF-κB signaling pathway. We showed that Tip110 regulates NF-κB activity. The expression of Tip110 potentiated TNF-α-induced NF-κB activity and deletion of the nuclear localization domain in Tip110 abrogated this potentiation activity. We then demonstrated that Tip110 altered IκBα phosphorylation and stability in the presence of TNF-α. Moreover, we found that Tip110 and USP15 opposingly regulated NF-κB activity by targeting IκBα protein stability. We further showed that Tip110 altered the expression of NF-κB-dependent proinflammatory cytokines. Lastly, by using whole-transcriptome analysis of Tip110 knockout mouse embryonic stem cells, we found several NF-κB and NF-κB-related pathways were dysregulated. Taken together, these findings add to the nuclear regulation of NF-κB activity by Tip110 through IκBα stabilization and provide new evidence to support the role of Tip110 in controlling cellular processes such as cancers that involve proinflammatory responses.

Keywords: Tip110/SART3, NF-kB, IkB kinase, USP15, inflammation

OPEN ACCESS

Edited by:
Yari Ciribilli,
University of Trento, Italy

Reviewed by:
Srimoyee Mukherjee,
Tufts University School of Medicine, United States
Takashi Suzuki,
Osaka University, Japan
Takashi Tanaka,
RIKEN Center for Integrative Medical Sciences (IMS), Japan

***Correspondence:**
Khalid Amine Timani
Khalid.timani@rosalindfranklin.edu

Specialty section:
This article was submitted to Molecular and Cellular Oncology, a section of the journal Frontiers in Oncology

Received: *24 December 2021*
Accepted: *21 March 2022*
Published: *21 April 2022*

Citation:
Timani KA, Rezaei S, Whitmill A, Liu Y and He JJ (2022) Tip110/SART3-Mediated Regulation of NF-κB Activity by Targeting IκBα Stability Through USP15. Front. Oncol. 12:843157. doi: 10.3389/fonc.2022.843157

BACKGROUND

Nuclear factor of κB (NF-κB) is a critical mediator of the cellular response to inflammatory cytokines, developmental signals, pathogens, and cellular stress in which its constitutive activation promotes tumor initiation and development (1, 2). NF-κB is activated by a mystifying array of stimuli, including biological agents such as tumor necrosis factor α (TNF-α), interleukin-1, bacterial

endotoxin, and phorbol esters and cytotoxic stimuli such as chemotherapeutic agents and oxidative stress (3). The activity of NF-κB is regulated through its interaction with inhibitor proteins (IκBs), which prevent DNA binding to the p65 subunit of NF-κB. The NF-κB/IκB complex is localized exclusively in the cytosol because of a nuclear export signal encoded in the IκB subunit and the masking of a nuclear localization signal (NLS) in the NF-κB subunit (4). Proinflammatory stimuli activate IκB kinase (IKK) to phosphorylate IκBα at two N-terminal serines, Ser32 and Ser36. This phosphorylation triggers ubiquitination at the N-terminal lysines, Lys20 and Lys21 in IκBα, leading to its degradation through the 26S proteasomal pathway and subsequent translocation of p65 to the nucleus, where it regulates transcription of target genes (5–7). Thus, identifying the molecular players that regulate NF-κB and characterization of the mechanistic pathways through which the molecular players affect NF-κB activation will provide clues for possible therapeutic strategies against inflammatory diseases and cancer.

HIV-1 Tat-interacting protein 110 (Tip110), also known as "squamous cell carcinoma antigen recognized by T cells 3" (SART3), is a nuclear protein that plays an important role in pre-mRNA splicing, spliceosome assembly, and embryonic development (8–15). Tip110 protein expression is very low in normal tissues and non-proliferating cells but becomes highly elevated in a number of malignant tumor cell lines and cancerous tissues as well as in stem cells. Tip110 has been proposed as a potential antigen for cancer immunotherapy (8, 16–19), and its mutations have been linked to inflammatory skin diseases (20). We have summarized the biological functions of Tip110 in a comprehensive review (8). Furthermore, we reported that exposure of a highly metastatic melanoma cell line to severe hypoxic conditions led to significant down-regulation of Tip110 both *in vitro* and *in vivo* (21). Also, we have shown that Tip110 regulates interleukin-8 (IL-8) expression and predicts the clinical outcomes in melanoma, indicating that Tip110 expression level could play a role in melanoma tumor progression (22). Furthermore, we and others reported that Tip110 interacts with and/or regulates several oncogenic proteins such as C-Myc, Y-box-binding protein 1 (YB-1), p53, ubiquitin specific peptidase 15 (USP15), and ubiquitin specific peptidase 4 (USP4) (9, 23–25). Interestingly, these Tip110-interacting partners play roles in NF-κB signaling through interaction or regulation of the signaling components of the NF-κB pathway (9, 10, 21, 24, 26, 27). Given the importance of NF-κB signaling in inflammation, immunity, and cell fate decision, we examined the possible role of Tip110 in the regulation of the NF-κB pathway.

In this study, we showed that Tip110 expression regulates TNF-α-induced NF-κB activation, and the nuclear localization signal on Tip110 is required for this activation. Then we explored the potential mechanism underlying the Tip110-mediated NF-κB activity by studying its effects on IκBα protein stability. Then we determined the role of Tip110-associated protein USP15, whose nuclear localization is affected by Tip110 expression, on Tip110-potentiated TNF-α-induced NF-κB activity. Finally, dysregulation of NF-κB and NF-κB-related signaling pathways by Tip110 was further substantiated by using whole-transcriptome analysis of Tip110 knockout cells.

RESULTS

Tip110 Activated NF-κB Transcriptional Activity

Tip110 is identified as an interacting partner with HIV-1 Tat protein that has been reported to enhance NF-κB activity (28, 29). USP15, another Tip110-interacting protein, that has been reported to regulate NF-κB activity (27, 30–32). In addition, Tip110 interacts with and/or regulates other proteins which are known to play a role on NF-κB by targeting NF-κB signaling components (9, 10, 21, 24, 26, 27). All those findings prompted us to investigate the possible role of Tip110 in the NF-κB signaling pathway. Transfection of luciferase-reporter vector pGL3-NF-κB(3)-Luc containing NF-κB responsive element with an increasing amount of Tip110 in 293T enhanced NF-κB transcriptional activity in a dose-dependent manner (**Figure 1A**). Treatment of Tip110 expressing cells with TNF-α further augmented NF-κB transcriptional activity compared to untreated cells (**Figure 1B**). On the contrary, Tip110 knockdown by siRNA in 293T led to inhibition in the NF-κB transcriptional activity in response to TNF-α treatment (**Figure 1C**). Interestingly, deletion of Tip110 nuclear localization signal (NLS) (**Figure 2A**) abolished the NF-κB transcriptional activity (**Figure 1D**).

Even though NF-κB and AP-1 transcription factors are regulated by different mechanisms, they appear to be activated by the same multitude of stimuli (33–35). Indeed, the activation of JNK by inflammatory cytokines or by stress is often accompanied by the nuclear translocation of NF-κB, and many genes require the concomitant activation of AP-1 and NF-κB, suggesting that these transcription factors work cooperatively (36, 37). To determine whether Tip110 expression would also regulate AP-1 transcriptional activity, 293T were transfected with a luciferase-reporter vector containing the AP-1 responsive element with an increasing amount of Tip110. The results showed that Tip110 expression suppressed AP-1 transcriptional activity in a dose-dependent manner (**Figure 1E**). A similar result was also found under phorbol 12-myristate 13-acetate (PMA) treatment (**Figure 1F**). Under our experimental settings, TNF-α showed low activation of AP-1 luciferase activity in 293T, and the effect was not significant; therefore, we used PMA, a known activator for AP-1 transcriptional activity. These data suggest that Tip110 activates NF-κB transcriptional activity through Tip110 nuclear localization but inhibits AP-1 transcriptional activity.

N-Terminal Domain on Tip110 Responsible for the NF-κB Activation

Tip110 contains 12 half-a-tetratricopeptide repeats (HAT) and an NLS at the N terminus and two RNA recognition motifs (RRM) at the C terminus. To identify the Tip110 domains involved in the regulation of NF-κB activity, a series of Tip110

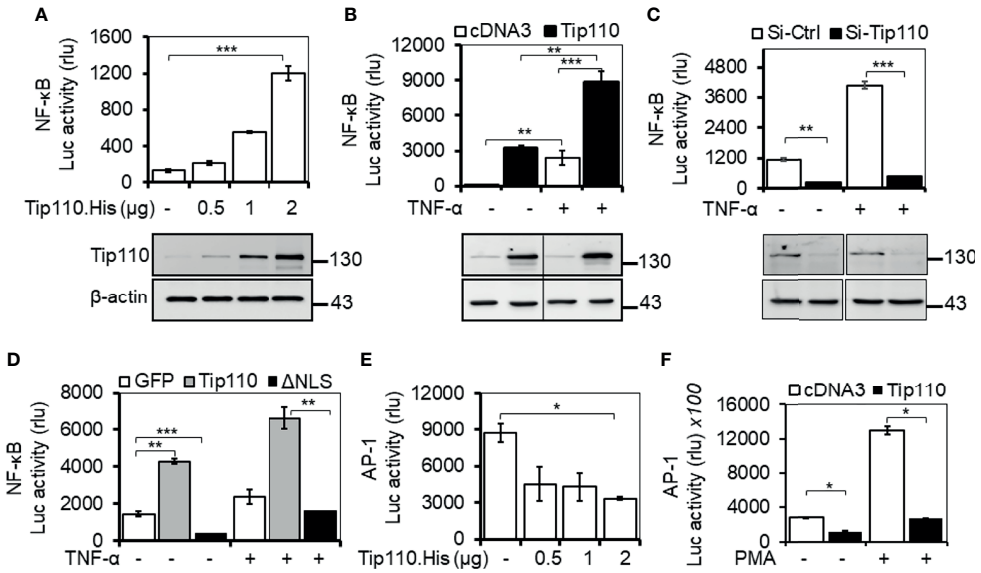

FIGURE 1 | Impact of Tip110 on NF-κB transcriptional activity. **(A-D)**. 293T were transfected with 0.06 μg pGL3-NF-κB(3)-luc and an increasing amount of Tip110. His **(A),** 2.5 μg Tip110.His **(B),** 50 nM Tip110-specific siRNA (si-Tip110) **(C)**, or 2 μg pGFP.Tip110 or pGFP.Tip110ΔNLS containing deletion of the nuclear localization signal (NLS) **(D)**. **(E, F)** 293T were transfected with 0.04 μg pAP-1-Luc and an increasing amount of Tip110.His **(E)** or 2.5 μg Tip110.His **(F)**. pcDNA3 **(A, B, E, F)**, control siRNA (Si-Ctrl, **C**), pGFP **(D)** was used to equalize the total amount of DNA or siRNA among the transfection, and pGFP was added to ensure comparable transfection efficiencies among all transfections. **(B–D)**, 10 ng/ml TNF-α **(F)** 100 ng/ml PMA were added 24 hr post-transfection and continued for either 18 or 6 hr, respectively. Cells were then harvested for the luciferase reporter gene assay, and Western blotting was used to determine the expression of Tip110. β-actin was used as an internal loading control **(A–C)**. The data were means ± SE from triplet samples and representative of three independent experiments. *$P < 0.05$, **$P < 0.01$, ***$P < 0.001$.

mutant proteins (**Figure 2A** (25, 28)**,** were analyzed. Similarly, 293T were transfected with wild-type Tip110 and its mutants together with the NF-κB reporter. Compared to wild-type Tip110, deletion of Tip110 N-terminal domain (Tip110ΔN), including the NLS, resulted in a decrease in the NF-κB activity (**Figure 2B**). Deletion up to 557 aa from the C-terminal, including the NLS, completely abolished NF-κB activity similar to the cDNA3-transfected control. While deletion of the C-terminal domain on Tip110 (Tip110ΔC and Tip110Δ785-963 mutants) led to higher NF-κB activity than the wild-type (**Figure 2B**). Western blotting was performed to confirm the expression of Tip110 mutant proteins (**Figure 2C**). These results demonstrated that an approximately 300 aa at the N-terminal domain, which includes the NLS region on Tip110, 556-785 aa, is required for the NF-κB activation.

We have previously shown that Tip110 is ubiquitinated and this ubiquitination is regulated by its associated-protein USP15 (25). Therefore, we then determined whether Tip110 ubiquitination would be affected by its intracellular localization. 293T were transfected with UB.HA alone or plus Tip110.His or Tip110ΔNLS.His on the presence or absence of pUSP15.Myc. Cells were treated with MG132, an inhibitor of 26S proteasome degradation, then collected for cell lysates. Tip110 expression was confirmed by Western blotting (**Figure 2D**, Input). Immunoprecipitation using anti-His antibody followed by Western blotting using anti-HA antibody led to the detection of a highly ubiquitinated Tip110ΔNLS mutant protein compared to wild-type Tip110 and the expression of USP15 deubiquitinated both Tip110 and its cytoplasmic mutant Tip110ΔNLS (**Figure 2D**, IP). Then we used the same strategy to determine whether TNF-α stimulation would alter Tip110 ubiquitination. 293T were transfected with Tip110.His or its control plasmid then either treated with TNF-α or left untreated. Immunoprecipitation assay data showed little effect in ubiquitinated Tip110 upon TNF-α stimulation compared to unstimulated cells with reference to the amount of Tip110 input (**Figure 2E**). Those results indicate that Tip110 ubiquitination level affects its intracellular localization and might be involved in NF-κB activity.

Tip110 Promoted TNF-α-Induced Nuclear Translocation of NF-κB p65

We and others have shown that a number of Tip110-associated proteins translocated to the nucleus when they co-expressed with Tip110 such as USP15, USP4, and YB-1 ((12, 25, 38), data not shown for YB-1). In addition, NF-κB activation is mainly associated with nuclear translocation of endogenous NF-κB p65 (2). Thus we analyzed the distribution of NF-κB p65 between the cytoplasm and nucleus in relation to Tip110 expression and TNF-α treatment by using an immunofluorescence assay. Expression of endogenous NF-κB p65 localized mainly in the cytoplasm and weak expression was also detected in the nucleus due to its continuous shuttling between both compartments (39) (**Figure 3A–I**). Treatment of cells with TNF-α for 30 min caused accumulation of NF-κB p65 in the nucleus (**Figure 3A–**

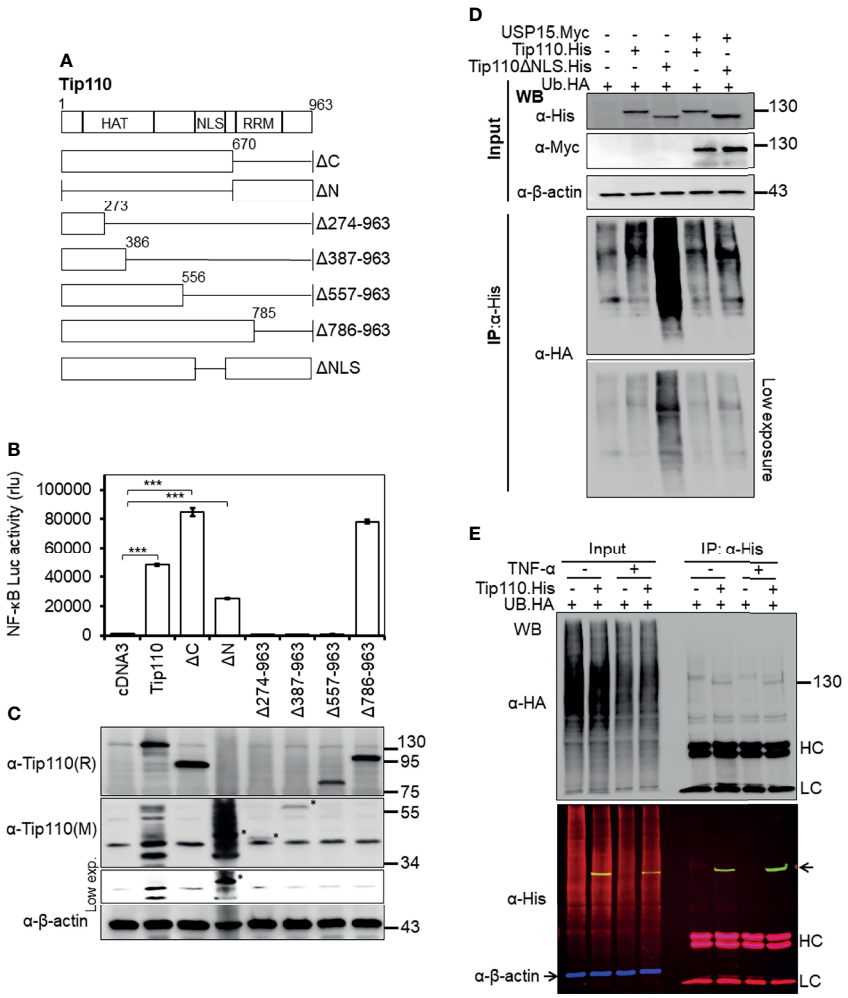

FIGURE 2 | Effects of Tip110 intracellular localization and ubiquitination on NF-κB activity. **(A)** Schematic of Tip110 and its respective deletion mutants. Tip110 consists of seven half-a-tetratricopeptide repeats (HAT), a nuclear localization signal (NLS), and two RNA recognition motifs (RRM). **(B, C)** 293T were transfected with 0.6 μg pGL3-NF-κB(3)-Luc and Tip110.His or one of the Tip110 deletion mutants. Cells were harvested 48 hr post-transfection for the luciferase reporter gene assay **(B)** and Western blotting for Tip110 and its mutant expression using a monoclonal (M) and polyclonal (R) anti-Tip110 antibody **(C)**. **(D)** 293T were transfected with UB.HA and Tip110.His, or Tip110ΔNLS, with and without USP15.Myc cultured for 48 hr, treated with MG132 (10 μM) for 20 hr, and then harvested for Tip110 expression by Western blotting using anti-His antibody (Input) or immunoprecipitated using an anti-HA antibody, followed by Western blotting using anti-HA antibody after the SDS-PAGE was run for a long time to capture polyubiquitinated smear above the Tip110 band. **(E)** 293T were transfected with UB.HA and Tip110.His, cultured for 24 hr, treated with TNF-α (10 ng/ml) for 30 min, and then harvested for expression of total ubiquitin, Tip110, and β-actin by Western blotting using anti-HA and anti-His antibody (Input) or immunoprecipitated using anti-His antibody followed by the same Western blotting to identify the amount of the ubiquitinated Tip110. An Alexa Fluor 488 (green), 555 (red), and 633 (purple) secondary antibodies were used to detect the Tip110, UB, and β-actin, respectively. Tip110 bands in the input appeared in yellow due to the overlay of green (Tip110) and red (ubiquitin) fluorescence. pcDNA3 was used to equalize the total amount of DNA among the transfection, and pGFP expression vector was added to ensure comparable transfection efficiencies among all transfections. β-actin was used as an internal loading control. The data were means ± SE from triplet samples and representative of three independent experiments. HC, IgG heavy; LC, IgG light chain. ***$P < 0.001$.

II). Tip110 overexpression showed no significant effect on p65 nuclear accumulation (**Figure 3A–III**). However, treatment of Tip110 expressing cells with TNF-α greatly enhanced NF-κB p65 nuclear accumulation compared to control expressing cells (**Figure 3A–IV**). On the other hand, Tip110 knockdown by siRNA in the presence or absence of TNF-α treatment has no significant effect on NF-κB p65 protein expression and localization pattern compared to si-RNA control cells (**Figures 3B–III, IV**). Then we determined whether Tip110 would be associated with NF-κB p65. 293T were transfected with Tip110 or vector control then treated with TNF-α for 20 hr. Cells were lysed, and an immunoprecipitation assay was performed. Tip110 and p65 were expressed (**Figure S1A**), but there was no complex formation between Tip110 and p65 (**Figure S1B**). These data together demonstrated that Tip110 expression altered NF-κB p65 nuclear accumulation only in the presence of TNF-α stimulation, suggesting that other mechanisms may also contribute to NF-κB activation by Tip110.

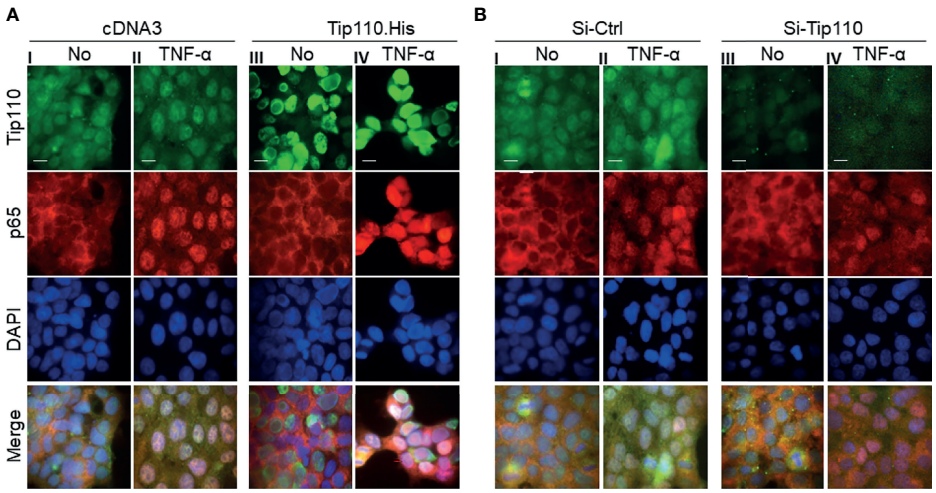

FIGURE 3 | Effects of Tip110 expression and TNF-α treatment on NF-κB p65 nuclear translocation. **(A)** 293T were transfected with 0.8 μg Tip110.His **(A)** 50 nM Si-Tip110 **(B)**, cultured for 24 hr, treated with 20 ng/ml TNF-α for 30 min, and then processed for immunostaining using anti-Tip110 and anti-p65 antibodies. The cells were counterstained with DAPI for nuclei. pcDNA3 or si-Ctrl was used as the respective controls. Representative micrographs were separately taken using fluorescence microscopy and used to make the composite (Merge). Magnification; 100X, Scale bar, 10μM.

Tip110 Altered IκBα Phosphorylation and Stability

The canonical NF-κB transactivation pathway involves IκBα phosphorylation and degradation (2). Thus, we next investigated whether Tip110 expression would alter IκBα expression and stability in the presence TNF-α stimulation. 293T were transfected with Tip110 expression vector or its control and treated with TNF-α for various lengths of time. Western blotting showed that under TNF-α stimulation, phosphorylated IκBα increased under the context of Tip110 expression (**Figure 4A**), which is paralleled with changes in the IκBα protein stability. To further investigate whether this effect could also be observed in normal primary cells which retain a native signaling pathways, we used primary mouse embryonic fibroblasts (MEF) under the context of limited amount of Tip110. Cells were transfected with siRNA-Tip110 or control siRNA, treated with TNF-α at various lengths of time up to 120 min, and harvested for Western blotting. Similarly, Tip110 knockdown led to decreases in IκBα phosphorylation and subsequent stabilization of the total amount of IκBα in the presence of TNF-α stimulation (**Figure 4B**). These results also showed that Tip110 had no significant effects on the amount of NF-κB p65 protein. These data suggest that Tip110 alters the phosphorylation status and stability of IκBα and subsequently regulates NF-κB activity under TNF-α stimulation.

Unexpectedly, no significant effect was detected on the basal level of IκBα in the absence of TNF-α treatment (**Figures 4A, B**). Thus to further examine whether Tip110 expression regulates IκBα protein turnover rate, a cycloheximide (CHX) chase assay was performed. 293T were transfected with IκBα.HA alone or plus Tip110.His or Tip110ΔNLS expression vectors, treated with CHX, to inhibit new protein synthesis, for various lengths of time, and harvested to determine Tip110 and IκBα protein expression by Western blotting. Tip110 overexpression accelerated IκBα degradation compared to its transfection control (**Figures 4C, D**), while expression of Tip110ΔNLS that previously showed an inhibitory effect on NF-κB activity (**Figure 1D**) showed no apparent effects on IκBα protein level compared to its transfection control (**Figures 4D, E**). Further, we observed that Tip110ΔNLS expression caused more accumulation of IκBα protein before the beginning of CHX treatment compared to Tip110 and the control (**Figures 4C, E**). Then we examined whether Tip110 or Tip110ΔNLS expressions affect the turnover rate of the nuclear targeted IκBα by using IκBα-Nuc.Myc expression plasmid. Interestingly, CHX chase assay showed that Tip110 expression stabilized the nuclear IκBα compared to its transfection control while the expression of Tip110ΔNLS accelerated nuclear IκBα degradation compared to Tip110 but still higher than the transfection control (**Figures 4E, F**). In addition, qRT-PCR results showed that Tip110 expression only had a little effect on the IκBα mRNA level at 2 hr, but had no effect at 24 hr following TNF-α treatment compared to the control transfection (**Figure 4G**). These data showed that the Tip110 affects IκBα phosphorylation under TNF-α treatment and the regulation of IκBα protein stability.

Tip110 and USP15 Opposingly Regulated NF-κB Activity by Targeting IκBα

We showed that nuclear localization was required for potentiation of TNF-α-induced NF-κB activation by Tip110 and different effect of Tip110 on the IκBα protein stability is dependent on its localization (**Figures 1**, **4**). The TNF-α-induced NF-κB signaling cascade is initiated within the cytoplasm (37). Furthermore, Tip110 interacts with USP15 and regulates its localization between the cytoplasm and nucleus (25, 38), while

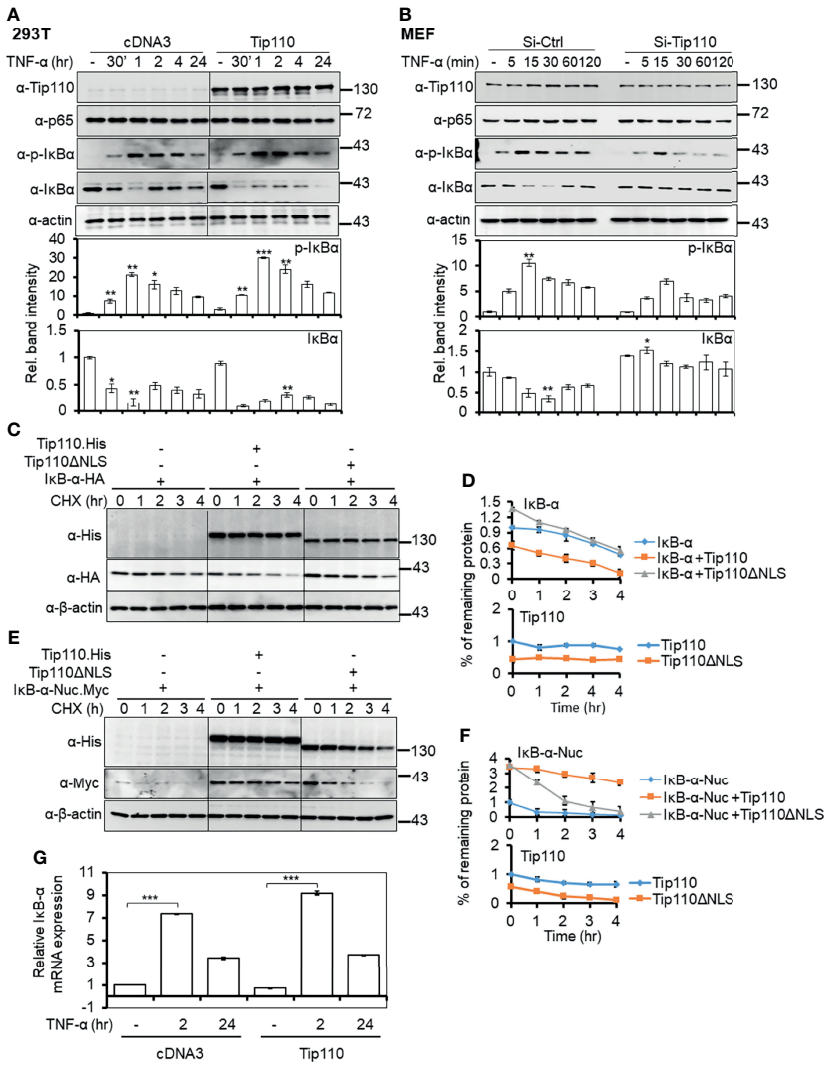

FIGURE 4 | Effects of Tip110 expression on IκBα phosphorylation and protein stability. **(A)** 293T were transfected with Tip110.His and its plasmid control, treated with 20 ng/ml of TNF-α for 0, 30 min, 1, 2 4 and 24 hr then harvested for Western blotting. pcDNA3 was used to equalize the total amount of DNA among the transfection. **(B)** Primary mouse embryonic fibroblasts (MEF) were transfected with 50 nM Si-Ctrl or Si-Tip110, cultured for 24 hr, treated with 20 ng/ml TNF-α for 0, 5, 15, 30, 60, or 120 min. 293T were transfected with **(C)** IκBα.HA or **(E)** IκBα.Nuc.Myc and Tip110.His or Tip110ΔNLS.His, cultured for 48 hr, treated with 20 μg/ml cycloheximide (CHX) for 0, 1, 2, 3, and 4 hr, and then harvested for Western blotting. Relative IκBα protein level was normalized to β-actin and expressed as a percentage of the untreated or as individual values **(D, F)**. **(G)** 293T were transfected with Tip110 or pcDNA3, cultured for 48 hr, treated with TNF-α (10 ng/ml) for 2 or 24 hr, and harvested for total RNA isolation and qRT-PCR for IκBα mRNA level. Relative IκBα mRNA was normalized to β-actin and calculated using the untreated as a reference. *P < 0.05, **P < 0.01, ***P < 0.001.

USP15 is shown to regulate NF-κB activity (27, 40, 41). Those findings together raised the possibility that USP15 might be the link between Tip110 and NF-κB activation. To test this possibility, 293T were transfected with pGL3-NF-κB(3)-Luc, Tip110, USP15, or USP15 mutants (**Figure 5A**). The data showed that the expression of USP15 inhibited NF-κB transcriptional activity (**Figure 5B**). Interestingly, increasing the amount of USP15 expression plasmid in the presence of Tip110 led to gradual decreases of Tip110-induced NF-κB activity in a dose-dependent manner (**Figure 5B**). Then we determined which USP15 domain was involved in the inhibition of NF-κB activity. The results showed that the N-terminal domain of USP15, which contains the domain present in ubiquitin-specific proteases (DUSP) and ubiquitin-like domain (UBL) (**Figure 5A**), was responsible for this inhibition as deletion of this domain (USP15ΔN) enhanced the NF-κB activity (**Figure 5C**). While deletion of the C-terminal domain, USP15ΔC, led to inhibition of NF-κB activity. Furthermore, co-expression of Tip110 with the USP15ΔC mutant led to reduction on the Tip110-induced NF-κB activity. In contrast, co-expression with the USP15ΔN mutant had no such effects (**Figure 5C**), indicating that the N-terminal domain of USP15,

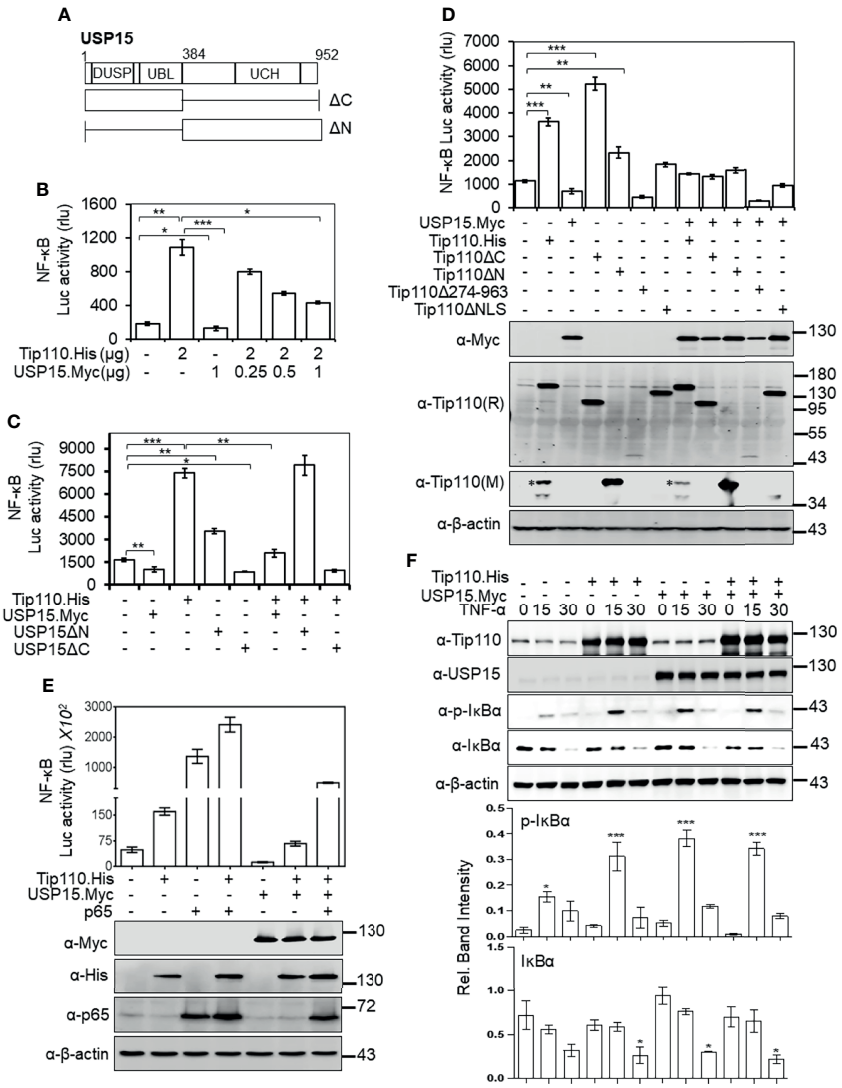

FIGURE 5 | USP15 abrogated Tip110-induced NF-κB activity by targeting IκBα. **(A)** Schematic of USP15 protein and its respective deletion mutants. USP15 contains three distinct domains: domain present in ubiquitin-specific proteases (DUSP), ubiquitin-like domain (UBL), ubiquitin C-terminal hydrolase (UCH). **(B)** 293T were transfected with pGL3-NF-κB(3)-Luc, Tip110.His, and an increasing amount of USP15.Myc, cultured 48 hr, and harvested for the luciferase reporter gene assay. **(C)** 293T were transfected with pGL3-NF-κB(3)-Luc, Tip110.His, USP15.Myc, USP15ΔN, or USP15ΔC, cultured for 48 hr, and harvested for the luciferase reporter gene assay. **(D)** 293T were transfected with pGL3-NF-κB(3)-luc,USP15.Myc, Tip110.His or Tip110 deletion mutants. **(E)** 293T were transfected with pGL3-NF-κB(3)-Luc, Tip110.His, USP15.Myc, and p65. Cells were processed the same as above, and Western blotting using indicated antibodies. pcDNA3 was used to equalize the total amount of DNA among the transfection, and pGFP expression vector was added to ensure comparable transfection efficiencies among all transfections. The data were means ± SE from triplet samples and representative of three independent experiments. **(F)** 293T were transfected with Tip110.His and/or USP15.Myc, treated with 20 ng/ml TNF-α for 15 or 30 min, and harvested for Western blotting using antibodies as indicated. *P < 0.05, **P < 0.01, ***P < 0.001.

which physically associates with Tip110 (25), is responsible for USP15 inhibitory function on Tip110-induced NF-κB activity.

Next, we examined the role of Tip110 mutants on NF-κB activity in the context of the USP15 expression. Expression of Tip110 mutant proteins in the presence of USP15 attenuated their NF-κB basal transcriptional activity (**Figure 5D**). Interestingly, co-expression of Tip110ΔNLS or Tip110Δ274-963 mutants with USP15 led to decreases in the NF-κB activity compared to the mutants alone, indicating that USP15 expression may also affect cytoplasmic expressed Tip110 mutants. To further verify the opposing effects of Tip110 and USP15 on the NF-κB activity, we utilized NF-κB p65 protein, which is known to activate NF-κB transcriptional activity in a reporter gene assay. The results showed an enhancement in the transcriptional activation of NF-κB by the co-expression of p65 and Tip110. Expression of USP15 abrogated this enhancement effect, yet the level was still higher than Tip110 alone due to the effect of p65, indicating that p65 expression reversed the inhibitory effect of USP15 on Tip110-induced NF-κB activity (**Figure 5E**). Then, we investigated whether the abrogation of

Tip110-enhanced NF-κB activity by USP15 was due to modulation of IκBα protein stability. 293T were transfected with Tip110 or USP15 alone, or in combination, then treated with TNF-α for 15 or 30 min. Similar to our previous observation, Tip110 expression led to increases in p-IκBα paralleled with decreases in IκBα protein level. While co-expression of USP15 and Tip110 reduced the IκBα protein level compared to the USP15 expressing cells only (**Figure 5F**), yet this reduction was not paralleled with increased in the p-IκBα, which is more likely due to the effect of Tip110 on the IκBα phosphorylation. Interestingly, expression of USP15 on the presence of TNF-α led to increase on IκBα phosphorylation compared to untreated cells which is not parallel with decrease on IκBα level. It has been reported that overexpression of USP15 potentiated TNF-α-induced NF-κB activation (42). In addition, deletion of USP15 N-terminal domain enhanced NF-κB activity (**Figure 5C**). Thus it's possible that USP15 regulates NF-κB at multiple mechanisms. These data further confirming the opposing effect of Tip110 and USP15 on IκBα stability.

As we previously alluded to, Tip110 expression promoted the nuclear translocation of USP15 where both are associated (25) and the above observations prompted us to examine whether Tip110 also targeted nuclear IκBα to regulate NF-κB activity. 293T were transfected same as above then treated with leptomycin B (LMB), a nuclear export inhibitor found to sequester NF-κB/IκBα complexes in the nucleus (43), alone or together with TNF-α. Then the cells were prepared for an NF-κB reporter gene assay. As reported previously, treatment of cells with LMB inhibited NF-κB activity while further inhibition was observed by combined treatment with TNF-α (**Figure S2A**) (39, 44). However, LMB treatment had no significant effect on NF-κB activity under the context of Tip110 expression compared to untreated cells, but inhibition of NF-κB activity was observed with combined treatment with TNF-α. Furthermore, LMB treatment led to decreases in p65-induced NF-κB transcriptional activity while Tip110 co-expression resulted in a marginal increase compared to p65 expression alone (**Figure S2B**). These data indicate that USP15 expression abrogated the effect of Tip110-induced NF-κB activity and that Tip110 could regulate both nuclear and cytoplasmic IκBα protein stability.

Tip110 Altered TNF-α-Induced NF-κB-Dependent Gene Expression

To gain further insight into the consequence of Tip110 effect in the TNF-α-induced NF-κB signaling pathway, we assessed the NF-κB dependent gene expression of various inflammatory cytokines when Tip110 was knocked down. 293T were transfected with control or Tip110 siRNA then stimulated with TNF-α for short (2 and 4 hr) and long (24 hr) lengths of time due to different stimulation kinetics exhibited by various cytokines in response to TNF-α treatment. The cells were harvested for the determination of mRNA level by qRT-PCR. In line with the previous findings, the overall expression of NF-κB target genes such as TNF-α and IL-6 were substantially decreased in Tip110 knockdown cells as compared to their respective control (**Figure 6**). While IL-8 expression showed no significant

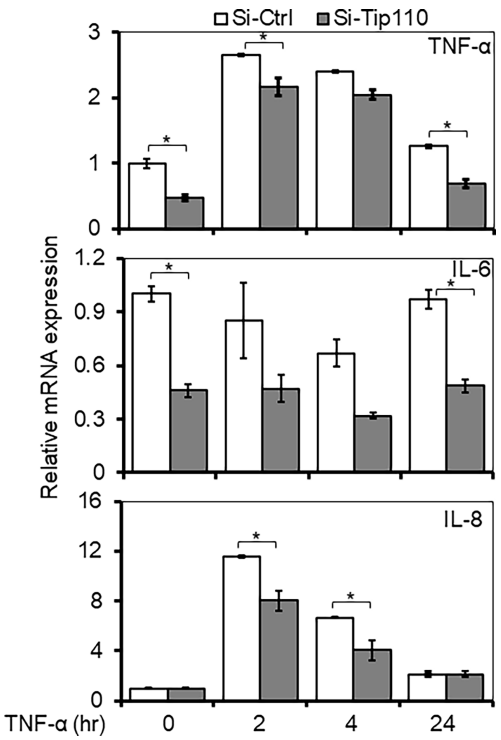

FIGURE 6 | Effects of Tip110 expression on NF-κB responsive gene expression. 293T were transfected with 50 nM of Si-Ctrl or Si-Tip110, cultured for 24 hr, treated with TNF-α (10 ng/ml) for 0, 2, 4 or 24 hr, and harvested for total RNA isolation and qRT-PCR for TNF-α, IL-6, and IL-8 mRNA expression. The relative mRNA expression was normalized to β-actin and expressed as fold increases over those in Si-Ctrl-transfected and untreated cells. The data were mean ± from triplicate samples. *$P < 0.05$.

reduction, indicating that these differences could reflect the quantitative requirement for NF-κB by different target genes under a limited amount of Tip110 or that the regulation of IL-8 by NF-κB under the context of Tip110 acted differently than other cytokines. Recently, we reported that knockdown of Tip110 in melanoma cell line resulted in the up-regulation of IL-8 expression while no such effect was observed in the cell lines from other cancer types (22).

Whole-Transcriptome Analysis of Tip110 Knockout Mouse Embryonic Stem Cells Revealed Dysregulation of NF-κB-Related Signaling Pathways

The possible role of Tip110 on NF-κB signaling pathway was further illustrated by an analysis of whole-transcriptome array data using Affymetrix Expression Console (TAC) and pathway analysis software that was generated previously during our investigation of the embryonic lethality instigated by knockout of Tip110 in mice (45). The microarray analysis data from the Tip110-knockout mESC revealed that several genes associated with NF-κB regulatory pathways were highly downregulated. Specifically, FGF4 (-17.8 fold) and GSTA4 (-46.7 fold) related to MAPK signaling cascades (**Figure 7A**), PMI (-4.97 fold) and

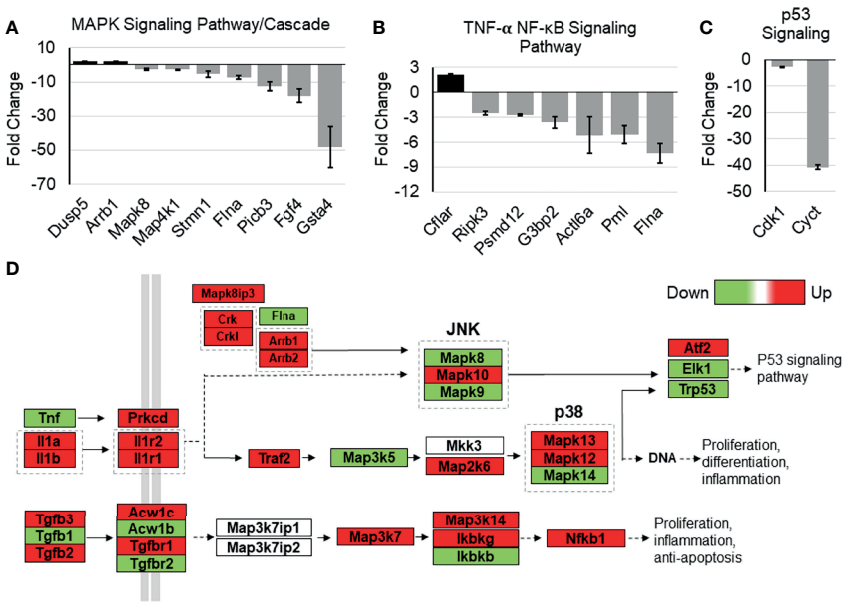

FIGURE 7 | Effects of Tip110 knockout on gene expression in several NF-κB-related signaling pathways. Affymetrix Transcriptome Analysis Console software provided a list of pathways found in WIKI Pathways Beta that were most perturbed by Tip110 loss. This information was used to construct bar graphs depicting the fold change of some of the associated genes. Genes associated with MAPK **(A)**, TNF-α-NF-κB **(B)**, p53 **(C)**, signaling pathways were included. **(D)** Data from Affymetrix microarray analysis of wild-type and Tip110 knockout-mouse embryonic stem cell RNA revealed the fold changes of genes in these networks. Genes are shown in red when upregulated and in green when downregulated. Pathway information was adapted from MAPK and other signaling pathways depicted in WIKI Pathways Beta.

FLNA (-7.26 fold) related to the TNF-α-NF-κB pathway (**Figure 7B**), CDK1 (-9.99 fold) and CYCT (-40.0 fold) related to p53 signaling pathway (**Figure 7C**), SPRY2 (-8.22 fold) related EGFR1 signaling pathway (**Figure S3A**), CDK5 (-8.4 fold) related to IL-6 signaling pathway (**Figure S3B**), and SSP1 (-39.2 fold) related to TGF-β1 receptor signaling pathway (**Figure S3C**). Interestingly, analysis of TNF-α-NF-κB, EGF, and TGF-β signaling cascades demonstrated that several genes within the cascade were also upregulated in the knockout Tip110 cells (**Figures 7D** and **S3D**), indicating there is a compensatory mechanism that was impacted these signaling pathways in the absence of Tip110, which may also explain the little effect of Tip110 on the basal level of IκBα and the gene expression of cytokines (**Figure 6**).

DISCUSSION

To date, there are a small number of nuclear-restricted proteins that have been reported to play a role in NF-κB signaling. However, the exact molecular mechanisms are not fully understood (46). Herein, we identified another nucleus-restricted protein, Tip110, to regulate NF-κB through a unique mechanism. Our results demonstrated that Tip110 activates NF-κB but while inhibits AP-1 activity (**Figure 1**). Nuclear localization of Tip110 was required for such activation as deletion of the NLS obliterated Tip110-induced NF-κB activity concomitant with an increase in Tip110 ubiquitination (**Figures 1**, **2**). We further investigated the potential molecular mechanisms and found that Tip110-associated shuttling protein, USP15, opposingly regulated NF-κB activity by targeting IκBα protein stability (**Figure 4**). Our findings were further substantiated using whole-transcriptome array data of Tip110 knockout mouse cells, which showed that several NF-κB and NF-κB-related pathways were dysregulated (**Figures 7** and **S3**).

Several Tip110-associated proteins have been identified (8). Interestingly, those Tip110-interacting partners have been found to play roles in NF-κB signaling through their interaction with and/or regulation of the signaling components of the NF-κB pathway (9, 10, 21, 24, 26, 27). We previously have shown that Tip110 bound to and enhanced Tat-mediated HIV-1 gene expression (28). It has been reported that HIV-1 Tat protein activates the NF-κB pathway *via* physical interaction with IκBα and p65 proteins (29). Persistent activation of NF-κB that occurs in HIV-1-infected cells results in the enhancement of the expression of proinflammatory cytokines and chemokines, which causes immune and neuron dysfunction due to chronic inflammation (47, 48). Furthermore, we also reported that Tip110 regulated several oncogenic proteins such as Y-box-binding protein 1 (YB-1), C-Myc, p53, USP15, and USP4 (9, 10, 21, 24) which regulate NF-κB signaling (49–54). These observations suggest a highly possible role of Tip110 in HIV-1-mediated chronic inflammation and cancer-associated inflammation *via* modulation of the NF-κB pathway.

Nuclear localization of Tip110 is required for its function on the NF-κB activity. Interestingly, the cytoplasmic expressed-

Tip110 mutant (Tip110ΔNLS) showed a higher ubiquitination level compared with its nuclear wild-type (**Figure 2D**). Meanwhile, this difference in the ubiquitination had little effect on the level of the expressed proteins (**Figure 5D**). Tip110 expression promoted the translocation of several associated nuclear-cytoplasmic shuttling proteins such as USP4 (38), USP15 (25, 38), and YB-1 [(8), data not shown] from the cytoplasm to the nucleus where they co-localized. The complex structure of the NLS on Tip110 and importin 2α is involved a bipartite binding, and removal of Tip110 NLS prevents the entry of USP4 or USP15 in the nucleus and abrogates their subsequent deubiquitinase activity (12, 55), which may explain the detection of a higher ubiquitinated form of cytoplasmic expressed Tip110ΔNLS mutant (**Figures 2D**, **4C, E**). Therefore, the NLS domain on Tip110 may play an important role in its ubiquitination and function, which merits further investigations.

Newly synthesized IκBα is accumulated in the cytoplasm but is also present in the nucleus, where it terminates NF-κB-dependent transcription (56). However, there is a requirement for the transcription of essential NF-κB-dependent genes in unstimulated cells, which requires a continual proteasome-mediated breakdown of IκBα. We found that Tip110 regulated the TNF-α-induced IκBα phosphorylation and subsequently affected its stability (**Figure 4**). However, the absence of Tip110 effect in basal level of IκBα protein (on the absence of TNF-α treatment) is likely due to the compensatory response caused by Tip110 expression as shown in **Figure 7** and **Figure S3**. Due to that, we performed CHX chase assay to determine the exogenous IκBα half-life (**Figures 4C–F**). Ectopic expression of Tip110 in the absence of TNF-α stimulation enhanced the IκBα degradation as shown by the CHX chase assay while the cytoplasmic-expressed Tip110 mutant stabilized IκBα (**Figure 4**). No interaction had been detected between Tip110 and IκBα (data not shown), and no significant effect on the IκBα mRNA level by Tip110 was observed (**Figure 4G**). Surprisingly, we found that knockdown of Tip110 also has a similar impact on the IκBα stability by the CHX chase assay. This observation further confirms the compensatory effect of Tip110 expression level as Tip110-transgenic homozygous mice apparently impacted embryonic development similar to the knockout mice [data not shown (45)].

It is important to note that activation of NF-κB transcriptional activity is not only a consequence of IκBα degradation initiated by a signaling cascade. One important example is p65, which is known to activate NF-κB transcriptional activity; however, overexpression of p65 has also been shown to increase synthesis and stabilization of IκBα (57, 58). Although Tip110 potentiated NF-κB activation, it had little effect on the basal level of IκBα protein. Therefore, we have not excluded other mechanisms such as modulation of p65 coactivators/corepressors, p65 post-translational modification, and Tip110-associated proteins that are known to play a role in NF-κB signaling. Here, we showed that Tip110-associated protein, USP15, opposingly regulates NF-κB activity by targeting IκBα protein stability.

USP15 is an oncogenic ubiquitously expressed protein that shared amino acid sequence homology with two other deubiquitinating enzymes (DUBs), USP4 and USP11 (59). However, Tip110 was found to interact with and promote nuclear translocation of USP4 and USP15 but not USP11, and this is due to β-hairpin of the linker region of the DUSP and UBL domains of both USP4 and USP15 proteins that were associated with the HAT domain of Tip110 (12, 23, 25, 38) In addition, the binding of USP15 to Tip110 is 20-fold stronger than USP4 (55). Interestingly, USP15 expression only led to Tip110 deubiquitination (25, 38). USP4 was found to inhibit TNF-α-induced NF-κB activation by targeting several upstream components of NF-κB signaling (26, 60–62). While IκBα acts as a substrate for USP15 and USP11, and this resulted in IκBα stabilization and inhibited NF-κB activation (27, 30, 63). Overexpression of USP15 inhibited Sendai Virus-induced activation of NF-κB by modulation of NF-κB phosphorylation (64). On the other hand, Zhou et al. showed that USP15 acts as positive regulator in TNF-α- and IL-1β-induced NF-κB activation through differential stabilization of TAB2/3 (42). Those observations prompted us to investigate whether Tip110-USP15 complex regulate NF-κB activity. We showed that USP15 expression obliterated Tip110-induced NF-κB activation (**Figures 5B, C**) and overexpression of Tip110 enhanced USP15-inhibited NF-κB activity (**Figures 5D, E**). Those observations were further confirmed under the context of NF-κB p65 which is known to activate NF-κB gene expression (65) (**Figure 5E**). The opposing effect of Tip110 and USP15 was a result of IκBα protein destabilization (**Figure 5F**). Unexpectedly, we observed stabilization of nuclear targeted IκBα under the context of Tip110 overexpression (**Figures 4E, F**) more likely as a result of the translocation of USP15 to the nucleus and promoted nuclear IκBα stability. Therefore, it is possible that under the pathophysiological condition, when the Tip110 level is elevated, USP15 is translocated from the cytoplasm to the nucleus and associated with Tip110. This promoted IκBα protein phosphorylation, degradation, and ultimately NF-κB activation.

It has been reported that pretreatment of cells with Leptomycin B (LMB), protein export inhibitor, inhibited NF-κB-dependent transcriptional activation mediated by TNF-α through the accumulation of IκBα in the nucleus where it became resistant to signal-induced degradation (66). We showed that LMB treatment had no effect on Tip110-induced NF-κB activity; however, in the presence of both TNF-α and LMB, Tip110 expression led to a reduction in the NF-κB activity but remained higher than transfected control (**Figure S2A**). Furthermore, synergetic activation of NF-κB was found by the co-expression of Tip110 and p65, and the addition of LMP led to a reduction in the NF-κB activity (**Figures 5E**, **S2A**). LMB treatment led to the rapid nuclear accumulation of IκBα and slower nuclear accumulation of p65 (67). Moreover, IκBα but not IκBβ is sensitive to LMB treatment in the nucleus (68). Therefore, Tip110 expression may affect IκBα protein in both cytoplasm and nucleus to regulate NF-κB activation since the localization of the p65 population is carefully controlled, presumably by the IκBα (56, 69). Thus, we speculated that other factors might also contribute to regulating IκBα stability by Tip110 in the nucleus.

Heterogeneous nuclear ribonucleoprotein A1 (hnRNPA1) is a nuclear protein that shuttles between the nucleus and the cytoplasm due to unknown conditions (70). Using proteomic study, we have shown that hnRNPA1 complexed with Tip110 (24). HnRNPA1 contributed to the control of NF-κB-dependent transcription through direct interaction and potentiation of IκBα degradation. Both nuclear and cytoplasmic expressed-hnRNPA1 proteins were able to bind with IκBα, but the nuclear hnRNAPA1 has shown a higher NF-κB transcriptional activity (71). Although the mechanism has not been investigated, the authors suggested that hnRNPA1 may act as a scaffold-like molecule, bringing IκBα into the optimal environment for signal induced-modification (72). Therefore, it is highly possible that Tip110/hnRNPA1/USP15 complex contributes to IκBα stability and NF-κB activation in the nucleus.

Recently, we reported the lethal effects of complete loss of Tip110 on mouse embryonic development. The whole-genome analysis data from knockout Tip110 embryonic stem cells compared to the wild-type (45) was utilized to elucidate the possible role of Tip110 knockout in the NF-κB pathway. The data showed that Tip110 knockout cells caused dysregulation of genes associated with NF-κB and NF-κB-related signaling pathways, including TNF-α-NF-κB, MAPK, p53, and IL-6 signaling (**Figures 7A–C** and **S3B**). Intriguingly, several genes in the EGF, TNF-α, and TGFβ receptor signaling cascade were found to be upregulated (**Figure 7D**). In the NF-κB pathway, TNF-α was down-regulated, while IL-1 cytokines and their receptors were upregulated. MAP3K5 and MAPK14 were downregulated while MAP2K6, MAPK13, and MAPK12 were upregulated. Also, TGFβ1 was downregulated while TGFβ2 and TGFβ3 were upregulated. IKKγ and NF-κB1 were upregulated, while IKKβ was down-regulated. The microarray data also showed that knockout of Tip110 cells caused dysregulation of several genes associated with apoptosis, mRNA processing, and proteasomal degradation (45). Therefore, loss of Tip110 may evoke a compensatory mechanism that may lead to an up-regulation of other proteins associated with signaling pathways at the transcriptional and/or translational level, strongly suggesting the important role of Tip110 expression in an inflammatory response. In addition, this compensatory mechanism has also been reported on the spliceosome recycling defect exerted by knockout of Tip110 in zebrafish (73).

In summary, the identification of nucleus-restricted protein Tip110 as a regulator of the NF-κB pathway unveils novel and exciting layers of regulatory specificity for NF-κB in the nucleus. In addition, our findings elucidate the important role of Tip110 expression in inflammatory diseases and cancer-related inflammation.

METHODS

Cell Culture and Transfection

HEK 293T cell line was purchased from American Tissue Culture Collection (ATCC) and cultured in Dulbecco's modified Eagle's medium (DMEM) containing 10% fetal bovine serum (FBS). Mouse embryonic fibroblasts (MEF) isolation was reported previously (25). Briefly, MEF cells were isolated from embryos of 13.5-14.5 days post coitus pregnant mice and cultured in DMEM with 10% FBS and 50 μM 2-β mercaptoethanol. All media contained 100 IU/ml penicillin, 100 μg/ml streptomycin. Plasmid DNA transfection was performed using the standard calcium phosphate precipitation method for 293T. MEF cells were transfected using Lipofectamine LTX (Invitrogen) according to the manufacturer's instructions. Si-RNA transfection was performed using Lipofectamine 2000 according to the manufacturer's instructions (Invitrogen).

DNA Plasmids and siRNA

Tip110.His, Tip110ΔN.His, Tip110ΔC.His, GFP-Tip110ΔNLS, Tip110ΔNLS.His, and GFP-Tip110 plasmids were described elsewhere (28, 74). Tip110Δ274-963.His, Tip110Δ387-963.His, Tip110Δ557-963.His, and Tip110Δ786-963.His plasmids were constructed in the backbone of pcDNA3 (Invitrogen) using standard PCR techniques with Tip110.His as a template and using EcoRI and XhoI cloning sites. USP15.Myc (1–952 aa), USP15ΔC.Myc (1–384 aa) and USP15ΔN.Myc (385-952 aa) were described elsewhere (25). NF-κB p65 was a kindly provided by Dr. Michael Klemsz of Indiana University School of Medicine. pNF-κB-luc and pAP-1-Luc were purchased from Clontech Laboratories Inc., CA. UB.HA plasmid was kindly provided by Dr. Mark Hannink of the University of Missouri. IκBα.HA plasmid was kindly provided by Dr. Michael Karin of the University of California (75). The IκBα-Nuc.Myc plasmid was constructed using IκBα.HA as a template, backbone of pCMV-Nuc-Myc (Addgene) and using SalI and NotI cloning sites. On-TARGETplus Tip110 siRNA (L-013447-01) and SiRNA control (D-001810-01) were purchased from Dharmacon.

Reporter Gene Assays

The firefly luciferase activity was measured using the luciferase assay substrate (Promega, Madison, WI) according to the manufacturer's instructions. Briefly, cells were washed with ice-cold PBS and lysed with 120 μl 1× firefly luciferase lysis buffer (Promega) at room temperature for 15 min. The lysates were centrifuged at 12,000 × *g* for 2 min to remove cell debris. The cleared lysates (5 μl) were then mixed with 20 μl firefly luciferase substrate (Promega), and the luciferase activity was measured using an Opticomp luminometer (MGM Instruments, Hamden, CT). The same cell lysates were then used for immunoblotting to confirm the protein expression.

Immunoblot and Immunoprecipitation Analysis

Cells were washed in cold PBS and lysed in lysis buffer (50 mM Tris.HCl, pH 8.0, 280 mM NaCl, 0.5% NP-40, 0.2 mM EDTA, 2 mM EGTA, 10% glycerol, 2 mM PMSF and protease inhibitor cocktail). Lysates were cleared of cell debris by centrifugation at 12,000 *x g* and fractionated on SDS-PAGE, followed by Western blotting. For detection of Tip110 and its mutants, we used polyclonal and monoclonal Tip110 antibodies (9, 28) because

not all of the Tip110 mutants were able to be recognized by the same antibody. Also, not all the constructed mutants in our study were tagged. Anti-His (abm), anti-HA (Santa Cruz Biotechnology; sc-7392), anti-p65 (Abcam; ab-7970), anti-Myc (Santa Cruz Biotechnology; sc-9E10), anti-USP15 (Santa Cruz Biotechnology; sc-100629), and anti-actin (Sigma A1978). For immunoprecipitation, 1 mg of cell lysates were incubated with 1 μg of primary antibody at 4°C on a rotating device overnight, and protein A agarose beads (Upstate) were then added for 45 min. Agarose beads were recovered and washed thoroughly three times with the above lysis buffer and processed for SDS-PAGE and Western blotting analysis.

Immunostaining

Cells were transfected on 24-well culture plates, fixed with 4% paraformaldehyde for 20 min, and then permeabilized with 0.5% Triton X-100 for 10 min. After extensive washing with PBS, the cells were blocked with 3% BSA and incubated with anti-p65 and anti-Tip110 antibodies (1:500) for 1 hr at room temperature in a humidified chamber. Then the cells were washed and incubated with either anti-Alexa Fluor 555 or anti-Alexa Fluor 488 secondary antibodies (Invitrogen; 1:500) for 1 hr and then 1 ng/ml 4,6-diamidino-2-phenylindole (DAPI) for 5 min to stain the nuclei. The coverslips were washed with PBS and mounted with fluoromount-G (SouthernBiotech) on glass slides. Fluorescence micrographs were taken using a Zeiss Model Axiovert 200 M microscope.

Quantitative RT-PCR Analysis of Gene Expression

RNA was extracted from cells using TRizol (Invitrogen) according to the manufacturer's instructions. RNA (1 μg) was converted to cDNA using the iScript cDNA synthesis kit (Bio-Rad, Hercules, CA) and used as the template for PCR using SsoAdvanced SYBR green Supermix and the CFX96 real-time PCR detection system (Bio-Rad). The quantitative reverse transcription-PCR (qRT-PCR) primers used and their sequences are as follows: for β-actin, 5′-AAA CTG GAA CGG TGA AGG TG-3′ and 5′-AGA GAA GTG GGG TGG CTT TT-3′; for TNF-α, 5′-TCT TCT CGA ACC CCG AGT GA-3′ and 5-CCT CTG ATG GCA CCA CCA G-3′; for IL-6, 5′-ACA ACA AAT TCG GTA GAT CCT CG-3′ and 5′-AGC CAT CTT TGG AAG GTT CAG G-3′; for IL-8, 5′-TGC CAA GGA GTG CTA AAG-3′ and 5′-TCT CAG CCC TCT TCA AAA-3′; and, for IκBα, 5′- ACC AAC TAC AAT GGC CAC AC-3′ and 5′- ATT ACA GGG CTC CTG AGC AT-3′. Threshold cycle (C_T) values were calculated using Bio-Rad CFX manager software. The $2^{-\Delta\Delta CT}$ value was calculated to represent the fold change of the target gene mRNA compared to untreated siRNA control and normalized using β-actin as the reference.

Cycloheximide Chase Assay

Cells were treated with 20 μg/ml cycloheximide (Sigma), and then the whole-cell lysates were prepared after different durations. The lysates were subjected to Western blotting analysis to identify the IκBα turnover rate alone or in the presence of Tip110 and Tip110ΔNLS. The amount of the remaining proteins was quantified by using densitometry and normalized to the β-actin.

Data Analysis

Where appropriate, values are expressed as means ± standard deviations (SD) from triplicate samples. All comparisons were made based on the control using a two-tailed Student's *t*-test and two-way analysis of variance (ANOVA) as appropriate. *P* values of <0.05 were considered statistically significant, <0.01 highly significant, and <0.001 strongly significant. If statistical significance (P <0.05) was determined by ANOVA, the data were further analyzed by Turkey's *post hoc* test for multi group Comparisons.

DATA AVAILABILITY STATEMENT

The original contributions presented in the study are included in the article/**Supplementary Material**. Further inquiries can be directed to the corresponding author.

AUTHOR CONTRIBUTIONS

KT: Conceptualized and executed the study, interpreted the data, and wrote the MS. SR: Helped in executing the experiments and editing the MS. AW: Analyzed whole-transcriptome array data, prepared related figures, and helped in editing the MS. YL: shared reagents and gave valuable inputs. JH: conceptualized the study, supervised experiments, supported the study, and contributed to writing the MS. All the authors approved the submission of the manuscript.

ACKNOWLEDGMENTS

We thank Dr. Michael Karin for providing pIκBα.HA expression plasmid. Dr. Michael Klemsz for providing NF-κB p65 expression plasmid. Dr. Mark Hannink for providing pUB.HA. Part of this work was performed at the UNTHSC. This work was supported by the startup funds (JJH) provided by Rosalind Franklin University Chicago Medical School.

SUPPLEMENTARY MATERIAL

The Supplementary Material for this article can be found online at: https://www.frontiersin.org/articles/10.3389/fonc.2022.843157/full#supplementary-material

REFERENCES

1. Hayden MS, Ghosh S. Shared Principles in NF-kappaB Signaling. *Cell* (2008) 132(3):344–62. doi: 10.1016/j.cell.2008.01.020
2. Karin M, Lin A. NF-kappaB at the Crossroads of Life and Death. *Nat Immunol* (2002) 3(3):221–7. doi: 10.1038/ni0302-221
3. Li Q, Verma IM. NF-kappaB Regulation in the Immune System. *Nat Rev Immunol* (2002) 2(10):725–34. doi: 10.1038/nri910
4. Ghosh S, Karin M. Missing Pieces in the NF-kappaB Puzzle. *Cell* (2002) 109 Suppl:S81–96. doi: 10.1016/S0092-8674(02)00703-1
5. Chen ZJ. Ubiquitin Signalling in the NF-kappaB Pathway. *Nat Cell Biol* (2005) 7(8):758–65. doi: 10.1038/ncb0805-758
6. Verma IM, Stevenson JK, Schwarz EM, Van Antwerp D, Miyamoto S. Rel/NF-Kappa B/I Kappa B Family: Intimate Tales of Association and Dissociation. *Genes Dev* (1995) 9(22):2723–35. doi: 10.1101/gad.9.22.2723
7. Vallabhapurapu S, Karin M. Regulation and Function of NF-kappaB Transcription Factors in the Immune System. *Annu Rev Immunol* (2009) 27:693–733. doi: 10.1146/annurev.immunol.021908.132641
8. Whitmill A, Timani KA, Liu Y, He JJ. Tip110: Physical Properties, Primary Structure, and Biological Functions. *Life Sci* (2016) 149:79–95. doi: 10.1016/j.lfs.2016.02.062
9. Liu Y, Timani K, Mantel C, Fan Y, Hangoc G, Cooper S, et al. TIP110/p110nrb/SART3/p110 Regulation of Hematopoiesis Through CMYC. *Blood* (2011) 117(21):5643–51. doi: 10.1182/blood-2010-12-325332
10. Liu Y, Timani K, Ou X, Broxmeyer HE, He JJ. C-MYC Controlled TIP110 Protein Expression Regulates OCT4 mRNA Splicing in Human Embryonic Stem Cells. *Stem Cells Dev* (2013) 22(5):689–94. doi: 10.1089/scd.2012.0271
11. Novotny I, Malinova A, Stejskalova E, Mateju D, Klimesova K, Roithova A, et al. SART3-Dependent Accumulation of Incomplete Spliceosomal snRNPs in Cajal Bodies. *Cell Rep* (2015) 10(3):429–40. doi: 10.1016/j.celrep.2014.12.030
12. Park JK, Das T, Song EJ, Kim EE. Structural Basis for Recruiting and Shuttling of the Spliceosomal Deubiquitinase USP4 by SART3. *Nucleic Acids Res* (2016) 44(11):5424–37. doi: 10.1093/nar/gkw218
13. Ruegger S, Miki TS, Hess D, Grosshans H. The Ribonucleotidyl Transferase USIP-1 Acts With SART3 to Promote U6 snRNA Recycling. *Nucleic Acids Res* (2015) 43(6):3344–57. doi: 10.1093/nar/gkv196
14. Harada K, Yamada A, Yang D, Itoh K, Shichijo S. Binding of a SART3 Tumor-Rejection Antigen to a pre-mRNA Splicing Factor RNPS1: A Possible Regulation of Splicing by a Complex Formation. *Int J Cancer* (2001) 93 (5):623–8. doi: 10.1002/ijc.1391
15. Zhao W, Liu Y, Timani KA, He JJ. Tip110 Protein Binds to Unphosphorylated RNA Polymerase II and Promotes its Phosphorylation and HIV-1 Long Terminal Repeat Transcription. *J Biol Chem* (2014) 289(1):190–202. doi: 10.1074/jbc.M113.529784
16. Fukuda K. Expression of the SART3 Antigens in Oral Cancers. *Kurume Med J* (2001) 48(1):55–8. doi: 10.2739/kurumemedj.48.55
17. Kawagoe N, Shintaku I, Yutani S, Etoh H, Matuoka K, Noda S, et al. Expression of the SART3 Tumor Rejection Antigen in Renal Cell Carcinoma. *J Urol* (2000) 164 (6):2090–5. doi: 10.1016/S0022-5347(05)66975-3
18. Murayama K, Kobayashi T, Imaizumi T, Matsunaga K, Kuramoto T, Shigemori M, et al. Expression of the SART3 Tumor-Rejection Antigen in Brain Tumors and Induction of Cytotoxic T Lymphocytes by its Peptides. *J Immunother* (2000) 23(5):511–8. doi: 10.1097/00002371-200009000-00001
19. Niiya F, Nishizaka S, Matsunaga K, Koufuji K, Mori M, Katai H, et al. Expression of SART3 Tumor-Rejection Antigen in Gastric Cancers. *Jpn J Cancer Res: Gann* (2000) 91(3):337–42. doi: 10.1111/j.1349-7006.2000.tb00950.x
20. Liu P, Zhang S, Yao Q, Liu X, Wang X, Huang C, et al. *Et Al*: Identification of a Genetic Locus for Autosomal Dominant Disseminated Superficial Actinic Porokeratosis on Chromosome 1p31.3-P31.1. *Hum Genet* (2008) 123(5):507–13. doi: 10.1007/s00439-008-0504-x
21. Timani KA, Liu Y, Fan Y, Mohammad KS, He JJ. Tip110 Regulates the Cross Talk Between P53 and Hypoxia-Inducible Factor 1alpha Under Hypoxia and Promotes Survival of Cancer Cells. *Mol Cell Biol* (2015) 35(13):2254–64. doi: 10.1128/MCB.00001-15
22. Timani KA, Gyorffy B, Liu Y, Mohammad KS, He JJ. Tip110/SART3 Regulates IL-8 Expression and Predicts the Clinical Outcomes in Melanoma. *Mol Cancer* (2018) 17(1):124. doi: 10.1186/s12943-018-0868-z
23. Long L, Thelen JP, Furgason M, Haj-Yahya M, Brik A, Cheng D, et al. The U4/U6 Recycling Factor SART3 has Histone Chaperone Activity and Associates With USP15 to Regulate H2B Deubiquitination. *J Biol Chem* (2014) 289 (13):8916–30. doi: 10.1074/jbc.M114.551754
24. Timani KA, Liu Y, He JJ. Tip110 Interacts With YB-1 and Regulates Each Other's Function. *BMC Mol Biol* (2013) 14:14. doi: 10.1186/1471-2199-14-14
25. Timani KA, Liu Y, Suvannasankha A, He JJ. Regulation of Ubiquitin-Proteasome System-Mediated Tip110 Protein Degradation by USP15. *Int J Biochem Cell Biol* (2014) 54:10–9. doi: 10.1016/j.biocel.2014.06.017
26. Fan YH, Yu Y, Mao RF, Tan XJ, Xu GF, Zhang H, et al. USP4 Targets TAK1 to Downregulate TNFalpha-Induced NF-kappaB Activation. *Cell Death Different* (2011) 18(10):1547–60. doi: 10.1038/cdd.2011.11
27. Schweitzer K, Bozko PM, Dubiel W, Naumann M. CSN Controls NF-kappaB by Deubiquitinylation of IkappaBalpha. *EMBO J* (2007) 26(6):1532–41. doi: 10.1038/sj.emboj.7601600
28. Liu Y, Li J, Kim BO, Pace BS, He JJ. HIV-1 Tat Protein-Mediated Transactivation of the HIV-1 Long Terminal Repeat Promoter is Potentiated by a Novel Nuclear Tat-Interacting Protein of 110 kDa, Tip110. *J Biol Chem* (2002) 277(26):23854–63. doi: 10.1074/jbc.M200773200
29. Fiume G, Vecchio E, De Laurentiis A, Trimboli F, Palmieri C, Pisano A, et al. *Et Al*: Human Immunodeficiency Virus-1 Tat Activates NF-kappaB *via* Physical Interaction With IkappaB-Alpha and P65. *Nucleic Acids Res* (2012) 40(8):3548–62. doi: 10.1093/nar/gkr1224
30. Borner C, Kraus J. Inhibition of NF-kappaB by Opioids in T Cells. *J Immunol* (2013) 191(9):4640–7. doi: 10.4049/jimmunol.1300320
31. Hayes SD, Liu H, MacDonald E, Sanderson CM, Coulson JM, Clague MJ, et al. Direct and Indirect Control of Mitogen-Activated Protein Kinase Pathway-Associated Components, BRAP/IMP E3 Ubiquitin Ligase and CRAF/RAF1 Kinase, by the Deubiquitylating Enzyme USP15. *J Biol Chem* (2012) 287 (51):43007–18. doi: 10.1074/jbc.M112.386938
32. Zhang L, Zhou F, Drabsch Y, Gao R, Snaar-Jagalska BE, Mickanin C, et al. *Et Al*: USP4 is Regulated by AKT Phosphorylation and Directly Deubiquitylates TGF-Beta Type I Receptor. *Nat Cell Biol* (2012) 14(7):717–26. doi: 10.1038/ncb2522
33. Karin M, Takahashi T, Kapahi P, Delhase M, Chen Y, Makris C, et al. Oxidative Stress and Gene Expression: The AP-1 and NF-kappaB Connections. *BioFactors* (2001) 15(2-4):87–9. doi: 10.1002/biof.5520150207
34. Lee SW, Han SI, Kim HH, Lee ZH. TAK1-Dependent Activation of AP-1 and C-Jun N-Terminal Kinase by Receptor Activator of NF-Kappab. *J Biochem Mol Biol* (2002) 35(4):371–6. doi: 10.5483/BMBRep.2002.35.4.371
35. Fujioka S, Niu J, Schmidt C, Sclabas GM, Peng B, Uwagawa T, et al. NF-kappaB and AP-1 Connection: Mechanism of NF-kappaB-Dependent Regulation of AP-1 Activity. *Mol Cell Biol* (2004) 24(17):7806–19. doi: 10.1128/MCB.24.17.7806-7819.2004
36. Locksley RM, Killeen N, Lenardo MJ. The TNF and TNF Receptor Superfamilies: Integrating Mammalian Biology. *Cell* (2001) 104(4):487–501. doi: 10.1016/S0092-8674(01)00237-9
37. Wajant H, Pfizenmaier K, Scheurich P. Tumor Necrosis Factor Signaling. *Cell Death Different* (2003) 10(1):45–65. doi: 10.1038/sj.cdd.4401189
38. Song EJ, Werner SL, Neubauer J, Stegmeier F, Aspden J, Rio D, et al. The Prp19 Complex and the Usp4Sart3 Deubiquitinating Enzyme Control Reversible Ubiquitination at the Spliceosome. *Genes Dev* (2010) 24 (13):1434–47. doi: 10.1101/gad.1925010
39. Birbach A, Gold P, Binder BR, Hofer E, de Martin R, Schmid JA. Signaling Molecules of the NF-Kappa B Pathway Shuttle Constitutively Between Cytoplasm and Nucleus. *J Biol Chem* (2002) 277(13):10842–51. doi: 10.1074/jbc.M112475200
40. D'Arcy P, Wang X, Linder S. Deubiquitinase Inhibition as a Cancer Therapeutic Strategy. *Pharmacol Ther* (2015) 147:32–54. doi: 10.1016/j.pharmthera.2014.11.002
41. Das T, Song EJ, Kim EE. The Multifaceted Roles of USP15 in Signal Transduction. *Int J Mol Sci* (2021) 22(9):4728. doi: 10.3390/ijms22094728
42. Zhou Q, Cheng C, Wei Y, Yang J, Zhou W, Song Q, et al. USP15 Potentiates NF-kappaB Activation by Differentially Stabilizing TAB2 and TAB3. *FEBS J* (2020) 287(15):3165–83. doi: 10.1111/febs.15202
43. Huang TT, Kudo N, Yoshida M, Miyamoto S. A Nuclear Export Signal in the N-Terminal Regulatory Domain of IkappaBalpha Controls Cytoplasmic Localization of Inactive NF-Kappab/IkappaBalpha Complexes. *Proc Natl Acad Sci USA* (2000) 97(3):1014–9. doi: 10.1073/pnas.97.3.1014

44. O'Connor S, Shumway S, Miyamoto S. Inhibition of IkappaBalpha Nuclear Export as an Approach to Abrogate Nuclear factor-kappaB-Dependent Cancer Cell Survival. *Mol Cancer Res: MCR* (2005) 3(1):42–9.
45. Whitmill A, Liu Y, Timani KA, Niu Y, He JJ. Tip110 Deletion Impaired Embryonic and Stem Cell Development Involving Downregulation of Stem Cell Factors Nanog, Oct4, and Sox2. *Stem Cells* (2017) 35(7):1674–86. doi: 10.1002/stem.2631
46. Wan F, Lenardo MJ. The Nuclear Signaling of NF-Kappab: Current Knowledge, New Insights, and Future Perspectives. *Cell Res* (2010) 20 (1):24–33. doi: 10.1038/cr.2009.137
47. McElhinny JA, MacMorran WS, Bren GD, Ten RM, Israel A, Paya CV. Regulation of I Kappa B Alpha and P105 in Monocytes and Macrophages Persistently Infected With Human Immunodeficiency Virus. *J Virol* (1995) 69 (3):1500–9. doi: 10.1128/jvi.69.3.1500-1509.1995
48. Hiscott J, Kwon H, Genin P. Hostile Takeovers: Viral Appropriation of the NF-kappaB Pathway. *J Clin Invest* (2001) 107(2):143–51. doi: 10.1172/JCI11918
49. Raj GV, Safak M, MacDonald GH, Khalili K. Transcriptional Regulation of Human Polyomavirus JC: Evidence for a Functional Interaction Between RelA (P65) and the Y-Box-Binding Protein, YB-1. *J Virol* (1996) 70(9):5944–53. doi: 10.1128/jvi.70.9.5944-5953.1996
50. Sinnberg T, Sauer B, Holm P, Spangler B, Kuphal S, Bosserhoff A, et al. MAPK and PI3K/AKT Mediated YB-1 Activation Promotes Melanoma Cell Proliferation Which is Counteracted by an Autoregulatory Loop. *Exp Dermatol* (2012) 21(4):265–70. doi: 10.1111/j.1600-0625.2012.01448.x
51. Klapproth K, Sander S, Marinkovic D, Baumann B, Wirth T. The IKK2/NF-{Kappa}B Pathway Suppresses MYC-Induced Lymphomagenesis. *Blood* (2009) 114(12):2448–58. doi: 10.1182/blood-2008-09-181008
52. Liu T, Zhou Y, Ko KS, Yang H. Interactions Between Myc and Mediators of Inflammation in Chronic Liver Diseases. *Mediators Inflammation* (2015) 2015:276850. doi: 10.1155/2015/276850
53. Wu H, Lozano G. NF-Kappa B Activation of P53. A Potential Mechanism for Suppressing Cell Growth in Response to Stress. *J Biol Chem* (1994) 269 (31):20067–74. doi: 10.1016/S0021-9258(17)32128-2
54. Lowe JM, Menendez D, Bushel PR, Shatz M, Kirk EL, Troester MA, et al. P53 and NF-kappaB Coregulate Proinflammatory Gene Responses in Human Macrophages. *Cancer Res* (2014) 74(8):2182–92. doi: 10.1158/0008-5472.CAN-13-1070
55. Zhang Q, Harding R, Hou F, Dong A, Walker JR, Bteich J, et al. Structural Basis of the Recruitment of Ubiquitin-Specific Protease USP15 by Spliceosome Recycling Factor Sart3. *J Biol Chem* (2016) 291(33):17283–92. doi: 10.1074/jbc.M116.740787
56. Arenzana-Seisdedos F, Thompson J, Rodriguez MS, Bachelerie F, Thomas D, Hay RT. Inducible Nuclear Expression of Newly Synthesized I Kappa B Alpha Negatively Regulates DNA-Binding and Transcriptional Activities of NF-Kappa B. *Mol Cell Biol* (1995) 15(5):2689–96. doi: 10.1128/MCB.15.5.2689
57. Scott ML, Fujita T, Liou HC, Nolan GP, Baltimore D. The P65 Subunit of NF-Kappa B Regulates I Kappa B by Two Distinct Mechanisms. *Genes Dev* (1993) 7(7A):1266–76. doi: 10.1101/gad.7.7a.1266
58. Perez P, Lira SA, Bravo R. Overexpression of RelA in Transgenic Mouse Thymocytes: Specific Increase in Levels of the Inhibitor Protein I Kappa B Alpha. *Mol Cell Biol* (1995) 15(7):3523–30. doi: 10.1128/MCB.15.7.3523
59. Vlasschaert C, Xia X, Coulombe J, Gray DA. Evolution of the Highly Networked Deubiquitinating Enzymes USP4, USP15, and USP11. *BMC Evol Biol* (2015) 15:230. doi: 10.1186/s12862-015-0511-1
60. Xiao N, Li H, Luo J, Wang R, Chen H, Chen J, et al. Ubiquitin-Specific Protease 4 (USP4) Targets TRAF2 and TRAF6 for Deubiquitination and Inhibits TNFalpha-Induced Cancer Cell Migration. *Biochem J* (2012) 441 (3):979–86. doi: 10.1042/BJ20111358
61. Li Z, Hao Q, Luo J, Xiong J, Zhang S, Wang T, et al. USP4 Inhibits P53 and NF-kappaB Through Deubiquitinating and Stabilizing HDAC2. *Oncogene* (2015) 35(22):2902–16. doi: 10.1038/onc.2015.349
62. Hou X, Wang L, Zhang L, Pan X, Zhao W. Ubiquitin-Specific Protease 4 Promotes TNF-Alpha-Induced Apoptosis by Deubiquitination of RIP1 in Head and Neck Squamous Cell Carcinoma. *FEBS Lett* (2013) 587(4):311–6. doi: 10.1016/j.febslet.2012.12.016
63. Sun W, Tan X, Shi Y, Xu G, Mao R, Gu X, et al. USP11 Negatively Regulates TNFalpha-Induced NF-kappaB Activation by Targeting on IkappaBalpha. *Cell Signall* (2010) 22(3):386–94. doi: 10.1016/j.cellsig.2009.10.008
64. Zhang H, Wang D, Zhong H, Luo R, Shang M, Liu D, et al. Ubiquitin-Specific Protease 15 Negatively Regulates Virus-Induced Type I Interferon Signaling *via* Catalytically-Dependent and -Independent Mechanisms. *Sci Rep* (2015) 5:11220. doi: 10.1038/srep11220
65. Schmitz ML, Baeuerle PA. The P65 Subunit is Responsible for the Strong Transcription Activating Potential of NF-Kappa B. *EMBO J* (1991) 10 (12):3805–17. doi: 10.1002/j.1460-2075.1991.tb04950.x
66. Rodriguez MS, Thompson J, Hay RT, Dargemont C. Nuclear Retention of IkappaBalpha Protects it From Signal-Induced Degradation and Inhibits Nuclear Factor kappaB Transcriptional Activation. *J Biol Chem* (1999) 274 (13):9108–15. doi: 10.1074/jbc.274.13.9108
67. Nelson G, Paraoan L, Spiller DG, Wilde GJ, Browne MA, Djali PK, et al. Multi-Parameter Analysis of the Kinetics of NF-kappaB Signalling and Transcription in Single Living Cells. *J Cell Sci* (2002) 115(Pt 6):1137–48. doi: 10.1242/jcs.115.6.1137
68. Huang TT, Miyamoto S. Postrepression Activation of NF-kappaB Requires the Amino-Terminal Nuclear Export Signal Specific to IkappaBalpha. *Mol Cell Biol* (2001) 21(14):4737–47. doi: 10.1128/MCB.21.14.4737-4747.2001
69. Zabel U, Baeuerle PA. Purified Human I Kappa B Can Rapidly Dissociate the Complex of the NF-Kappa B Transcription Factor With its Cognate DNA. *Cell* (1990) 61(2):255–65. doi: 10.1016/0092-8674(90)90806-P
70. Pinol-Roma S, Dreyfuss G. Shuttling of pre-mRNA Binding Proteins Between Nucleus and Cytoplasm. *Nature* (1992) 355(6362):730–2. doi: 10.1038/355730a0
71. Hay DC, Kemp GD, Dargemont C, Hay RT. Interaction Between Hnrnpa1 and IkappaBalpha Is Required for Maximal Activation of NF-kappaB-Dependent Transcription. *Mol Cell Biol* (2001) 21(10):3482–90. doi: 10.1128/MCB.21.10.3482-3490.2001
72. Sahu I, Sangith N, Ramteke M, Gadre R, Venkatraman P. A Novel Role for the Proteasomal Chaperone PSMD9 and Hnrnpa1 in Enhancing IkappaBalpha Degradation and NF-kappaB Activation - Functional Relevance of Predicted PDZ Domain-Motif Interaction. *FEBS J* (2014) 281(11):2688–709. doi: 10.1111/febs.12814
73. Trede NS, Medenbach J, Damianov A, Hung LH, Weber GJ, Paw BH, et al. *Et Al*: Network of Coregulated Spliceosome Components Revealed by Zebrafish Mutant in Recycling Factor P110. *Proc Natl Acad Sci USA* (2007) 104 (16):6608–13. doi: 10.1073/pnas.0701919104
74. Liu Y, Kim BO, Kao C, Jung C, Dalton JT, He JJ. Tip110, the Human Immunodeficiency Virus Type 1 (HIV-1) Tat-Interacting Protein of 110 kDa as a Negative Regulator of Androgen Receptor (AR) Transcriptional Activation. *J Biol Chem* (2004) 279(21):21766–73. doi: 10.1074/jbc.M314321200
75. Zandi E, Chen Y, Karin M. Direct Phosphorylation of IkappaB by IKKalpha and IKKbeta: Discrimination Between Free and NF-kappaB-Bound Substrate. *Science* (1998) 281(5381):1360–3. doi: 10.1126/science.281.5381.1360

Conflict of Interest: The authors declare that the research was conducted in the absence of any commercial or financial relationships that could be construed as a potential conflict of interest.

frontiers | Frontiers in Oncology

ORIGINAL RESEARCH
published: 30 May 2022
doi: 10.3389/fonc.2022.872444

SIRT4-Catalyzed Deacetylation of Axin1 Modulates the Wnt/β-Catenin Signaling Pathway

Yuting Wang[1,2†], Jicheng Yue[3†], Mingzhe Xiao[4†], Xiaomei Lu[5] and Yuen Eugene Chin[1*]*

[1] Institutes of Biology and Medical Sciences, Soochow University School of Medicine, Suzhou, China, [2] The Affiliated Wuxi People's Hospital of Nanjing Medical University, Wuxi, China, [3] Peninsula Cancer Research Center, Binzhou Medical University, Yantai, China, [4] Institute of Health Sciences, Shanghai Institutes for Biological Sciences, Chinese Academy of Sciences, Shanghai, China, [5] Cancer Hospital of Xinjiang Medical University, Urumqi, China

OPEN ACCESS

Edited by:
Yih-Cherng Liou, National University of Singapore, Singapore

Reviewed by:
Roland Piekorz, Heinrich Heine University of Düsseldorf, Germany
Martha Robles-Flores, National Autonomous University of Mexico, Mexico
Shu-Yong Lin, Xiamen University, China

****Correspondence:***
Xiaomei Lu
luxiaomei@xjmu.edu.cn
Yuen Eugene Chin
chinyue@suda.edu.cn

[†]These authors have contributed equally to this work

Specialty section:
This article was submitted to Molecular and Cellular Oncology, a section of the journal Frontiers in Oncology

Received: *22 February 2022*
Accepted: *27 April 2022*
Published: *30 May 2022*

Citation:
Wang Y, Yue J, Xiao M, Lu X and Chin YE (2022) SIRT4-Catalyzed Deacetylation of Axin1 Modulates the Wnt/β-Catenin Signaling Pathway. Front. Oncol. 12:872444. doi: 10.3389/fonc.2022.872444

Axin1 is a fundamental scaffolding protein of the destruction complex in the canonical Wnt signaling pathway, which plays a critical role in various biological processes. However, how Axin1 is regulated in the activation of the canonical Wnt signaling pathway remains elusive. Here, we report that Axin1 is constitutively acetylated in resting cells. Upon stimulation with Wnt, SIRT4 translocates from mitochondria to the cytoplasm and catalyzes Axin1 deacetylation, thus turning off the destruction complex. In this process, Lys147, a residue in the RGS domain of Axin1, plays a key role. We proved that the Axin1-K147R mutant impairs the assembly of β-TrCP to the destruction complex, which leads to β-catenin accumulation even without Wnt stimulation. In summary, our work proposes a new model for better understanding the initial stage of the canonical Wnt signaling pathway in which SIRT4 translocates from mitochondria into the cytoplasm to deacetylate Axin1-K147 after Wnt stimulation, which results in reduced assembly of β-TrCP to the destruction complex.

Keywords: Axin1, SIRT4, deacetylation, β-catenin, Wnt signaling pathway

INTRODUCTION

The Wnt/β-catenin signaling cascade plays a crucial role in regulating many biological processes, especially those involved in cell or organ development. Abnormal Wnt/β-catenin signaling often leads to cell or organ developmental failure or diseases (1–3). In the absence of Wnt ligands, cytosolic β-catenin is maintained at an extremely low level in the cytoplasm by finely regulated continuous synthesis and degradation machinery. β-catenin degradation takes place within a so-called destruction complex, which includes axis inhibition scaffold proteins (Axin1 and Axin2), adenomatous polyposis coli (APC), glycogen synthase kinase-3β (GSK3β), casein kinase-1 (CK-1), protein phosphatase 2A (PP2A) and E3-ubiquitin ligase β-TrCP (4, 5). During the degradation process, cytosolic β-catenin captured by the destruction complex is sequentially phosphorylated by CK-1 and GSK3β in a conserved Ser/Thr-rich sequence near the amino terminus, a process requiring scaffolding of the kinases and β-catenin by Axin (6). Phosphorylated β-catenin can therefore be recognized by β-TrCP and subjected to protein degradation through the ubiquitin–proteasome pathway (7, 8). In the Wnt-on state, Wnt ligands combine their receptor with Frizzled or LRP5/6 to recruit disheveled proteins to the cell membrane, ensuing the dissociation of the

destruction complex and ultimately preventing β-catenin degradation. Subsequently, β-catenin accumulates in the cytoplasm and then translocates into the nucleus. In the nucleus, β-catenin is engaged in TCF/LEF transcription factors to regulate the Wnt signaling pathway (9).

In the canonical Wnt signaling pathway, the main function of Axin1 is to tether most components of the β-catenin destruction complex together (10). At least in frog embryos, it is the least abundant member of all components of the destruction complex (11). Thus, it is supposed that Axin1 is a rate-limiting protein in the destruction complex. When the amount of the rate-limiting protein Axin1 increases to some extent, the degradation of β-catenin mediated by the destruction complex rises greatly (12). In short, a small change in Axin1 is enough to regulate the degradation of β-catenin (13, 14). Therefore, we speculated that in addition to protein quantity, posttranslational modification (PTM) of Axin1 may be important to balance the cellular Wnt signaling response.

Acetylation is a kind of protein posttranslational modification that generally neutralizes the positive charges of lysine residues and regulates protein interactions within a hydrophobic complex (15, 16). PTM changes are usually the first steps of many signaling pathways. We analyzed the PTM of destruction complex components in the early stage of Wnt signaling and found that Axin1 deacetylation is critical for proper Wnt signal transduction. Generally, deacetylation is controlled by histone deacetylases (HDACs). HDACs include classical zinc-dependent HDACs and NAD^+-dependent HDACs, which are also known as silent mating-type information regulator 2 homologs (sirtuins) (17). Sirtuins are highly conserved from bacteria to humans (18). Seven SIRT family members (SIRT1–7) have been identified in mammals. They have diverse subcellular localizations and functions (19). Among them, SIRT4 is a multifunctional protein with enzymatic activities such as deacetylation (20), ADP-ribosyl transfer (21), and lipoamidase (22) activity. Generally, SIRT4 is supposed to be localized in the mitochondria and is involved in regulating metabolism and metabolic homeostasis (23, 24). However, it was recently proved that a small amount of SIRT4 presents in both cytosol and nucleus (25, 26). Interestingly, our preliminary results showed that SIRT4 could translocate from mitochondria to the cytoplasm after Wnt stimulation.

Here, we demonstrated that deacetylation of Axin1 regulates the canonical Wnt/β-catenin signaling pathway. Deacetylation of Axin1 is mediated by SIRT4, which translocates from mitochondria to the cytoplasm in response to Wnt stimulation. We provided strong evidence that SIRT4-mediated deacetylation of Lys147 was one of the crucial reactions in activation of the canonical Wnt signaling pathway, which results in reduced assembly of β-TrCP to the destruction complex. As a consequence, β-TrCP-catalyzed ubiquitination and ubiquitin-proteasome-dependent degradation of β-catenin were significantly inhibited.

RESULTS

Axin1 Is Deacetylated During Wnt Signaling Pathway Activation

Since Axin1 is considered to be a rate-limiting factor of the destruction complex (11), we sought to investigate whether dynamic acetylation of Axin1 occurs in the activation of the Wnt signaling pathway. To obtain enough Axin1 protein from HEK293T cells, a cell line with an intact Wnt signaling cascade and a high level of Wnt autocrine signaling (14), we pooled HEK293T cells from two 15 cm culture dishes. Axin1 was immunoprecipitated and analyzed by western blot with an anti-panacetylated lysine antibody. It was noted that acetylation of Axin1 was removed rapidly after Wnt3a stimulation (**Figure 1A**). We confirmed that deacetylation of Axin1 is widespread in the activation of the Wnt signaling pathway. Axin1 of NTERA-2, a pluripotent human embryonic carcinoma cell with an intact canonical Wnt/β-catenin cascade and a low level of Wnt autocrine signaling, and Axin1 of HCT116, a human colorectal carcinoma cell with a β-catenin mutation, were analyzed. Deacetylation of Axin1 was also observed after Wnt3a stimulation (**Figures 1B, C**).

SIRT4 Translocates to the Cytoplasm to Regulate the Acetylation Levels of Axin1 and Promote β-Catenin Protein Accumulation

We next sought to identify the enzyme that mediates the deacetylation of Axin1 and thus treated cells with the HDAC family inhibitor TSA or the SIRT family inhibitor NAM. It was noted that deacetylation of Axin1 was retarded by the SIRT

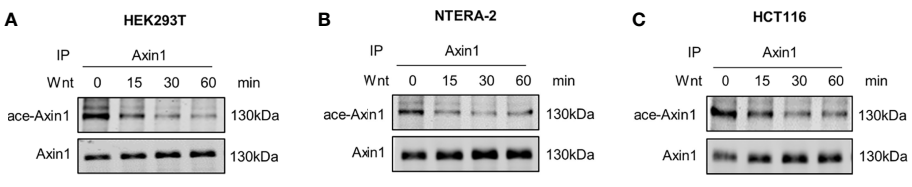

FIGURE 1 | Axin1 is deacetylated during Wnt signaling pathway activation. **(A)** HEK293T (human embryonic kidney 293 cell), **(B)** NTERA-2 (pluripotent human embryonic carcinoma cell), **(C)** HCT116 (human colorectal carcinoma cell) cells were stimulated with Wnt3a-conditioned medium. Cell lysates at the indicated time points were collected and subjected to immunoprecipitation with anti-Axin1 antibody. The precipitated Axin1 protein was then subjected to SDS-PAGE followed by western blot analysis with the indicated antibodies.

family inhibitor NAM but not the HDAC family inhibitor TSA (**Figure 2A**). Therefore, we concluded that SIRT family members have an effect on this deacetylation process. However, it is not clear which SIRT member is responsible for Axin1 deacetylation in Wnt signaling pathway activation. To answer this question, we overexpressed seven members of the SIRT family and investigated their effects on Axin1 acetylation levels. Overexpression of SIRT4 significantly downregulated the acetylation level of Axin1 (**Figure 2B**). On the other hand, by knocking down endogenous SIRT4 with a specific siRNA, we noticed that the acetylation level of Axin1 was obviously upregulated (**Figure 2C**). Importantly, SIRT4 knockdown retarded Wnt3a-induced deacetylation of Axin1 (**Figure 2D**) similar to NAM treatment (**Figure 2A**). In addition, the inactivated mutant SIRT4-H161Y was co-overexpressed with Axin1 to confirm the deacetylation effect of SIRT4 on Axin1, SIRT4-H161Y lost the deacetylation effect on Axin1 compared with SIRT4-WT (**Figure 2E**). Normally, SIRT4 is located in mitochondria (21). To amplify SIRT4's effect on Axin1 deacetylation, we constructed a mitochondrial targeting sequence deletion mutant SIRT4-Δsig, which lost the ability to enter mitochondria. Interestingly, when SIRT4 was retained in the cytoplasm more Axin1 was deacetylated (**Figure 2F**). Finally, we purified both Axin1 and SIRT4 proteins and performed an *in vitro* deacetylation assay. It was shown that SIRT4 could directly catalyze the deacetylation of Axin1 (**Figure 2G**).

Previous studies have found that Axin1 is a core component of the destruction complex, which is located in the cytoplasm, whereas SIRT4 is a protein located in mitochondria (21). We hypothesized that SIRT4 could translocate from mitochondria to the cytoplasm in response to Wnt stimulation. After treatment with Wnt3a-conditioned medium, we isolated the mitochondria and cytoplasm of HEK293T cells and detected SIRT4 protein levels. The results showed that SIRT4 decreased in the mitochondria and increased in the cytoplasm (**Figure 2H**). A small amount of SIRT4 enriched in the cytoplasmic fraction before Wnt stimulation supports the report that a tiny amount of SIRT4 is located in the cytosol (25). To further confirm this, with the help of a SIRT4-GFP fusion protein, we observed distinct separation of green (SIRT4-GFP) and red (MitoTracker) fluorescence, indicating that SIRT4 was translocated from mitochondria to the cytoplasm in a time-dependent manner after Wnt3a stimulation (**Figure 2I**). In addition, we noticed that Wnt treatment increased the interaction between SIRT4 and Axin1 in a time-dependent manner (**Figure 2J**). Taken together, our results confirm that Wnt3a regulates the subcellular localization of SIRT4, which catalyzes the deacetylation of Axin1.

Given that the deacetylation of Axin1 is SIRT4 dependent, we speculated that SIRT4 may affect the activation of the canonical Wnt signaling pathway. Then, we explored the effect of SIRT4 on the Wnt signaling pathway. β-catenin is the key effector responsible for transduction of the Wnt signaling pathway to the nucleus (4). The accumulation of cytoplasmic β-catenin is the key switch in the canonical Wnt pathway (4). To study the effect of SIRT4 on the Wnt signaling pathway, we detected the level of β-catenin. Interestingly, overexpression of SIRT4 upregulated cellular β-catenin protein levels (**Figure 3A**). In contrast, SIRT4 knockout robustly downregulated β-catenin protein levels in MEFs (**Figure 3B**). Furthermore, overexpression of SIRT4 increased Wnt3a stimulation-induced β-catenin accumulation (**Figure 3C**). When cells were transfected with siSIRT4, we found that knockdown of endogenous SIRT4 significantly inhibited Wnt3a-induced β-catenin accumulation (**Figure 3D**). Correspondingly, the transcription of the target genes of canonical Wnt signaling was enhanced by SIRT4 overexpression (**Figure 3E**), while Sirt4 knockout inhibited it (**Figure 3F**). These results indicated that SIRT4 plays an important role in promoting canonical Wnt signaling pathway activation. However, we were not sure whether SIRT4-mediated deacetylation of Axin1 plays a key role in this process.

SIRT4-Regulated Deacetylation of the Axin1-K147 Residue Is Crucial for the Activation of the Wnt/β-Catenin Signaling Pathway

We confirmed that SIRT4-mediated deacetylation of Axin1 is a crucial step in β-catenin accumulation. Human Axin1 was purified and subjected to mass spectrometric analysis, and eight lysine residues with acetylation were detected: Lys53, Lys147, Lys408, Lys513, Lys521, Lys571, Lys790 and Lys791, which are distributed in different domains of Axin1 (**Figure 4A**). Mutants of Axin1 (K53R, K147R, K408R, K513R, K521R, K571R, K790R or K791R), whose lysine at positions 53, 147, 408, 513, 521, 571, 790 or 791 was replaced with arginine to mimic the nonacetylated state of the lysine residue, were prepared. Then, we transfected HEK293T cells with vectors encoding wild-type or mutant Axin1 to determine the effect of the change on the biological function of Axin1. Our results revealed that the K147R Axin1 mutant dramatically increased β-catenin protein levels (**Figure 4B**), implying that Axin1 could not assemble functional destruction complexes if Lys147 could not be acetylated. Next, we constructed another mutant of Lys147 (K147Q). This mutant had a replacement of the lysine at position 147 with glutamine to mimic the acetylated state of the lysine residue. Wild-type Axin1 and the K147Q mutant obviously decreased the β-catenin amount, whereas similar amounts of the K147R mutant lost the property of wild-type Axin1 to some extent (**Figure 4C**). We transfected HEK293T cells with Axin1-WT and Axin1-K147R and then treated them with Wnt3a. Our results showed that in the Axin1-WT group, intracellular β-catenin significantly accumulated after Wnt3a stimulation. While overexpression of Axin1-K147R significantly upregulated β-catenin protein levels compared with Axin1-WT and only slightly upregulated the level of β-catenin protein in the Axin1-K147R group when stimulated by Wnt3a (**Figure 4D**). This result suggested that Axin1-K147R significantly obstructs Wnt-regulated β-catenin accumulation. However, although Axin1-K147R significantly inhibited Wnt-regulated β-catenin accumulation, β-catenin protein was still slightly upregulated. We hypothesized that Wnt may regulate endogenous Axin1 deacetylation and further promote β-catenin accumulation. These data suggested that the acetylation level of the Axin1-K147 residue was involved in the regulation of Axin1 function. In addition, sequence alignment

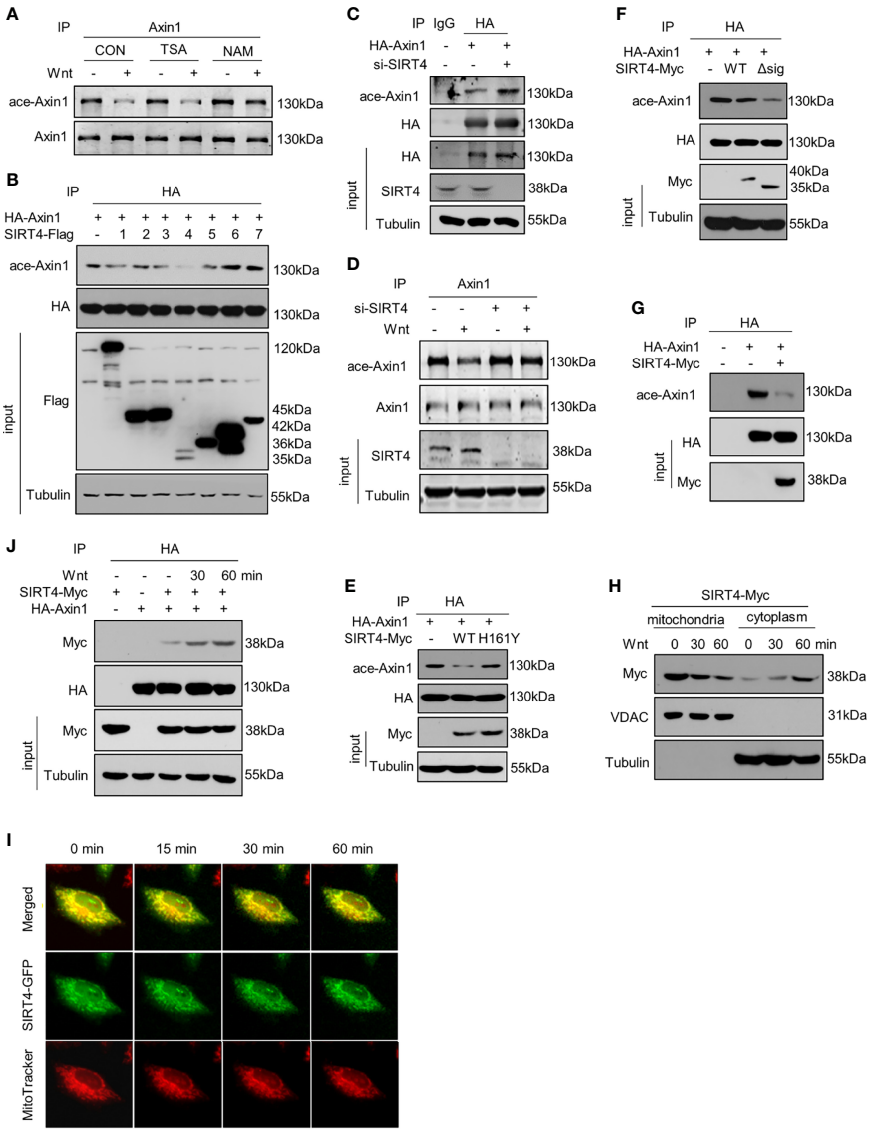

FIGURE 2 | SIRT4 translocates to the cytoplasm and regulates the acetylation levels of Axin1 **(A)** HEK293T cells overexpressing HA-Axin1 were treated with the HDAC inhibitor TSA (2 μM) or SIRT inhibitor NAM (5 mM) for 2 hour, followed by treatment with Wnt3a-conditioned medium for 30 minutes. Stimulated lysates were subjected to immunoprecipitation using an Axin1 antibody and were subjected to SDS-PAGE followed by western blot analysis using the indicated antibodies. **(B)** HA-Axin1 with/without Flag-tagged sirtuins (1-7) were overexpressed in HEK293T cells, HA-Axin1 was immunoprecipitated, and the acetylation levels of Axin1 were analyzed by western blot. Tubulin protein levels were used as loading control. **(C)** HA-Axin1 with/without siSIRT4 RNA were overexpressed in HEK293T cells. HA-Axin1 was immunoprecipitated with anti-HA, and the acetylation levels of Axin1 were analyzed by western blot. Tubulin protein levels were used as loading control. **(D)** Immunoprecipitation analysis of Axin1 acetylation in HEK293T cells transfected with siSIRT4, followed by western blot analysis using the indicated antibodies after Wnt3a-conditioned medium stimulation. Tubulin protein levels were used as loading control. **(E)** HA-Axin1 was coexpressed with SIRT4-Myc or SIRT4-H161Y-Myc in HET293T cells for 48h. HA-Axin1 was immunoprecipitated with anti-HA, and the acetylation levels of Axin1 were analyzed by western blot. Tubulin protein levels were used as loading control. **(F)** HA-Axin1 was coexpressed with SIRT4-Myc or SIRT4-Δsig-Myc in HET293T cells for 48 h. HA-Axin1 was immunoprecipitated with anti-HA, and the acetylation levels of Axin1 were analyzed by western blot. Tubulin protein levels were used as loading control. **(G)** HA-Axin1 and SIRT4-Myc were overexpressed respectively in HET293T cells. The proteins were purified 48 h later, an *in vitro* deacetylation assay was performed and the acetylation levels of Axin1 were analyzed by western blot. **(H)** HEK293T cells transfected with SIRT4-Myc for 48 h were treated with Wnt3a-conditioned medium for indicated times and fractioned into cytoplasmic and mitochondrial fractions. The cell fractions were then analyzed by western blot with the indicated antibodies. VDAC was used as a loading control for mitochondria proteins. Tubulin was used as a loading control for cytoplasm proteins. **(I)** Hela cells were transfected with SIRT4-GFP, and 48 hours later, the cells were stained with MitoTrackerer™ Red CMXRos for 10 min and then treated with Wnt3a-conditioned medium for the indicated time. For the same scope, both green (SIRT4) and red (mitochondria) fluorescence were captured with a Leica Microsystem at the indicated time points after treatment with Wnt3a-conditioned medium. **(J)** HA-Axin1 was coexpressed with or without SIRT4-Myc in HET293T cells for 48 h. Some cells were treated with Wnt3a-conditioned medium as indicated. HA-Axin1 was immunoprecipitated with anti-HA, and the interaction between Axin1 and SIRT4 was detected by western blot.

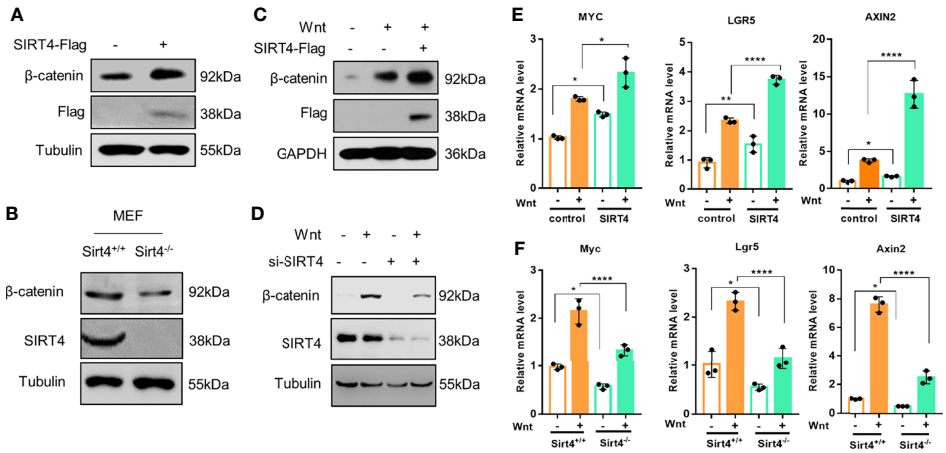

FIGURE 3 | SIRT4 positively regulates the Wnt/β-catenin signaling pathway. **(A)** HEK293T cells were transfected with EV and SIRT4-Flag respectively, the cells were collected and the whole cell lysates were analyzed by western blot with the indicated antibodies. **(B)** Sirt4$^{+/+}$ MEFs and Sirt4$^{-/-}$ MEFs were prepared from WT and Sirt4 knockout mice respectively and maintained in DMEM with 10% FBS. Whole cell lysates were analyzed by western blot with the indicated antibodies. **(C)** HEK293T cells were transfected with EV or SIRT4-Flag, the cells were treated with Wnt3a-conditioned medium for 30 min. The whole cell lysates were analyzed by western blot with the indicated antibodies. **(D)** HEK293T cells were transfected with/without siSIRT4 for 48 h, then the cells were treated with Wnt3a-conditioned medium for 30 min. The whole cell lysates were analyzed by western blot with the indicated antibodies. **(E)** HEK293T cells were transfected with EV and SIRT4-Flag respectively, the cells were treated with Wnt3a-conditioned medium for 3 h. Total RNA was extracted with TRIzol, and the mRNA levels of β-catenin target genes (AXIN2, LGR5 and MYC) were analyzed with RT-qPCR (n = 3; error bars represent ± SD, *p < 0.05, **p < 0.01, ****p < 0.0001; two-way ANOVA with multiple comparisons followed by Bonferroni *post hoc* test). **(F)** Sirt4$^{+/+}$ MEFs and Sirt4$^{-/-}$ MEFs were stimulated with Wnt3a for 3 h. Total RNA was extracted with TRIzol, and the mRNA levels of β-catenin target genes (Axin2, Lgr5 and Myc) were analyzed with RT-qPCR (n = 3; error bars represent ± SD, *p<0.05, **** p < 0.0001; two-way ANOVA with multiple comparisons followed by Bonferroni *post hoc* test).

revealed that Axin1-K147 was a highly conserved residue among different species (**Figure 4A**).

Although Axin1-K147 is a key residue in the regulation of Axin1 function, whether deacetylation of Axin1-K147 is a major contributor to SIRT4-mediated Axin1 deacetylation has still not been confirmed. We then coexpressed SIRT4 and Axin1 in HEK293T cells. The acetylation level of the K147R mutant decreased significantly compared to that of the wild type (**Figure 4E**, lane 1 vs lane 3). While the acetylation level of Axin1-WT was decreased by SIRT4 (**Figure 4E**, lane 1 vs lane 2), the acetylation level of Axin1-K147R was not affected by SIRT4 overexpression (**Figure 4E**, lane 3 vs lane 4), indicating that SIRT4-mediated deacetylation of Axin1 mainly occurred at Lys147. Consistently, while the β-catenin level in the Axin1-WT group was increased significantly by SIRT4, further β-catenin accumulation in the Axin1-K147R group was abolished (**Figure 4E**, panel 4).

Consistently, while Axin1-WT and the Axin1-K147Q mutant decreased the TOP/FOP flash ratio and the transcription levels of β-catenin target genes dramatically, the Axin1-K147R mutant failed to induce such events (**Figures 4F, G**). Taken together, these results implied that SIRT4-mediated deacetylation of the Axin1-K147 residue is a crucial step in the activation of the canonical Wnt/β-catenin signaling pathway.

SIRT4-Catalyzed Deacetylation of Axin1-K147 Reduces the Accessibility of β-TrCP to the Destruction Complex

The results above suggest that SIRT4 promotes β-catenin accumulation by regulating Axin1 acetylation. Next, we further explored the mechanism by which SIRT4 regulates β-catenin protein accumulation. Axin1 is a rate-limiting protein in the destruction complex, and it is commonly thought of as a scaffold that supports the stable presence of the destruction complex. Coimmunoprecipitation (co-IP) with HA-Axin1 showed that most components of the destruction complex were precipitated (**Figure 5A**). Intriguingly, although Lys147 is located in the RGS domain, a domain interacts with the SAMP domain of APC, and Axin1-K147R mutation did not damage the Axin1-APC interaction (**Figure 5B**). However, when the same amount of β-TrCP was immunoprecipitated, the Axin1-K147R mutant significantly reduced its interaction with β-TrCP compared with Axin1-WT (**Figure 5C**). In addition, overexpression of SIRT4 also reduced the interaction between Axin1 and β-TrCP (**Figure 5D**). Consistently, SIRT4 overexpression also decreased the protein level of β-TrCP precipitated with β-catenin (**Figure 5E**). Furthermore, SIRT4 overexpression reduced the interaction between β-TrCP and several components of the destruction complex (β-catenin, Dvl2 and GSK3β) (**Figure 5F**). Taken together, our findings demonstrated that SIRT4-mediated deacetylation of Axin1-K147 would result in reduced assembly of β-TrCP to the destruction complex.

Conventionally, β-TrCP is recruited by phosphorylated β-catenin; however, the Axin1-K147R mutation did not affect the assembly of GSK3β to the destruction complex (**Figure 5A**), and the levels of phosphorylated β-catenin in the destruction complex were not impaired by the K147R mutation (**Figure 5G**). We are not sure how deacetylation of Axin1-K147 can impair the interaction between β-TrCP and phosphorylated β-catenin.

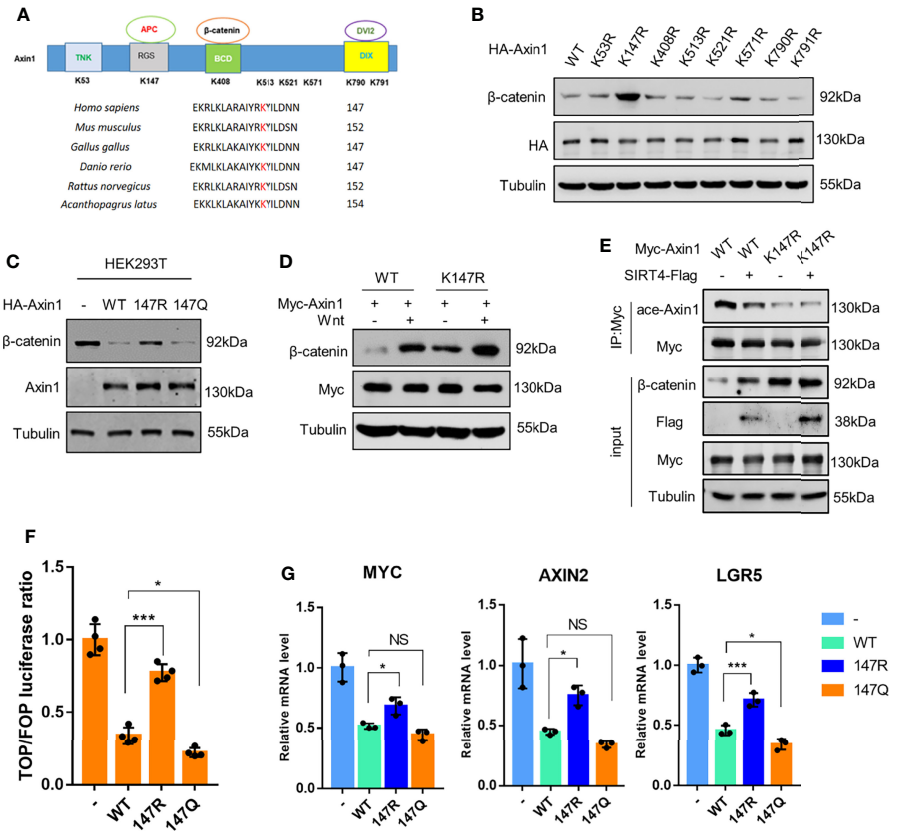

FIGURE 4 | SIRT4-regulated deacetylation of the Axin1-K147 residue is crucial for the activation of the canonical Wnt/β-catenin signaling pathway. **(A)** Mass spectrometry analysis of the potential acetylation sites of Axin1. Multiple sequence alignment among species showed a conserved Lys147 residue in Axin1. **(B)** HA-Axin1 mutants (K53R, K147R, K408R, K513R, K521R, K571R, K790R, K791R) were overexpressed in HEK293T cells respectively, the whole cell lysates were analyzed by western blot with the indicated antibodies. **(C)** HEK293T cells were transfected with HA-Axin1-WT, HA-Axin1-K147R or HA-Axin1-K147Q. The whole cell lysates were analyzed by western blot with the indicated antibodies. **(D)** HEK293T cells were transfected with Myc-Axin1-WT or Myc-Axin1-K147R and then treated with Wnt3a conditioned medium for 30 min. The whole cell lysates were analyzed by western blot with the indicated antibodies. **(E)** HEK293T cells were cotransfected with Myc-Axin1/Myc-Axin1-K147R and SIRT4-Flag as indicated. The whole cell lysates were collected and analyzed by western blot with the indicated antibodies as input, Myc-Axin1 was immunoprecipitated with anti-Myc and the acetylation levels were analyzed by western blot. **(F)** Dual-luciferase reporter assay of TOP/FOP activity in HEK293T cells transfected with HA-Axin1-WT, HA-Axin1-K147R or HA-Axin1-K147Q (n=4; error bars represent ± SD, *p<0.05, ***P<0.0001; ordinary one-way ANOVA with multiple comparisons followed by Holm-Sidak's test). **(G)** HEK293T cells were transfected with HA-Axin1-WT, HA-Axin1-K147R and HA-Axin1-K147Q respectively. Total RNA was extracted with TRIzol and the mRNA levels of β-catenin target genes (AXIN2, LGR5 and MYC) were analyzed with RT-qPCR (n = 3; error bars represent ± SD, *p<0.05, ***p<0.001; n=0.3>0.05 NS, no significant; ordinary one-way ANOVA with multiple comparisons followed by Holm-Sidak's test).

SIRT4 Downregulates the Ubiquitination of β-Catenin

Due to the decreased accessibility of β-TrCP to the destruction complex, we found that the levels of polyubiquitinated β-catenin were changed significantly. Compared to Axin1-WT, the levels of the polyubiquitinated β-catenin were inhibited by the Axin1-K147R mutation, whereas they were robustly increased by the K147Q mutation (**Figure 6A**). In line with our hypothesis, we found that SIRT4 overexpression dramatically inhibited the levels of polyubiquitinated β-catenin (**Figure 6B**).

Therefore, we concluded that SIRT4-mediated Axin1 deacetylation promotes β-catenin accumulation by reducing the levels of polyubiquitinated β-catenin and reducing its degradation speed. We confirmed that the expression of β-catenin was not promoted (**Figure 6C**). When protein translation was inhibited by CHX (cycloheximide), compared to the EV group, we found that the degradation speed of β-catenin was increased significantly because of the overexpression of Axin1-WT, but conversely, no perceptible change was observed when Axin1-K147R was overexpressed (**Figure 6D**). Similarly, SIRT4 overexpression also decreased the degradation speed of β-catenin (**Figure 6E**). In conclusion, SIRT4-mediated deacetylation of Axin1-K147 promotes β-catenin accumulation by reducing the ubiquitin-dependent degradation of β-catenin.

DISCUSSION

The Wnt/β-catenin signaling pathway plays a critical role in maintaining the self-renewal growth of embryonic stem cells and

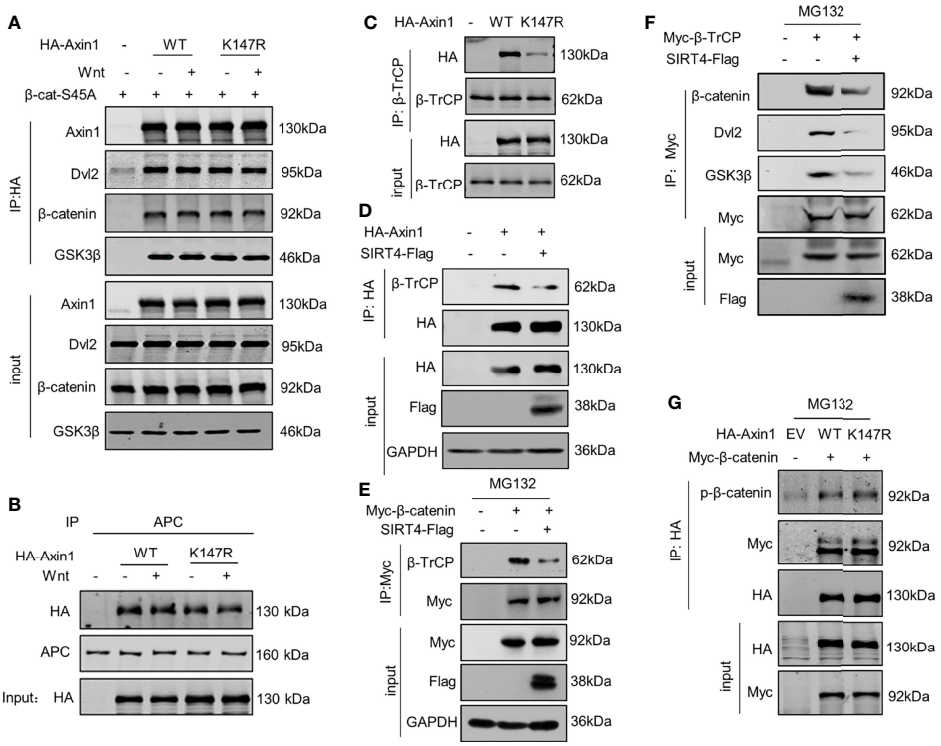

FIGURE 5 | SIRT4-catalyzed deacetylation of Axin1-K147 reduces accessibility of β-TrCP to the destruction complex. **(A)** Both WT and K147R mutant HA-tagged Axin1 were cotransfected with 6×Myc-β-catenin-S45A. Cells were treated with Wnt3a-conditioned medium as indicated for 30 minutes before samples were collected. HA-Axin1 was immunoprecipitated with anti-HA beads. Immunoprecipitated proteins were analyzed by western blotting with the indicated antibodies. **(B)** HA-Axin1-WT or HA-Axin1-K147R were transfected in HEK293T cells as indicated. The cells were treated with Wnt3a-conditioned medium for 30 minutes and then were collected and subjected to coimmunoprecipitation with anti-APC. Axin1 and APC were detected by western blot with anti-HA or anti-APC antibody respectively. **(C)** HEK293T cells were transfected with HA-Axin1-WT/K147R respectively, whole cell lysates were collected, β-TrCP was immunoprecipitated with anti-β-TrCP. Both whole cell lysates and precipitates were analyzed by western blot with the indicated antibodies. **(D)** HEK293T cells were cotransfected with HA-Axin1 and SIRT4-Flag as indicated, whole cell lysates were collected, HA-Axin1 was immunoprecipitated with anti-HA. Both whole cell lysates and precipitates were analyzed by western blot with the indicated antibodies. **(E)** HEK293T cells were cotransfected with Myc-β-catenin and SIRT4-Flag as indicated, and then treated with 10 mM MG132 for 4 h, the whole cell lysates were collected, Myc-β-catenin was immunoprecipitated with anti-Myc. Both whole cell lysates and precipitates were analyzed by western blot with the indicated antibodies. **(F)** HEK293T cells were cotransfected with Myc-β-TrCP and SIRT4-Flag as indicated, and then treated with 10 mM MG132 for 4 h, the whole cell lysates were collected, Myc-β-TrCP was immunoprecipitated with anti-Myc. Both whole cell lysates and precipitates were analyzed by western blot with indicated antibodies. **(G)** HEK293T cells were cotransfected with Myc-β-catenin and HA-Axin1 (WT or K147R) as indicated with treated 10 mM MG132 for 4 h, and then whole cell lysates were collected, HA-Axin1 was immunoprecipitated with anti-HA. Both whole cell lysates and precipitates were analyzed by western blot with indicated antibodies.

the development of various organs (27). In the regulation of the canonical Wnt signaling pathway, several components undergo numerous posttranslational modifications. One of the most well established is the sequential phosphorylation of the N-terminus of β-catenin in the destruction complex, which is required for β-TrCP-mediated ubiquitination (5). Acetylation of the canonical Wnt signaling pathway has also been intensively researched. (28–32). Distinct from the phosphorylation of β-catenin, acetylation of β-catenin occurs and functions outside of the destruction complex. In addition, acetylation of GSK3β, one component of the destruction component, was reported to reduce kinase activity and thus enhance β-catenin accumulation. In contrast, SIRT2-mediated deacetylation of GSK3β increases the phosphorylation level of β-catenin, which results in β-catenin degradation (33). In summary, acetylation of both GSK3β and β-catenin promotes Wnt/β-catenin pathway activation. However, the features of Axin1 acetylation are quite different. Deacetylation of Axin1 occurs in the destruction complex, which is dependent on Wnt stimulation. Even though several sirtuin proteins are involved in the Wnt signaling pathway, SIRT4 seems to be the only member that responds rapidly to Wnt stimulation and accumulates in the cytosol. Our work supports the report that SIRT4 is present within both the cytosol and nucleus (25, 26). However, how SIRT4 translocates from mitochondria to the cytoplasm and interacts with the destruction complex after Wnt stimulation remains elusive. In addition to direct deacetylation, SIRT1 positively regulates the translation of Dishevelled proteins in several cell lines and thus changes the gene expression of classic Wnt/Dvl target genes (34). As the SIRT1 and Dvl complex, it is reasonable to infer that some components of the destruction complex were substrate of SIRT1.

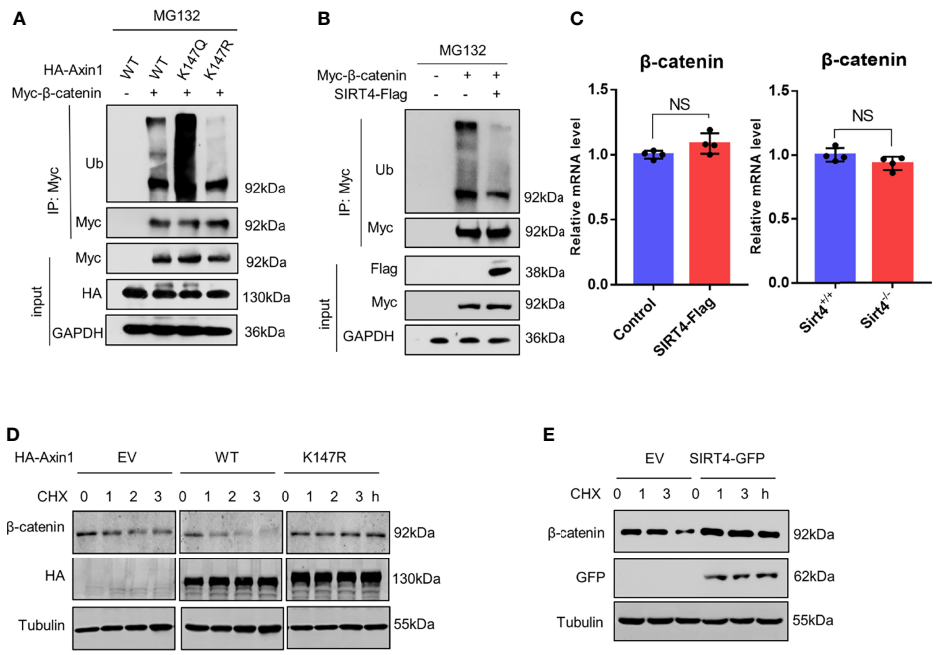

FIGURE 6 | SIRT4 downregulates the ubiquitination of β-catenin. **(A)** HEK293T cells were cotransfected with Myc-β-catenin and HA-Axin1 (WT, K147Q or K147R) as indicated, the cells were treated with 10 mM MG132 for 4 h, and then whole cell lysates were collected, Myc-β-catenin was immunoprecipitated with anti-Myc. Both whole cell lysates and precipitates were analyzed by western blot with the indicated antibodies. **(B)** HEK293T cells were cotransfected with Myc-β-catenin and SIRT4-Flag as indicated, the cells were treated with 10 mM MG132 for 4 h, and then whole cell lysates were collected, Myc-β-catenin was immunoprecipitated with anti-Myc. Both whole cell lysates and precipitates were analyzed by western blot with the indicated antibodies. **(C)** RT–qPCR analysis of the mRNA of β-catenin (CTNNB) in HEK293T cells transfected with SIRT4-Flag. RT–qPCR analysis of the mRNA of β-catenin (CTNNB) in Sirt4$^{+/+}$ MEFs or Sirt4$^{-/-}$ MEFs (n=4, error bars represent ± SD, p=0.08>0.05 in HEK293T cells, p=0.1>0.05 in MEFs cells. NS-not significant, unpaired, two-tailed, parametric t-test were used). **(D)** HEK293T cells were transfected with HA-Axin1 (WT or K147R) as indicated, the cells were treated with 1 μM cycloheximide (CHX) for the indicated times. Whole cell lysates were collected and analyzed by western blot with the indicated antibodies. **(E)** HEK293T cells were transfected with or without SIRT4-GFP as indicated, the cells were treated with 1 μM cycloheximide (CHX) for the indicated times. Whole cell lysates were collected and analyzed by western blot with indicated antibodies.

Several acetylated lysine residues were identified on Axin1, and it is reasonable to speculate that the residue located in a functional domain of Axin1 is crucial for its function. Unexpectedly, when Lys147 was mutated, the Axin1-APC interaction seemed to remain intact; however, the abundance of β-TrCP in the destruction complex was reduced. It was reported that upon Wnt treatment, β-catenin is released from the destruction complex after a while disassociation of the destruction complex and GSK3β sequestration could then occur together with Axin1 degradation, which usually takes hours to be observed (13, 14, 35), whereas deacetylation of Axin1 is an early event within 30 minutes at the initial stage.

MATERIALS AND METHODS

Cell Culture and Transfection

HEK293T, NTERA-2, and HCT116 cells were obtained from the American Type Culture Collection, and L-Wnt3a-producing cells were a kind gift from Pro. Xiaoren Zhang. HEK293T, NTERA-2 and L-Wnt-3a cells were cultured in DMEM (high glucose) (HyClone) supplemented with 10% fetal bovine serum (FBS) (Gemini), 100 units/ml penicillin and 100 μg/ml streptomycin (Sangon Biotech, Shanghai). HCT116 cells were cultured in RPMI-1640 medium (HyClone) supplemented with 10% FBS, 100 units/ml penicillin and 100 μg/ml streptomycin. Cell transfection was carried out with Lipofectamine 2000 transfection reagent following the manufacturer's instructions for Invitrogen (Thermo Fisher Scientific, Waltham, MA). For siRNA transfection, cells were seeded in 6-well plates (1×10^6 cells/well) and incubated for 48 h at 37°C with 5% CO_2. Then the cells were transfected with siRNA using siRNA mate reagent (GenePharma) after reaching 70% confluence.

Plasmid Construct

SIRT4-Flag was cloned into the 5' FLAG-pcDNA 3.0 vector. Human or mouse Axin1 was cloned into 5'FLAG-pCS2. SIRT4-Myc and SIRT4-Δsig-Myc were cloned into the Myc-N1 vector. K53R, K147R, K408R, K513R, K521R, K571R, K790R, K791R and K147Q mutants of Axin1 and H161Y mutant of SIRT4 were generated according to the site-directed mutagenesis protocol of Stratagene, Agilent Technologies Inc. (Santa Clara, CA). Human β-catenin was cloned into a 5'6xmyc-pcDNA 3.0 vector and introduced according to the site-directed mutagenesis protocol. All constructs were confirmed by Sanger sequencing analysis.

Antibodies and Reagents

The following primary antibodies were commercially obtained: anti-acetylated-lysine antibody (Cell Signaling Technology, 9441); anti-SIRT4 antibody (Abcam, ab10140); anti-β-catenin antibody (Cell Signaling Technology, 9562); anti-HA antibody (Santa Cruz, sc-7392); anti-Myc antibody (Santa Cruz, sc-40); anti-Flag antibody (Sigma, F1804); anti-tubulin antibody (Sigma, T619); anti-phospho-S33/37/T41 β-catenin antibody (Cell Signaling Technology, 9561); anti-β-TrCP antibody (Cell Signaling Technology, 4394); anti-β-TrCP antibody (Cell Signaling Technology, 11984) and anti-dishevelled 2 antibody (Abcam, ab228804); anti-GSK3β antibody (Cell Signaling Technology, 12456); anti-APC antibody (Abcam, ab40778). FLAG peptide was purchased from Sigma–Aldrich (St. Louis, MO). Small interfering RNAs (siRNAs) against SIRT family mRNAs were purchased from Santa Cruz Biotechnology, Inc. (SIRT1 siRNA (h), sc-40986, SIRT3 siRNA (h), sc-61555, SIRT4 siRNA (h), sc-63024, SIRT5 siRNA (h), sc-63026, SIRT6 siRNA (h), sc-63028, SIRT7 siRNA (h), sc-63030). Chemicals, including NAM (A2984) and TSA (T1952), were obtained from Sigma. Wnt3a-conditioned medium was derived from stably transfected L-Wnt3a cells.

Luciferase Reporter Assay

HEK293T cells were seeded in 24-well plates and transfected with 5 ng TK-Renilla and 30 ng TOP-flash or FOP-flash reporter constructs. Cells were treated with Wnt3a-conditioned medium for 12 h and lysed with passive lysis buffer. Luciferase activity was measured using a Dual Luciferase Reporter Assay System (Promega Corporation, E1960) according to the manufacturer's instructions.

Immunoprecipitation (IP), Coimmunoprecipitation (co-IP) and Pull-Down Assay

Cells were washed with PBS and collected at 3000 rpm for 5 min at 4°C. For co-IP and IP, cells were lysed with co-IP buffer (50 mM Tris pH 8.0, 0.5% NP-40, 1 mM EDTA, 150 mM NaCl) or RIPA on ice and clarified at 12000 rpm for 10 min at 4°C. The lysate was incubated with primary antibody for 2-4 hours at 4°C, followed by the addition of a 50% slurry of protein A/G magnetic beads (B23202, Bimake) and incubation overnight at 4°C or direct incubation with antibody-conjugated beads overnight at 4°C. Flag-tagged proteins were purified by anti-FLAG M2 affinity gel (A2220, Sigma) following the manufacturer's instructions. A peptide pulldown assay was performed in buffer PD (20 mM HEPES, pH 7.9, 20% v/v glycerol, 0.2 mM EDTA, 0.2% Triton X-100, 2 mM DTT). The western blots were scanned and analyzed on a LI-COR system (Odyssey).

Mass Spectrometry Analysis

Flag-tagged Axin1 was transfected with Lipofectamine 2000 into HEK293T cells, which were cultured in 10-cm Petri dishes. After 48 hours, cells from two dishes were collected to immunoprecipitate Axin1. The immunoprecipitated Axin1 was then separated by SDS–PAGE. Peptides were extracted and analyzed with a Thermo LC–MS/MS system.

RNA Isolation and Quantitative RT–PCR

RNA was extracted from cells with TRIzol reagent (Invitrogen), and cDNA was prepared with a PrimeScript RT Reagent kit (Takara) according to the manufacturer's instructions. Real-time PCR (MYC: GGCTCCTGGCAAAAGGTCA, CTGCGTAGTTGT GCTGATGT, LGR6: AGCCCTGT GAGTACCTCTTTG, CAG CACCAGTCCATTGCAGA, AXIN2: TACACTCCTTATT GGGCGA TCA, TTGGCTACTCGTAAAGTTTTGGT, CTN NB1: CATCTACACAGTTTGATGCTGCT, GCAGTTTT GTCAGTTCAGGGA, Myc: ATGCCCCTCAACGTGAACTTC, CGCAACATAGG ATGGAGAGCA, Lgr6: GAGGACGGCA TCATGCTGTC, GCTCCGTGAGGTTGTTCATACT, Axin2: TGACTCTCCTTCCAGATCCCA, TGCCCACACTAGGC TGACA) was performed with SYBR Green Master Mix (YEASEN) on an ABI QuantStudio (Applied Biosystems). Relative quantitation of gene expression was calculated with the ΔΔCt method.

In Vitro Deacetylation Assay

HA-Axin1 and SIRT4-Myc were overexpressed respectively in HET293T cells. The proteins were purified, and an *in vitro* deacetylation assay was performed as previously described (36).

Cytosolic β-Catenin and Mitochondrial Fraction Preparation

To collect cytosolic proteins from mammalian cells, cells were collected and washed with PBS and incubated in fraction buffer (10 mM KCl, 10 mM Tris pH 7.5, 2 mM EDTA with PMSF and protease inhibitor added) on ice for 30 min. The cells were then stroke 30 times with a 1 mL syringe needle and centrifuged at 12000 rpm for 40 min at 4°C. The supernatant was collected as the cytosolic fraction containing cytosolic β-catenin. Mitochondria were extracted using a Mitochondria Isolation Kit (Sigma) following the manufacturer's protocol. In brief, 2×10^7 cells were pelleted by centrifuging the harvested cell suspension, and then mitochondria isolation reagent was added to the cell pellets. The cell resuspension was centrifuged at 700 × g for 10 min at 4°C, and then the supernatant was transferred to a new 1.5 ml tube and centrifuged at 12,000 × g for 15 min at 4°C. The supernatant (cytosolic fraction) was transferred to a new tube, and the pellet contained the isolated mitochondria. The pellet was further lysed to yield the final mitochondrial lysate. The extracted proteins were prepared for subsequent western blotting analysis.

Statistical Analysis

All data are presented as the means ± SD. For single comparisons, an unpaired two-tailed Student's t tests were used, $p < 0.05$ was considered statistically significant, NS indicate no significant. Statistical significance is indicated by asterisks (* $p < 0.05$, ** $p < 0.01$, *** $p < 0.001$). For multiple groups comparisons, one-way ANOVA Holm-Sidak's test were used and two-way ANOVAs with Bonferroni *post hoc* test for assessing the combination of SIRT4 overexpression/knockout and Wnt treatment. The Statistical analyses were performed using the GraphPad Prism 7.0 and SPSS 23.0 software package.

DATA AVAILABILITY STATEMENT

The original contributions presented in the study are included in the article/**Supplementary Material**. Further inquiries can be directed to the corresponding authors.

AUTHOR CONTRIBUTIONS

The conceptualization and supervision were carried out by YC and XL. The investigation was carried out by YW and MX, and these authors contributed equally. YW and JY provided critical intellectual input for experimental design and prepared the manuscript. All authors contributed to the article and approved the submitted version.

FUNDING

This research was supported by the National Natural Science Foundation of China (Grant Nos. 82030077, 81530083, 81820108023, 31700789) and the National Key Research and Development Project (2016YFC1302402, U1603284, 2018YFC1705505).

ACKNOWLEDGMENTS

We thank Dr. Lin Li (Shanghai Institute of Biochemistry and Cell Biology, CAS) for the gift of Axin1 and Wnt3a plasmids and Dr. Weijun Pan (Shanghai Institute of Biochemistry and Cell Biology, CAS) for technical assistance.

SUPPLEMENTARY MATERIAL

The Supplementary Material for this article can be found online at: https://www.frontiersin.org/articles/10.3389/fonc.2022.872444/full#supplementary-material

REFERENCES

1. Kim SE, Huang H, Zhao M, Zhang X, Zhang A, Semonov MV, et al. Wnt Stabilization of β-Catenin Reveals Principles for Morphogen Receptor-Scaffold Assemblies. *Science* (2013) 340(6134):867–70. doi: 10.1126/science.1232389
2. Voloshanenko O, Erdmann G, Dubash TD, Augustin I, Metzig M, Moffa G, et al. Wnt Secretion is Required to Maintain High Levels of Wnt Activity in Colon Cancer Cells. *Nat Commun* (2013) 4:2610. doi: 10.1038/ncomms3610
3. Mazzoni SM, Fearon ER. AXIN1 and AXIN2 Variants in Gastrointestinal Cancers. *Cancer Lett* (2014) 355(1):1–8. doi: 10.1016/j.canlet.2014.09.018
4. MacDonald BT, Tamai K, He X. Wnt/beta-Catenin Signaling: Components, Mechanisms, and Diseases. *Dev Cell* (2009) 17(1):9–26. doi: 10.1016/j.devcel.2009.06.016
5. Stamos JL, Weis WI. The β-Catenin Destruction Complex. *Cold Spring Harb Perspect Biol* (2013) 5(1):a007898. doi: 10.1101/cshperspect.a007898
6. Zeng X, Tamai K, Doble B, Li S, Huang H, Habas R, et al. A Dual-Kinase Mechanism for Wnt Co-Receptor Phosphorylation and Activation. *Nature* (2005) 438(7069):873–7. doi: 10.1038/nature04185
7. Aberle H, Bauer A, Stappert J, Kispert A, Kemler R. Beta-Catenin is a Target for the Ubiquitin-Proteasome Pathway. *EMBO J* (1997) 16(13):3797–804. doi: 10.1093/emboj/16.13.3797
8. Liu C, Kato Y, Zhang Z, Do VM, Yankner BA, He X. Beta-Trcp Couples Beta-Catenin Phosphorylation-Degradation and Regulates Xenopus Axis Formation. *Proc Natl Acad Sci U.S.A.* (1999) 96(11):6273–8. doi: 10.1073/pnas.96.11.6273
9. Nusse R, Clevers H. Wnt/β-Catenin Signaling, Disease, and Emerging Therapeutic Modalities. *Cell* (2017) 169(6):985–99. doi: 10.1016/j.cell.2017.05.016
10. Liu C, Li Y, Semenov M, Han C, Baeg GH, Tan Y, et al. Control of Beta-Catenin Phosphorylation/Degradation by a Dual-Kinase Mechanism. *Cell* (2002) 108(6):837–47. doi: 10.1016/s0092-8674(02)00685-2
11. Lee E, Salic A, Krüger R, Heinrich R, Kirschner MW. The Roles of APC and Axin Derived From Experimental and Theoretical Analysis of the Wnt Pathway. *PloS Biol* (2003) 1(1):E10. doi: 10.1371/journal.pbio.0000010
12. Dajani R, Fraser E, Roe SM, Yeo M, Good VM, Thompson V, et al. Structural Basis for Recruitment of Glycogen Synthase Kinase 3beta to the Axin-APC Scaffold Complex. *EMBO J* (2003) 22(3):494–501. doi: 10.1093/emboj/cdg068
13. Kim S, Jho EH. The Protein Stability of Axin, a Negative Regulator of Wnt Signaling, is Regulated by Smad Ubiquitination Regulatory Factor 2 (Smurf2). *J Biol Chem* (2010) 285(47):36420–6. doi: 10.1074/jbc.M110.137471
14. Li VS, Ng SS, Boersema PJ, Low TY, Karthaus WR, Gerlach JP, et al. Wnt Signaling Through Inhibition of β-Catenin Degradation in an Intact Axin1 Complex. *Cell* (2012) 149(6):1245–56. doi: 10.1016/j.cell.2012.05.002
15. Struhl K. Histone Acetylation and Transcriptional Regulatory Mechanisms. *Genes Dev* (1998) 12(5):599–606. doi: 10.1101/gad.12.5.599
16. Wang D, Kon N, Lasso G, Jiang L, Leng W, Zhu WG, et al. Acetylation-Regulated Interaction Between P53 and SET Reveals a Widespread Regulatory Mode. *Nature* (2016) 538(7623):118–22. doi: 10.1038/nature19759
17. Shakespear MR, Iyer A, Cheng CY, Das Gupta K, Singhal A, Fairlie DP, et al. Lysine Deacetylases and Regulated Glycolysis in Macrophages. *Trends Immunol* (2018) 39(6):473–88. doi: 10.1016/j.it.2018.02.009
18. Imai S, Guarente L. NAD+ and Sirtuins in Aging and Disease. *Trends Cell Biol* (2014) 24(8):464–71. doi: 10.1016/j.tcb.2014.04.002
19. Seto E, Yoshida M. Erasers of Histone Acetylation: The Histone Deacetylase Enzymes. *Cold Spring Harb Perspect Biol* (2014) 6(4):a018713. doi: 10.1101/cshperspect.a018713
20. Anderson KA, Huynh FK, Fisher-Wellman K, Stuart JD, Peterson BS, Douros JD, et al. SIRT4 Is a Lysine Deacylase That Controls Leucine Metabolism and Insulin Secretion. *Cell Metab* (2017) 25(4):838–55.e15. doi: 10.1016/j.cmet.2017.03.003
21. Haigis MC, Mostoslavsky R, Haigis KM, Fahie K, Christodoulou DC, Murphy AJ, et al. SIRT4 Inhibits Glutamate Dehydrogenase and Opposes the Effects of Calorie Restriction in Pancreatic Beta Cells. *Cell* (2006) 126(5):941–54. doi: 10.1016/j.cell.2006.06.057
22. Mathias RA, Greco TM, Oberstein A, Budayeva HG, Chakrabarti R, Rowland EA, et al. Sirtuin 4 is a Lipoamidase Regulating Pyruvate Dehydrogenase Complex Activity. *Cell* (2014) 159(7):1615–25. doi: 10.1016/j.cell.2014.11.046
23. Pirinen E, Lo Sasso G, Auwerx J. Mitochondrial Sirtuins and Metabolic Homeostasis. *Best Pract Res Clin Endocrinol Metab* (2012) 26(6):759–70. doi: 10.1016/j.beem.2012.05.001
24. van de Ven RAH, Santos D, Haigis MC. Mitochondrial Sirtuins and Molecular Mechanisms of Aging. *Trends Mol Med* (2017) 23(4):320–31. doi: 10.1016/j.molmed.2017.02.005
25. Ramadani-Muja J, Gottschalk B, Pfeil K, Burgstaller S, Rauter T, Bischof H, et al. Visualization of Sirtuin 4 Distribution Between Mitochondria and the Nucleus, Based on Bimolecular Fluorescence Self-Complementation. *Cells* (2019) 8(12):1583. doi: 10.3390/cells8121583
26. Bergmann L, Lang A, Bross C, Altinoluk-Hambüchen S, Fey I, Overbeck N, et al. Subcellular Localization and Mitotic Interactome Analyses Identify SIRT4 as a Centrosomally Localized and Microtubule Associated Protein. *Cells* (2020) 9(9):1950. doi: 10.3390/cells9091950
27. Clevers H. Wnt/beta-Catenin Signaling in Development and Disease. *Cell* (2006) 127(3):469–80. doi: 10.1016/j.cell.2006.10.018
28. Lévy L, Wei Y, Labalette C, Wu Y, Renard CA, Buendia MA, et al. Acetylation of Beta-Catenin by P300 Regulates Beta-Catenin-Tcf4 Interaction. *Mol Cell Biol* (2004) 24(8):3404–14. doi: 10.1128/mcb.24.8.3404-3414.2004

29. Chocarro-Calvo A, García-Martínez JM, Ardila-González S, de la Vieja A, García-Jiménez C. Glucose-Induced β-Catenin Acetylation Enhances Wnt Signaling in Cancer. *Mol Cell* (2013) 49(3):474–86. doi: 10.1016/j.molcel.2012.11.022
30. Hoffmeyer K, Junghans D, Kanzler B, Kemler R. Trimethylation and Acetylation of β-Catenin at Lysine 49 Represent Key Elements in ESC Pluripotency. *Cell Rep* (2017) 18(12):2815–24. doi: 10.1016/j.celrep.2017.02.076
31. Zhang Y, Wang S, Kang W, Liu C, Dong Y, Ren F, et al. CREPT Facilitates Colorectal Cancer Growth Through Inducing Wnt/β-Catenin Pathway by Enhancing P300-Mediated β-Catenin Acetylation. *Oncogene* (2018) 37 (26):3485–500. doi: 10.1038/s41388-018-0161-z
32. Chen X, Wang C, Jiang Y, Wang Q, Tao Y, Zhang H, et al. Bcl-3 Promotes Wnt Signaling by Maintaining the Acetylation of β-Catenin at Lysine 49 in Colorectal Cancer. *Signal Transduct Target Ther* (2020) 5(1):52. doi: 10.1038/s41392-020-0138-6
33. Sarikhani M, Mishra S, Maity S, Kotyada C, Wolfgeher D, Gupta MP, et al. SIRT2 Deacetylase Regulates the Activity of GSK3 Isoforms Independent of Inhibitory Phosphorylation. *Elife* (2018) 7:e32952. doi: 10.7554/eLife.32952
34. Holloway KR, Calhoun TN, Saxena M, Metoyer CF, Kandler EF, Rivera CA, et al. SIRT1 Regulates Dishevelled Proteins and Promotes Transient and Constitutive Wnt Signaling. *Proc Natl Acad Sci USA* (2010) 107(20):9216–21. doi: 10.1073/pnas.0911325107
35. Taelman VF, Dobrowolski R, Plouhinec JL, Fuentealba LC, Vorwald PP, Gumper I, et al. Wnt Signaling Requires Sequestration of Glycogen Synthase Kinase 3 Inside Multivesicular Endosomes. *Cell* (2010) 143(7):1136–48. doi: 10.1016/j.cell.2010.11.034
36. Song HY, Park S-H, Kang H-J, Vassilopoulos A. Deacetylation Assays to Unravel the Interplay Between Sirtuins (SIRT2) and Specific Protein-Substrates. *J Visualized Experiments JoVE* (2016) 108):53563. doi: 10.3791/53563

Conflict of Interest: The authors declare that the research was conducted in the absence of any commercial or financial relationships that could be construed as a potential conflict of interest.

Publisher's Note: All claims expressed in this article are solely those of the authors and do not necessarily represent those of their affiliated organizations, or those of the publisher, the editors and the reviewers. Any product that may be evaluated in this article, or claim that may be made by its manufacturer, is not guaranteed or endorsed by the publisher.

frontiers | Frontiers in Oncology

ORIGINAL RESEARCH
published: 25 July 2022
doi: 10.3389/fonc.2022.927358

Stabilization of CCDC102B by Loss of RACK1 Through the CMA Pathway Promotes Breast Cancer Metastasis *via* Activation of the NF-κB Pathway

Jing Si[1,2,3†], *Rong Guo*[1,2,4†], *Bingqiu Xiu*[1,2], *Weiru Chi*[1,2], *Qi Zhang*[1,2], *Jianjing Hou*[1,2], *Yonghui Su*[1,2], *Jiajian Chen*[1,2], *Jingyan Xue*[1,2], *Zhi-Ming Shao*[1,2], *Jiong Wu*[1,2,5*] *and Yayun Chi*[1,2*]

[1] Department of Breast Surgery, Key Laboratory of Breast Cancer in Shanghai, Fudan University Shanghai Cancer Center, Shanghai, China, [2] Department of Oncology, Fudan University Shanghai Medical College, Shanghai, China, [3] Department of Breast Disease, The First Hospital of Jiaxing and The Affiliated Hospital of Jiaxing University, Jiaxing, China, [4] Department of Breast Surgery, The Third Affiliated Hospital of Kunming Medical University, Yunnan Cancer Hospital, Kunming, China, [5] Collaborative Innovation Center for Cancer Medicine, Shanghai Medical College, Fudan University, Shanghai, China

OPEN ACCESS

Edited by:
Yi Zhang,
First Affiliated Hospital of Zhengzhou University, China

Reviewed by:
Noritaka Yamaguchi,
Chiba University, Japan
Ying Lin,
Sun Yat-Sen University, China

***Correspondence:**
Yayun Chi
yychi@126.com
Jiong Wu
wujiong1122@vip.sina.com

†These authors have contributed equally to this work

Specialty section:
This article was submitted to Molecular and Cellular Oncology, a section of the journal Frontiers in Oncology

Received: 24 April 2022
Accepted: 20 June 2022
Published: 25 July 2022

Citation:
Si J, Guo R, Xiu B, Chi W, Zhang Q, Hou J, Su Y, Chen J, Xue J, Shao Z-M, Wu J and Chi Y (2022) Stabilization of CCDC102B by Loss of RACK1 Through the CMA Pathway Promotes Breast Cancer Metastasis via Activation of the NF-κB Pathway. Front. Oncol. 12:927358. doi: 10.3389/fonc.2022.927358

Background: Breast cancer is one of the leading causes of cancer-related death among women, and the pathological status of axillary lymph nodes is an important predictor of prognosis. However, the mechanism involved in this early stage of metastasis remains largely unknown.

Methods: Microarray analysis was used to carry out differential genomics analyses between matched pairs of metastatic sentinel lymph node tissues and breast primary tumors. The CRISPR/Cas9 gene editing system was used for *in vivo* screening by transplanting a loss-of-function cell pool into immunocompromised mice. MAGeCK was used to analyze the screening results. Survival analysis was performed *via* the Kaplan–Meier method. Cell proliferation, wound healing, migration and invasion assays were performed to confirm the phenotype. A tail vein model and subcutaneous xenotransplanted tumor model were used for the *in vivo* study. The relationship between coiled-coil domain containing 102B (CCDC102B) and receptor for activated C kinase 1 (RACK1) was examined using coimmunoprecipitation, mass spectrometry, nuclear protein extraction and immunofluorescence assays. The primary biological functions and pathways related to CCDC102B were enriched by RNA sequencing.

Results: We identified CCDC102B through screening and found that it was significantly upregulated in metastatic lesions in lymph nodes compared to matched primary tumors. Increased expression of CCDC102B promoted breast cancer metastasis *in vitro* and *in vivo*. Additionally, high expression of CCDC102B was correlated with poor clinical outcomes in breast cancer patients. We further identified that CCDC102B was stabilized by the loss of RACK1, a protein negatively correlated with breast cancer metastasis. Mechanistically, we found that RACK1 promoted CCDC102B lysosomal

degradation by mediating chaperone-mediated autophagy (CMA). The aggressive behavior of CCDC102B in breast cancer cells could be reversed by the expression of RACK1. Moreover, CCDC102B was correlated with the significant enrichment of NF-κB pathway components. Overexpressing CCDC102B led to less interaction between RACK1 and IKKa. Thus, CCDC102B positively regulates the NF–κB pathway by interacting with RACK1.

Conclusion: Taken together, our findings uncover a novel role of CCDC102B in breast cancer metastasis. CCDC102B serves as a potential metastasis promoter by regulating the activation of the NF-κB pathway and can be degraded by RACK1 *via* CMA.

Keywords: breast cancer, CRISPR/Cas9, CCDC102B, RACK1, chaperone-mediated autophagy, NF-κB pathway

INTRODUCTION

Breast cancer is one of the most common malignant diseases and the leading global cause of cancer-related deaths among women (1–3). With the progress of precision medicine, the overall survival of breast cancer patients has improved in recent years, but metastasis is still the leading cause of treatment failure and mortality (4, 5). Thus, it is important to understand the mechanisms underlying the metastatic process and find effective therapeutic targets. For breast cancer patients, the pathological status of axillary lymph nodes (LNs) is one of the most important predictors of prognosis (6, 7). Theoretically speaking, metastasis to the sentinel lymph nodes (SLNs) is the earliest stage of all kinds of metastasis. However, the mechanism involved in this early stage of metastasis remains largely unknown. Fortunately, the application of sentinel lymph node biopsy (SLNB) has provided us with an opportunity to study the mechanism of early-stage LN metastasis in breast cancer. Thus, novel metastasis-promoting genes may be identified by comparing the genetic changes between SLN metastasis tissues and primary tumor tissues.

The clustered regularly interspaced short palindromic repeats (CRISPR)-associated (Cas) protein 9 system, first discovered in bacteria as part of an adaptive immune system, is now a powerful genome editing technology that has been extensively applied in various cell types and organisms (8, 9). The CRISPR/Cas9 system includes a nonspecific Cas9 nuclease and a set of programmable sequence-specific CRISPR RNAs, which can guide Cas9 to cleave DNA and generate double-strand breaks at target sites (10, 11). Thus, the specificity of CRISPR/Cas9-mediated DNA cleavage requires target sequences matching CRISPR RNA. Recent advances in the CRISPR/Cas9 system enable the acceleration of cancer research by providing an efficient technology to dissect the mechanisms of tumorigenesis and identify targets for drug development, providing great promise for the treatment of cancer (8, 9, 12).

Coiled-coil domains, mostly composed of approximately 200 amino acids, are structural motifs that have been widely identified in proteins distributed in living creatures (13). Due to the specific coiled-coil structure, these proteins adopt different spatial confirmations to regulate a series of biological functions. Previous studies have indicated that coiled-coil domain containing (CCDC) proteins play important roles in tumorigenesis and progression through regulating intracellular signal transduction, the transcription of genetic information, the cell cycle, differentiation, apoptosis, etc. (14–18). Recently, increasing evidence has confirmed that CCDC proteins are associated with cancer metastasis (19–22). CCDC102B was first identified as an age-correlated DNA methylation marker for forensic use (23–25). With further research, CCDC102B was identified as a new centrosome linker protein that is required for maintaining centrosome cohesion and was found to be associated with the development of myopic maculopathy (26, 27). However, few studies have focused on the function and mechanism of CCDC102B in the development and metastasis of breast cancer, especially in the early stage of the transition from primary cancer to metastatic tumors.

The ubiquitin–proteasome system and autophagy–lysosome system are two main pathways for protein degradation in eukaryotes (28, 29). In general, the ubiquitin–proteasome system targets short-lived proteins for proteasome-mediated degradation through polyubiquitination (29). In contrast, the autophagy–lysosome system targets long-lived proteins and organelles for degradation in lysosomes (28). There are three types of autophagy involved in lysosomal degradation: macroautophagy, microautophagy, and chaperone-mediated autophagy (CMA) (28). Distinct from other autophagy types, the CMA pathway is the lysosomal degradation process in which substrates are selectively recognized by a cytosolic chaperone in the presence of a consensus pentapeptide called the Lys-Phe-Glu-Arg-Gln (KFERQ)-like motif (30). Substrates containing KFERQ-like motifs are recognized by HSPA8 and then bind to LAMP2A, a CMA receptor that mediates the translocation of substrate in the lysosomal lumen for degradation (28, 30–34).

In this study, we identified CCDC102B *via* CRISPR/Cas9 screening *in vivo* and found that it was significantly upregulated in metastatic LNs compared with primary tumors, which led to a poor prognosis in breast cancer patients. Overexpression of CCDC102B could promote breast cancer metastasis *in vitro* and *in vivo*. Mechanistically, receptor for activated C kinase 1 (RACK1), which was negatively correlated with breast cancer prognosis, bound to the third coiled-coil structure of CCDC102B, which includes two putative KFERQ-like motifs, and participated in the lysosomal degradation of CCDC102B through CMA. Furthermore, we found that CCDC102B could

activate the NF−κB pathway by interacting with RACK1. Taken together, our findings demonstrate that CCDC102B plays a crucial role in promoting early-stage breast cancer metastasis and could serve as a novel predictor of clinical outcomes in breast cancer patients and a potential therapeutic target for mitigating breast cancer metastasis.

MATERIALS AND METHODS

Cell Lines and Cell Culture

The MDA-MB-231, BT549 and HEK293T cell lines were purchased from the American Type Culture Collection (ATCC) (Manassas, VA, USA) and cultured according to ATCC instructions. The MDA-MB-231 BO cell line is a subline of MDA-MB-231 with a high osteolytic metastasis tendency and was a generous gift from Dr. Toshiyuki Yoneda (The University of Texas, USA) (35, 36). The MDA-MB-231 LM2 cell line is a subline of MDA-MB-231 cells with a high lung metastasis tendency, which was described previously (37). All cell lines were cultured in DMEM containing 10% FBS (Life Technologies), 100 U/ml penicillin and 100 μg/ml streptomycin (Invitrogen) at 37°C in a humidified incubator with 5% CO2. All cell lines were genotyped (Genewiz) and routinely tested for Mycoplasma contamination (Vazyme).

Tissue Samples and Microarray Analysis

Five pairs of primary tumors and SLN macrometastatic loci were collected and confirmed by hematoxylin and eosin (H&E) staining at Fudan University Shanghai Cancer Center. Patients were preoperatively diagnosed with invasive ductal carcinoma (IDC) with clinically negative nodal status. The negative status of non-SLNs and a tumor cell percentage of over 70% in metastatic SLN loci were pathologically confirmed. All protocols were reviewed and approved by an independent institutional review board at Fudan University. All patients gave their written informed consent before inclusion in this study.

Primary tumor lesions and SLN macrometastatic loci were subjected to RNA extraction with TRIzol reagent. Paired samples were analyzed by Shanghai Qiming Biotechnology Co. Ltd. with Affymetrix GeneChip Human Transcriptome Array 2.0.

RNA Isolation, RT–PCR and RT–qPCR

Total RNA was extracted from cells or tissues using TRIzol reagent (Thermo Fisher Scientific) according to the manufacturer's protocol with DNase treatment. Subsequently, RNA was reverse transcribed into cDNA using oligo (dT) primers and a reverse transcription system according to the protocol of the RevertAid First Strand cDNA Synthesis Kit (Thermo Fisher Scientific). The single-stranded cDNA was amplified by PCR and overlap PCR using primers in **Supplementary Table 1**.

For RT–qPCR, RNA was reverse transcribed with the PrimeScript RT Reagent Kit (TaKaRa Biotechnology). Real-time PCR was performed with SYBR Premix Ex Taq (TaKaRa Biotechnology) using an ABI Prism 7900 instrument (Applied Biosystems). The relative expression of genes was quantified to ACTB (beta-actin) mRNA. Relative gene expression was calculated with the $2^{-\Delta\Delta CT}$ method (38). The primer sequences used in this study are shown in **Supplementary Table 1**.

CRISPR/Cas9 Knockout Pooled Library Cloning

DNA oligonucleotide library synthesis was performed on a microarray as previously described (39). The 1091 unique oligonucleotide sequences targeting 182 genes in our study were from the GeCKO library (**Supplementary Table 2**). Additionally, 409 nontargeted sequences were included as controls (**Supplementary Table 2**). A total of 1500 oligonucleotides with full lengths of 74 nt were amplified by PCR using Q5® High-Fidelity DNA Polymerase (NEB) and purified on a 2% agarose E-Gel EX (Life Technologies) using the Wizard SV Gel and PCR Clean-up System (Promega). The lentiGuide-Puro vector (Addgene #52963) was digested with BsmBI (NEB) at 55°C for 2 hours and gel-purified on a 1% agarose E-Gel EX (Life Technologies) using a Wizard SV Gel and PCR Clean-up System (Promega). The Gibson ligation reaction (NEB) was performed using 10 ng of inserts and 25 ng of vector at 50°C for 30 min. From the ligation, 2 μl of the reaction was transformed into 50 μl of *E. coli* DH5α Electro-Cells (TaKaRa Biotechnology) according to the manufacturer's protocol using a GenePulser (BioRad). To ensure representation, 8 parallel transformations were performed using the same ligation reaction and plated onto 245 mm×245 mm plates (Corning) with ampicillin (100 μg/ml) for selection, which yielded 300× library coverage with over 450,000 colonies. Plasmid DNA was extracted using the EndoFree Maxi Plasmid Kit (TIANGEN) after scraping the colonies off the plates.

Lentivirus Packaging and Infection

The open reading frames (ORFs) of CCDC102B and RACK1 were all cloned from MDA-MB-231 cDNA and inserted into pCDH-CMV-Puro with or without a C-terminus 3×FLAG tag and pcDNA3.1-myc vector, respectively. The sgRNA oligos of CCDC102B and RACK1 were annealed and cloned into lentiGuide-Puro using BsmBI (**Supplementary Table 3**). Lentivirus was produced by cotransfecting HEK293T cells with specific plasmids together with psPAX2 and pMD2G. After 72 hours, viral supernatants were collected, filtered, and concentrated by ultracentrifugation. Lentivirus infected cells with the addition of polybrene (Sigma–Aldrich) at a working concentration of 8 μg/ml. Cells were incubated with lentivirus for 12 hours before changing the medium to FBS containing DMEM. For knockout, cells were transfected with lentiCas9-Blast (Addgene #52962) and lentiGuide-Puro. Infected cells were selected with puromycin (Sigma–Aldrich) at 2 μg/ml or blasticidin (Sigma–Aldrich) at 5 μg/ml for 1 week. For knockout cells, single colonies were found by seeding cells in 96-well plates at a very low density and confirmed by western blot.

Cell Transduction by CRISPR/Cas9 Pooled Library

MDA-MB-231 BO-Cas9 cells were transduced with a CRISPR/Cas9 knockout pooled library *via* spinfection. To find the optimal volume of virus to achieve a multiplicity of infection (MOI) of 0.3, tests were performed by spinfecting 3.5×10^5 cells with different volumes of virus. In detail, 3.5×10^5 cells per well were plated into a 24-well plate with polybrene at a working concentration of 8 μg/ml, and each well received different amounts of virus; a control group without transduction was also included (**Supplementary Table 4**). The 24-well plate was centrifuged at 2000 g for 2 hours at 37°C. After spinning, the media was changed to standard media without polybrene. The cells were incubated for 24 hours and trypsinized using trypsin (Corning). The cells in each well were divided equally into four wells, and three of them underwent puromycin selection. As soon as the cells were all dead in the control wells without transduction, the cells were counted to calculate the efficiency of transduction, which was defined as the cell count in wells with puromycin selection divided by the cell count in wells with no puromycin multiplied by 100 (**Supplementary Table 4**). Finally, the volume of virus yielding an MOI closest to 0.3 (80 μl) was selected. Large-scale cell transduction was conducted in the same way with 80 μl of virus per well, and cells were pooled together into large flasks for puromycin selection and further research.

Animal Studies

For CRISPR/Cas9 screening *in vivo*, 2×10^6 MDA-MB-231 BO-Cas9 or MDA-MB-231 BO-Cas9 lentiGuide-CRISPR cells in 100 μl of sterile PBS were injected into BALB/c nude mice (6-8 weeks old) *via* the tail vein. Bioluminescence imaging was carried out by an IVIS-200 system (Xenogen) with intraperitoneal injection of 150 mg/kg D-Luciferin in each mouse 8 weeks after injection to monitor metastasis in the lungs. Lungs were fixed in polyformaldehyde for paraffin embedding.

To create a subcutaneous xenotransplanted tumor model for CCDC102B research, 2×10^6 MDA-MB-231 LM2 pCDH-3×FLAG or MDA-MB-231 LM2 pCDH-3×FLAG-CCDC102B cells in 100 μl of sterile PBS were injected subcutaneously into fat pats of nude mice. Tumor progression was monitored by measuring the diameter of the tumor every 3 days. The xenografts were fixed in polyformaldehyde for paraffin embedding. To investigate tumor metastasis, 1×10^6 MDA-MB-231 LM2 pCDH-3×FLAG or MDA-MB-231 LM2 pCDH-3×FLAG-CCDC102B cells were injected intravenously. Tumor metastasis to the lungs was monitored by bioluminescence imaging. The lungs were fixed in polyformaldehyde for paraffin embedding.

BALB/c nude mice were housed under specific-pathogen-free (SPF) conditions at the animal care facility of Shanghai Laboratory Animal Center (SLAC). All animal procedures were conducted in compliance with relevant institutional and national guidelines and regulations of Shanghai Medical Experimental Animal Care Commission.

Deep Sequencing Processing

To confirm the plasmid DNA of the CRISPR/Cas9 knockout pooled library, deep sequencing was performed as described (39). Agencourt AMPure XP Bead Clean-Up (NEB) was used for DNA purification after each PCR step using High-Fidelity 2X PCR Master Mix (NEB). Amplicons from the second PCR were attached to Illumina adaptors and barcodes and sequenced using a HiSeq 3000 (Illumina). Primer sequences to amplify sgRNAs in each step are shown in **Supplementary Table 1**.

Genomic DNA from metastatic lungs and MDA-MB-231 BO-Cas9 lentiGuide-CRISPR cells before animal injection was harvested using the DNeasy Blood & Tissue Kit (Qiagen) according to the manufacturer's protocol. The amount of genomic DNA of human transduced cells in mouse metastatic lungs was calculated as previously described (40). Two steps of PCR and DNA purification were performed as described above. To achieve 300× coverage over the library, the amount of input genomic DNA in each sample was calculated for the first PCR as described (39). Amplified sgRNA target sites were subjected to high-throughput genomic DNA sequencing using a HiSeq 3000 (Illumina). Primer sequences for the human-specific standard curve are shown in **Supplementary Table 1**.

All sequencing datasets were evaluated using FastQC (version 0.11.2) to ensure high quality. We mapped the reads to the reference genomic sequence and analyzed these datasets using MAGeCK analysis (41).

RNA-Seq Analysis and Gene Set Enrichment Analysis (GSEA)

MDA-MB-231 cells were transduced with control or CCDC102B, and total RNA was extracted using TRIzol reagent. For RNA-Seq analysis of cell lines (CCDC102B overexpressing versus control), the raw sequencing reads were aligned to the human reference genome (release version hg19) using TopHat. Gene expression levels were calculated according to the fragments per kilobase of transcript per million mapped reads (FPKM) values. GSEA was used to identify pathways enriched among differentially expressed genes.

Study Population

Patients with invasive ductal breast cancer who were diagnosed and operated on between January 2008 and December 2009 in Fudan University Shanghai Cancer Center (FUSCC) with no neoadjuvant therapy were included. Paraffin-embedded tissues and clinical data for these patients were collected. A total of 212 patients were included with a median follow-up of 74.5 months. Diagnosis was verified by two independent pathologists in the Department of Pathology of FUSCC. Postoperative therapy was suggested according to guidelines. This study was approved by the Ethics Committee of FUSCC, and all participants signed informed consent documents.

Tissue Microarrays (TMAs) and IHC Staining

TMAs were constructed from paraffin-embedded breast cancer samples obtained from the breast cancer patients described above. Tissue cylinders 2 mm in diameter were punched from marked tumor areas in each sample and inserted into a recipient paraffin wax block. Each sample was punched twice into the microarray to compare staining patterns in different areas of the same tumor in the same patient. Paraffin-embedded 4-mm-thick slides of TMAs were made and stained with 1:200 CCDC102B antibody (Abcam) using standard immunohistochemistry (IHC) protocols. Scores were calculated by multiplying the percentage of cells (scale: 0–3) and the intensity of protein expression (scale: 0–3). Procedures were conducted by experienced pathologists. IHC scores were verified by two independent researchers. All protocols were reviewed and approved by the review board at Fudan University. Informed consent was obtained from all patients. In addition, paraffin-embedded samples of xenotransplanted tumors and metastatic lungs were sliced and stained with 1:200 CCDC102B antibody (Abcam).

Western Blot Analysis

Total cell lysates were extracted, and western blot analysis was conducted according to standard procedures. Briefly, protein lysates from cultured cells were harvested with RIPA buffer containing proteinase and phosphatase inhibitors. Samples were resolved by SDS–PAGE and transferred to PVDF membranes (Millipore). The membranes were blocked in 5% skim milk or 5% BSA and incubated with primary antibodies and then HRP-conjugated secondary antibodies. The antibodies used in this study are listed in **Supplementary Table 5**.

Cell Proliferation, Wound Healing and Transwell Assays

Cell proliferation, wound healing and Transwell assays were performed as previously described (42). Cell proliferation and wound healing were imaged by an IncuCyte ZOOM System (Essen Bioscience). For the Transwell assay, cells were incubated at 37°C for different times according to their migration ability. The images of three random fields of migrated cells were analyzed by ImageJ. All experiments were conducted in triplicate.

Coimmunoprecipitation (Co-IP) and Mass Spectrometry

Lentivirus-infected cells with a 3×FLAG tag were collected, and IP lysis buffer (Thermo) with protease inhibitor cocktail (Thermo) was added. Cell lysates were put on ice for 30 min followed by centrifugation at 12000 rpm for 15 min at 4°C. Meanwhile, magnetic beads (Sigma) were washed with PBS and blocked in 5% BSA for 1 hour at 4°C. The beads were washed again 3 times with IP lysis buffer. After spinning the cell lysates, a 5% volume of supernatant was saved as input, and the rest of the supernatant was added to beads for incubation overnight at 4°C. The next day, the beads were washed 6 times with IP lysis buffer. Proteins were eluted by 0.1 M glycine-hydrochloride solution and boiled with 1x SDS loading buffer as well as input. Samples were subjected to western blotting and resolved with SDS–PAGE. The protein gel was fixed with glacial acetic acid as a fixing solution and silver stained with a Fast Silver Stain Kit (Beyotime) according to the manufacturer's protocol. Differential bands of different lentivirus-infected cells were cut and analyzed by LC–MS/MS (Shanghai Applied Protein Technology, Shanghai, China). MS spectra were searched using MASCOT version 2.4.01 (Matrix Science, London, UK) against the RefSeq human protein database (National Center for Biotechnology Information). For the IP experiment, western blotting was used with standard protocols to test the immunoprecipitated proteins.

Immunofluorescence

MDA-MB-231 cell lines grown on coverslips were fixed with 4% paraformaldehyde for 30 min at room temperature, permeabilized with 0.2% Triton X-100 for 10 min at room temperature, blocked in 1% BSA for 1 hour at room temperature and incubated with primary antibodies overnight at 4°C. The slides were then incubated with Alexa 555–conjugated or Alexa 488–conjugated secondary antibodies (Cell Signaling Technology) for 2 hours at room temperature. DNA staining was performed using Fluoroshield Mounting Medium with DAPI (Abcam). Images were captured with a Leica SP5 confocal laser microscope (Leica Microsystems, Buffalo Grove, USA).

Statistical Analysis

Statistical analyses were performed using SPSS version 23.0 and Prism GraphPad 8.0. T tests were used to calculate the P values for most of the experiments. Survival curves were plotted using the Kaplan–Meier method and were compared using log-rank tests. The experiments were repeated three times independently with similar results obtained, and the results of a representative experiment are shown in the tables or figures.

RESULTS

CRISPR Screening *In Vivo* Identified CCDC102B as a Candidate Metastasis Promoter in Breast Cancer

Gene microarray and comparative genomics analyses were used to define the differentially expressed genes between metastatic SLNs and matched primary tumors in breast cancer patients (**Supplementary Table 1A**, **Supplementary Figures 1A–C**). To identify candidate functional metastasis promoters in breast cancer, we chose genes that were 1.5-fold upregulated in metastatic SLNs compared with matched primary tumors and performed a CRISPR/Cas9-based knockout screen in MDA-MB-231 BO cells. We infected MDA-MB-231 BO cells with the CRISPR/Cas9 knockout pooled library of 2000 single-guide RNAs (sgRNAs) targeting 182 genes and injected 2×10^6 transduced cells into the tail vein of immunocompromised BALB/c nude mice (**Figure 1A**). After 8 weeks, 75% (n=4) of

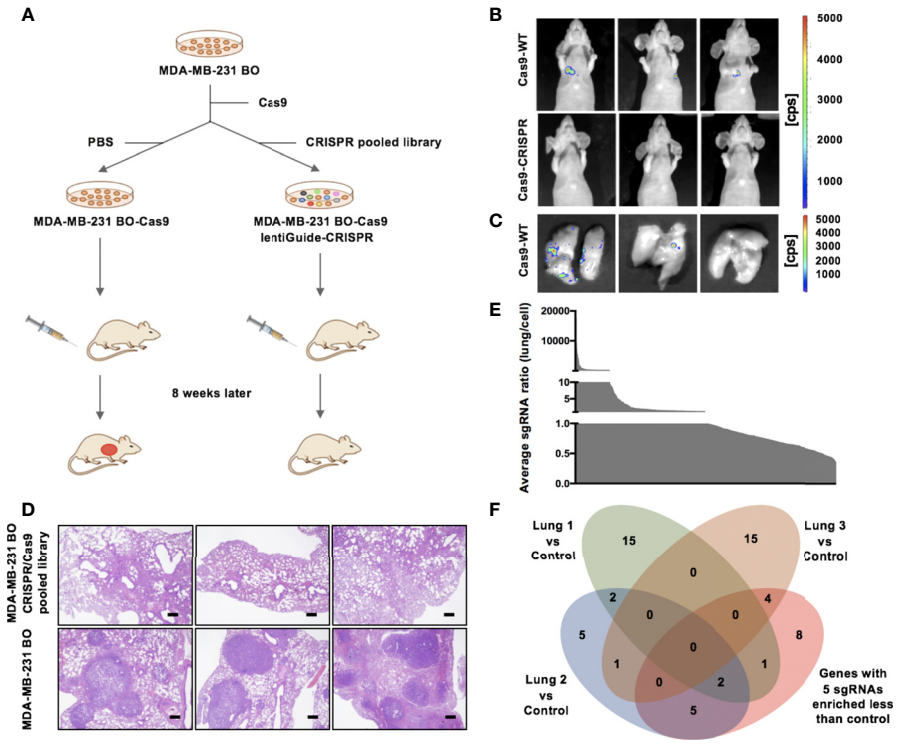

FIGURE 1 | CRISPR/Cas9 screening identifies CCDC102B as a metastasis promoter. **(A)** Outline of the CRISPR/Cas9 screening strategy. **(B)** BLI of three representative mice in each group 8 weeks after injection with transduced cells. (n=6 of each group) **(C)** BLI of three representative lungs in control group mice with metastasis. (n=6 of each group) **(D)** Representative images of H&E staining of lung metastasis in each group 8 weeks after injection with transduced cells. Scale bars: 500 μm. (n=6 of each group) **(E)** Average ratio of all individual sgRNAs in lungs versus cell pool. **(F)** Venn diagram of candidate breast cancer metastasis promoter selection.

mice that received the control cells had lung metastasis, whereas only one out of six mice that received the sgRNA library showed metastasis (**Figures 1B–D**).

To identify candidate sgRNAs that drive breast cancer metastasis, we used high-throughput sequencing and MAGeCK analysis to assess the representation of sgRNAs in three lungs that received the sgRNA library and the preinjected cells with the CRISPR pooled library (**Supplementary Table 1B**, **Supplementary Figures 1D–F**). The average ratio of all individual sgRNAs in the lungs versus the cell pool was measured (**Figure 1E**). Although the sgRNA library consisted of ~6 sgRNAs per gene, no experimental group showed greater enrichment of all 6 sgRNAs than the control group. We listed all 20 targets for which 5 sgRNAs were more enriched in the control group than the experimental groups (**Supplementary Table 1C**). Additionally, we listed the top 20 genes that were the least enriched in metastatic lungs compared to the initial cell pool according to MAGeCK analysis (**Supplementary Table 1D**). We merged the results of these lists (**Figure 1F** and **Supplementary Table 1E**), which revealed genes not only targeting known tumor promoters (e.g., JAK3 and SELL) and tumor promoters with demonstrated roles in other tissues (e.g., CD27, PROX1 and PSIP1) but also genes not previously described as tumor promoters (e.g., CCDC102B and C16orf54). These results showed that our approach was suited to identifying metastasis promoters in breast cancer. We identified CCDC102B, newly described as a tumor-related gene, as a candidate metastasis promoter in breast cancer.

Increased Expression of CCDC102B Correlates With Poor Clinical Outcomes in Breast Cancer

To validate the increase in CCDC102B in LN metastatic loci, we analyzed its expression by qRT–PCR in breast cancer patients with LN metastasis (n=20). CCDC102B expression was significantly increased in LN metastatic loci compared with primary tumors (P=0.011, **Figure 2A**). Further examination of the expression of CCDC102B by western blot analysis of primary tumors and corresponding metastatic LNs (n=5) showed that CCDC102B expression was significantly higher in metastatic LNs than in primary tumors (**Figure 2B**). To explore the role of CCDC102B in breast cancer, we examined the expression of CCDC102B in 212 breast tumor samples and analyzed the correlation between CCDC102B expression and the clinicopathological characteristics of breast cancer patients (**Supplementary Table 2A**). IHC staining of a TMA confirmed that CCDC102B was expressed in breast tumor tissues (**Figure 2C**), and semiquantitative scoring revealed that the

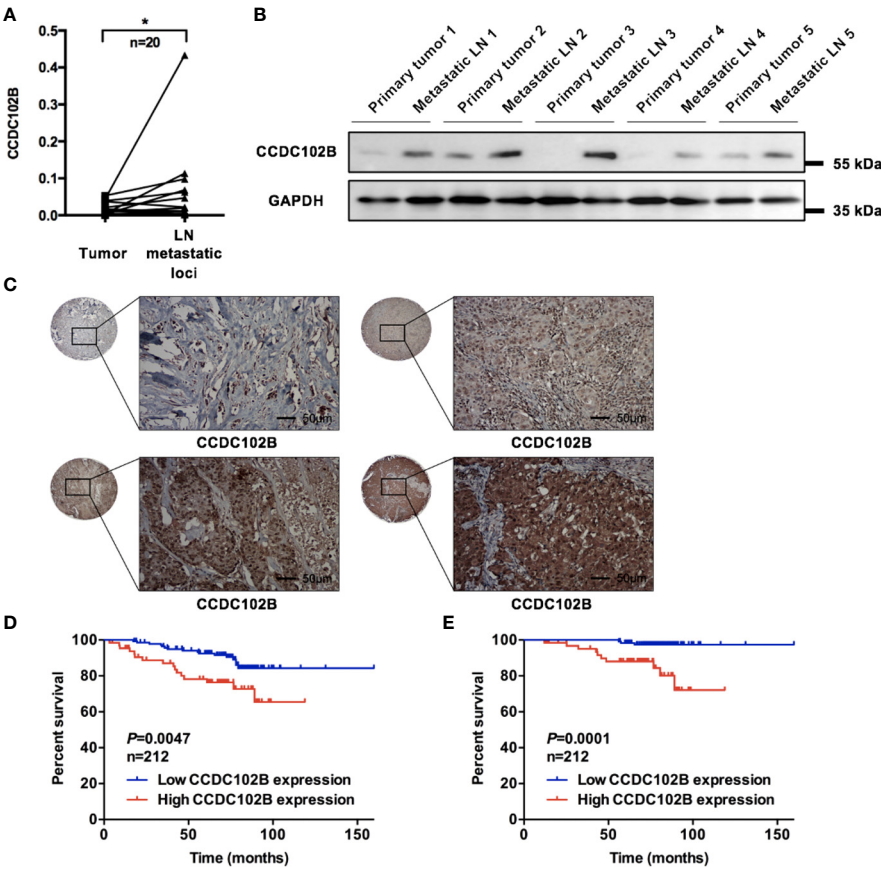

FIGURE 2 | Increased expression of CCDC102B correlates with poor clinical outcome. **(A)** Relative expression of CCDC102B in primary breast cancer tissues (tumor) and their corresponding LN metastatic loci in a 20-paired-sample cohort (Wilcoxon matched-pairs signed rank test). Normalized to β-ACTIN. (*P=0.011) **(B)** Expression of CCDC102B in primary tumors and corresponding metastatic LNs. **(C)** Breast tumor tissue microarray from 212 breast cancer patients using immunohistochemistry to determine CCDC102B expression. Scale bars: 50 μm. **(D, E)** Kaplan-Meier analysis and Log-rank test of recurrence-free survival (RFS) and overall survival (OS) with different expression of CCDC102B in breast cancer patients. *P ≤ 0.05.

high expression of CCDC102B was correlated with younger age (P=0.033) and higher histological grade (P=0.019). We found that high expression of CCDC102B was associated with LN metastasis (P=0.052) (**Supplementary Figure 2A**). In addition, the bc-GenExMiner 3.0 database was used to explore the correlation between CCDC102B expression and nodal status in breast cancer patients (43). With analysis of targeted expression of CCDC102B in breast cancer patients with different nodal status, we found significantly higher expression of CCDC102B in LN-positive patients (P=0.0005, **Supplementary Figure 2B**).

Based on the TMA data, we analyzed the correlation between CCDC102B expression and the prognosis of breast cancer patients, which showed that CCDC102B was an independent predictive factor of both recurrence-free survival (RFS) and overall survival (OS) (P=0.009 and P=0.002, respectively, **Supplementary Tables 2B, C**). Kaplan–Meier analysis indicated that high expression of CCDC102B was associated with poor clinical outcomes. When all patients were considered as a whole group, patients with high CCDC102B expression showed significantly reduced RFS and OS compared with that of those with low CCDC102B expression (P=0.0047 and P=0.0001, respectively, **Figures 2D, E**), which was similar to the clinical outcomes observed from the Gene Expression Omnibus (GEO) database (Affymetrix HGU133A and HGU133+2 microarrays) (44) (**Supplementary Figures 2C, D**). The median survival time of breast cancer patients with high CCDC102B expression was 70.30 months, which was significantly shorter than that of patients with low CCDC102B expression (75.87 months). When these tumors were divided into luminal A, luminal B, HER2+ and triple-negative breast cancer (TNBC) subtypes, high expression of CCDC102B showed a particularly strong correlation with poor clinical outcome in HER2+ and TNBC (**Supplementary Figures 2E, F**). Taken together, these results demonstrated that increased expression of CCDC102B was

correlated with poor clinical outcomes in breast cancer, suggesting that CCDC102B was associated with increased metastatic ability in breast cancer.

CCDC102B Promotes Breast Cancer Cell Migration and Metastasis *In Vitro* and *In Vivo*

To investigate the role of CCDC102B in breast cancer migration and metastasis, we analyzed the expression of CCDC102B in breast cancer cells (**Supplementary Figure 3A**) and developed three CCDC102B-overexpressing stable breast cancer cell line models (MDA-MB-231, BT549, and MDA-MB-231 LM2) for *in vitro* and *in vivo* studies. Western blot analysis and qRT–PCR both demonstrated that the CCDC102B expression level was strongly increased (**Supplementary Figure 3B**). In parallel, stable CCDC102B-targeting CRISPR/Cas9 knockout breast cancer cell line models (MDA-MB-231 and BT549) were established with distinct sgRNAs. Single colonies were selected from breast cancer cells transduced with CCDC102B-targeting CRISPR/Cas9, and knockout efficiency was examined with western blot analysis and qRT–PCR (**Supplementary Figure 3C**). Overexpression of CCDC102B significantly enhanced the migration and invasion ability in Transwell assays of MDA-MB-231, BT549, and MDA-MB-231 LM2 cells (**Figures 3A, B** and **Supplementary Figures 3D–F**) and also

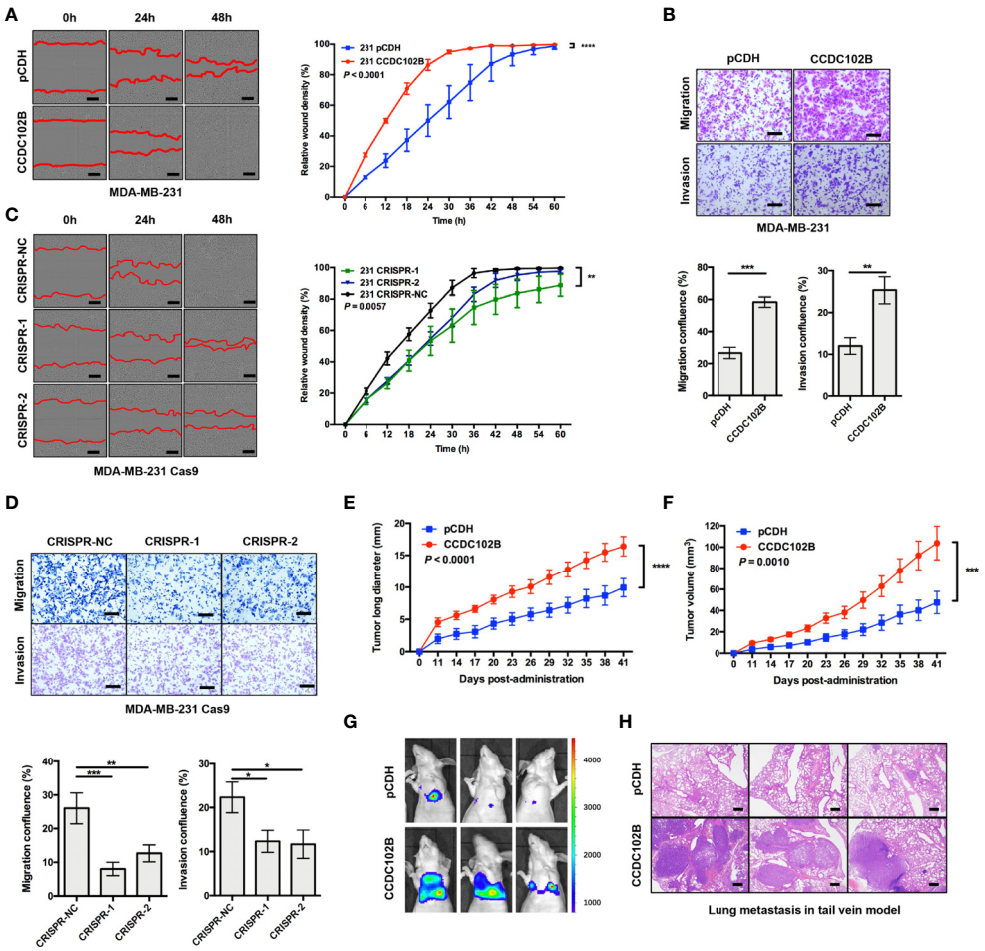

FIGURE 3 | CCDC102B promotes breast cancer metastasis. **(A, B)** Wound healing assay and Transwell assay in MDA-MB-231 cells. CCDC102B overexpressed cells and the corresponding control cells were used. Representative photos and quantitative analysis were shown. Relative wound density was determined by IncuCyte. Confluence of Transwell was analyzed by ImageJ. n=3, biological replicates. Scale bars: 100 μm. **(C, D)** Wound healing assay and Transwell assay in MDA-MB-231 Cas9 cells. CCDC102B KO cells by CRISPR system and the corresponding control cells were used. Representative photos and quantitative analysis were shown. Relative wound density was determined by IncuCyte. Confluence of Transwell was analyzed by Image J. n=3, biological replicates. Scale bars: 100 μm. **(E, F)** Tumor long diameter and tumor volume were measured in orthotopic xenograft breast cancer model with overexpressed CCDC102B cells and the corresponding control cells. (Unpaired t test was performed on the day 41, n=12 of each group) **(G)** BLI of three representative mice in each group 6 weeks after injection with transduced cells in tail vein model. (n=6 of each group) **(H)** Representative images of H&E staining of lung metastasis in each group 6 weeks after injection with transduced cells in tail vein model. (n=6 of each group) Scale bars: 500 μm. *P ≤ 0.05; **P ≤ 0.01; ***P ≤ 0.001; ****P ≤ 0.0001.

increased proliferation (**Supplementary Figure 3G**). In contrast, knockout of endogenous CCDC102B in MDA-MB-231 and BT549 cells resulted in significant decreases in proliferation, migration and invasion (**Figures 3C, D** and **Supplementary Figures 3H–J**).

To further validate the potential significance of CCDC102B in breast cancer metastasis *in vivo*, we generated an orthotopic xenograft breast cancer model using stable CCDC102B-overexpressing MDA-MB-231 LM2 cells. The growth of xenograft tumors and body weight were monitored. We found that the long tumor diameters and tumor volumes were significantly increased when CCDC102B was overexpressed (**Figures 3E, F** and **Supplementary Figure 3K**), while body weight was similar in the two groups (**Supplementary Figure 3L**). In addition, we developed a metastasis model with intravenous delivery of stable CCDC102B-overexpressing MDA-MB-231 LM2 cells with a retroviral construct expressing a GFP/luciferase fusion protein into the tail vein of nude mice. Tumor cell colonization and outgrowth in the lungs were monitored 6 weeks after the injection. We observed significantly increased lung metastasis in mice injected with CCDC102B-overexpressing cells compared with corresponding control mice with similar body weights in the two groups (**Figures 3G, H** and **Supplementary Figure 3M**). Taken together, these findings confirmed that high CCDC102B expression promoted breast cancer cell metastasis *in vitro* and *in vivo*.

RACK1 Decreases the Stability of CCDC102B Through the Lysosome Pathway

To explore the underlying mechanism of CCDC102B-induced promotion of tumor metastasis, co-IP followed by mass spectrometry (MS) was employed to identify potential interaction partners binding to CCDC102B. RACK1 was identified as a major protein in CCDC102B-overexpressing samples (**Figure 4A** and **Supplementary Figure 4A**, **Supplementary Table 4A**). Next, we validated the interaction between CCDC102B and RACK1 by IP experiments using MDA-MB-231 cells stably overexpressing CCDC102B-Flag (**Figure 4B**). The endogenous interaction was further confirmed (**Figure 4C**).

RACK1, which contains seven Trp-Asp 40 (WD40) repeats, is a scaffold protein with diverse functions that has been reported to interact with several receptors and regulate signaling pathways (45–49). To determine the functional significance of the

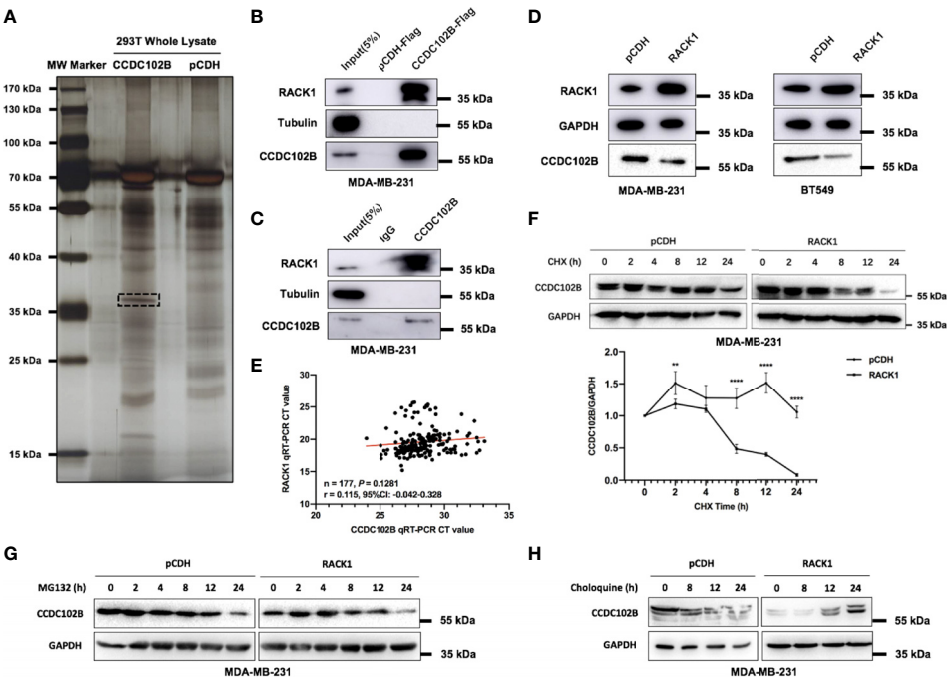

FIGURE 4 | CCDC102B interacts with RACK1. **(A)** Co-IP identified potential interaction partners binding to CCDC102B. **(B)** Immunoprecipitation experiments validated interaction between CCDC102B and RACK1 using MDA-MB-231 stably overexpressing CCDC102B-Flag. **(C)** Immunoprecipitation experiments to validate endogenous interaction between CCDC102B and RACK1. **(D)** Overexpression of RACK1 significantly decreased the expression level of CCDC102B in both MDA-MB-231 cells and BT549 cells. **(E)** Gene expression profile correlation between CCDC102B and RACK1 using qRT-PCR analysis in 177 breast cancer patients. (Spearman r) **(F)** Overexpression RACK1 decreased the stability of CCDC102B and shortened the half-life of CCDC102B. Quantitative analysis was analyzed by ImageJ. (**P = 0.0010; ****P < 0.0001) n=3, biological replicates. **(G)** MG132 treatment did not significantly alter the protein levels of CCDC102B. **(H)** Choloquine treatment resulted in an accumulation of CCDC102B in a time-dependent manner.

association between CCDC102B and RACK1, we examined the expression level of RACK1 (**Supplementary Figure 4B**). Interestingly, we noticed that overexpression of RACK1 significantly decreased the expression level of CCDC102B in MDA-MB-231 and BT549 cells (**Figure 4D**). In contrast, CRISPR/Cas9 knockout of RACK1 led to increased expression of CCDC102B (**Supplementary Figure 4C**). The negative correlation of RACK1 and CCDC102B expression was not due to repressed transcription, as revealed by qRT–PCR analysis in breast cancer patients (n=177) (**Figure 4E**). Similar results were shown with the bc-GenExMiner 3.0 database when analysis with gene correlation between CCDC102B and RACK1, indicating that there was little transcriptional correlation between CCDC102B and RACK1 (**Supplementary Figure 4D**) (43). Therefore, we hypothesized that the association between CCDC102B and RACK1 was mediated by cellular posttranslational processing. To investigate the effect of RACK1 on CCDC102B stability, MDA-MB-231 cells transfected with empty vector or RACK1 were incubated with 100 μM cycloheximide (CHX). The results showed that overexpression of RACK1 decreased the stability and shortened the half-life of CCDC102B (**Figure 4F**). Together, these results suggest that RACK1 promotes the degradation of CCDC102B.

The ubiquitin–proteasome system and autophagy–lysosome system are two main pathways for protein degradation in eukaryotes (28, 29). To delineate which pathway is responsible for RACK1-mediated CCDC102B degradation, MDA-MB-231 cells transfected with empty vector or RACK1 were treated with 2 μM proteasome inhibitor MG132 or 10 μM lysosome inhibitor chloroquine. We found that MG132 treatment did not significantly alter the protein levels of CCDC102B (**Figure 4G**), while chloroquine treatment resulted in the accumulation of CCDC102B in a time-dependent manner (**Figure 4H**). Thus, these data suggest that RACK1 promotes CCDC102B degradation mainly through the lysosome pathway.

RACK1 Promotes CCDC102B Lysosomal Degradation by Mediating CMA

There are three types of autophagy involved in lysosomal degradation. To determine whether macroautophagy contributes to the regulation of CCDC102B, 3-methyladenine (3-MA), a selective inhibitor of macroautophagy that blocks the formation of autophagosomes, was used to treat MDA-MB-231 cells transfected with empty vector or RACK1 vector. Western blot analysis showed that 5 mM 3-MA had no significant effects on the stability of CCDC102B (**Figure 5A**), which indicated that

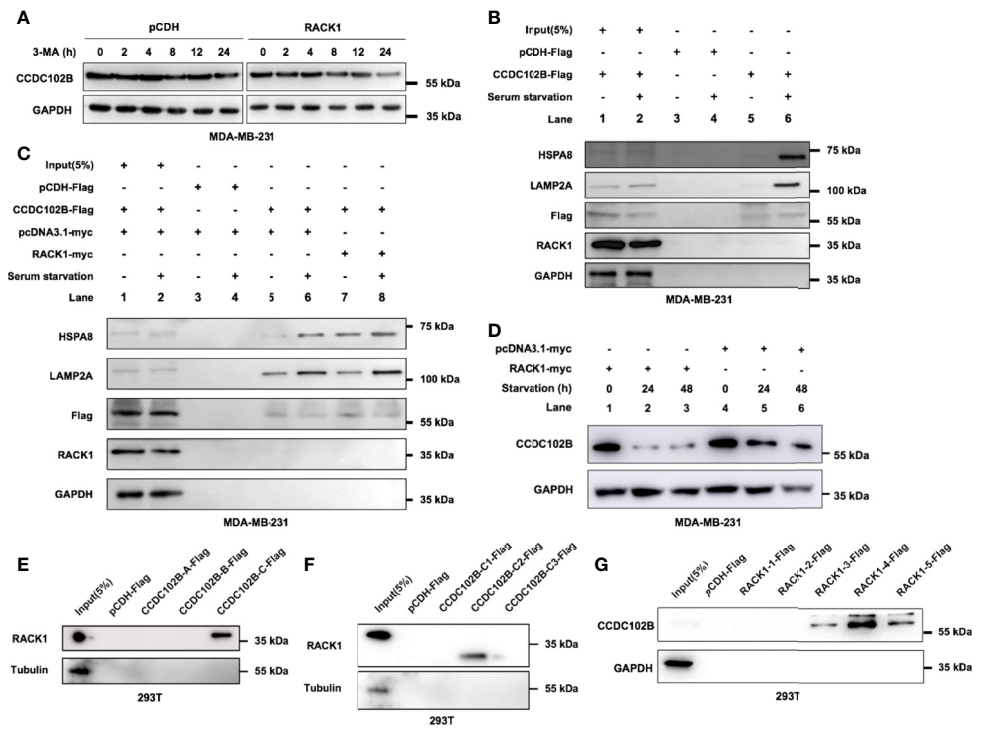

FIGURE 5 | RACK1 promotes CCDC102B degradation. **(A)** 3-MA had no significant effects on the stability level of CCDC102B. **(B)** MDA-MB-231 cells were cultured in complete or serum-free medium for 24h, and then subjected to IP and immunoblotting. CCDC102B overexpressed cells and the corresponding control cells were used. **(C)** MDA-MB-231 cells were cultured in complete or serum-free medium for 24h, and then subjected to IP and immunoblotting. CCDC102B overexpressed cells, RACK1 overexpressed cells and the corresponding control cells were used. **(D)** MDA-MB-231 cells were cultured in serum-free medium for the indicated times and analyzed by immunoblotting. RACK1 overexpressed cells and the corresponding control cells were used. **(E)** RACK1 interacted with CCDC102B-C. (**F**) RACK1 interacted with CCDC102B-C2. **(G)** CCDC102B interact with RACK1-3.

macroautophagy is not responsible for the lysosomal degradation of CCDC102B.

CMA is one of the three types of autophagy and is responsible for the selective degradation of proteins bearing a KFERQ-like motif (30). Interestingly, after reviewing the amino acid sequence of CCDC102B, we found seven putative KFERQ-like motifs at its N-terminus, namely, ^{146}QKEAL^{150}, ^{156}QDLKL^{160}, ^{352}LERLQ^{356}, ^{374}QGLER^{378}, ^{386}QVKEM^{390}, ^{449}NRVDQ^{453} and ^{490}QRSLD^{494}, indicating that CCDC102B may be a CMA substrate. The KFERQ-like motif in the substrate is first selectively recognized by HSPA8, which recruits proteins to the lysosome, and then the substrate binds to LAMP2A, a CMA receptor that mediates the translocation of substrate in the lysosomal lumen for degradation (28, 30–34). To explore whether CCDC102B interacts with HSPA8 and LAMP2A, MDA-MB-231 cells transfected with empty vector or CCDC102B were cultured under serum starvation conditions, a well-established inducer of CMA, and IP assays were performed. The results showed that, compared with complete medium growth conditions, serum starvation enhanced the interactions between CCDC102B and HSPA8 and CCDC102B and LAMP2A (**Figure 5B**). In addition, overexpression of RACK1 further enhanced these interactions (**Figure 5C**). To demonstrate the role of RACK1 and CMA in CCDC102B degradation, we investigated the effect of RACK1 overexpression and serum starvation on the stability level of CCDC102B. Western blot analysis showed that the expression level of CCDC102B in MDA-MB-231 cells was decreased in a time-dependent manner following serum starvation and was further decreased by RACK1 overexpression (**Figure 5D**). Therefore, RACK1 enhanced the CMA-mediated lysosomal degradation of CCDC102B.

To further map the specific binding regions in CCDC102B and RACK1, a series of truncations were constructed according to the structures of the proteins with confirmation by western blot analysis (**Supplementary Figures 5A–C**). IP assays in 293T cells were performed with different truncations. The results showed that CCDC102B-C2, which included two KFERQ-like motifs, ^{374}QGLER^{378} and ^{386}QVKEM^{390}, and the #5 WD40 domain in RACK1 were required for their interaction (**Figures 5F–H**). These data suggest that the interaction of RACK1 with the CCDC102B domain, including the KFERQ-like motif, may help expose the KFERQ-like motif and enhance recognition to promote CMA. Thus, RACK1 promotes CCDC102B lysosomal degradation by mediating CMA.

RACK1 Decreases the Stability of CCDC102B and Inhibits Breast Cancer Metastasis

Previous studies have shown that RACK1 regulates tumor metastasis by either promoting or inhibiting the progression of different tumor types and by regulating their microenvironments (47, 50–53). To validate the role of RACK1 in breast cancer, we analyzed the expression with qRT–PCR in breast cancer patients with LN metastasis (n=20) and found that RACK1 was similarly expressed in LN metastatic loci and primary tumors (P=0.7543, **Figure 6A**). Western blot analysis of primary tumors and corresponding metastatic LNs (n=4) also confirmed that RACK1 was similarly and ubiquitously expressed in both tissue types (**Figure 6B**). The bc-GenExMiner 3.0 database was used to explore the correlation between RACK1 expression and nodal status in breast cancer patients (43). With analysis of targeted expression of RACK1 in breast cancer patients with different nodal status, the results showed no significant difference in RACK1 expression between metastatic LN-positive and metastatic LN-negative patients (P=0.0936, **Supplementary Figure 6A**). In addition, clinical outcomes from the GEO database (Affymetrix HGU133A and HGU133+2 microarrays) (44) indicated that RACK1 expression was not associated with RFS in breast cancer patients (**Supplementary Figure 6B**), while OS was significantly correlated with RACK1 expression (**Supplementary Figure 6C**).

Furthermore, we investigated the role of RACK1 in breast cancer cell migration and metastasis. The results showed that overexpression of RACK1 significantly inhibited the migration and invasion of MDA-MB-231 and BT549 cells in Transwell assays (**Figures 6C, D**) and also slowed cell proliferation (**Supplementary Figure 6D**). However, there was no significant difference between the control and RACK1 overexpression groups in wound healing assays (**Supplementary Figure 6E**). In contrast, knockout of endogenous RACK1 in MDA-MB-231 cells resulted in the significant enhancement of migration and invasion (**Figure 6E**). These data suggest that RACK1 plays a role in metastasis inhibition in breast cancer.

Considering that RACK1 decreased the stability of CCDC102B, we hypothesized that RACK1 might exert its effects on breast cancer cell metastasis by regulating the degradation of CCDC102B. To verify this notion, functional rescue tests in breast cancer cells were performed. The results showed that the migration of MDA-MB-231 cells was significantly impaired by RACK1 overexpression, while RACK1-reduced cell migration was remarkably enhanced in CCDC102B-overexpressing cells (**Figure 6F**). On the other hand, the enhancement of the migration of RACK1 knockout breast cancer cells was attenuated by CCDC102B knockout (**Figure 6G**). Taken together, our results demonstrated that RACK1 inhibits breast cancer metastasis by decreasing the stability of CCDC102B.

CCDC102B Activates the NF–κB Pathway by Interacting With RACK1

To further investigate the molecular mechanisms of increased metastasis in CCDC102B-overexpressing breast cancer cells, we performed RNA sequencing in MDA-MB-231 cells transfected with the CCDC102B-overexpressing vector and the corresponding control vector. Gene set enrichment analysis (GSEA) showed that genes with expression changes (fold change > 1.5) were significantly associated with cancer development and metastasis, such as the NF–κB pathway (**Figure 7A** and **Supplementary Table 7A, B**), supporting the role of CCDC102B in breast cancer cell proliferation and metastasis. Functional rescue tests were performed showing that the migration of breast cancer cells was significantly

the

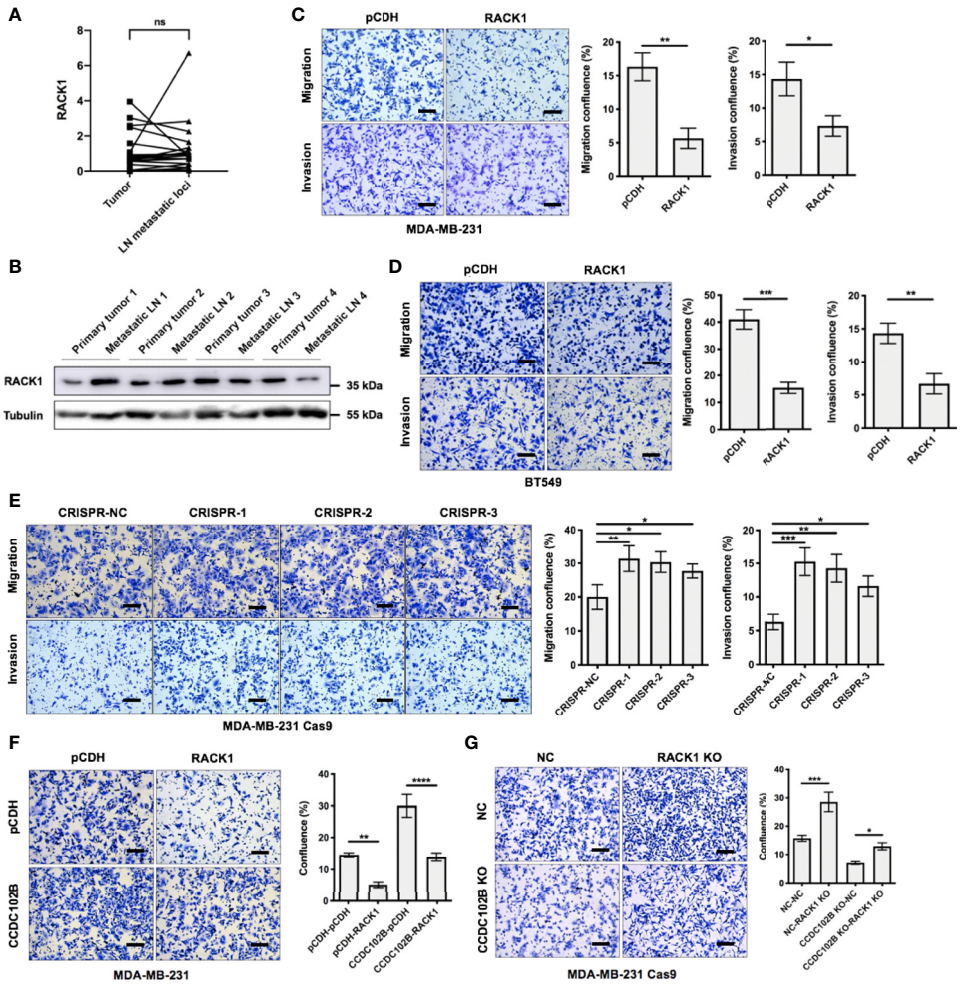

FIGURE 6 | RACK1 inhibits breast cancer metastasis. **(A)** Relative expression of RACK1 in primary breast cancer tissues (tumor) and their corresponding LN metastatic loci in a 20-paired-sample cohort (Wilcoxon matched-pairs signed rank test). Normalized to β-ACTIN. **(B)** Expression of RACK1 in primary tumors and corresponding metastatic LNs. **(C, D)** Transwell assay in MDA-MB-231 cells and BT549 cells. RACK1 overexpressed cells and the corresponding control cells were used. Representative photos and quantitative analysis were shown. Confluence of Transwell was analyzed by ImageJ. n=3, biological replicates. Scale bars: 100 μm. **(E)** Transwell assay in MDA-MB-231 Cas9 cells. RACK1 KO cells by CRISPR system and the corresponding control cells were used. Representative photos and quantitative analysis were shown. Confluence of Transwell was analyzed by ImageJ. n=3, biological replicates. Scale bars: 100 μm. **(F, G)** Cell functional rescue tests with Transwell assay in MDA-MB-231 cells and MDA-MB-231 Cas9 cells. CCDC102B overexpressed cells, RACK1 overexpressed cells, CCDC102B KO cells, RACK1 KO cells and the corresponding control cells were used. Representative photos and quantitative analysis were shown. Confluence of Transwell was analyzed by ImageJ. n=3, biological replicates. Scale bars: 100 μm. ns, $P > 0.05$; *$P \leq 0.05$; **$P \leq 0.01$; ***$P \leq 0.001$; ****$P \leq 0.0001$.

impaired by CCDC102B knockout, while was remarkably enhanced in NF−κB activated cells (**Figure 7B**). Western blot analysis confirmed that overexpressed CCDC102B was associated with increased p65, phospho-p65 (Ser536) and epithelial-mesenchymal transition (EMT) in MDA-MB-231 cells (**Figure 7C**). In addition, immunohistochemistry was performed in both orthotopic xenograft tumors and metastatic lungs in nude mice, showing that p65 was significantly increased in models with CCDC102B-overexpressing MDA-MB-231 LM2 cells (**Supplementary Figures 7A, B**).

Previous studies showed that RACK1, as a negative regulator of NF-κB signaling, interacts with the IKK complex and interferes with recruitment of the IKK complex to TRAF2, which is a critical step for IKK phosphorylation (54). To further verify this, we performed functional rescue tests in breast cancer cells, showing that RACK1-reduced cell migration was remarkably enhanced in NF−κB activated cells (**Supplementary Figure 7C**). Western blot analysis also confirmed that RACK1 overexpression was associated with decreased p65 (**Supplementary Figure 7D**). However, IP assays showed that CCDC102B had no interaction with the IKK complex (**Supplementary Figure 7E**), suggesting that CCDC102B was not associated with the recruitment of the IKK complex. We hypothesized that CCDC102B activates the NF−κB pathway by interacting with RACK1, which decreases the interference with IKK

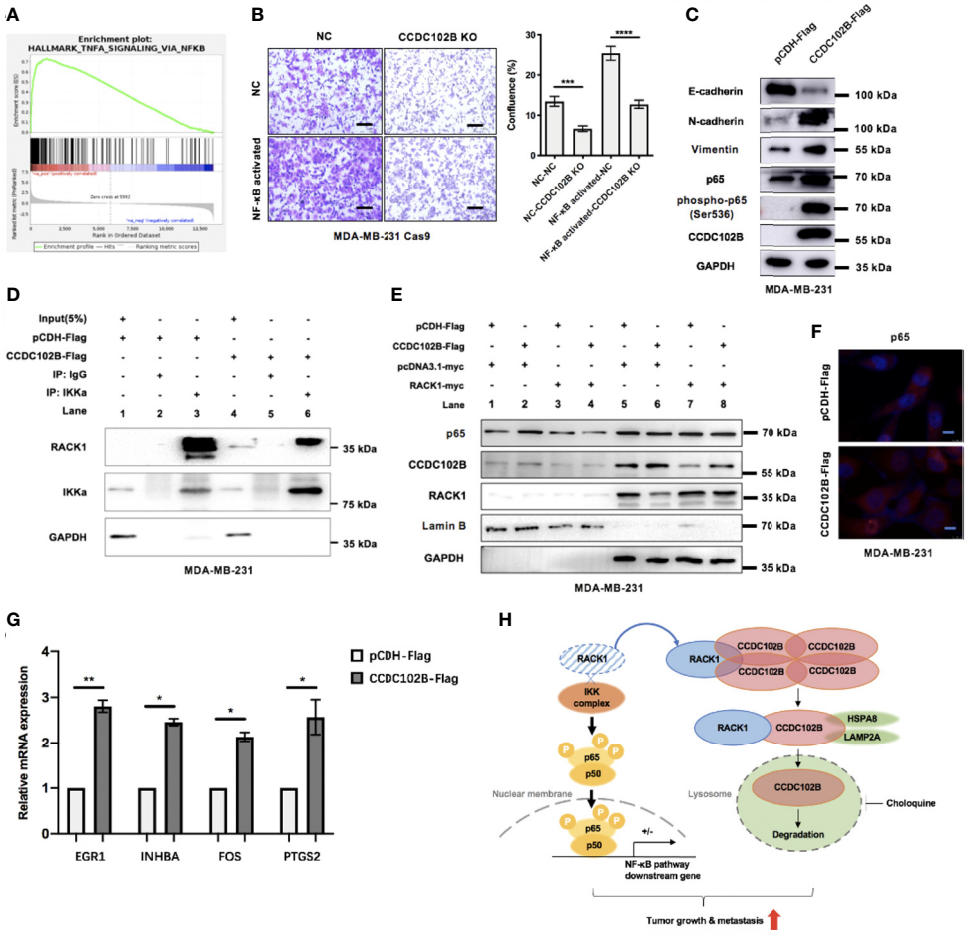

FIGURE 7 | CCDC102B activates NF−κB pathway by interacting with RACK1. **(A)** GSEA showed CCDC102B was significantly associated with NF−κB pathway. **(B)** Cell functional rescue tests with Transwell assay in MDA-MB-231 Cas9 cells. CCDC102B KO cells, NF−κB activated cells and the corresponding control cells were used. Representative photos and quantitative analysis were shown. Confluence of Transwell was analyzed by ImageJ. n=3, biological replicates. Scale bars: 100 μm. **(C)** Overexpressed CCDC102B was associated with increased p65, phospho-p65 (Ser536) and EMT in MDA-MB-231. **(D)** Overexpressed CCDC102B led to less interaction between RACK1 and IKKα. **(E)** Movement of p65 into cell nucleus was promoted by CCDC102B, which could be decreased by overexpressed RACK1. **(F)** Immunofluorescence showed movement of p65 into cell nucleus promoted by CCDC102B. Scale bars: 10 μm. **(G)** Expression of NF−κB pathway target genes in CCDC102B-overexpressing MDA-MB-231 cells measured by qRT-PCR. n=3, biological replicates. **(H)** Schematic diagram of CCDC102B regulating breast cancer metastasis *via* NF−κB pathway. *P ≤ 0.05; **P ≤ 0.01; ***P ≤ 0.001; ****P ≤ 0.0001.

complex recruitment and phosphorylation. To verify this hypothesis, we performed IP assays with MDA-MB-231 cells transfected with empty vector or CCDC102B vector. The results showed that, compared with the corresponding control cells, cells overexpressing CCDC102B exhibited less interaction between RACK1 and IKKa (**Figure 7D**). Moreover, we verified that the translocation of p65 into the cell nucleus was promoted by CCDC102B *via* western blot analysis and immunofluorescence (**Figures 7E, F**). Additionally, western blot analysis was performed to verify the decreased translocation of p65 into the cell nucleus with RACK1 overexpression (**Figure 7E**). We further analyzed the expression of several NF−κB pathway target genes showed in GSEA and confirmed that these highly ranked genes were overexpressed at transcription level in CCDC102B-overexpressing MDA-MB-231 cells (**Figure 7G**). Thus to sum up, CCDC102B positively regulates the NF−κB pathway by interacting with RACK1 (**Figure 7H**).

DISCUSSION

In this study, we presented several interesting findings concerning the biological function and regulatory mechanism of CCDC102B in breast cancer. For the first time, we identified CCDC102B as a significantly enriched protein in metastatic LNs compared to primary tumors *via* gene microarray analysis, comparative genomics analysis and *in vivo* CRISPR/Cas9-based knockout screening. We found that increased CCDC102B expression

correlated with poor RFS and OS in breast cancer patients and could promote the migration and invasion of breast cancer cells. Moreover, overexpression of CCDC102B remarkably accelerated tumor growth and lung metastasis in breast cancer xenograft models. Therefore, CCDC102B could serve as an independent prognostic factor in breast cancer. Furthermore, we found a mutual effect between CCDC102B and RACK1. On the one hand, CCDC102B binds to RACK1 and interferes with the interaction between RACK1 and the IKK complex, which leads to activation of NF-κB signaling. On the other hand, RACK1 promotes the degradation of CCDC102B through CMA. Thus, the interaction between CCDC102B and RACK1 regulates the metastatic ability of breast cancer.

Previous studies have demonstrated the critical roles of RACK1 in regulating the processes of cancer cell proliferation, adhesion, migration, invasion and metastasis (45–49). RACK1, ubiquitously expressed in a wide range of tissues, was initially identified as an anchoring protein for protein kinase C (55). With an increasing number of reports showing its interaction with a large number of signaling transduction complexes and signaling pathways, such as Src family kinases, HIF-1, the Hedgehog pathway, the AKT pathway and the NF-κB pathway, RACK1 has been widely perceived as a platform for integrating diverse signaling activities (50–54, 56–59). The NF-κB pathway was also significantly enriched in CCDC102B-overexpressing breast cancer cells. Thus, all of these reports indicate the relationship among RACK1, CCDC102B and the NF-κB pathway, which has important functions in breast cancer metastasis. Generally, the NF-κB pathway comprises a family of transcription factors involved in the regulation of various biological response signaling pathways, which play a key role in cancer development, metastasis and resistance (60–63). Accordingly, NF-κB pathway activation increases NF-κB translocation in the nucleus and regulates gene expression. RACK1, identified as an IKK signalosome component, represses IKK activity and subsequent NF-κB activation through interaction with the IKK complex (54). In our study, we proposed that CCDC102B activates the NF−κB pathway by interacting with RACK1, which controls the sensitivity of NF-κB signaling by regulating IKK activation. Because CCDC102B was not found to be associated with the recruitment of the IKK complex, more questions about the mechanism of interaction among CCDC102B, RACK1 and the IKK complex were raised. One hypothesis is that CCDC102B competitively interacts with RACK1 with the same binding site of the IKK complex. Another hypothesis is that the interaction between CCDC102B and RACK1 influences the functional dimer formation of RACK1. Further research is needed to further clarify the mechanism.

Moreover, we provided evidence for the first time that CCDC102B undergoes lysosomal degradation *via* the CMA pathway. According to the mechanism by which cargo is delivered to lysosomes, autophagy can be classified as macroautophagy, microautophagy, or CMA (28). Distinct from other autophagy types, CMA is the first lysosomal degradation process in which substrates are selectively recognized by a cytosolic chaperone and tagged for degradation in lysosomes (32, 64). This process involves substrate recognition, unfolding, translocation, and degradation (32). By degrading specific target proteins, the CMA pathway is involved in a variety of cellular activities, including its critical role in the development of diseases (32, 64–68). CMA degrades proteins that contain a consensus pentapeptide called a KFERQ-like motif, which includes glutamine on one of the sides, one or two of the positive residues K and R, one or two of the hydrophobic residues F, L, I or V and one of the negatively charged E or D residues (30, 64). Proteins containing KFERQ-like motifs are recognized by HSPA8 and interact with LAMP2A, which helps with transportation to the lysosomal surface (28, 30–34). In this study, we demonstrated that CCDC102B, containing seven putative KFERQ-like motifs, was degraded in lysosomes by the CMA pathway. Serum starvation enhanced the interactions between CCDC102B and HSPA8 and between CCDC102B and LAMP2A. Furthermore, we found decreased expression of CCDC102B with serum starvation, which could be further decreased by RACK1 overexpression. Therefore, RACK1 enhanced the CMA-mediated lysosomal degradation of CCDC102B. With further mapping of specific binding regions in CCDC102B and RACK1, we found that RACK1, interacting with the CCDC102B domain including a KFERQ-like motif, promotes CCDC102B lysosomal degradation by mediating CMA. One possible mechanism of RACK1 was increased exposure of the KFERQ-like motif and enhanced recognition for the CMA process. Taken together, these results showed that CCDC102B protein levels are regulated by CMA-mediated lysosomal degradation, which could be enhanced by RACK1 overexpression.

Therefore, we believe that there is an interesting balance between CCDC102B and RACK1 (**Figure 7G**). When the expression level of CCDC102B is relatively low, which means that RACK1 is far more abundant than CCDC102B, the role of RACK1 is dominant; it promotes the CMA-mediated degradation of CCDC102B. Although CCDC102B can upregulate the NF-κB pathway, it is quickly degraded in the presence of excess RACK1. Generally, there will be no great impact on tumor development or metastasis. Nevertheless, when the expression level of CCDC102B is relatively high, which means RACK1 is far less abundant than CCDC102B, the role of CCDC102B is dominant. With little degradation, excess CCDC102B binds with RACK1, which may compete with IKK binding, resulting in NF-κB pathway activation and eventually promoting tumor development or metastasis. Thus, CCDC102B expression is one of the key predictors of early-stage metastasis in breast cancer.

In summary, we uncovered the interaction between CCDC102B and RACK1, which could be one of the mechanisms involved in the early-stage metastasis of breast cancer. As CCDC102B expression is upregulated in breast tumors, the discovery of novel drugs targeting CCDC102B could suppress breast cancer growth and mitigate

metastasis. These emerging findings provide new mechanistic insights into early-stage breast cancer metastasis and define novel therapeutic targets for breast cancer.

DATA AVAILABILITY STATEMENT

The datasets presented in this study can be found in online repositories. The names of the repository/repositories and accession number(s) can be found in the article/**Supplementary Material**.

ETHICS STATEMENT

The studies involving human participants were reviewed and approved by Fudan University. The patients/participants provided their written informed consent to participate in this study. The animal study was reviewed and approved by Shanghai Medical Experimental Animal Care Commission.

AUTHOR CONTRIBUTIONS

JS and YC designed and performed the experiments, analyzed data and wrote the paper. RG performed some of the experiments, analyzed data and provided some critical ideas. BX, WC, QZ, JC and JX performed some of the experiments and analyzed data. JC and JX provided the patients samples for clinical data analysis. JW and YC initiated the study, organized, designed, and revised the paper. All authors contributed to the article and approved the submitted version.

FUNDING

This work was supported by grants from National Natural Science Foundation of China (Grant No. 81902674, 81874115, 82072919 and 81302297).

ACKNOWLEDGMENTS

We thank Dr. Xin Hu and Dr. Peng Ji for their kind help on the initiation of this research.

SUPPLEMENTARY MATERIAL

The Supplementary Material for this article can be found online at: https://www.frontiersin.org/articles/10.3389/fonc.2022.927358/full#supplementary-material

REFERENCES

1. Zhou M, Wang H, Zeng X, Yin P, Zhu J, Chen W, et al. Mortality, Morbidity, and Risk Factors in China and Its Provinces, 1990-2017: A Systematic Analysis for the Global Burden of Disease Study 2017. *Lancet* (2019) 394(10204):1145–58. doi: 10.1016/S0140-6736(19)30427-1
2. Bray F, Ferlay J, Soerjomataram I, Siegel RL, Torre LA, Jemal A. Global Cancer Statistics 2018: GLOBOCAN Estimates of Incidence and Mortality Worldwide for 36 Cancers in 185 Countries. *CA Cancer J Clin* (2018) 68 (6):394–424. doi: 10.3322/caac.21492
3. Siegel RL, Miller KD, Jemal A. Cancer statistics, 2020. *CA Cancer J Clin* (2020) 70(1):7–30. doi: 10.3322/caac.21590
4. Miller KD, Nogueira L, Mariotto AB, Rowland JH, Yabroff KR, Alfano CM, et al. Cancer Treatment and Survivorship Statistics. *CA Cancer J Clin* (2019) 69(5):363–85. doi: 10.3322/caac.21565
5. Peart O. Metastatic Breast Cancer. *Radiol Technol* (2017) 88(5):519M–39M.
6. Malter W, Hellmich M, Badian M, Kirn V, Mallmann P, Kramer S. Factors Predictive of Sentinel Lymph Node Involvement in Primary Breast Cancer. *Anticancer Res* (2018) 38(6):3657–62. doi: 10.21873/anticanres.12642
7. van Diest PJ, de Boer M, van Deurzen CH, Tjan-Heijnen VC. Micrometastases and Isolated Tumor Cells in Breast Cancer Are Indeed Associated With Poorer Outcome. *J Clin Oncol* (2010) 28(9):e141–142. doi: 10.1200/JCO.2009.26.7575
8. Zhan T, Rindtorff N, Betge J, Ebert MP, Boutros M. CRISPR/Cas9 for Cancer Research and Therapy. *Semin Cancer Biol* (2019) 55:106–19. doi: 10.1016/j.semcancer.2018.04.001
9. Doudna JA, Charpentier E. Genome Editing. the New Frontier of Genome Engineering With CRISPR-Cas9. *Science* (2014) 346(6213):1258096. doi 10.1126/science.1258096
10. Zhang F, Wen Y, Guo X. CRISPR/Cas9 for Genome Editing: Progress, Implications and Challenges. *Hum Mol Genet* (2014) 23(R1):R40–46. doi: 10.1093/hmg/ddt394
11. Hsu PD, Lander ES, Zhang F. Development and Applications of CRISPR-Cas9 for Genome Engineering. *Cell* (2014) 157(6):1262–78. doi: 10.1016/j.cell.2014.05.010
12. Chen M, Mao A, Xu M, Weng Q, Mao J, Ji J. CRISPR-Cas9 for Cancer Therapy: Opportunities and Challenges. *Cancer Lett* (2019) 447:48–55. doi: 10.1016/j.canlet.2019.01.017
13. Burkhard P, Stetefeld J, Strelkov SV. Coiled Coils: A Highly Versatile Protein Folding Motif. *Trends Cell Biol* (2001) 11(2):82–8. doi: 10.1016/S0962-8924(00)01898-5
14. Radulovich N, Leung L, Ibrahimov E, Navab R, Sakashita S, Zhu CQ, et al. Coiled-Coil Domain Containing 68 (CCDC68) Demonstrates a Tumor-Suppressive Role in Pancreatic Ductal Adenocarcinoma. *Oncogene* (2015) 34(32):4238–47. doi: 10.1038/onc.2014.357
15. Li CF, Wu WR, Chan TC, Wang YH, Chen LR, Wu WJ, et al. Transmembrane and Coiled-Coil Domain 1 Impairs the AKT Signaling Pathway in Urinary Bladder Urothelial Carcinoma: A Characterization of a Tumor Suppressor. *Clin Cancer Res* (2017) 23(24):7650–63. doi: 10.1158/1078-0432.CCR-17-0002
16. Chen M, Ni J, Chang HC, Lin CY, Muyan M, Yeh S. CCDC62/ERAP75 Functions as a Coactivator to Enhance Estrogen Receptor Beta-Mediated Transactivation and Target Gene Expression in Prostate Cancer Cells. *Carcinogenesis* (2009) 30(5):841–50. doi: 10.1093/carcin/bgn288
17. Occhionorelli M, Santoro F, Pallavicini I, Gruszka A, Moretti S, Bossi D, et al. The Self-Association Coiled-Coil Domain of PML Is Sufficient for the Oncogenic Conversion of the Retinoic Acid Receptor (RAR) Alpha. *Leukemia* (2011) 25 (5):814–20. doi: 10.1038/leu.2011.18
18. Kim H, Huang J, Chen J. CCDC98 Is a BRCA1-BRCT Domain-Binding Protein Involved in the DNA Damage Response. *Nat Struct Mol Biol* (2007) 14(8):710–5. doi: 10.1038/nsmb1277
19. Dickson I. NETs Promote Liver Metastasis. *Via CCDC25. Nat Rev Gastroenterol Hepatol* (2020) 17(8):451. doi 10.1038/s41575-020-0345-1
20. Yang L, Liu Q, Zhang X, Liu X, Zhou B, Chen J, et al. DNA of Neutrophil Extracellular Traps Promotes Cancer Metastasis. *Via CCDC25. Nat* (2020) 583 (7814):133–8. doi 10.1038/s41586-020-2394-6
21. Wang J, Wu X, Dai W, Li J, Xiang L, Tang W, et al. The CCDC43-ADRM1 Axis Regulated by YY1, Promotes Proliferation and Metastasis of Gastric Cancer. *Cancer Lett* (2020) 482:90–101. doi: 10.1016/j.canlet.2020.03.026

22. Wang J, Liu G, Liu M, Xiang L, Xiao Y, Zhu H, et al. The FOXK1-CCDC43 Axis Promotes the Invasion and Metastasis of Colorectal Cancer Cells. *Cell Physiol Biochem* (2018) 51(6):2547–63. doi: 10.1159/000495924
23. Pan C, Yi S, Xiao C, Huang Y, Chen X, Huang D. The Evaluation of Seven Age-Related CpGs for Forensic Purpose in Blood From Chinese Han Population. *Forensic Sci Int Genet* (2020) 46:102251. doi: 10.1016/j.fsigen.2020.102251
24. Freire-Aradas A, Phillips C, Mosquera-Miguel A, Giron-Santamaria L, Gomez-Tato A, Casares de Cal M, et al. Development of a Methylation Marker Set for Forensic Age Estimation Using Analysis of Public Methylation Data and the Agena Bioscience EpiTYPER System. *Forensic Sci Int Genet* (2016) 24:65–74. doi: 10.1016/j.fsigen.2016.06.005
25. Park JL, Kim JH, Seo E, Bae DH, Kim SY, Lee HC, et al. Identification and Evaluation of Age-Correlated DNA Methylation Markers for Forensic Use. *Forensic Sci Int Genet* (2016) 23:64–70. doi: 10.1016/j.fsigen.2016.03.005
26. Hosoda Y, Yoshikawa M, Miyake M, Tabara Y, Shimada N, Zhao W, et al. CCDC102B Confers Risk of Low Vision and Blindness in High Myopia. *Nat Commun* (2018) 9(1):1782. doi: 10.1038/s41467-018-03649-3
27. Xia Y, Huang N, Chen Z, Li F, Fan G, Ma D, et al. CCDC102B Functions in Centrosome Linker Assembly and Centrosome Cohesion. *J Cell Sci* (2018) 131 (23):1–12. doi: 10.1242/jcs.222901
28. Mizushima N, Levine B, Cuervo AM, Klionsky DJ. Autophagy Fights Disease Through Cellular Self-Digestion. *Nature* (2008) 451(7182):1069–75. doi: 10.1038/nature06639
29. Ravid T, Hochstrasser M. Diversity of Degradation Signals in the Ubiquitin-Proteasome System. *Nat Rev Mol Cell Biol* (2008) 9(9):679–90. doi: 10.1038/nrm2468
30. Dice JF. Peptide Sequences That Target Cytosolic Proteins for Lysosomal Proteolysis. *Trends Biochem Sci* (1990) 15(8):305–9. doi: 10.1016/0968-0004(90)90019-8
31. Bandyopadhyay U, Sridhar S, Kaushik S, Kiffin R, Cuervo AM. Identification of Regulators of Chaperone-Mediated Autophagy. *Mol Cell* (2010) 39(4):535–47. doi: 10.1016/j.molcel.2010.08.004
32. Kaushik S, Cuervo AM. Chaperone-Mediated Autophagy: A Unique Way to Enter the Lysosome World. *Trends Cell Biol* (2012) 22(8):407–17. doi: 10.1016/j.tcb.2012.05.006
33. Cuervo AM, Dice JF. A Receptor for the Selective Uptake and Degradation of Proteins by Lysosomes. *Science* (1996) 273(5274):501–3. doi: 10.1126/science.273.5274.501
34. Chiang HL, Terlecky SR, Plant CP, Dice JF. A Role for a 70-Kilodalton Heat Shock Protein in Lysosomal Degradation of Intracellular Proteins. *Science* (1989) 246(4928):382–5. doi: 10.1126/science.2799391
35. Hiraga T, Kizaka-Kondoh S, Hirota K, Hiraoka M, Yoneda T. Hypoxia and Hypoxia-Inducible Factor-1 Expression Enhance Osteolytic Bone Metastases of Breast Cancer. *Cancer Res* (2007) 67(9):4157–63. doi: 10.1158/0008-5472.CAN-06-2355
36. Stark AM, Anuszkiewicz B, Mentlein R, Yoneda T, Mehdorn HM, Held-Feindt J. Differential Expression of Matrix Metalloproteinases in Brain- and Bone-Seeking Clones of Metastatic MDA-MB-231 Breast Cancer Cells. *J Neurooncol* (2007) 81(1):39–48. doi doi: 10.1007/s11060-006-9207-0
37. Minn AJ, Gupta GP, Siegel PM, Bos PD, Shu W, Giri DD, et al. Genes That Mediate Breast Cancer Metastasis to Lung. *Nature* (2005) 436(7050):518–24. doi: 10.1038/nature03799
38. Livak KJ, Schmittgen TD. Analysis of Relative Gene Expression Data Using Real-Time Quantitative PCR and the 2(-Delta Delta C(T)) Method. *Methods* (2001) 25(4):402–8. doi: 10.1006/meth.2001.1262
39. Shalem O, Sanjana NE, Hartenian E, Shi X, Scott DA, Mikkelson T, et al. Genome-Scale CRISPR-Cas9 Knockout Screening in Human Cells. *Science* (2014) 343 (6166):84–7. doi: 10.1126/science.1247005
40. Song P, Xie Z, Guo L, Wang C, Xie W, Wu Y. Human Genome-Specific Real-Time PCR Method for Sensitive Detection and Reproducible Quantitation of Human Cells in Mice. *Stem Cell Rev Rep* (2012) 8(4):1155–62. doi: 10.1007/s12015-012-9406-3
41. Li W, Xu H, Xiao T, Cong L, Love MI, Zhang F, et al. MAGeCK Enables Robust Identification of Essential Genes From Genome-Scale CRISPR/Cas9 Knockout Screens. *Genome Biol* (2014) 15(12):554. doi: 10.1186/s13059-014-0554-4
42. Xiu B, Chi Y, Liu L, Chi W, Zhang Q, Chen J, et al. LINC02273 Drives Breast Cancer Metastasis by Epigenetically Increasing AGR2 Transcription. *Mol Cancer* (2019) 18(1):187. doi: 10.1186/s12943-019-1115-y
43. Jezequel P, Frenel JS, Campion L, Guerin-Charbonnel C, Gouraud W, Ricolleau G, et al. Bc-GenExMiner 3.0: New Mining Module Computes Breast Cancer Gene Expression Correlation Analyses. *Database (Oxford)* (2013) 2013:bas060. doi: 10.1093/database/bas060
44. Gyorffy B, Lanczky A, Eklund AC, Denkert C, Budczies J, Li Q, et al. An Online Survival Analysis Tool to Rapidly Assess the Effect of 22,277 Genes on Breast Cancer Prognosis Using Microarray Data of 1,809 Patients. *Breast Cancer Res Treat* (2010) 123(3):725–31. doi: 10.1007/s10549-009-0674-9
45. McCahill A, Warwicker J, Bolger GB, Houslay MD, Yarwood SJ. The RACK1 Scaffold Protein: A Dynamic Cog in Cell Response Mechanisms. *Mol Pharmacol* (2002) 62(6):1261–73. doi: 10.1124/mol.62.6.1261
46. Shen S, Feng H, Le Y, Ni J, Yu L, Wu J, et al. RACK1 Affects the Progress of G2/M by Regulating Aurora-A. *Cell Cycle* (2019) 18(18):2228–38. doi: 10.1080/15384101.2019.1642065
47. Wu H, Song S, Yan A, Guo X, Chang L, Xu L, et al. RACK1 Promotes the Invasive Activities and Lymph Node Metastasis of Cervical Cancer*via* galectin-1. *Cancer Lett* (2020) 469:287–300. doi: 10.1016/j.canlet.2019.11.002
48. Duff D, Long A. Roles for RACK1 in Cancer Cell Migration and Invasion. *Cell Signal* (2017) 35:250–5. doi: 10.1016/j.cellsig.2017.03.005
49. Fan Y, Si W, Ji W, Wang Z, Gao Z, Tian R, et al. Rack1 Mediates Tyrosine Phosphorylation of Anxa2 by Src and Promotes Invasion and Metastasis in Drug-Resistant Breast Cancer Cells. *Breast Cancer Res* (2019) 21(1):66. doi: 10.1186/s13058-019-1147-7
50. Dan H, Liu S, Liu J, Liu D, Yin F, Wei Z, et al. RACK1 Promotes Cancer Progression by Increasing the M2/M1 Macrophage Ratio*via* the NF-kappaB pathway in oral squamous cell carcinoma. *Mol Oncol* (2020) 14(4):795–807. doi: 10.1002/1878-0261.12644
51. Cao J, Zhao M, Liu J, Zhang X, Pei Y, Wang J, et al. RACK1 Promotes Self-Renewal and Chemoresistance of Cancer Stem Cells in Human Hepatocellular Carcinoma Through Stabilizing Nanog. *Theranostics* (2019) 9(3):811–28. doi: 10.7150/thno.29271
52. Swaminathan G, Cartwright CA. Rack1 Promotes Epithelial Cell-Cell Adhesion by Regulating E-Cadherin Endocytosis. *Oncogene* (2012) 31 (3):376–89. doi: 10.1038/onc.2011.242
53. Mamidipudi V, Dhillon NK, Parman T, Miller LD, Lee KC, Cartwright CA. RACK1 Inhibits Colonic Cell Growth by Regulating Src Activity at Cell Cycle Checkpoints. *Oncogene* (2007) 26(20):2914–24. doi: 10.1038/sj.onc.1210091
54. Yao F, Long LY, Deng YZ, Feng YY, Ying GY, Bao WD, et al. RACK1 Modulates NF-kappaB Activation by Interfering With the Interaction Between TRAF2 and the IKK Complex. *Cell Res* (2014) 24(3):359–71. doi: 10.1038/cr.2013.162
55. Ron D, Chen CH, Caldwell J, Jamieson L, Orr E, Mochly-Rosen D. Cloning of an Intracellular Receptor for Protein Kinase C: A Homolog of the Beta Subunit of G Proteins. *Proc Natl Acad Sci USA* (1994) 91(3):839–43. doi: 10.1073/pnas.91.3.839
56. Kraus S, Gioeli D, Vomastek T, Gordon V, Weber MJ. Receptor for Activated C Kinase 1 (RACK1) and Src Regulate the Tyrosine Phosphorylation and Function of the Androgen Receptor. *Cancer Res* (2006) 66(22):11047–54. doi: 10.1158/0008-5472.CAN-06-0596
57. Liu YV, Baek JH, Zhang H, Diez R, Cole RN, Semenza GL. RACK1 Competes With HSP90 for Binding to HIF-1alpha and Is Required for O(2)-Independent and HSP90 Inhibitor-Induced Degradation of HIF-1alpha. *Mol Cell* (2007) 25(2):207–17. doi: 10.1016/j.molcel.2007.01.001
58. Li Y, Sun X, Gao D, Ding Y, Liu J, Chen J, et al. Dual Functions of Rack1 in Regulating Hedgehog Pathway. *Cell Death Differ* (2020) 27(11):3082–96. doi: 10.1038/s41418-020-0563-7
59. Liu B, Wang C, Chen P, Wang L, Cheng Y. RACK1 Promotes Radiation Resistance in Esophageal Cancer *Via* Regulating AKT Pathway and Bcl-2 Expression. *Biochem Biophys Res Commun* (2017) 491(3):622–8. doi: 10.1016/j.bbrc.2017.07.153
60. Dolcet X, Llobet D, Pallares J, Matias-Guiu X. NF-kB in Development and Progression of Human Cancer. *Virchows Arch* (2005) 446(5):475–82. doi: 10.1007/s00428-005-1264-9
61. Khongthong P, Roseweir AK, Edwards J. The NF-KB Pathway and Endocrine Therapy Resistance in Breast Cancer. *Endocr Relat Cancer* (2019) 26(6):R369–80. doi: 10.1530/ERC-19-0087

62. Gaptulbarova KA, Tsyganov MM, Pevzner AM, Ibragimova MK, Litviakov NV. NF-kB as a Potential Prognostic Marker and a Candidate for Targeted Therapy of Cancer. *Exp Oncol* (2020) 42(4):263–9.
63. Zinatizadeh MR, Schock B, Chalbatani GM, Zarandi PK, Jalali SA, Miri SR. The Nuclear Factor Kappa B (NF-kB) Signaling in Cancer Development and Immune Diseases. *Genes Dis* (2021) 8(3):287–97. doi: 10.1016/j.gendis.2020.06.005
64. Kaushik S, Cuervo AM. The Coming of Age of Chaperone-Mediated Autophagy. *Nat Rev Mol Cell Biol* (2018) 19(6):365–81. doi: 10.1038/s41580-018-0001-6
65. Juste YR, Cuervo AM. Analysis of Chaperone-Mediated Autophagy. *Methods Mol Biol* (2019) 1880:703–27. doi: 10.1007/978-1-4939-8873-0_47
66. Rios J, Sequeida A, Albornoz A, Budini M. Chaperone Mediated Autophagy Substrates and Components in Cancer. *Front Oncol* (2020) 10. doi: 10.3389/fonc.2020.614677
67. Cuervo AM, Wong E. Chaperone-Mediated Autophagy: Roles in Disease and Aging. *Cell Res* (2014) 24(1):92–104. doi: 10.1038/cr.2013.153
68. Hou T, Fan Y, Dan W, Liu B, Wang Z, Zeng J, et al. Chaperone-Mediated Autophagy in Cancer: Advances From Bench to Bedside. *Histol Histopathol* (2020) 35(7):637–44. doi: 10.14670/HH-18-202

Conflict of Interest: The authors declare that the research was conducted in the absence of any commercial or financial relationships that could be construed as a potential conflict of interest.

Publisher's Note: All claims expressed in this article are solely those of the authors and do not necessarily represent those of their affiliated organizations, or those of the publisher, the editors and the reviewers. Any product that may be evaluated in this article, or claim that may be made by its manufacturer, is not guaranteed or endorsed by the publisher.

frontiers | Frontiers in Oncology

TYPE Original Research
PUBLISHED 06 December 2022
DOI 10.3389/fonc.2022.842205

OPEN ACCESS

EDITED BY
Yusuke Suenaga,
Chiba Cancer Center, Japan

REVIEWED BY
Kiyohiro Ando,
Saitama Cancer Center, Japan
Kazuhiro Murakami,
Kanazawa University, Japan

*CORRESPONDENCE
Shifeng Xu
shifengxu2008@163.com

†These authors have contributed equally to this work

SPECIALTY SECTION
This article was submitted to Molecular and Cellular Oncology, a section of the journal Frontiers in Oncology

RECEIVED 23 December 2021
ACCEPTED 04 November 2022
PUBLISHED 06 December 2022

CITATION
Zhang Z, Wang X, Nie P, Qin Y, Shi J and Xu S (2022) DEPDC1B promotes development of cholangiocarcinoma through enhancing the stability of CDK1 and regulating malignant phenotypes.
Front. Oncol. 12:842205.
doi: 10.3389/fonc.2022.842205

DEPDC1B promotes development of cholangiocarcinoma through enhancing the stability of CDK1 and regulating malignant phenotypes

Zhenhai Zhang[1†], Xinxing Wang[1†], Peihua Nie[2], Yejun Qin[3], Junping Shi[4] and Shifeng Xu[1*]

[1]Department of Hepatobiliary Surgery, Shandong Provincial Hospital Affiliated to Shandong First Medical University, Jinan, Shandong, China, [2]Department of Ophthalmology and Otorhinolaryngology, Shandong Provincial Third hospital, Jinan, Shandong, China, [3]Department of Pathology, Shandong Provincial Hospital Affiliated to Shandong First Medical University, Jinan, Shandong, China, [4]Medical Department, OrigiMed, Shanghai, China

Cholangiocarcinoma (CCA) is the second most common primary tumor of the hepatobiliary system. At present, the therapeutic efficiency of cholangiocarcinoma is fairly low and the prognosis is poor. The root cause is that the molecular mechanism of the occurrence and development of CCA is largely unclear. This work intended to clarify the role of DEP domain-containing protein 1B (DEPDC1B) in the progress of CCA through cellular biology research strategies and further clarify the molecular mechanism of CCA. Clinical tissue-related detection showed that the expression level of DEPDC1B in tumor tissues was significantly higher than that in normal tissues and was positively correlated with tumor grade. Knockdown of the endogenous DEPDC1B of CCA cells can significantly inhibit cell proliferation and migration, while promoting cell apoptosis and blocking the cell cycle. DEPDC1B overexpression induced the opposite effects. Studies in animal models also showed that the downregulation of DEPDC1B can reduce the tumorigenicity of CCA cells. In addition, through gene profiling analysis and molecular biology studies, we found that CDK1 may be an important downstream mediator of DEPDC1B, the protein stability of which was significantly decreased through the ubiquitin–proteasome system in DEPDC1B knockdown cells. Moreover, knockdown of CDK1 can weaken the promotion of CCA caused by DEPDC1B overexpression. In summary, our research showed that DEPDC1B plays an important role in the development of CCA and its targeted inhibition may become one of the important methods to inhibit the progress of CCA.

KEYWORDS

cholangiocarcinoma, DEPDC1B, CDK1, tumor promotor, ubiquitination

Introduction

Cholangiocarcinoma (CCA) is the most common invasive malignancy, originating from the biliary system and involving the intrahepatic, perihepatic, and distal bile ducts (1–3). Due to the heterogeneity and origin of CCA, it can be simply divided into intrahepatic CCA (iCCA) and extrahepatic CCA (eCCA) according to the location (4). Globally, the incidence of iCCA showed an annual growth trend of 4%, whereas the incidence of eCCA remained largely unchanged (5). Although surgery is the preferred treatment for all disease subtypes, only a small number of patients (approximately 35%) can undergo effective surgical excision (2, 6). For patients with advanced or unresectable CCA, the standard treatment options available are gemcitabine and cisplatin (7). However, the treatment effectiveness of CCA is limited, and the median overall survival is usually less than 1 year (8). Fortunately, the genetic pattern of each subtype of CCA was gradually determined with the development of comprehensive exome and transcriptome sequencing (9). Therefore, a deeper understanding of the molecular mechanism of cholangiocarcinoma is an indispensable part of the establishment of accurate medical treatment. In particular, promising molecular targets for precision medicine deserve further exploration.

DEPDC1B (DEP domain-containing protein 1B) is a 61-kDa protein encoded by 529 amino acids on human chromosome 5q12, containing an N-terminal DEP domain and a C-terminal Rho-GAP (GTPase-activated protein)-like domain (10). The DEP domain is a spherical domain of about 90 amino acids, which mediates the localization of the cell membrane and the determination of cell polarity (11, 12). The Rho-GAP domain is involved in transduction of the Rho GTPase signal and regulation of cell growth, cell movement, cell differentiation, cytoskeleton reorganization, and cell cycle (13). DEPDC1B has an unstable expression in the procession of cell cycle and accumulates to the peak in the G2 phase, whose function is similar to that of cell-cycle regulator cyclin B (10). Moreover, accumulating evidence demonstrated that DEPDC1B is overexpressed in diverse types of cancers such as non-small cell lung cancer, oral cancer, prostate cancer, soft tissue sarcoma, cervical cancer, and malignant melanoma (14–19). For example, knockdown of DEPDC1B inhibits the cellular behavior of malignant melanoma by slowing cell proliferation and inducing apoptosis (19). Analogously, downregulation of DEPDC1B can hinder the progression of glioblastoma (20). In addition, DEPDC1B promotes the migration and invasion of pancreatic cancer through the Rac1/PAK1-LIMK1-Cofilin1 signal pathway (21). Furthermore, DEPDC1B is recognized as a key regulator of mouse and human myoblast proliferation (22). On the other hand, DEPDC1B is identified as a new diagnostic and prognostic biomarker of hepatocellular carcinoma and prostate cancer, which has significant clinical value (23, 24). However, the biological function and potential mechanism of DEPDC1B in CCA is still a mystery.

In this study, the level of DEPDC1B in CCA was detected through immunohistochemistry analysis, showing that 1) the expression of DEPDC1B in CCA tissues is observably higher than in normal tissues and 2) CCA tissues with a more advanced malignant grade tend to express a higher DEPDC1B level. More evidence proving the promotion of CCA by DEPDC1B was provided by further biological studies, which displayed that DEPDC1B depletion could disturb the proliferation and migration capability of CCA cells while inducing cell apoptosis by regulating apoptosis- or epithelial–mesenchymal transition (EMT)-related proteins. Moreover, the inhibited tumorigenicity of CCA cells by DEPDC1B knockdown was also manifested *in vitro* by colony formation assay and *in vivo* by mouse xenograft models. The exploration of downstream mechanisms further recognized the involvement of CDK1, which is a critical regulatory factor in cell cycle and a well-known tumor promotor, in DEPDC1B-induced promotion of CCA. These results indicated the essential role of DEPDC1B in the development of CCA, which may act as an effective therapeutic target in the development of targeted drugs against CCA.

Material and methods

Cell lines and cell culture

Human cholangiocarcinoma cell lines HCCC-9810, QBC939, HUCCT1, and RBE were purchased from Hangzhou Bena Technology. Cells were cultured in 90% RPMI-1640 containing 10% FBS. All cells were grown in an incubator at 37°C with 5% CO_2.

Immunohistochemistry analysis and Ki-67 immunostaining

CCA tissue microarray (TMA, Cat. #GA802, Xian Alenabio Co., Ltd.) images of 78 spots were taken from 73 patients with cholangiocarcinoma, including 41 patients with eCCA, 27 patients with iCCA, and five patients with intrahepatic bile duct tissue. Related information and written informed consent were also provided. The experiment was approved by the Ethics Committee of Shandong Provincial Hospital. For immunohistochemistry (IHC) staining, sections were incubated with primary anti-DEPDC1B (Cat. #bs-14356R, BIOSS) at 4°C overnight. A secondary antibody was added and incubated for 2 h at room temperature. The tissue microarrays were stained with diaminobenzidine and examined under a microscope with ×200 and ×400 objective. IHC scoring of specimens was classified into four categories based on the sum of the staining intensity (varied from weak to strong) and staining extent scores, graded as 0 (0%), 1 (1%–25%), 2 (26%–50%), 3 (51%–75%), or 4 (76%–100%).

For Ki-67 immunostaining, slides were incubated with antibody to Ki-67 (Cat. #Ab16667, Abcam) and the secondary antibody and stained with hematoxylin and eosin (Cat. #BA4041, BA4022, Baso). Stained slides were examined with a microscope. All antibodies used in IHC are listed in Table S1.

Human apoptosis antibody array

Detection of related genes in the human apoptosis signaling pathway was performed using Human Apoptosis Antibody Array (R&D Systems) following the manufacturer's instructions. Briefly, the transfected HCCC-9810 were collected, washed, and then lysed with lysis buffer and total proteins were extracted. Protein concentrations were measured using the BCA Protein Assay Kit (HyClone-Pierce). Each array antibody membrane was blocked, then incubated with protein samples (0.5 mg/ml) overnight at 4°C and continuously incubated with an HRP-linked streptavidin conjugate for 1 h. Enhanced chemiluminescence (ECL) (Amersham) was used for visualizing and signaling the spots.

Construction of stable knockdown and overexpressed cells and transfection

Full-length human DEPDC1B and SMURF1 complementary DNA was amplified by PCR and cloned into a lentivirus vector (Shanghai Biosciences) for gene overexpression. Lentiviruses expressing shDEPDC1B or shCDK1 and shCtrl or empty vectors were purchased from Shanghai Biosciences, Co., Ltd. Designed sequences for DEPDC1B and CDK1 are detailed in Table S2. HCCC-9810 and QBC939 were chosen to establish stable DEPDC1B knockdown models, whereas HUCCT1 cells were used for stable DEPDC1B or CDK1 knockdown, stable DEPDC1B overexpression, and CDK1 knockdown experiments. Cells (2×10^5) at 80% confluence were seeded into six-well dishes, and RNA-expressing BR-V-108 vectors (1×10^8 TU/ml) were added for transfection using Lipofectamine 2000 Reagent (Thermo Fisher Scientific). After culturing for 72 h, cell infection efficiency was evaluated by microscopic fluorescence.

RNA extraction and RT-qPCR

RNA from experiment cells were extracted using TRIzol Reagent (QIAGEN), and the quality of total RNA was evaluated using a NanoDrop 2000 spectrophotometer (Thermo Fisher Scientific) according to the manufacturer's instructions. Total RNA (2.0 μg) was reverse transcribed into cDNA, and quantitative real-time PCR with related primers (shown in Table S3) was conducted using SYBR Green Master Mix Kit (Vazyme) on the Applied Biosystems 7500 Real-Time PCR system. GAPDH was utilized as internal control. A relative quantitative analysis in gene expression data was performed using the $2^{-\Delta\Delta Ct}$ method.

Western blotting assay

For Western blotting (WB) assay, each experiment group's cells were lysed in ice-cold IP lysis buffer and the total proteins were collected. The BCA Protein Assay Kit (HyClone-Pierce) was applied for protein concentrations detection. Equal amounts of proteins (20 μg) were separated by 10% SDS-PAGE (Invitrogen) and transferred onto PVDF membranes. After blocking with TBST solution containing 5% non–fat milk, the membranes were incubated with specific primary antibodies (Table S1) and fluorescently conjugated secondary antibodies, followed by the detection with enhanced chemiluminescence (ECL) (Amersham). The quantification of blots was performed by ImageJ and shown in the following corresponding blots as protein/GAPDH.

For Co-IP, cell lysate was prepared as WB assay, and 1.0–1.2 mg proteins were incubated with normal rabbit IgG (as control) for 2 h, followed by 2 h of incubation with 20-μl protein A/G beads. The cleared protein antibody bead complex was incubated at 100°C for 10 min. Then, the proteins in the immunocomplex were separated by 10% SDS-PAGE as WB assay and used for immunoblotting to identify interacting proteins.

Flow cytometry for apoptosis and cell cycle

Apoptosis and cell cycle were detected using the Annexin V-APC Apoptosis Detection Kit (eBioscience, Cat. #88-8007) and Cell Cycle PI Staining Reagent (Sigma, Cat. #P4170), respectively. Lentivirus transfected cells were inoculated in six-well plates in triplicate and cultured for 5 days until cell confluence reached 85%. After being trypsinized, cells were harvested and stained with 5 μl Annexin V-APC for 15 min in the dark. For cell-cycle detection, cells were collected and stained with propidium Iodide. Apoptosis analysis and cell-cycle distribution were measured using FACSCalibur (BD Biosciences).

Cell proliferation assay

Cell viability was measured using the MTT assay kit (Genview, Cat #JT343). Cells (2,000 cells/well) in the

exponential growth phase were seeded into a 96-well plate. After incubation for 1, 2, 3, 4, and 5 days at 37°C, cells were stained with 20 µl MTT reagent (5 mg/ml) and OD490 values were measured by a microplate reader (Tecan).

Celigo cell counting assay

Transfected HUCCT1 cells were cultured for 72 h, and then the cells were seeded into 96-well plates (2,000 cells/well) and further cultured for 5 days. A Celigo image cytometer (Nexcelom Bioscience) was applied for cell counting for 5 consecutive days, and a cell proliferation curve was drawn.

Wound healing assay

Lentivirus transfected cells were seeded at 5×10^4 cells per well onto 96-well dishes until cell confluence reached 90%. Scratches were made by a 96-wounding replicator (V&P Scientific). Images were captured at 0 and 24 h by a fluorescence microscope and analyzed using ImageJ software for the cell migration rate.

Transwell assay

Migration assays were performed using 24-well plates inserted using an 8-µm-pore-size Transwell filter insert (Cat. #3422, Corning). Transfected HUCCT1 cells (5×10^4 cells/well) were harvested and seeded in the 24-well plate and cultured for 24 h. Medium supplemented with 30% FBS was added in the lower chamber. Non-metastatic cells were removed with a cotton swab, cells within the membrane were fixed with 4% formaldehyde and stained with Giemsa, and the migration ability of cells was analyzed.

GeneChip analysis

Gene expression profiling analysis was completed with Affymetrix GeneChip PrimeView Human Gene Expression Array according to the manufacturer's instruction. Total RNA was extracted using the RNeasy Kit (Sigma). The concentration and values of A260/A280 of total RNA were determined using the NanoDrop 2000 (Thermo Fisher Scientific). The RNA integrity number (RIN) was evaluated with Agilent 2100 and Agilent RNA 6000 Nano Kit (Agilent). Raw data statistical significance assessment was accomplished using a Welch t-test with Benjamini–Hochberg FDR ($|\text{fold change}| \geq 2.0$ and FDR < 0.05 as significant). Significant difference analysis and functional analysis based on Ingenuity Pathway Analysis (IPA) (Qiagen) were executed.

In vivo tumorigenicity assay

Our animal study was reviewed and approved by the Ethics Committee of Shandong Provincial Hospital and performed at the Animal Center of Provincial Hospital Affiliated to Shandong First Medical University. Four-week-old BALB/c female nude mice were purchased from Beijing Vital River Laboratory Animal Technology Co., Ltd., and housed at 22°C with a 12-h light/dark cycle-controlled condition. For *in vivo* tumor formation, 0.2 ml stably expressing shDEPDC1B or shCtrl HUCCT1 cell suspension with a density of 2×10^7 cells/ml was subcutaneously injected into 20 mice (randomly divided into shDEPDC1B group and shCtrl group). The growth of tumor was monitored, and tumor volume was recorded around 1 month later using L and W (L represents the longest dimension and W means the dimension perpendicular to length) and calculated as $\pi/6 \times L \times W^2$. Tumor volume was calculated two to three times weekly. Pentobarbital sodium was used as the anesthetics. Bioluminescence imaging by the IVIS Spectrum Imaging System (Perkin Elmer) was performed. Then, mice were sacrificed and the tumor tissues were removed for Ki-67 immunostaining.

Statistical analysis

Data are expressed as the mean ± SD, and all statistical analysis was performed using SPSS 17.0 (IBM) or GraphPad Prism 6.01 (GraphPad Software). *P*-values were determined using Student's T-test or one-way ANOVA. The DEPDC1B expression difference between cholangiocarcinoma tissues and adjacent normal tissues was analyzed with rank-sum test analysis. The relation of DEPDC1B expression and tumor characteristics in cholangiocarcinoma patients was analyzed with Mann–Whitney U analysis and Spearman rank correlation analysis. $P < 0.05$ was considered statistically significant.

Results

DEPDC1B was upregulated in CCA tissues and highly expressed in CCA cells

We aimed to explore the role of DEPDC1B in CCA. First, IHC analysis was used to reveal differences in the expression of DEPDC1B between CCA tissues and normal tissues; these analyses indicated the upregulated expression of DEPDC1B in CCA (Figure 1A). The statistical analysis of expression data collected from 73 CCA tissues and five normal tissues also highlighted the significantly higher expression levels of DEPDC1B in CCA ($P < 0.001$, Table 1). A correlation analysis between DEPDC1B expression and the clinical parameters of

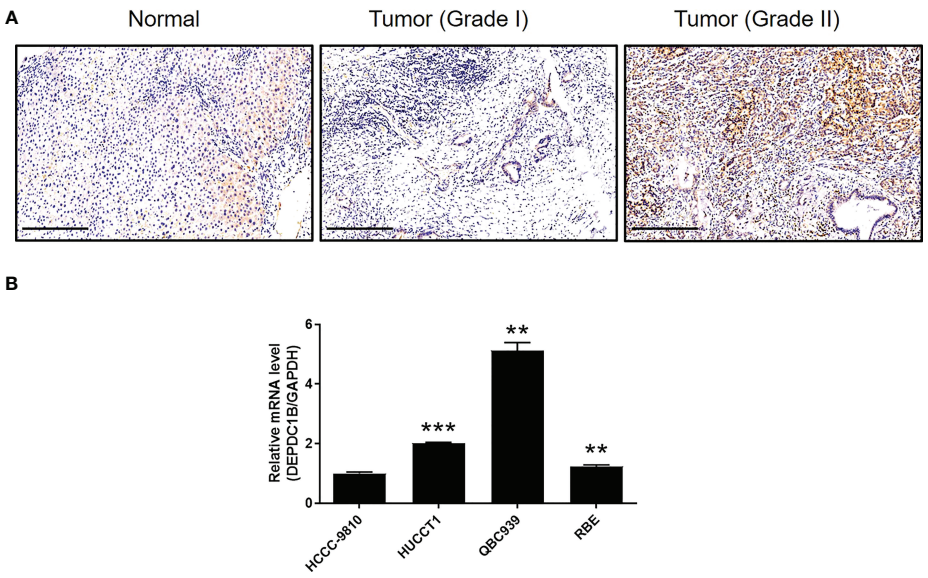

FIGURE 1
DEPDC1B was upregulated in CCA tissues and expressed in CCA cells. **(A)** The expression level of DEPDC1B was detected by IHC analysis in CCA tissues and normal tissues (scale bar = 250 μm). **(B)** The mRNA expression of DEPDC1B in HCCC-9810, HUCCT1, QBC939, and RBE cell lines was detected by qPCR. Data were shown as mean ± SD (n = 3). $^{**}P < 0.01$, $^{***}P < 0.001$.

patients with CCA revealed that DEPDC1B expression was significantly upregulated in patients with a more advanced tumor grade ($P < 0.05$, Figure 1A and Table 2); these findings were further verified by Spearman rank correlation analysis (Table S4). Collectively, the higher expression levels of DEPDC1B in more serious cases of CCA suggested the potential role of DEPDC1B in the promotion of CCA. In addition, the endogenous expression of DEPDC1B in CCA cell lines including HCCC-9810, HUCCT1, QBC939, and RBE was detected by qPCR, exhibiting the expression of DEPDC1B in all cell lines (Figure 1B).

The depletion of DEPDC1B inhibited the development of CCA *in vitro*

We constructed a cell model of DEPDC1B deficiency by designing lentiviral vectors to silence DEPDC1B and thus allow us to investigate the role of this protein in CCA. Fluorescence signals were observed in >80% of cells, thus providing evidence of a successful transfection (Figure S1). Moreover, the significant downregulation of DEPDC1B mRNA and protein levels was demonstrated by qPCR ($P < 0.001$) and Western blotting (Figures 2A, B), respectively, thus confirming the successful knockdown of DEPDC1B in both HCCC-9810 and QBC939 cells. MTT assays further showed that cells in which DEPDC1B had been depleted (shDEPDC1B) grew significantly slower than those without DEPDC1B depletion (shCtrl) ($P < 0.001$, Figure 2C). Apoptosis is another key factor in cell proliferation; we used flow cytometry to determine cell apoptosis in CCA cells with or without DEPDC1B knockdown. As expected, cells with DEPDC1B deficiency exhibited a significantly larger population of apoptotic cells than the shCtrl group ($P < 0.001$, Figure 2D). Analysis of the cell-cycle distribution demonstrated that the downregulation of DEPDC1B in HCCC-9810 and QBC939 cells led to cell-cycle

TABLE 1 Expression patterns of DEPDC1B in CCA tissues and normal tissues revealed in immunohistochemistry analysis.

DEPDC1B expression	Tumor tissue		Normal tissue	
	Cases	Percentage	Cases	Percentage
Low	31	42.5%	5	100%
High	42	57.5%	0	–

P < 0.001.

TABLE 2 Relationship between DEPDC1B expression and tumor characteristics in patients with CCA.

Features	No. of patients	DEPDC1B expression		*P* value
		Low	High	
All patients	73	31	42	
Age (years)				0.381
<59	35	13	22	
≥59	38	18	20	
Gender				0.593
Male	38	15	23	
Female	35	16	19	
Grade				<0.001
I	10	9	1	
II	37	18	19	
III	22	3	19	
Lymphatic metastasis (N)				0.652
N0	57	25	32	
N1	16	6	10	
T Infiltrate				0.073
T1	6	4	2	
T2	34	16	18	
T3	30	11	19	
T4	3	0	3	

arrest in the G2 phase ($P < 0.001$, Figure 2E). In order to further investigate the mechanism underlying the ability of DEPDC1B to regulate cell apoptosis, we performed an antibody array to identify apoptosis-related proteins that exhibit interactions with DEPDC1B. We demonstrated that DEPDC1B depletion induced the upregulated expression of Caspase3, p21, p27, and p53 and the downregulation of IGF-I, IGF-II, Survivin, sTNF-R1, TNF-β, and XIAP (Figure 2F). We also used wound-healing assays to demonstrate the reduced mobility of HCCC-9810 and QBC939 cells in the shDEPDC1B group ($P < 0.001$, Figure 2G); this reduction was associated with the upregulation of E-cadherin and the downregulation of N-cadherin and Vimentin (Figure 2H). Collectively, these data suggested that DEPDC1B plays a vital role in the development of CCA by regulating cell proliferation and cell apoptosis. Moreover, CCA cell migration was influenced by DEPDC1B through the regulation of epithelial–mesenchymal transition-related proteins.

DEPDC1B knockdown suppressed tumor growth *in vivo*

We constructed and maintained a mouse model by injecting HUCCT1 cells, which possessed the highest efficiency in tumorigenesis *in vivo*, with or without a DEPDC1B knockdown vector. *In vivo* bioluminescence imaging revealed a significantly weaker total bioluminescence intensity, as well as a smaller tumor burden, in the shDEPDC1B group ($P < 0.001$, Figures 3A, B). Moreover, the smaller volume and weight of the solid tumors in the shDEPDC1B group also suggested that tumor growth slowed down when DEPDC1B was silenced ($P < 0.01$, Figures 3C–E). Furthermore, we observed a lower Ki67 index, as well as lower proliferative activity, in the tumors removed from mice in the shDEPDC1B group (Figure 3F). Furthermore, TUNEL analysis suggested that apoptosis of xenografts was much stronger in shDEPDC1B groups than in the control group (Figure 3G).

DEPDC1B may regulate CCA by targeting CDK1

Given the clear regulatory role of DEPDC1B in CCA, we next attempted to identify the mechanisms underlying this effect. We conducted 3 v 3 RNA-seq to identify differentially expressed genes (DEGs) between cells in the shDEPDC1B group and the shCtrl group of HCCC-9810 cells. Based on a threshold of simultaneous $|\text{fold change}| \geq 2$ and a FDR < 0.05 (the *P* value after Benjamini–Hochberg analysis), we identified 319 DEGs that were upregulated in shDEPDC1B cells compared with shCtrl cells and 828 DEGs that were downregulated (Figure S2A, Figure 4A). The enrichment of all 1,147 DEGs in canonical signaling pathways, or IPA disease and function, was assessed by

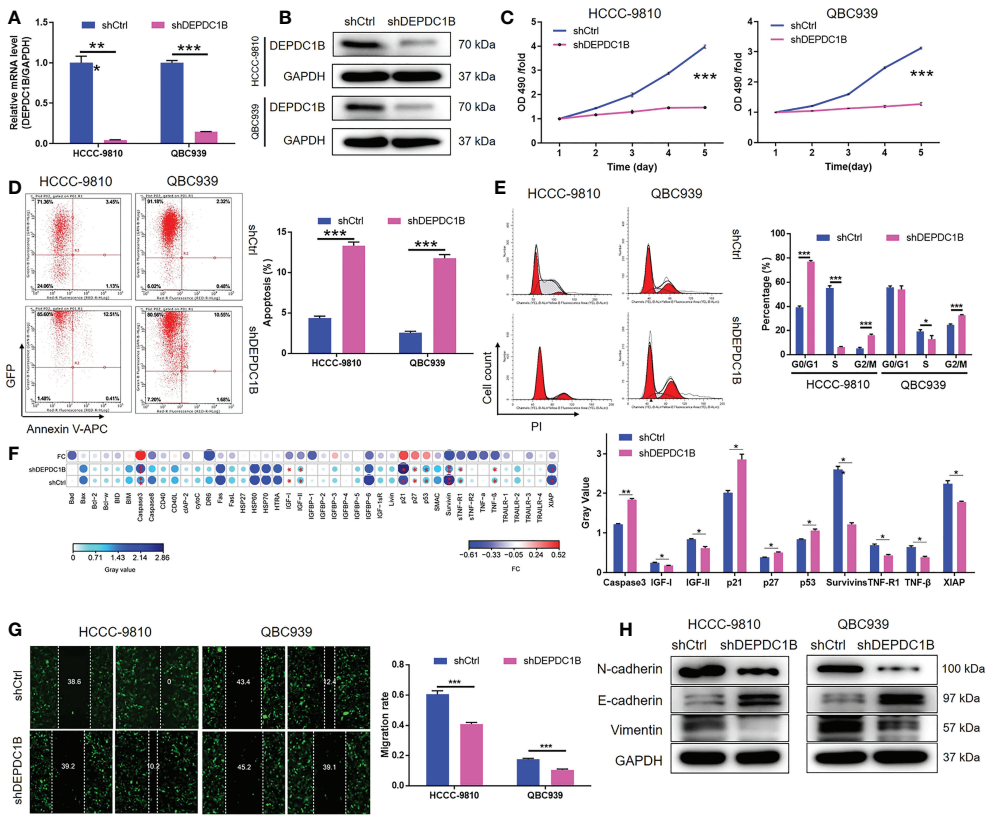

FIGURE 2
DEPDC1B knockdown inhibited CCA development *in vitro*. **(A, B)** Cell models with or without DEPDC1B knockdown were constructed by transfecting shDEPDC1B or shCtrl. The knockdown efficiency of DEPDC1B in HCCC-9810 and QBC939 cells was assessed by qPCR **(A)** and Western blotting **(B)**. **(C)** MTT assay was employed to show the effects of DEPDC1B on cell proliferation of HCCC-9810 and QBC939 cells. **(D)** Flow cytometry was performed to detect the cell apoptosis of HCCC-9810 and QBC939 cells with or without DEPDC1B knockdown. **(E)** Cell-cycle distribution was estimated in HCCC-9810 and QBC939 cells with or without DEPDC1B knockdown. **(F)** Human Apoptosis Antibody Array was performed to detect and compare the expression of apoptosis-related proteins in HCCC-9810 cells with or without DEPDC1B knockdown. **(G)** The effects of DEPDC1B on the cell migration ability of HCCC-9810 and QBC939 cells were evaluated by wound healing assay. **(H)** Western blotting was performed to show the effects of DEPDC1B knockdown on expression of EMT-related proteins. The representative images were selected from at least three independent experiments. Data were shown as mean ± SD (n = 3). $^{*}P < 0.05$, $^{**}P < 0.01$, $^{***}P < 0.001$.

IPA (Figures 4B, C). Based on bioinformatics and IPA of the DEPDC1B-associated interaction network built on the known interaction between related molecules (Figures 4B–E), several DEGs with the highest fold change in expression were subjected to verification by qPCR and Western blotting in HCCC-9810 and QBC939 cells (Figures S2B, 4D and S2C). Of these, CDK1, a key member of the cyclin and cell-cycle regulation pathway, was considered to be a promising candidate as the target for DEPDC1B. Notably, the expression of CDK1 showed a similar expression pattern as DEPDC1B in CCA tissues in that higher expression levels were observed in CCA tissues than in normal tissues (Figure 4F). The abundant expression of CDK1 in CCA cells was also demonstrated by qPCR (Figure 4G). Collectively, these data indicated that CDK1 may represent a potential target for DEPDC1B during the regulation of CCA.

DEPDC1B may regulate CDK1 expression through the ubiquitin–proteasome system

Although the mechanism by which DEPDC1B regulates CDK1 on the RNA level is still unclear, we unexpectedly found that DEPDC1B knockdown could distinctly decrease the protein stability of CDK1 in HUCCT1 cells (Figure 5A), in which the treatment of cycloheximide (CHX) blocked the biosynthesis of proteins. Based on these, we proposed that DEPDC1B may regulate the protein level of CDK1 through the ubiquitin–proteasome system, which plays an important role in the degradation of endogenous proteins. Through the application of UbiBrowser (http://ubibrowser.ncpsb.org.cn/ubibrowser/home/index), CDK1 was predicted as a substrate

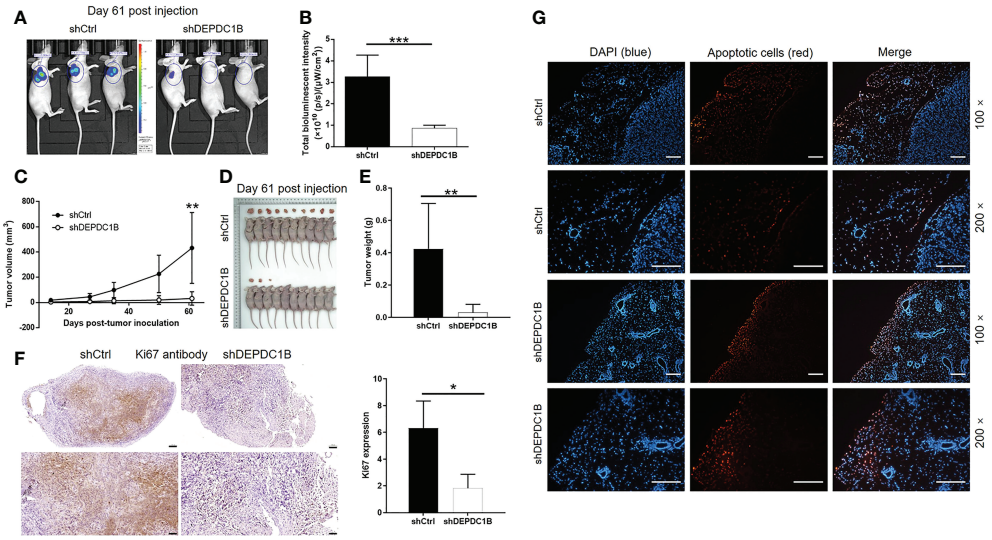

FIGURE 3
DEPDC1B knockdown inhibited CCA development *in vivo*. **(A, B)** *In vivo* imaging was performed to evaluate the tumor burden in mice of shDEPDC1B and shCtrl groups at day 61 post tumor inoculation. **(C)** Fourteen days post injection of HUCCT1 cells with or without DEPDC1B knockdown, the volume of tumors formed in mice was measured and calculated at indicated time intervals. **(D, E)** Mice were sacrificed at day 61 post injection, and the tumors were removed for collecting photos **(D)** and weighing **(E)**. **(F)** The expression of Ki67 in sections of xenografts was detected by IHC analysis (scale bar = 100 μm). **(G)** TUNEL analysis was performed in xenografts of shDEPDC1B and shCtrl groups (scale bar = 200 μm). Data were shown as mean ± SD (n = 3). $^{*}P < 0.05$, $^{**}P < 0.01$, $^{***}P < 0.001$.

of E3 ligase SMURF1 (Figure 5B). Indeed, the overexpression of SMURF1 could also decline the protein stability of CDK1 (Figure 5C). Moreover, the regulatory effects of DEPDC1B knockdown and SMURF1 overexpression on CDK1 protein level could be partially eliminated by the treatment of MG132, a proteasome inhibitor, indicating the potential involvement of the ubiquitin–proteasome system (Figure 5D). Accordingly, we revealed that knockdown of DEPDC1B could actually enhance the ubiquitination of CDK1 (Figure 5E). Therefore, we believed that DEPDC1B could upregulate the expression of CDK1 through inhibiting its ubiquitination as well as enhancing its protein stability, which may be resulted from the interaction between DEPDC1B and SMURF1 (Figure 5F). In addition, we also made some attempts to explore the underlying mechanism by which DEPDC1B regulates the SMURF1-mediated ubiquitination of CDK1. On the one hand, it was demonstrated that DEPDC1B knockdown/overexpression could downregulate/upregulate the mRNA and protein levels of SMURF1 in HUCCT1 cells (Figure S3). On the other hand, a series of immunoprecipitation assays showed that overexpression of DEPDC1B could apparently prevent the interaction between SMURF1 and CDK1 (Figure 5G), which was promoted by DEPDC1B knockdown (Figure 5H). Collectively, we believe that DEPDC1B may regulate the protein level of CDK1 through influencing SMURF1-mediated protein ubiquitination.

CDK1 knockdown blocked the development of CCA *in vitro*

In order to identify the role of CDK1 in the development of CCA, we carried out a range of functional experiments following the construction of HUCCT1 cells in which CDK1 had been knocked down by lentivirus-delivered shCDK1–3 (Figure S4). Transfection and knockdown efficiencies were evaluated by a combination of fluorescence imaging, qPCR, and Western blotting ($P < 0.001$, Figures S5 and S6A). Celigo cell counting assays indicated that the growth of HUCCT1 cells transfected with shCDK1 slowed down significantly whereas cells that had been transfected with shCtrl grew normally ($P < 0.01$, Figure S6B). We also counted the number of colonies formed by cells after 14 days of culture; there was a significant difference between the shCDK1 group (fewer colonies) and the shCtrl group (more colonies) ($P < 0.001$, Figure S6C). The effects of CDK1 knockdown on cell apoptosis were also similar to those induced by DEPDC1B knockdown; the proportion of apoptotic cells in the shCDK1 group increased by approximately 14-fold ($P < 0.001$, Figure S6D). Finally, wound-healing assays and Transwell assays showed that HUCCT1 cells in which CDK1 had been knocked down were significantly less motile ($P < 0.001$, Figures S6E, F). In summary, CDK1 exhibited similar regulatory effects on the development of CCA with DEPDC1B; however, the association between CDK1 and DEPDC1B remains unclear.

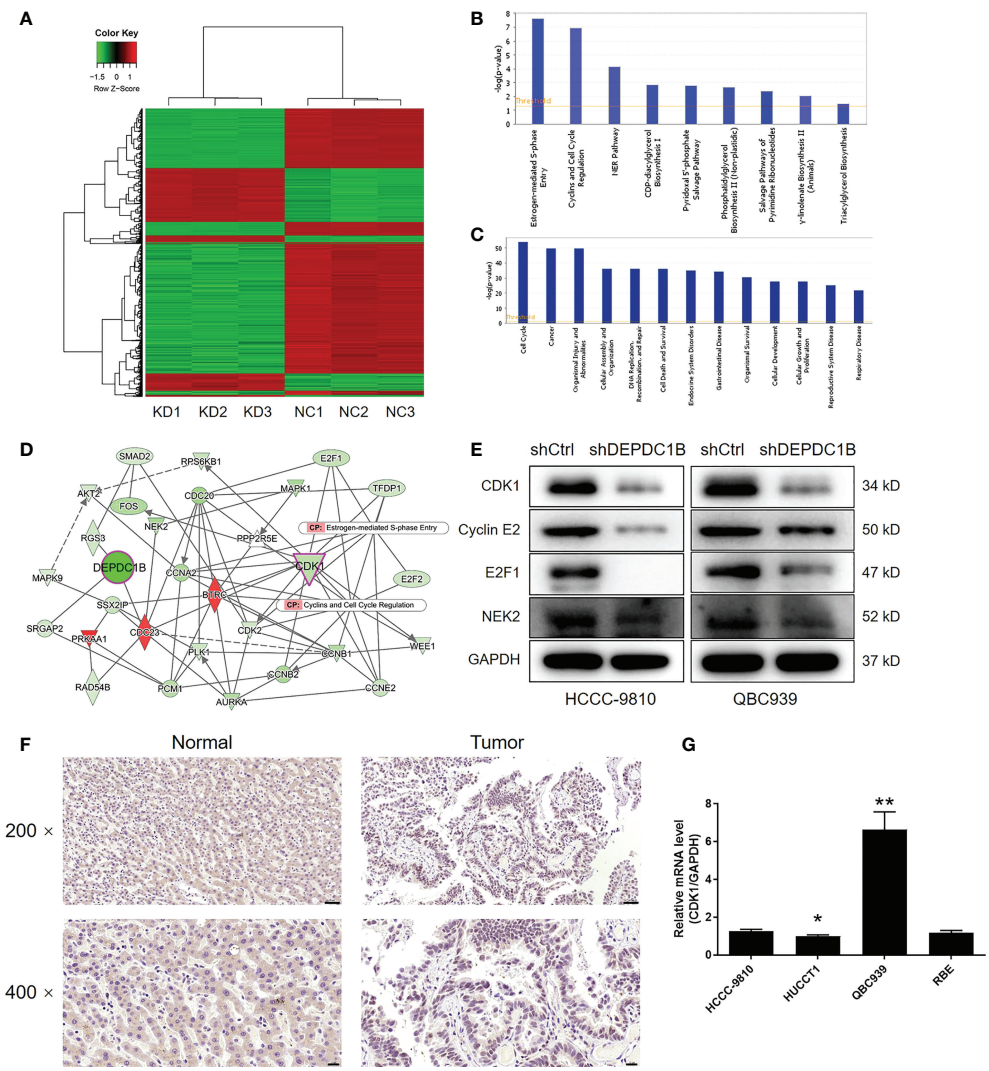

FIGURE 4
The exploration and verification of downstream underlying DEPDC1B-induced regulation of CCA. **(A)** A PrimeView Human Gene Expression Array was performed to identify the differentially expressed genes (DEGs) between the shDEPDC1B and shCtrl groups of HCCC-9810 cells. **(B, C)** The enrichment of DEGs in the canonical signaling pathway **(B)** and IPA disease and function **(C)** was analyzed by IPA. **(D)** A DEPDC1B-associated interaction network constructed by IPA revealed the potential linkage between DEPDC1B and CDK1. **(E)** Western blotting was used to detect the expression of several selected DEGs in HCCC-9810 and QBC939 cells with or without DEPDC1B knockdown. **(F)** The expression of CDK1 in CCA tissues and normal tissues was evaluated by IHC analysis (scale bar = 50 μm for ×200, 20 μm for ×400). **(G)** The mRNA expression of CDK1 in HUCCT1, QBC939, RBE. and HCCC-9810 cell lines was detected by qPCR. The representative images were selected from at least three independent experiments. Data were shown as mean ± SD (n = 3). *$P < 0.05$, **$P < 0.01$.

CDK1 knockdown alleviated the regulatory effects of DEPDC1B overexpression on CCA

Next, we constructed HUCCT1 cells that overexpressed DEPDC1B and cells that overexpressed DEPDC1B but in which CDK1 had been knocked down. These cell groups were then used to investigate the synergistic effects of DEPDC1B and CDK1 on CCA. The transfection of HUCCT1 cells by DEPDC1B overexpression plasmids (Figure S7A) led to a significant upregulation of DEPDC1B ($P < 0.001$, Figures S7B, C) and a significantly faster rate of cell proliferation ($P < 0.001$, Figure 6A). We also found that the overexpression of DEPDC1B promoted the formation of colonies ($P < 0.001$, Figure 6B). Interestingly, we failed to observe the expected inhibition of cell apoptosis; this may have been attributed to the low apoptosis rate in the shCtrl group (Figure 6C). Furthermore, the overexpression of DEPDC1B promoted cell motility in HUCCT1 cells, as demonstrated by wound healing and

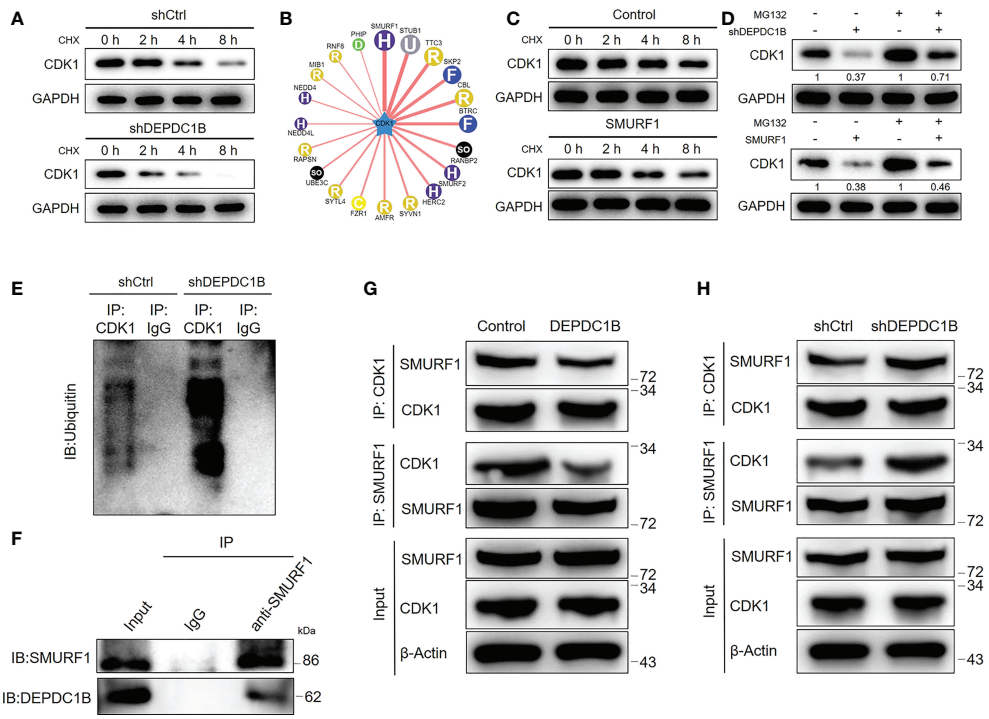

FIGURE 5
DEPDC1B regulates CDK1 expression through the ubiquitin–proteasome system. **(A)** The protein level of CDK1 was detected in shCtrl and shDEPDC1B HUCCT1 cells upon the treatment of cyclohexane (CHX) for indicated times. **(B)** The UbiBrowser online tool was used for predicting the E3 ligase of CDK1. **(C)** The protein level of CDK1 was detected in HUCCT1 cells with or without SMURF1 overexpression upon the treatment of cyclohexane (CHX) for indicated times. **(D)** The regulatory effects of the CDK1 protein level by DEPDC1B knockdown or SMURF1 overexpression were evaluated with or without treatment of proteasome inhibitor MG132. **(E)** An immunoprecipitation assay was performed for assessing the ubiquitination modification of CDK1 in shCtrl and shDEPDC1B HUCCT1 cells. **(F)** The interaction between DEPDC1B and SMURF1 was detected and verified by a co-immunoprecipitation assay using the IgG or SMURF1 antibody for obtaining a protein complex. **(G, H)** Total lysates of CCA cells with or without DEPDC1B overexpression **(G)** or DEPDC1B knockdown **(H)** were subjected to immunoprecipitation using anti-CDK1 or anti-SMURF1, followed by Western blotting analysis using indicated antibodies. All groups of cells were treated with MG132 to inhibit the function of proteasome.

Transwell assays ($P < 0.001$, Figures 6D, E). A comparative analysis of results produced by the DEPDC1B group (DEPDC1B overexpression) and the DEPDC1B+shCDK1 group (DEPDC1B overexpression + CDK1 knockdown) demonstrated that the effects of DEPDC1B overexpression on cell proliferation, colony formation, cell apoptosis, and cell migration could all be alleviated or even reversed by the knockdown of CDK1 ($P < 0.001$, Figures S8 and 6A–E). These results clearly indicate the effects of DEPDC1B overexpression on CCA and suggest that CDK1 may be involved.

Discussion

Herein, we presented the first study reporting the role of DEPDC1B in CCA. In this study, it was found that DEPDC1B expression was higher in CCA tissues than in normal tissues, or in CCA tissues with a more advanced tumor grade, showing the potential participation of DEPDC1B in CCA development. The role of DEPDC1B was also proved by the subsequent *in vitro* investigation of the cell phenotype, which indicated the inhibition of cell proliferation, cell migration, the facilitation of cell apoptosis, and the arrest of cell cycle in the G2 phase. The simulation of *in vivo* CCA growth in the xenograft animal models further demonstrate the DEPDC1B knockdown-induced suppression of tumor growth.

A human apoptosis antibody array was utilized to explore how DEPDC1B regulates cell apoptosis and identified a variety of apoptosis-related proteins that are changed by DEPDC1B. For example, the shDEPDC1B group of CCA cells expressed a much lower level of Caspase3, an essential participator in cell apoptosis (25). Similarly, the suppression of cell apoptosis of CCA by DEPDC1B knockdown may also result from the downregulation of Survivin, which is a new member of the anti-apoptotic protein family (26). Meanwhile, some other apoptosis-associated factors such as IGF-I and IGF-II were also regulated by DEPDC1B. Otherwise, it has been well documented that EMT, which is an important biological process in development, specifically

10.3389/fonc.2022.842205

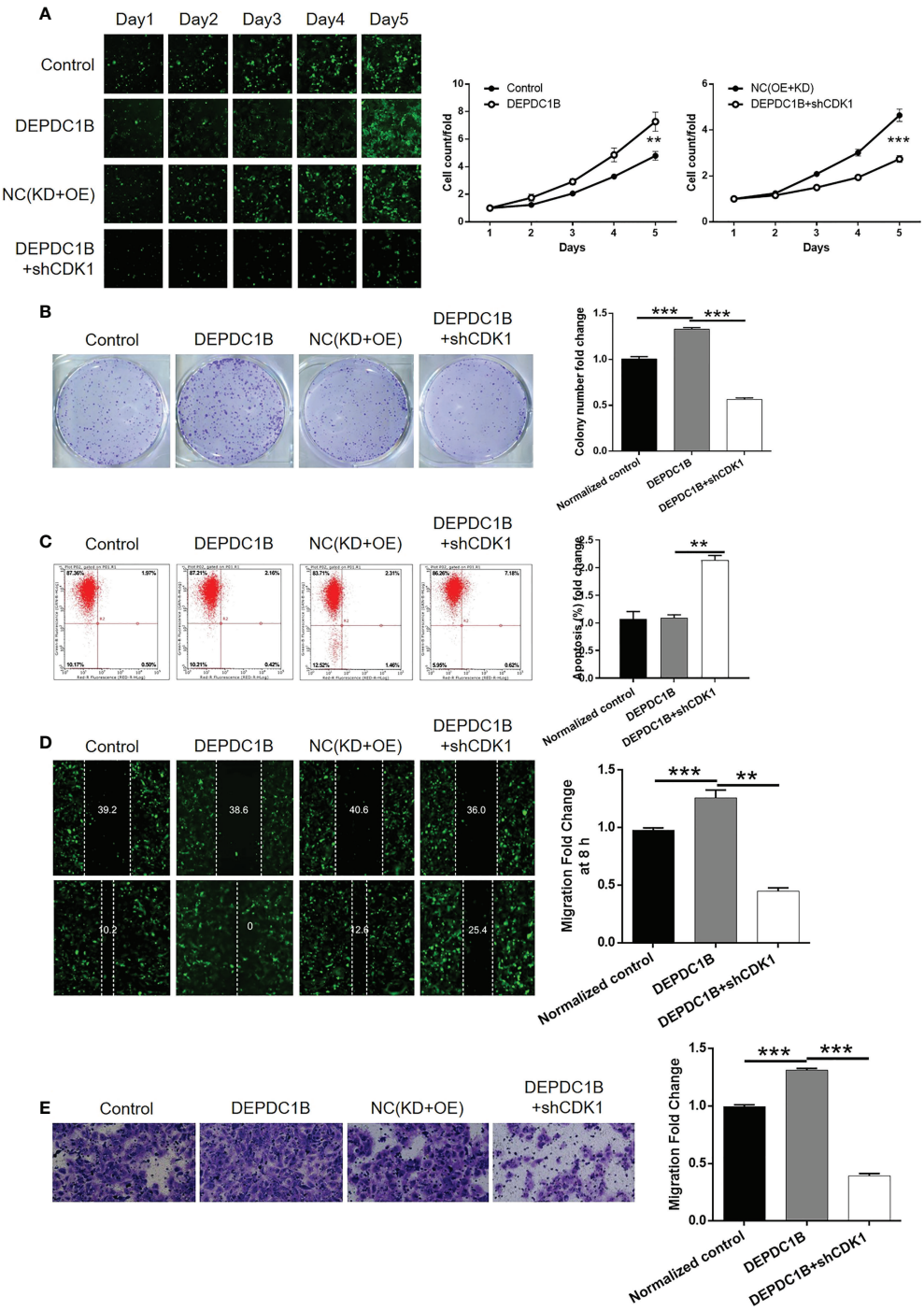

FIGURE 6
Knockdown of CDK1 attenuated the effects of CCA cells by DEPDC1B overexpression. HUCCT1 cells transfected with control plasmids, DEPDC1B overexpression plasmids, NC(OE+KD), and simultaneous DEPDC1B overexpression plasmids, and shCDK1 were subjected to the detection of cell proliferation by Celigo cell counting assay **(A)**, colony formation **(B)**, cell apoptosis by flow cytometry **(C)**, cell migration by wound healing assay **(D)**, and cell migration by Transwell assay **(E)**. The representative images were selected from at least three independent experiments. Data were shown as mean ± SD (n = 3). $^{**}P < 0.01$, $^{***}P < 0.001$.

participates in the metastasis of malignant tumors (27, 28). In this study, the upregulation of epithelial cell marker E-cadherin and the downregulation of stromal cell markers N-cadherin and Vimentin in the shDEPDC1B group of CCA cells suggested that DEPDC1B may promote CCA cell migration through affecting the EMT process.

Human cells have more than 13 cyclin–dependent kinases (CDKs) and more than 25 cyclins that form a variety of CDK–cyclin complexes at different stages of the cell cycle, which exert a specific role in the process of the cell cycle (29). In addition, cyclin–dependent kinase 1 (CDK1) is an important modulator for a variety of biological behaviors, including cytoskeleton recombination, chromosome segregation, and daughter cell formation and separation (30). CDK1 participates in the regulation of the G2 phase as part of the cyclin A complex. For example, CDK1 is involved in G2/M transformation through the formation of a complex with cyclin B (31). The inactivation of CDK1 induces G2/M arrest in the cell cycle and the production of polyploid cells (32). Importantly, CDK1 was identified to be upregulated in a variety of malignant tumors, such as colorectal cancer (33), prostate cancer (34), bladder cancer (35), ovarian cancer (36), and breast cancer (37). Additionally, a high expression of CDK1 predicts a poor prognosis of pancreatic ductal adenocarcinoma (38). Yamamura et al. put forward that expression of p-CDK1 may be a prognostic indicator of CCA and that the CDK pathway may be a therapeutic target of CCA treatment (39). Therefore, the expression of CDK1 is closely correlated with the development and progress of various cancers including CCA, which makes it a potential promising target for molecular targeted therapy. In this study, based on mechanistic research, CDK1 was proposed as the downstream target of DEPDC1B in the regulation of CCA, whose upregulation in CCA agreed with previous studies. More importantly, it was also clarified that the effects of DEPDC1B overexpression on CCA cell phenotypes, including cell proliferation, colony formation, apoptosis, and migration could be alleviated or even eliminated by the simultaneous knockdown of CDK1. All the above results suggested that CDK1 may mediate the DEPDC1B-induced regulation of CCA. Actually, CDK1 was also found to be a downstream effector in the DEPDC1B-related regulation of hepatocellular carcinoma (40). Furthermore, a previous report indicating the role of DEPDC1B in pancreatic cancer development through targeting the Akt/Gsk3b/Snail pathway also provides support for the alleviation of DEPDC1B overexpression-induced effects by CDK1 knockdown (41). More importantly, it has been previously indicated that CDK1 could be regulated by posttranslational modification such as ubiquitination (42). Herein, we also discovered that DEPDC1B may regulate the protein stability as well as protein level of CDK1 through influencing SMURF1-mediated CDK1 ubiquitination. However, the regulatory mechanism by which DEPDC1B regulates the mRNA level of CDK1 still needs to be explored and investigated.

In summary, the outcomes of this study provided a novel insight into the biological functions of DEPDC1B in the development and progression of CCA and preliminarily explored the underlying mechanism. Herein, DEPDC1B was identified as a tumor promotor in CCA, the knockdown of which could inhibit CCA development. Moreover, DEPDC1B formed a signal axis together with CDK1 to induce the promotion of CCA and could be considered a promising therapeutic target of CCA treatment.

Data availability statement

The original contributions presented in the study are included in the article/Supplementary Material. Further inquiries can be directed to the corresponding author.

Ethics statement

The experiment was approved by Ethics committee of Shandong Provincial Hospital. The patients/participants provided their written informed consent to participate in this study. This study was reviewed and approved by Ethics committee of Shandong Provincial Hospital.

Author contributions

SX designed this program. SX, XW, and YQ operated the cell and animal experiments. PN and JS conducted the data collection and analysis. SX produced the manuscript which was checked by SX, JS, ZZ, and XW. All authors contributed to the article and approved the submitted version.

Funding

This work was financially supported by the Jinan Clinical Medicine Science and Technology Innovation Plan (No. 201907073) and Natural Science Foundation of Shandong Province (No. ZR2022MH169).

Conflict of interest

Author JS was employed by Origimed at the time of writing. The remaining authors declare that the research was conducted in the absence of any commercial or financial relationships that could be construed as a potential conflict of interest.

Publisher's note

Supplementary material

The Supplementary Material for this article can be found online at: https://www.frontiersin.org/articles/10.3389/fonc.2022.842205/full#supplementary-material

References

1. Nataliya R, Gregory JG. Cholangiocarcinoma. *Lancet* (2014) 383:2168–79. doi: 10.1016/S0140-6736(13)61903-0

2. Doherty B, Nambudiri VE, Palmer WC. Update on the diagnosis and treatment of cholangiocarcinoma. *Curr Gastroenterol Rep* (2017) 19:2. doi: 10.1007/s11894-017-0542-4

3. Oliveira IS, Kilcoyne A, Everett JM, Mino-Kenudson M, Harisinghani MG, Ganesan K. Cholangiocarcinoma: Classification, diagnosis, staging, imaging features, and management. *Abdom Radiol* (2017) 42:1637–49. doi: 10.1007/s00261-017-1094-7

4. Lendvai G, Szekerczés T, Illyés I, Dóra R, Kontsek E, Gógl A, et al. Cholangiocarcinoma: Classification, histopathology and molecular carcinogenesis. *Pathol Oncol Res* (2020) 26:3–15. doi: 10.1007/s12253-018-0491-8

5. Gad MM, Saad AM, Faisaluddin M, Gaman MA, Ruhban IA, Jazieh KA, et al. Epidemiology of cholangiocarcinoma; united states incidence and mortality trends. *Clin Res Hepatol Gas* (2020) 44:885-93. doi: 10.1016/j.clinre.2020.03.024

6. Rizvi S, Khan SA, Hallemeier CL, Kelley RK, Gores GJ. Cholangiocarcinoma–evolving concepts and therapeutic strategies. *Nat Rev Clin Oncol* (2017) 15:95–111. doi: 10.1038/nrclinonc.2017.157

7. Krasinskas AM. Cholangiocarcinoma. *Surg Pathol Clinics* (2018) 11:403–29. doi: 10.1016/j.path.2018.02.005

8. Sadeghi S, Bejjani A, Finn R. Systemic therapy for primary liver tumors: Cholangiocarcinoma and hepatocellular carcinoma. *Surg Oncol Clin N Am* (2019) 28:695–715. doi: 10.1016/j.soc.2019.06.015

9. Rizvi S, Khan SA, Hallemeier CL, Kelley RK, Gores GJ. Cholangiocarcinoma — evolving concepts and therapeutic strategies. *Nat Rev Clin Oncol* (2018) 15:95–111. doi: 10.1038/nrclinonc.2017.157

10. Marchesi S, Montani F, Deflorian G, D'Antuono R, Cuomo A, Bologna S, et al. DEPDC1B coordinates de-adhesion events and cell-cycle progression at mitosis. *Dev Cell* (2014) 31:420–33. doi: 10.1016/j.devcel.2014.09.009

11. Consonni SV, Gloerich M, Spanjaard E, Bos JL. CAMP regulates DEP domain-mediated binding of the guanine nucleotide exchange factor Epac1 to phosphatidic acid at the plasma membrane. *Proc Natl Acad Sci* (2012) 109:3814. doi: 10.1073/pnas.1117599109

12. Consonni SV, Maurice MM, Bos JL. DEP domains: Structurally similar but functionally different. *Nat Rev Mol Cell Bio* (2014) 15:357–62. doi: 10.1038/nrm3791

13. Peck J, Douglas G, Wu CH, Burbelo PD. Human RhoGAP domain-containing proteins: Structure, function and evolutionary relationships. *FEBS Lett* (2002) 528:27–34. doi: 10.1016/S0014-5793(02)03331-8

14. Yang Y, Liu L, Cai J, Wu J, Guan H, Zhu X, et al. DEPDC1B enhances migration and invasion of non-small cell lung cancer cells *via* activating wnt/β-catenin signaling. *Biochem Bioph Res Co* (2014) 450:899–905. doi: 10.1016/j.bbrc.2014.06.076

15. Su Y, Liang C, Huang C, Peng C, Chen CC, Lin M, et al. A putative novel protein, DEPDC1B, is overexpressed in oral cancer patients, and enhanced anchorage-independent growth in oral cancer cells that is mediated by Rac1 and ERK. *J BioMed Sci* (2014) 21:67. doi: 10.1186/s12929-014-0067-1

16. Bai S, Chen T, Du T, Chen X, Lai Y, Ma X, et al. High levels of DEPDC1B predict shorter biochemical recurrence-free survival of patients with prostate cancer. *Oncol Lett* (2017) 14:6801–8. doi: 10.3892/ol.2017.7027

17. Pollino S, Benassi MS, Pazzaglia L, Conti A, Bertani N, Righi A, et al. Prognostic role of XTP1/DEPDC1B and SDP35/DEPDC1A in high grade soft-tissue sarcomas. *Histol Histopathol* (2018) 33:11959. doi: 10.14670/HH-11-959

18. Zhang F, Zhou Q. Knockdown of BRCC3 exerts an anti–tumor effect on cervical cancer in vitro. *Mol Med Rep* (2018) 18:4886–94. doi: 10.3892/mmr.2018.9511

19. Xu Y, Sun W, Zheng B, Liu X, Luo Z, Kong Y, et al. DEPDC1B knockdown inhibits the development of malignant melanoma through suppressing cell proliferation and inducing cell apoptosis. *Exp Cell Res* (2019) 379:48–54. doi: 10.1016/j.yexcr.2019.03.021

20. Chen X, Guo Z, Cao D, Chen Y, Chen J. Knockdown of DEPDC1B inhibits the development of glioblastoma. *Cancer Cell Int* (2020) 20:310. doi: 10.1186/s12935-020-01404-7

21. Zhang S, Shi W, Hu W, Ma D, Yan D, Yu K, et al. DEP domain-containing protein 1B (DEPDC1B) promotes migration and invasion in pancreatic cancer through the Rac1/PAK1-LIMK1-Cofilin1 signaling pathway. *Oncotargets Ther* (2020) 13:1481–96. doi: 10.2147/OTT.S229055

22. Figeac N, Pruller J, Hofer I, Fortier M, Ortuste Quiroga HP, Banerji CRS, et al. DEPDC1B is a key regulator of myoblast proliferation in mouse and man. *Cell Proliferat* (2020) 53:e12717. doi: 10.1111/cpr.12717

23. Sun Y, Zhang Z. In silico identification of crucial genes and specific pathways in hepatocellular cancer. *Genet Test Mol Bioma* (2020) 24:296–308. doi: 10.1089/gtmb.2019.0242

24. Ma Z, Wang J, Ding L, Chen Y. Identification of novel biomarkers correlated with prostate cancer progression by an integrated bioinformatic analysis. *Medicine* (2020) 99. doi: 10.1097/MD.0000000000021158

25. Fornari F, Pollutri D, Patrizi C, La Bella T, Marinelli S, Casadei Gardini A, et al. In hepatocellular carcinoma miR-221 modulates sorafenib resistance through inhibition of caspase-3–mediated apoptosis. *Clin Cancer Res* (2017) 23:3953. doi: 10.1158/1078-0432.CCR-16-1464

26. Martínez-García D, Manero-Rupérez N, Quesada R, Korrodi-Gregório L, Soto-Cerrato V. Therapeutic strategies involving survivin inhibition in cancer. *Med Res Rev* (2019) 39:887–909. doi: 10.1002/med.21547

27. Chen T, You Y, Jiang H, Wang ZZ. Epithelial–mesenchymal transition (EMT): A biological process in the development, stem cell differentiation, and tumorigenesis. *J Cell Physiol* (2017) 232:3261–72. doi: 10.1002/jcp.25797

28. Liao T, Yang M. Revisiting epithelial-mesenchymal transition in cancer metastasis: The connection between epithelial plasticity and stemness. *Mol Oncol* (2017) 11:792–804. doi: 10.1002/1878-0261.12096

29. Liao Y, Feng Y, Shen J, Hornicek FJ, Duan Z. The roles and therapeutic potential of cyclin-dependent kinases (CDKs) in sarcoma. *Cancer Metast Rev* (2016) 35:151–63. doi: 10.1007/s10555-015-9601-1

30. Prevo R, Pirovano G, Puliyadi R, Herbert KJ, Rodriguez-Berriguete G, O Docherty A, et al. CDK1 inhibition sensitizes normal cells to DNA damage in a cell cycle dependent manner. *Cell Cycle* (2018) 17:1513–23. doi: 10.1080/15384101.2018.1491236

31. Yang Y, Xue K, Li Z, Zheng W, Dong W, Song J, et al. C-myc regulates the CDK1/cyclin B1 dependent–G2/M cell cycle progression by histone H4 acetylation in raji cells. *Int J Mol Med* (2018) 41:3366–78. doi: 10.3892/ijmm.2018.3519

32. Zhou J, Han S, Qian W, Gu Y, Li X, Yang K. Metformin induces miR-378 to downregulate the CDK1, leading to suppression of cell proliferation in hepatocellular carcinoma. *Oncotargets Ther* (2018) 11:4451–9. doi: 10.2147/OTT.S167614

33. Wang L, Sun K, Wu D, Xiu Y, Chen X, Chen S, et al. DLEU1 contributes to ovarian carcinoma tumourigenesis and development by interacting with miR-490-3p and altering CDK1 expression. *J Cell Mol Med* (2017) 21:3055–65. doi: 10.1111/jcmm.13217

34. Sung W, Lin Y, Wu P, Yen H, Lai H, Su T, et al. High nuclear/cytoplasmic ratio of Cdk1 expression predicts poor prognosis in colorectal cancer patients. *BMC Cancer* (2014) 14:951. doi: 10.1186/1471-2407-14-951

35. Heo J, Noh B, Lee S, Lee H, Kim Y, Lim J, et al. Phosphorylation of TFCP2L1 by CDK1 is required for stem cell pluripotency and bladder carcinogenesis. *EMBO Mol Med* (2020) 12:e10880. doi: 10.15252/emmm.201910880

36. Li J, Zhi X, Shen X, Chen C, Yuan L, Dong X, et al. Depletion of UBE2C reduces ovarian cancer malignancy and reverses cisplatin resistance *via*

downregulating CDK1. *Biochem Bioph Res Co* (2020) 523:434–40. doi: 10.1016/j.bbrc.2019.12.058

37. Izadi S, Nikkhoo A, Hojjat-Farsangi M, Namdar A, Azizi G, Mohammadi H, et al. CDK1 in breast cancer: Implications for theranostic potential. *Anti-Cancer Agent Me* (2020) 20:758–67. doi: 10.2174/1871520620666200203125712

38. Piao J, Zhu L, Sun J, Li N, Dong B, Yang Y, et al. High expression of CDK1 and BUB1 predicts poor prognosis of pancreatic ductal adenocarcinoma. *Gene* (2019) 701:15–22. doi: 10.1016/j.gene.2019.02.081

39. Yamamura M, Sato Y, Takahashi K, Sasaki M, Harada K. The cyclin –dependent kinase pathway involving CDK1 is a potential therapeutic target for cholangiocarcinoma. *Oncol Rep* (2019) 43:306–17. doi: 10.3892/or.2019.7405

40. Dang X, Pan Q, Lin Z, Wang H, Li L, Li L, et al. Overexpressed DEPDC1B contributes to the progression of hepatocellular carcinoma by CDK1. *Aging* (2021) 13:20094–115. doi: 10.18632/aging.203016

41. Liu X, Li T, Wu W, Li J, Wei L, Qian Y, et al. DEPDC1B promotes migration and invasion in pancreatic ductal adenocarcinoma by activating the Akt/GSK3β/Snail pathway. *Oncol Lett* (2020) 20:146. doi: 10.3892/ol.2020.12009

42. Sisinni L, Maddalena F, Condelli V, Pannone G, Simeon V, Li Bergolis V, et al. TRAP1 controls cell cycle G2–m transition through the regulation of CDK1 and MAD2 expression/ubiquitination. *J Pathol* (2017) 243:123–34. doi: 10.1002/path.4936

frontiers | Frontiers in Oncology

TYPE Original Research
PUBLISHED 06 January 2023
DOI 10.3389/fonc.2022.1009508

OPEN ACCESS

EDITED BY
Zhe-Sheng Chen,
St. John's University, United States

REVIEWED BY
Makoto Makishima,
Nihon University, Japan
Nikolai Chepelev,
Health Canada, Canada

*CORRESPONDENCE
Shuang Liu
shuangliu2016@csu.edu.cn
Yongguang Tao
taoyong@csu.edu.cn

SPECIALTY SECTION
This article was submitted to Molecular and Cellular Oncology, a section of the journal Frontiers in Oncology

RECEIVED 08 August 2022
ACCEPTED 25 November 2022
PUBLISHED 06 January 2023

CITATION
Liu Y, Ouyang L, Mao C, Chen Y, Liu N, Chen L, Shi Y, Xiao D, Liu S and Tao Y (2023) Inhibition of RNF182 mediated by Bap promotes non-small cell lung cancer progression.
Front. Oncol. 12:1009508.
doi: 10.3389/fonc.2022.1009508

Inhibition of RNF182 mediated by Bap promotes non-small cell lung cancer progression

Yating Liu[1,2,3], Lianlian Ouyang[1,2], Chao Mao[1,2], Yuanbing Chen[1,2], Na Liu[1,2], Ling Chen[1,2], Ying Shi[1,2], Desheng Xiao[1], Shuang Liu[4]* and Yongguang Tao[1,2,5]*

[1]Department of Pathology, Xiangya Hospital, Central South University, Key Laboratory of Carcinogenesis and Cancer Invasion, Ministry of Education, Hunan, Changsha, China, [2]National Health Commission (NHC) Key Laboratory of Carcinogenesis (Central South University), Cancer Research Institute and School of Basic Medicine, Central South University, Changsha, Hunan, China, [3]Postdoctoral Research Station of Clinical Medicine & Department of Hematology and Critical Care Medicine, The 3rd Xiangya Hospital, Central South University, Changsha, China, [4]Department of Oncology, Institute of Medical Sciences, National Clinical Research, Center for Geriatric Disorders, Xiangya Hospital, Central South University, Changsha, Hunan, China, [5]Hunan Key Laboratory of Early Diagnosis and Precision Therapy in Lung Cancer, Second Xiangya Hospital, Central South University, Changsha, China

Introduction: Ubiquitylation that mediated by ubiquitin ligases plays multiple roles not only in proteasome-mediated protein degradation but also in various cellular process including DNA repair, signal transduction and endocytosis. RING finger (RNF) proteins form the majority of these ubiquitin ligases. Recent studies have demonstrated the important roles of RNF finger proteins in tumorigenesis and tumor progression. Benzo[a]pyrene (BaP) is one of the most common environmental carcinogens causing lung cancer. The molecular mechanism of Bap carcinogenesis remains elusive. Considering the critical roles of RNF proteins in tumorigenesis and tumor progression, we speculate on whether Bap regulates RNF proteins resulting in carcinogenesis.

Methods: We used GEO analysis to identify the potential RING finger protein family member that contributes to Bap-induced NSCLC. We next used RT-qPCR, Western blot and ChIP assay to investigate the potential mechanism of Bap inhibits RNF182. BGS analyses were used to analyze the methylation level of RNF182.

Results: Here we reported that the carcinogen Bap suppresses the expression of ring finger protein 182 (RNF182) in non-small cell lung cancer (NSCLC) cells, which is mediated by abnormal hypermethylation in an AhR independent way and transcriptional regulation in an AhR dependent way. Furthermore, RNF182 exhibits low expression and hypermethylation in tumor tissues. RNF182 also significantly suppresses cell proliferation and induces cell cycle arrest in NSCLC cell lines.

Conclusion: These results demonstrated that Bap inhibits RNF182 expression to promote lung cancer tumorigenesis through activating AhR and promoting abnormal methylation.

KEYWORDS

RNF182, Bap, AhR, NSCLC, methylation

Introduction

Lung cancer is the leading cause of cancer-related deaths worldwide. Non-small cell lung cancer (NSCLC), including adenocarcinoma (LUAD) and squamous cell carcinoma (LUSC), is the most common type of lung cancer (1, 2). A large amount of somatic mutations, abnormally inactivated tumor suppressor genes and activated oncogenic factors contribute to lung carcinogenesis (3, 4).

Benzo(a)pyrene (Bap) is a member of the polycyclic aromatic hydrocarbon (PAH) family and Bap is usually produced when organic matters incompletely burned. Cigarette smoke and well-done barbecued-meat contain high levels of Bap and are common sources of general population Bap exposure (5, 6). Bap and its key metabolite benzo(a)pyrene-7,8-diol-9,10-epoxide (BPDE), form adducts with DNA and lead to mutagenic and carcinogenetic effects. Although Bap is recognized as one of the most common environmental pollutants and carcinogens causing lung cancer (6), the molecular mechanism of Bap carcinogenesis remains elusive.

Bap is a potent natural ligand of AhR which is a ligand-activated transcription factor of the basic helix-loop-helix/Per-Arnt-Sim family. Once binding to its ligands, AhR translocates into the nucleus and regulates a battery of gene expression. Activation of AhR is one of the mechanisms responsible for adverse effects of Bap (7–11).

Ubiquitin-protein enzymes (E3s) are of particular concern in ubiquitination, as they not only transfer activated ubiquitin from ubiquitin-conjugating enzymes to protein substrates but also confer substrate specificity (12). Recently, the RING finger protein family, a complex set of E3s that contain RNF domain, was demonstrated to play important roles in tumorigenesis and tumor progression (13–16). Considering the critical roles of RNF proteins, we speculate on whether Bap regulates RNF proteins resulting in carcinogenesis. Hence, we screened the RNF family genes which expression were altered in Bap key metabolite BPDE-treated lung fibroblasts cells through GEO database (GSE19510) and found that RNF182 was decreased significantly in a dose-dependent way. Next, the biological function experiments of RNF182, including cell proliferation, colony formation and cell cycle phase distribution demonstrated that inhibition of RNF182 promotes NSCLC progression. Moreover, the low expression of RNF182 is significantly associated with patients poor clinical outcome. These results suggested that RNF182 may function as a tumor suppressor in NSCLC and inhibition of RNF182 may contribute to NSCLC inition and progression.

On the other hand, we revealed that RNF182 was inhibited by Bap through both AhR-mediated regulation and DNA methylation. These findings may clarify the mechanism of Bap-mediated abnormal downregulation of RNF182 in NSCLC and identify new diagnostic, prognostic and therapeutic schedule in NSCLC.

Materials and methods

Ethics approval and consent to participate

This study was conducted at the Cancer Research Institute and the Third Xiangya Hospital, Central South University, Hunan, China. All of the protocols were reviewed and approved (No.2021-S055) by the IRB of Third Xiangya Hospital, Central South University and performed in accordance with national guidelines.

Data acquisition and databases

National Center for Biotechnology Information Gene Expression Omnibus (GEO) (https://www.ncbi.nlm.nih.gov/geo/) is a public functional genomics database that are provided to help users query and download experiments and curated gene expression profiles. Search was conducted using "Benzo(a)pyrene and lung" key words. Series GSE19510 (Dataset: GDS3706) provided the expression profiling of lung WI-38 fibroblasts exposed to BPDE (17).

The Cancer Genome Atlas (TCGA) (https://www.cancer.gov/) is a public funded project that aims to catalogue and discover major cancer-causing genomic alterations to create a comprehensive "atlas" of cancer genomic profiles (18).

Gene Expression Profiling Interactive Analysis (GEPIA) (http://gepia.cancer-pku.cn/) is a newly developed interactive web server for analyzing the RNA sequencing expression data tumors and normal samples from the TCGA and the GTEx projects, using a standard processing pipeline (19). Entering gene name "RNF182", choosing "Expression on Box Plots" parts, and selecting LUAD and LUSC datasets to get the expression of RNF182 in LUAD and LUSC datasets.

The UCSC (https://genome.ucsc.edu/) genome browser database is a free website that that allows scientists to visualize gene expression and metadata annotation distribution throughout a single-cell dataset or multiple datasets. The CpG islands of RNF182 were obtained by searching RNF182 in the genome browser part in UCSC database.

Cell lines and plasmids

The human lung bronchus cell line HBE (CRL- 2741) and lung carcinomatous cell lines A549 (CCL-185) were obtained from American Type Culture Collection (University Boulevard, Manassas, VA, USA). The human lung carcinomatous cell line PC9 was stored in the Department of Molecular Biology, Cancer Research Institute (Central South University, Hunan, China). The cell lines were characterized by mycoplasma detection,

DNA fingerprinting, isozyme detection, and cell viability by the provider. HBE and PC9 were cultured in Roswell Park Memorial Institute 1640 Media (Gibco) supplemented with 10% FBS, penicillin, and streptomycin. A549 cells were cultured in Dulbecco's Modified Eagle's Medium/Nutrient Mixture F-12 (Gibco) supplemented with 10% FBS, penicillin, and streptomycin.

Cells were seeded about 30% density in 6 well plate. After cells growing adherence for 24 hours, cells were exposed to Bap at different times (24h, 48h and 72h) and concentration (10μM, 20μM and 40μM) and finally collected for Western blot and RT-qPCR analyses. For BGS analysis, cells were seeded about 30% density in 6 well plate and continuously exposed to vehicle control (dimethyl sulfoxide, DMSO), Bap (Sigma) or ITE (Targetmol, USA) after 24 hours cell culture. Bap were freshly added to cells each time after overnight cell attachment (40μM,72h). ITE were freshly added every 8 hours and cell media were changed (10μM, 8h*3).

AhR shRNA vectors and control (GV248) were purchased from GeneChem (www.genechem.com.cn). Lentiviral shRNA clones targeting human RNF182 (#4 TTGCTAGG TTTGCTCTACTTC; #5 CCTCGTTATTCTTATGGTGTA) and the nontargeting control construct were purchased from GeneChem. Lentiviral particles were produced in 293T cells. A549 and PC9 cell lines that were transfected and selected with puromycin at a concentration of 2 μg/ml.

Western blot and antibody

The cells were washed with PBS and harvested by scraping and centrifugation at 500 g for 5 min. The harvested cells were washed with PBS and lysed for 30 min in the IP lysis buffer with proteinase inhibitor. Then the soluble fraction was collected by centrifugation at 12,000 g for 15min. Protein lysates were quantified and resolved on SDS-PAGE gels, transferred to PVDF membranes (Millipore) and immunoblotted with primary antibody, followed by incubation with a secondary antibody. Antibody signals were detected using an enhanced chemiluminescence system. The following antibodies were used: RNF182 (Abcam, #ab156127, 1:500), β-actin (Proteintech, #66009-1-lg, 1:1000), AhR (Santa Cruz, sc-5579).

Cell proliferation and colony formation

Details of these procedures have been previously described (20, 21). Briefly, for cell proliferation, 1000 cells were seeded into 96-well plates and incubated with CellTiter 96 AQueous One Solution Cell Proliferation Assay (Promega #G3581) (MTS: media=1:9) for 1 hour in indicated times. After incubation, the absorbance at 490 nm was measured by multimode reader (Bio-TeK, EL800).

For the colony formation assay, 500 cells were seeded into 6-well plates in appropriate media. After 2 weeks, the cells were washed with PBS, fixed in methanol and stained with crystal violet. Colonies were counted using ImageJ (1.47 v, NIH, USA).

Cell cycle analysis

Details of cell cycle analysis have been previously described (20). Briefly, PC9 cells were harvested and washed with PBS and fixed in 70% ice-cold ethanol overnight. After centrifugation at 800 rpm for 5 min, cells were washed with ice-cold PBS and resuspended in 0.5 mL PBS containing PI (50 μg/mL) and RNase (100 μg/mL) for 15 min in the dark. Subsequently, the cell cycle distribution was analyzed by flow cytometry (BD Biosciences, FACS Canto II).

Real-time quantitative PCR

RNA was extracted from cell lines using RNAiso Plus (Takara) according to the manufacturer's protocol. cDNA was synthesized by RNA (1 μg) using a Prime-Script™ RT Reagent Kit with gDNA Eraser (Takara). Amplification and semiquantification of transcripts were performed using FastStart Universal SYBR Green Master Mix (Roche) and specific primers on a 7500 Fast Real Time PCR System (Applied Biosystems, Life Technologies). Amplification was performed at 95°C for 10 min, followed by 40 cycles of 15 s at 95°C and 1 min at 60°C. Fold change in gene expression was calculated using the 2−ΔΔCt method. mRNA expression was normalized against β-actin, allowing comparison of mRNA levels. The primers used were list as below:

RNF182 (F: GTCCTCCAACTGCCTGGTCATA; R: GTGGTGACAGAGTCGAAACTCG); RNF141 (F: TCCTCTGTAACATCTTGTCAGGC; R: CTGTGAGCACAAGGCAGGATGA); RNF130 (F: GCCAGTTACCATGACTCATCCAG; R: GGCTGAAGTTCTTCGGTGGCAT); RNF110 (F: CACTATCGTGGAGTGCCTGCAT; R: GGTTTTATGGACCTGCACGTCAC); RNF150 (F: TCAGCCGTGGTCATCTTCAACG; R: CGGTGATGTTTCTTTCCAGCAGG); RNF24 (F: GTGTGCCTAGAAGACTTCAAGCC; R: GCTGTAGAACTGGCATGTTGCAC); RNF220 (F: ACCGATGACCTCCACCATTCAG; R: CTGCCCTTCATCTTGCTTCCTC); RNF11 (F: GCCTAAAGGAGTTTATGACCCTG; R: GTCCAGGTGATAGATGTGCATGC); RNF121 (F: GTGCAGACTACATGGCATCTACC; R: GATTGCAGGACAGCCTATACGTG); RNF7 (F: AGGCGACAAGATGTTCTCCCTC; R: TCAGCTTGACATCTAAGACAGGC); RNF181 (F: GACTGCCATTGAGATGCCTTGC; R: GCCTTATCTCGTCTGTGCTCCT); RNF26 (F: CAGGACCATCAGAGTGACACCT; R: GCAACACTGTCTTGCTCTGGTC); RNF34 (F:

GGAACTGGTAGAGAAAGTAAACCG; R: ACACAGG CTGTCGTCTTCCTCA); CYP1A1 (F: GATTGAGCAC TGTCAGGAGAAGC; R: ATGAGGCTCCAGGAGATAGCA0G);

Chromatin immunoprecipitation assays

ChIP assays were performed essentially as described previously (20, 21). Breifly, 10 cm dish cells (90% confluence) were fixed with formaldehyde (1% final volume concentration, Sigma) for 10 min at room temperature. Fixation was stopped by addition of 1/10 volume 1.25 M glycine and incubated for 5 min at room temperature. Sonication was performed using a Qsonica sonicator (6 min, 20 s on, 20 s off), and 400 μg protein-chromatin complex was used for each chromatin immunoprecipitation. Antibody against AhR (Santa Cruz, sc-5579), H3K27ac (Proteintech, 39135) or normal rabbit IgG (Cell signaling technology #2729S) as a negative control were used for ChIP assays. Antibody-protein complexes were captured using Protein A/G Mix Magnetic Beads (Millpore). ChIP DNA was analyzed by qPCR using FastStart Universal SYBR Green Master Mix (Roche) in an ABI-7500 instrument (Applied Biosystems) using primers:

(RNF182-ChIP-F: CAGCGCCGTAGAGACAAAGC; RNF182-ChIP-R: GGCTGCGGCGGCGCCTGGGAG).

Bisulfite genomic sequencing of DNA

Genomic DNA was extracted from A549 cells, PC9 cells, NSCLC carcinoma tissues and adjacent tissues using ONE-4-ALL Genemic DNA Mini-Preps Kit (Bio Basic Canada INC, B618503) and treated with sodium bisulfite using a Zymo DNA Modification kit (Zymo Research, D5030T). The amplified fragments were subcloned into the T-vector (Takara, 6013). The primers #1 (F: TTTAGGGTTTATGGTAGATGT TTAG, R: AAATATAATCTCACTCCACCCAAC) and primers#2 (F: GGTTGGGTGG AGTGAGATTATATT, R: CCACACCTTT CTCCTATAAAACTATACC) were used for subcloned. Six colonies were chosen randomly and were sequenced using the Primer RV-M by Sangon Biotech.

Statistical analyses

Results are shown as the mean ± SEM or SD. Significant differences between two groups were analyzed by unpaired Student's t-test (two-tailed) if data were normally distributed; otherwise, data were analyzed by Kolmogorov–Smirnov test. All statistical analyses were performed using Prism 8.0 GraphPad software. A p-value < 0.05 was considered statistically significant.

Results

Bap inhibits the mRNA and protein level of RNF182

To identify the potential RING finger protein family member that contributes to Bap-induced NSCLC, we analyzed the relative expression of RING finger protein family member in GEO database (GSE19510) of gene expression profiles of lung fibroblasts cells WI-38 (17), and found that RNF182 was significantly downregulated by BPDE in a dose-dependent way (Figures 1A, B). Next, Bap was prepared and used to treat HBE (normal lung epithelial cells) and A549 (lung adenocarcinoma) cells, and the results showed that treatment of the cells with Bap significantly downregulated mRNA expression of RNF182 in both HBE and A549 cells (Figures 1C, D). We further confirmed that Bap downregulated RNF182 at mRNA levels in dose- and time-dependent manners in HBE and A549 cells (Figures 1E, F). Consistently, Western blot analysis confirmed that Bap downregulated RNF182 protein levels in dose- and time-dependent manners in A549 cells (Figure 1G).

RNF182 expression is decreased in tumor tissues in NSCLC

To explore the expression of RNF182 in NSCLC, we examined the relative level of RNF182 in LUAD tissues (n=483) compared with normal tissues (n=347) and LUSC tissues (n=486) compared with normal tissues (n=338) through Gepia database (http://gepia.cancer-pku.cn). We found that RNF182 expression was significantly decreased in both LUAD and LUSC samples compared with the normal tissues (Figure 2A). Moreover, we detected the mRNA level (n=32) and protein level (n=5) of RNF182 in NSCLC tissues compared with adjacent normal tissues (Figures 2B, C). RNF182 expression was significantly decreased in NSCLC tumor tissues. Next, through K-M plotter analysis, we observed that low expression of RNF182 was associated with poor survival in LUAD patients (logrank P=4.3e-05) and lung cancer patients (logrank P=3.6e-07) (Figures 2D, E). However, there were no differences in survival between the two groups in LUSC patients (Figure 2F).

Taken together, these observations revealed that RNF182 expression is inhibited in NSCLC tumor tissues and that its low expression in NSCLC patients is associated with poor clinical outcome, indicating that NSCLC progression is associated with RNF182 alteration.

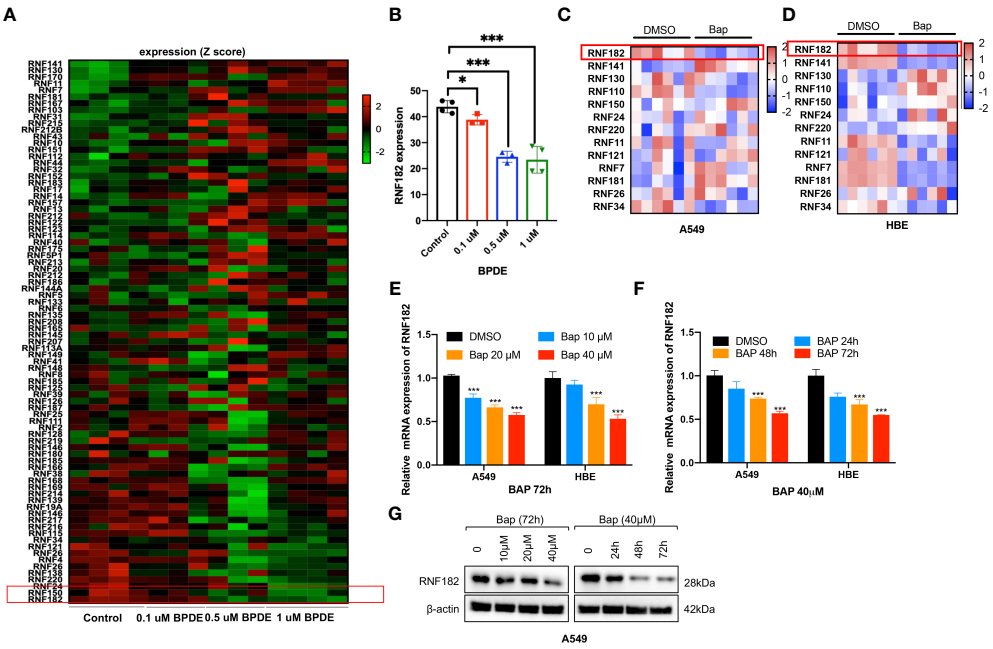

FIGURE 1
Bap inhibits the mRNA and protein level of RNF182 in LUAD cells. **(A)** GEO database (GSE19510) showed that BPDE inhibits mRNA expression of RNF182 in a dose-dependent manner in normal human lung WI-38 fibroblasts. **(B)** Quantitative results of RNF182 in A. (mean± SD, n=4). p-values are indicated (*$p < 0.05$, ***$p < 0.001$) in each panel (two-sided Student's t-test). BPDE exposure groups were compared to the control group. **(C, D)** Heatmap of RNF family members mRNA expression in A549 and HBE cells treated with Bap (40μM, 72h). **(E)** RT-qPCR shows the mRNA levels of RNF182 in A549 and HBE cells in a dose-dependent manner in response to BaP. (mean± SD, n=3). p-values are indicated (***$p < 0.001$) in each panel (two-sided Student's t-test). Bap exposure group were compared to the control group. **(F)** RT-qPCR shows the mRNA levels of RNF182 in A549 and HBE cells in a time-dependent manner in response to BaP. (mean± SD, n=3). p-values are indicated (***$p < 0.001$) in each panel (two-sided Student's t-test). Bap exposure group were compared to the control group. **(G)** Western blot shows the levels of RNF182 protein in A549 cells in a time- and dose-dependent manner in response to BaP.

RNF182 inhibits malignant progression of NSCLC

To further uncover the physiological role of RNF182 in NSCLC, we depleted expression of RNF182 using independent shRNA hairpins in PC9 cells that RNF182 is high expressed (Figure 3A). RNF182 knockdown significantly increased cell colony formation (Figure 3B) and cell proliferation (Figure 3C). Furthermore, we also found that RNF182 knockdown reversed the induction of cell cycle arrest in G1 phase (Figures 3D, E).

These results suggested that RNF182 significantly inhibits NSCLC tumorigenesis and growth *in vitro*.

Aryl hydrocarbon receptor-mediates Bap-inhibited RNF182

Aryl hydrocarbon receptor (AhR) mediates Bap-induced gene expression like CXCL13 and SMARCA6 in lung epithelia cells (22, 23). Bap triggered the activation of AhR *via* nuclear relocation of AhR (23). Interestingly, a significant negative correlation was observed between RNF182 and AhR in NSCLC patient samples (n=594, p=0.0004, R=-0.1445) based on TCGA database (Figure 4A). To further examine the regulation of AhR in RNF182, we knocked down AhR with two separate short hairpin RNAs (shRNAs) in A549 cell line that AhR is high expressed. The results demonstrated that knockdown of AhR in A549 cells increased RNF182 expression (Figure 4B). AhR agonist also inhibited RNF182 at mRNA level and AhR antagonist reversed the inhibition of AhR agonist in RNF182. CYP1A1, a well-known target gene of AhR, was used to confirm agonist and antagonist effects (Figures 4C, D). Chromatin immunoprecipitation (ChIP) were conducted to test AhR and RNF182 interaction, and the results showed that Bap treatment promoted the enrichment of AhR in the RNF182 promoter, indicating that Bap decreases RNF182 expression *via* promoting the recruitment of AhR to RNF182 promoter (Figures 4E, F).

Taken together, our results demonstrated that RNF182 was downregulated by AhR, which functions as a transcription factor and inhibits RNF182 expression by binding to its promoter region.

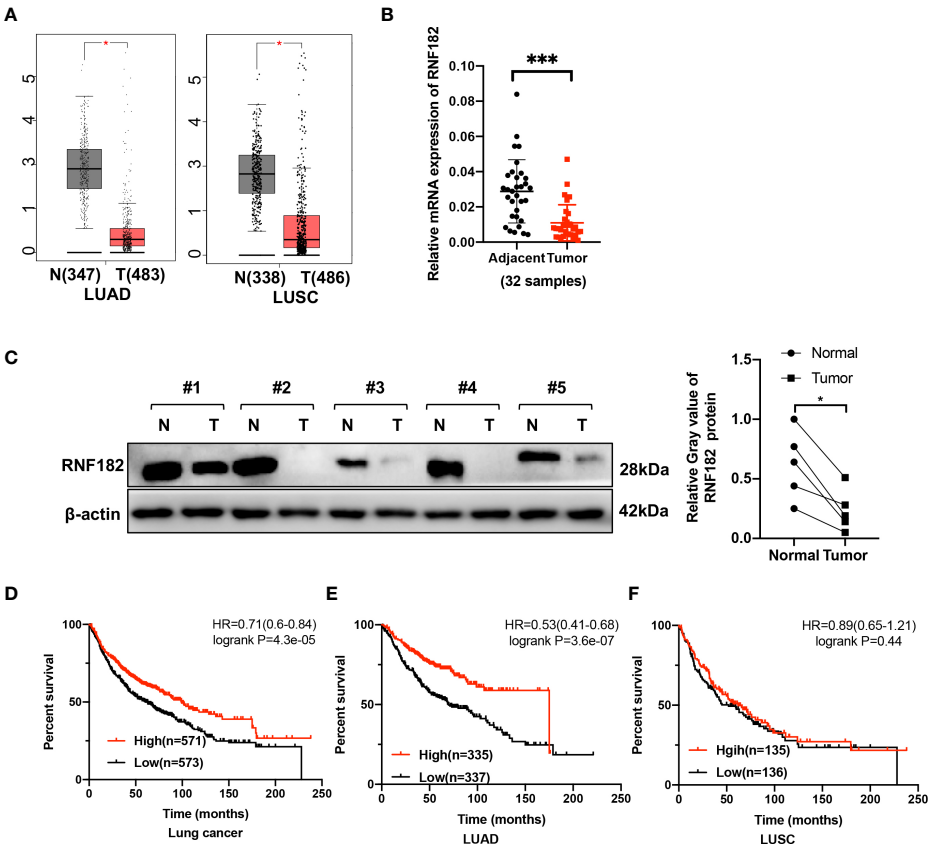

FIGURE 2
RNF182 expression is decreased in tumors tissues and associated with prognosis in LUAD patients. **(A)** Box plot showed RNF182 expression (transcript per million, TPM) is decreased in LUAD and LUSC tumor tissue. Data were adapted from Gepia. **(B)** Relative mRNA expression of RNF182 in LUAD patients (mean± SD, n=32). p-values are indicated (***$p < 0.001$) in each panel (two-sided Student's t-test). **(C)** RNF182 protein level in LUAD tumor tissues and adjacent tissues (n=5). p-values are indicated (*$p < 0.05$) in each panel (two-sided Student's t-test). **(D, E)** Kaplan-Meier survival curves showing that patients with low expression of RNF182 had a worse prognosis than patients with high expression of RNF182 in lung cancer and LUAD patients. **(F)** Kaplan-Meier showing that RNF182 expression and prognosis in LUSC patients.

RNF182 is hypermethylated in NSCLC tumor tissues

A CpG island was observed at the promoter region of RNF182 in the UCSC database. Abnormal DNA methylation has been found in cancer cells, especially at silenced tumor suppressor genes (24). Next, we tested whether downregulation of RNF182 in tumor tissues was caused by DNA methylation. Aberrant hypermethylation in a CpG island of RNF182 was detected in LUAD and LUSC tissues compared with normal tissues *via* several probes through Shiny Methylation Analysis Resource Tool (SMART) (Figures 5A, B). Moreover, an evident anticorrelation between RNF182 expression levels and methylation intensity was observed in these samples (Figures 5C, D). We further analyzed RNF182 CpG sites methylation in more details by using bisulfite genomic sequencing (BGS) analysis. Consistently, extensive methylation was detected in tumor tissues (n=4), whereas low levels of methylation were observed in adjacent tissues (n=4) (Figures 5E, F).

As Bap exposure has been reported to alter gene methylation in previous studies (25–28), we next detected the methylation level of RNF182 in A549 and PC9 cells treated with Bap by using bisulfite genomic sequencing analysis to confirm whether Bap exposure could alter RNF182 methylation. Interestingly, when treated with Bap, aberrant hypermethylation of RNF182 was observed *via* BGS analysis (Figures 5G, H).

To further confirm whether AhR contributes to Bap-mediates aberrant hypermethylation of RNF182, we detected the methylation level of RNF182 in A549 knockdown AhR cells treated with Bap by BGS analysis. We found that A549 AhR knockdown cells also exerts hypermethylation when treated with Bap (Figures 6A, B), which indicates that Bap mediates RNF182 hypermethylation in an AhR-independent way. We also used anther AhR agonist-ITE, a putative endogenous AHR ligand, to confirm the aberrant hypermethylation of RNF182 caused by

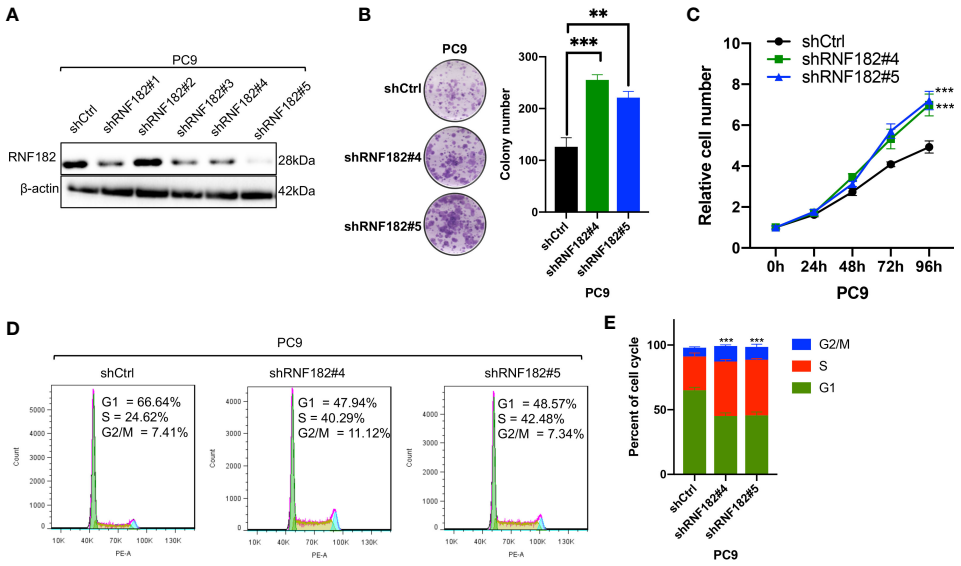

FIGURE 3
RNF182 inhibits malignant progression of NSCLC. **(A)** Western blot analysis was conducted to detect RNF182 protein levels in PC9 cells stably transfected with distinct RNF182 shRNA expression vectors or a control vector (shCtrl). **(B)** Colony formation assay of PC9 cell lines. (mean± SD, n=32). p-values are indicated (**$p < 0.01$, ***$p < 0.001$) in each panel (two-sided Student's t-test). **(C)** MTS assay of PC9 cell lines. (mean ± SD, n=5). p-values were obtained by two-way ANOVA (***$p < 0.001$). **(D)** PI-FACS analysis showing that RNF182 affects cell cycle progression in PC9 cells. **(E)** Quantification of PI-FACS analysis. (mean± SD, n=3). p-values are indicated (***$p < 0.001$) in each panel (two-sided Student's t-test).

AhR activation or Bap metabolic activation. As shown in Figures 6C, D, the methylation intensity of RNF182 showed similar levels both in A549 and PC9 cells, suggesting that AhR activation does not contribute to hypermethylation of RNF182. To test the effect of Bap on the gene methylation in a transient or in a persistent way, we treated A549 cells with Bap (40μM) for 72h and were cultured for 72h after remove Bap from the media. The BGS analysis showed that even Bap was removed from the culture media, the hypermethylation of RNF182 was still observed in Bap treated cells (Figures 6E, F), indicating that Bap effects on gene methylation may be a persistent way.

As Bap has been reported to alter histone H3 posttranslational modifications (29), a key mechanism of epigenetics, we next investigated whether Bap addition changes the histone acetylation patterns in the CYP1A1 gene and the RNF182 gene. It was found that CYP1A1 and RNF182 promoter region were dramatically enriched with H3K27ac through UCSC database. To confirm this, we conducted ChIP assay with the use of anti-H3K27ac antibody. ChIP assay showed that Bap promotes the enrichment of H3K27ac on the promoter of CYP1A1 both in A549 and PC9 cells (Figure 6G), but does not promote the enrichment of H3K27ac on the promoter of RNF182 (Figure 6H).

Collectively, the above results demonstrated that RNF182 is downregulated in NSCLC through its hypermethylation mediated by Bap through an AhR independent way.

Discussion

In this study, we provided evidence that RNF182 plays a critical role in suppressing NSCLC progression. Our findings suggested that RNF182 exerts a tumor suppressor effect in NSCLC through inhibiting cell growth and promoting cell cycle arrest that are key characteristics of cancer progression (30). Moreover, we found that RNF182 expression is significantly downregulated in LUAD tumor tissues compared with that in matched adjacent tissues, and the downregulation of RNF182 is strongly correlated with poor prognosis in LUAD patients. The reduced expression is linked closely to promoter methylation, as confirmed by methylation analyses in clinical tissues through public database and bisulfate genomic sequencing, indicating that promoter methylation is the principal regulatory mechanism of RNF182 inactivation in NSCLC.

RNF182, a member of RING E3 ubiquitin ligase family, has previously been reported to associate with innate immune system (31), cancers (20), Alzheimer's disease (32), ischemia-reperfusion injury (33) and various biological functions such as nuclear factor-kappa B (NF-κB) (31)and apoptosis (34). For example, multiple studies have demonstrated that RNF182 could bind with p65 and increase its ubiquitination and degradation (20, 31, 35), which is a well-known transcription factor of NF-κB, to modulate cell proliferation and inflammatory response

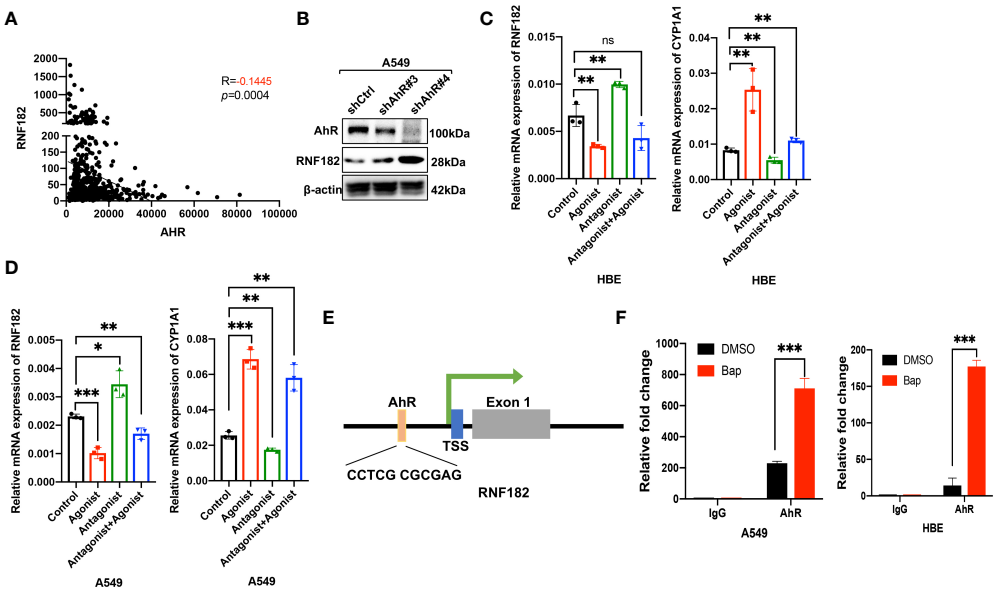

FIGURE 4
Aryl hydrocarbon receptor-mediates Bap- inhibited RNF182. **(A)** The correlation between AhR and RNF182 mRNA expression in LUAD patients (n=594). Data are adapted from TCGA. R=-0.1445, p=0.0004. **(B)** Western blot analysis showing the expression of RNF182 in AhR knockdown cell lines. **(C, D)** Relative mRNA expression of RNF182 and CYP1A1 in HBE **(C)** and A549 **(D)** cells treated with AhR agonist and Antagonist. (mean ± SD, n=3). p-values are indicated (*$p < 0.05$, **$p < 0.01$, ***$p < 0.001$, ns means "no significance") in each panel (two-sided Student's t-test). Each group was compared to the control group. **(E)** The AhR binding site is located at the upstream of the RNF182 transcription start site (TSS) **(F)** ChIP assay was performed using BaP-treated or untreated HBE and A549 cells. (mean± SD, n=3). p-values are indicated (***$p < 0.001$) in each panel (two-sided Student's t-test).

(31). RNF182 also contributes to myocardial ischemia-reperfusion injury (MIRI) *via* inhibiting mTOR signaling pathway (33). Considering the important physiological functions and tumor suppressive effects of RNF182, further study of the upstream regulatory mechanism of RNF182 will undoubtedly be helpful to the treatment of NSCLC.

Cigarette smoke is the leading cause of the lung cancer-related death, accounting for more than 87% (14, 36). Cigarette smoke and environmental pollutants contains high level of Bap, which is a member of the polycyclic aromatic hydrocarbon (PAH) family (6, 37–39). Accumulating evidence indicates that Bap exposure contributes to inducing cancer stem cell (CSC)-like property (40), immune destruction (36) and cell malignant transformation (6, 39). However, the underlying mechanisms of how Bap exposure induces epigenetics dysregulation in NSCLC has been poorly understood.

AhR is a ligand-activated transcriptional factor that regulates divers process, including malignant transformation, hematopoietic cell development, and fate determination of immune cell lineages (36, 41–43). Recent studies showed that Bap mediates target genes expression through inducing the translocation of AhR from cytoplasm to nucleus (9, 23, 44). Here, we reported that RNF182 is a target of AhR, and the expression level of RNF182 is inhibited by Bap through the AhR signaling pathway. Bap promotes AhR binding to the promoter of RNF182 and finally results to the decreased expression of RNF182. These results demonstrated that Bap-mediated AhR signaling is critical for promoting cancer progression and tumorigenicity in NSCLC cells.

Recent studies have shown that BaP can adversely modify human epigenetic characteristics, leading to health disorders (45–48). Several studies used Bap and its key metabolite BPDE to study modulation of DNA methylation *in vitro*. BPDE was shown to bind to DNA, which resulted in the methylated DNA formation and alteration of DNA methyltransferase (DNMT) (46, 47). Consistently, other two studies have described BaP-induced hypo- and hypermethylation *in vitro* cell line models (48, 49). Our studies demonstrated that Bap induced RNF182 aberrant hypermethylation in A549 and PC9 cell lines, and the decreased expression of RNF182 is associated with aberrant hypermethylation. This study suggested that Bap inhibits the expression of RNF182 to promote NSCLC progression.

The mechanisms responsible for DNA methylation response to Bap exposure are complex and not well understood. One of the most studied mechanisms of Bap-induced aberrant promoter methylation is BPDE-DNA adducts formation (48, 50, 51). Other mechanism such as Bap-mediated disruption of DNA methyltransferases (52, 53) has been also proposed to be involved in changing DNA methylation. Oxidative stress induced by Bap exposure could also influence the expression

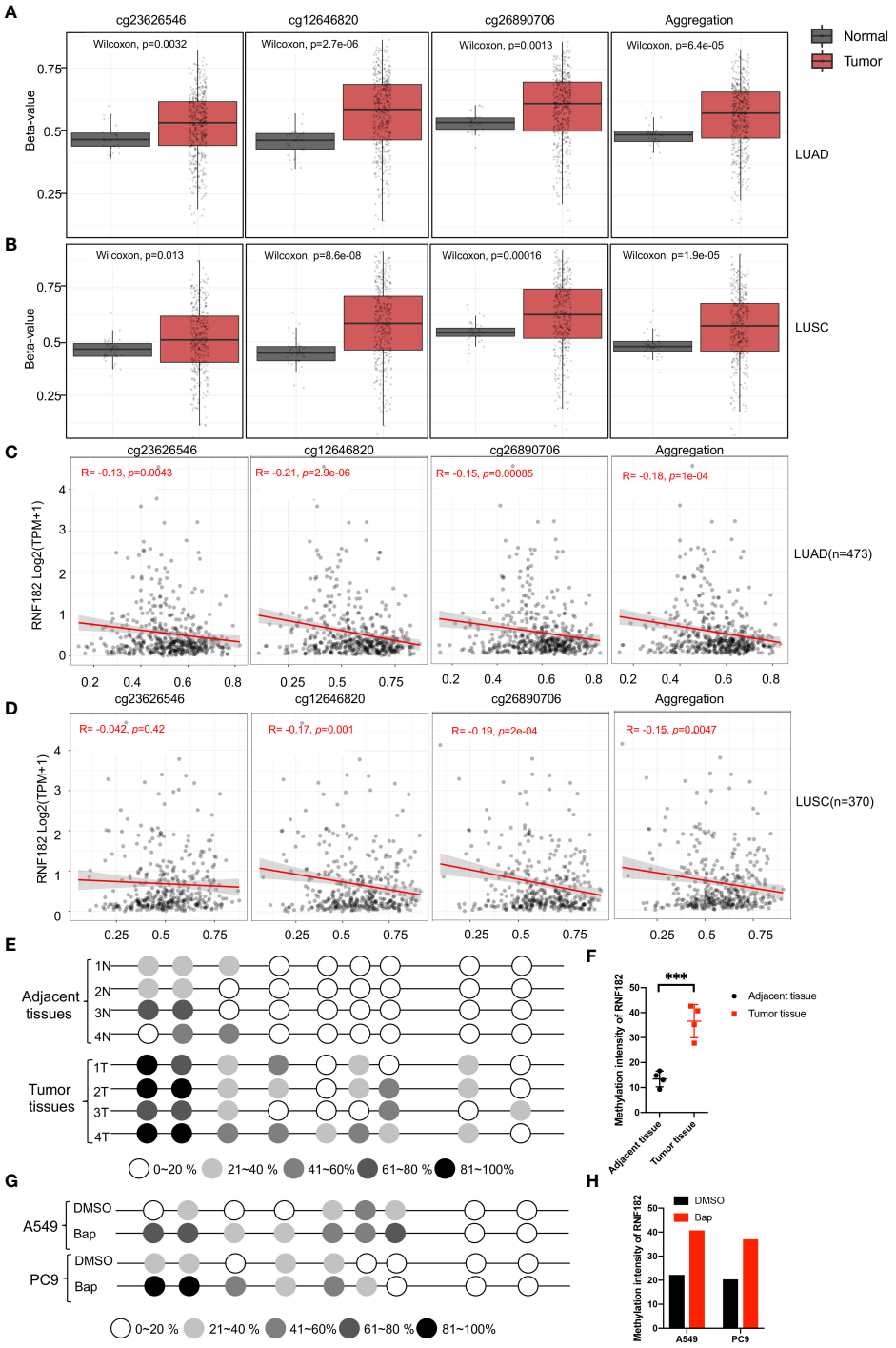

FIGURE 5
Methylation of RNF182 in LUAD and LUSC samples. **(A, B)** Several probes detected methylation level of RNF182 in LUAD **(A)** and LUSC **(B)**. The data are adapted from SMART App, a web application for comprehensively analyzing the DNA methylation data of TCGA project. **(C, D)** RNF182 expression and methylation shows a negative correlation in LUAD **(C)** and LUSC **(D)**. The data are adapted from SMART App, a web application for comprehensively analyzing the DNA methylation data of TCGA project. **(E)** Methylation status of RNF182 CpG sites in NSCLC tumor tissues (n=4) and adjacent tissues assayed by bisulfate genomic sequencing (BGS). The degree of methylation was calculated by the number of methylated colonies in each CpG site divided by the total number of colonies in the same CpG sites (n=6). **(F)** Methylation intensity and of RNF182 in NSCLC tumor and adjacent tissues (mean± SD, n=4). p-values are indicated (***$p < 0.001$) in each panel (two-sided Student's t-test). **(G)** Methylation status of RNF182 CpG sites in A549 cells and PC9 cells treated with Bap (40μM, 72h) /DMSO assayed by bisulfate genomic sequencing (BGS).The degree of methylation was calculated by the number of methylated colonies in each CpG site divided by the total number of colonies in the same CpG sites (n=6). **(H)** Methylation intensity and of RNF182 in A549 cells and PC9 cells.

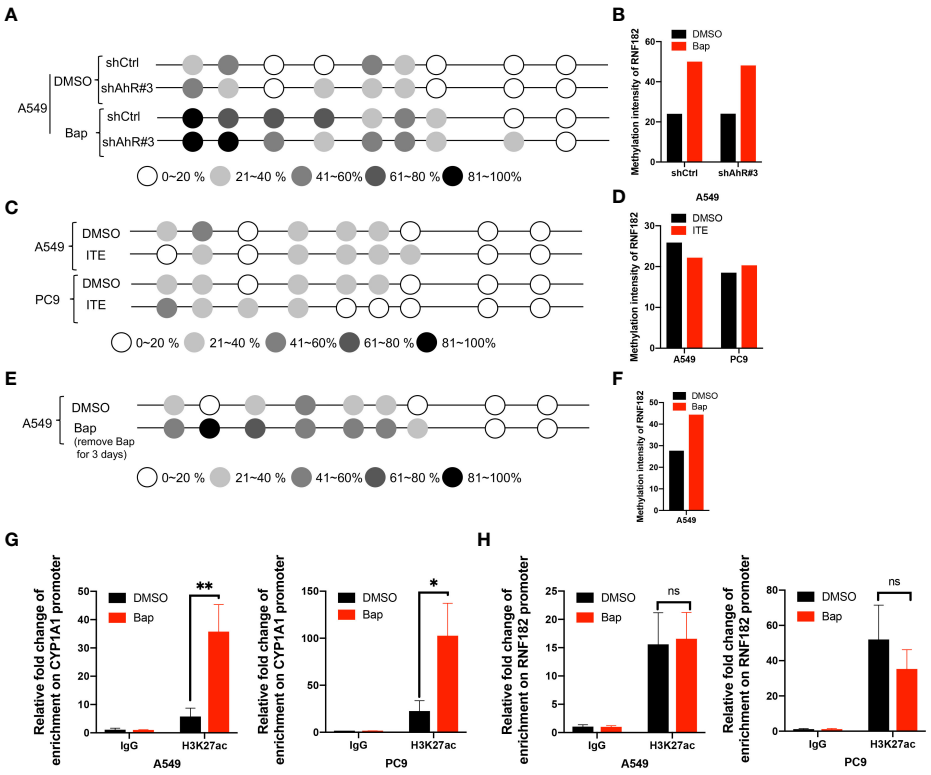

FIGURE 6
Bap mediates-RNF182 hypermethylation through an AhR-independent way. **(A)** Methylation status of RNF182 CpG sites in A549 shCtrl cells and shAhR#3 cells treated with Bap (40μM, 72h) /DMSO assayed by BGS.The degree of methylation was calculated by the number of methylated colonies in each CpG site divided by the total number of colonies in the same CpG sites (n=6). **(B)** Methylation intensity and of RNF182 in A549 shCtrl cells and shAhR#3 cells. **(C)** Methylation status of RNF182 CpG sites in A549 cells and PC9 cells treated with ITE (10μM, 8h*3) /DMSO assayed by BGS. The degree of methylation was calculated by the number of methylated colonies in each CpG site divided by the total number of colonies in the same CpG sites (n=6). **(D)** Methylation intensity and of RNF182 in A549 and PC9 cells treated with ITE (10μM, 8h*3) /DMSO. **(E)** Methylation status of RNF182 CpG sites in A549 cells assayed by BGS. A549 cells were treated with Bap (40μM) for 72h and were cultured for 72h after remove Bap from the media. The degree of methylation was calculated by the number of methylated colonies in each CpG site divided by the total number of colonies in the same CpG sites (n=6). **(F)** Methylation intensity and of RNF182 in A549 cells that were treated with Bap (40μM) for 72h and were cultured for 72h after remove Bap from the media. **(G)** ChIP assay was performed showing the enrichment of H3K27ac on the promoter of CYP1A1in DMSO/Bap-treated A549 and PC9 cells. (mean± SD, n=3). p-values are indicated (*$p < 0.05$, **$p < 0.01$) in each panel (two-sided Student's t-test). **(H)** ChIP assay was performed showing the enrichment of H3K27ac on the promoter of RNF182 in DMSO/Bap-treated A549 and PC9 cells. (mean± SD, n=3). p-values are indicated (ns means "no significance") in each panel (two-sided Student's t-test).

of DNA methyltransferase. Our study demonstrated that Bap exposure induces hypermethylation of RNF182 promoter in an AhR independent way as knockdown of AhR did not rescue the hypermethylation of RNF182 caused by Bap exposure. And ITE, an endogenous AhR ligand, also exerts no effects on the methylation patterns of RNF182. These results suggested that AhR may not be involved in aberrant DNA methylation of RNF182 caused by Bap exposure. The mechanism of Bap effects on the hypermethylation of RNF182 remains to be addressed in the future studies.

In addition to inducing hypermethylation of RNF182, Bap could activate AhR to suppress the expression of RNF182. AhR is involved in the control of many genes upon recognition of its binding motifs to regulate diverse process, including malignant transformation, hematopoietic cell development, and fate determination of immune cell lineages (43, 54). AhR could function as a transcriptional promoter or a transcriptional suppressor. For example, AhR suppressed ILC2s expression and functions through the counteraction of Gfil (a positive regulator of ILC2s) at the promoter but enhanced ILC3 maintenance to protect the host from citrobacter rodentium infection (55). Moreover, a study focused on cardiac differentiation demonstrated that TCDD impairs human embryonic stem cell cardiac differentiation by promoting AhR binding and repression of key mesoderm genes (56). Our results also showed that Bap can activate AhR binding to inhibit

RNF182 expression. Hence, Bap induced suppression of RNF182 through hypermethylation in an AhR independent way, and transcriptional regulation in an AhR dependent way.

However, the specific mechanisms underlying the anti-tumor role of RNF182 have not been thoroughly elucidated to date, and further investigations are needed. What's more, the mechanism of Bap effects on the hypermethylation of RNF182 remains to be addressed in the future studies. And Bap activates AhR to repress RNF182 expression, the potential transcriptional factor that inhibited by AhR also need further studies.

In conclusion, this study demonstrated that RNF182 functions as a tumor suppressor *via* suppressing NSCLC cells proliferation and inducing cell cycle arrest. Furthermore, RNF182 is inactivation and hypermethylation in NSCLC tumor tissues. Further molecular mechanism research revealed that AhR is activated by Bap in NSCLC cell lines and its activation decreases the expression of RNF182. In addition, Bap exposure induces hypermethylation of RNF182, leading to the suppression of RNF182. These findings imply that RNF182 plays an important role in suppressing NSCLC and Bap exposure significantly increases NSCLC risk through inhibiting the expression of RNF182.

Data availability statement

The raw data supporting the conclusions of this article will be made available by the authors, without undue reservation.

Ethics statement

The studies involving human participants were reviewed and approved by the IRB of Third Xiangya Hospital (No.2021-S055), Central South University. The patients/participants provided their written informed consent to participate in this study.

Author contributions

YT, YS, DX, and SL designed/planned the study and wrote the paper. YL performed experiments using the three types of cells and analyzed data. LO, CM, LC and NL participated in writing the paper. YC and YT participated in discussion of related experiments. YL and LO performed experiments and analyzed data. All authors contributed to the article and approved the submitted version.

Funding

This work is supported by National Natural Science Foundation of China [81872285(YS), 81874139 and 82073097 (SL), 82072594 (YT), 82073136 (DX)], Natural Science Foundation of Hunan Province [2021JJ30907 (YS)], [2020JJ5790 (CM)], [2021JJ40937 (YL)], China Postdoctoral Science Foundation [2021M700173(YL)] and the Hunan Provincial Key Area R&D Program [2021SK2013(YT)].

Conflict of interest

The authors declare that the research was conducted in the absence of any commercial or financial relationships that could be construed as a potential conflict of interest.

Publisher's note

References

1. Salama M, Liu M, Clarke C, Espaillat M, Haley J, Jin T, et al. PKCα is required for akt-mTORC1 activation in non-small cell lung carcinoma (NSCLC) with EGFR mutation. *Oncogene* (2019) 38:7311–28. doi: 10.1038/s41388-019-0950-z

2. Glanville A, Wilson B. Lung transplantation for non-small cell lung cancer and multifocal bronchioalveolar cell carcinoma. *Lancet Oncol* (2018) 19:e351–8. doi: 10.1016/S1470-2045(18)30297-3

3. Nokin M, Ambrogio C, Nadal E, Santamaria D. Targeting infrequent driver alterations in non-small cell lung cancer. *Trends Cancer* (2021) 7:410–29. doi: 10.1016/j.trecan.2020.11.005

4. Icard P, Simula L, Fournel L, Leroy K, Lupo A, Damotte D, et al. The strategic roles of four enzymes in the interconnection between metabolism and oncogene activation in non-small cell lung cancer: Therapeutic implications. *Drug Resist Updates Rev Commentaries Antimicrob Anticancer Chemother* (2022) 63:100852. doi: 10.1016/j.drup.2022.100852

5. Hecht SS. Tobacco carcinogens, their biomarkers and tobacco-induced cancer. *Nat Rev Cancer* (2003) 3:733–44. doi: 10.1038/nrc1190

6. Wang Z. Mechanisms of the synergistic lung tumorigenic effect of arsenic and benzo(a)pyrene combined- exposure. *Semin Cancer Biol* (2021) 76:156–62. doi: 10.1016/j.semcancer.2021.05.002

7. Bukowska B, Sicińska P. Influence of benzo(a)pyrene on different epigenetic processes. *Int J Mol Sci* (2021) 22:13453. doi: 10.3390/ijms222413453

8. An L, Shi Q, Fan M, Huang G, Zhu M, Zhang M, et al. Benzo[a]pyrene injures BMP2-induced osteogenic differentiation of mesenchymal stem cells through AhR reducing BMPRII. *Ecotoxicol Environ Saf* (2020) 203:110930. doi: 10.1016/j.ecoenv.2020.110930

9. Sun Y, Shi Z, Lin Y, Zhang M, Liu J, Zhu L, et al. Benzo(a)pyrene induces MUC5AC expression through the AhR/mitochondrial ROS/ERK pathway in airway epithelial cells. *Ecotoxicol Environ Saf* (2021) 210:111857. doi: 10.1016/j.ecoenv.2020.111857

10. Wang E, Liu X, Tu W, Do D, Yu H, Yang L, et al. Benzo(a)pyrene facilitates dermatophagoides group 1 (Der f 1)-induced epithelial cytokine release through aryl hydrocarbon receptor in asthma. *Allergy* (2019) 74:1675–90. doi: 10.1111/all.13784

11. Ye G, Gao H, Zhang X, Liu X, Chen J, Liao X, et al. Aryl hydrocarbon receptor mediates benzo[a]pyrene-induced metabolic reprogramming in human lung epithelial BEAS-2B cells. *Sci Total Environ* (2021) 756:144130. doi: 10.1016/j.scitotenv.2020.144130

12. Buetow L, Huang D. Structural insights into the catalysis and regulation of E3 ubiquitin ligases. *Nat Rev Mol Cell Biol* (2016) 17:626–42. doi: 10.1038/nrm.2016.91

13. Senft D, Qi J, Ronai Z. Ubiquitin ligases in oncogenic transformation and cancer therapy. *Nat Rev Cancer* (2018) 18:69–88. doi: 10.1038/nrc.2017.105

14. Wu Z, Liu H, Sun W, Du Y, He W, Guo S, et al. RNF180 mediates STAT3 activity by regulating the expression of RhoC *via* the proteasomal pathway in gastric cancer cells. *Cell Death Dis* (2020) 11:881. doi: 10.1038/s41419-020-03096-3

15. Sun W, Ma G, Zhang L, Wang P, Zhang N, Wu Z, et al. DNMT3A-mediated silence in ADAMTS9 expression is restored by RNF180 to inhibit viability and motility in gastric cancer cells. *Cell Death Dis* (2021) 12:428. doi: 10.1038/s41419-021-03628-5

16. Zhu J, Li X, Su P, Xue M, Zang Y, Ding Y. The ubiquitin ligase RNF181 stabilizes ERα and modulates breast cancer progression. *Oncogene* (2020) 39:6776–88. doi: 10.1038/s41388-020-01464-z

17. Dreij K, Rhrissorrakrai K, Gunsalus KC, Geacintov NE, Scicchitano DA. Benzo[a]pyrene diol epoxide stimulates an inflammatory response in normal human lung fibroblasts through a p53 and JNK mediated pathway. *Carcinogenesis* (2010) 31:1149–57. doi: 10.1093/carcin/bgq073

18. Tomczak K, Czerwińska P, Wiznerowicz M. The cancer genome atlas (TCGA): An immeasurable source of knowledge. *Contemp Oncol (Pozn)* (2015) 19:A68–77. doi: 10.5114/wo.2014.47136

19. Tang Z, Li C, Kang B, Gao G, Li C, Zhang Z. GEPIA: A web server for cancer and normal gene expression profiling and interactive analyses. *Nucleic Acids Res* (2017) 45:W98–W102. doi: 10.1093/nar/gkx247

20. Liu Y, Ouyang L, Mao C, Chen Y, Li T, Liu N, et al. PCDHB14 promotes ferroptosis and is a novel tumor suppressor in hepatocellular carcinoma. *Oncogene* (2022) 41:3570–83. doi: 10.1038/s41388-022-02370-2

21. Liu Y, Mao C, Wang M, Liu N, Ouyang L, Liu S, et al. Cancer progression is mediated by proline catabolism in non-small cell lung cancer. *Oncogene* (2020) 39:2358–76. doi: 10.1038/s41388-019-1151-5

22. Wang G, Cheng X, Zhou B, Wen Z, Huang Y, Chen H, et al. The chemokine CXCL13 in lung cancers associated with environmental polycyclic aromatic hydrocarbons pollution. *eLife* (2015) 4:e09419 doi: 10.7554/eLife.09419

23. Mao C, Wang M, Qian B, Ouyang L, Shi Y, Liu N, et al. Aryl hydrocarbon receptor activated by benzo (a) pyrene promotes SMARCA6 expression in NSCLC. *Am J Cancer Res* (2018) 8:1214–27.

24. Mao C, Wang X, Liu Y, Wang M, Yan B, Jiang Y, et al. A G3BP1-interacting lncRNA promotes ferroptosis and apoptosis in cancer *via* nuclear sequestration of p53. *Cancer Res* (2018) 78:3484–96. doi: 10.1158/0008-5472.Can-17-3454

25. Fu Y, Wang W, Li X, Liu Y, Niu Y, Zhang B, et al. LncRNA H19 interacts with s-adenosylhomocysteine hydrolase to regulate LINE-1 methylation in human lung-derived cells exposed to benzo[a]pyrene. *Chemosphere* (2018) 207:84–90. doi: 10.1016/j.chemosphere.2018.05.048

26. Zhang Z, Xing X, Jiang S, Qiu C, Mo Z, Chen S, et al. Global H3K79 di-methylation mediates DNA damage response to PAH exposure in Chinese coke oven workers. *Environ pollut (Barking Essex 1987)* (2021) 268:115956. doi: 10.1016/j.envpol.2020.115956

27. Zhang W, Yang J, Lv Y, Li S, Qiang M. Paternal benzo[a]pyrene exposure alters the sperm DNA methylation levels of imprinting genes in F0 generation mice and their unexposed F1-2 male offspring. *Chemosphere* (2019) 228:586–94. doi: 10.1016/j.chemosphere.2019.04.092

28. Lin S, Ren A, Wang L, Santos C, Huang Y, Jin L, et al. Aberrant methylation of Pax3 gene and neural tube defects in association with exposure to polycyclic aromatic hydrocarbons. *Clin Epigenet* (2019) 11:13. doi: 10.1186/s13148-019-0611-7

29. Sadikovic B, Andrews J, Carter D, Robinson J, Rodenhiser DI. Genome-wide H3K9 histone acetylation profiles are altered in benzopyrene-treated MCF7 breast cancer cells*. *J Biol Chem* (2008) 283:4051–60. doi: 10.1074/jbc.M707506200

30. Frost E, Taylor G, Baker M, Lovell-Badge R, Sutherland J. Establishing and maintaining fertility: The importance of cell cycle arrest. *Genes Dev* (2021) 35:619–34. doi: 10.1101/gad.348151.120

31. Cao Y, Sun Y, Chang H, Sun X, Yang S. The E3 ubiquitin ligase RNF182 inhibits TLR-triggered cytokine production through promoting p65 ubiquitination and degradation. *FEBS Lett* (2019) 593:3210–9. doi: 10.1002/1873-3468.13583

32. Liu Q, Lei J, Sikorska M, Liu R. A novel brain-enriched E3 ubiquitin ligase RNF182 is up regulated in the brains of alzheimer's patients and targets ATP6V0C for degradation. *Mol Neurodegeneration* (2008) 3:4. doi: 10.1186/1750-1326-3-4

33. Wang J, Wei Z, Gao Y, Liu C, Sun J. Activation of the mammalian target of rapamycin signaling pathway underlies a novel inhibitory role of ring finger protein 182 in ventricular remodeling after myocardial ischemia-reperfusion injury. *J Cell Biochem* (2018) 120:7635–48. doi: 10.1002/jcb.28038

34. Nectoux J, Fichou Y, Rosas-Vargas H, Cagnard N, Bahi-Buisson N, Nusbaum P, et al. Cell cloning-based transcriptome analysis in rett patients: Relevance to the pathogenesis of rett syndrome of new human MeCP2 target genes. *J Cell Mol Med* (2010) 14:1962–74. doi: 10.1111/j.1582-4934.2010.01107.x

35. Jiang H, Lin X, Liang W, Li Y, Yu X. Friedelin alleviates the pathogenesis of collagenase-induced tendinopathy in mice by promoting the selective autophagic degradation of p65. *Nutrients* (2022) 14:1–18. doi: 10.3390/nu14081673

36. Wang GZ, Zhang L, Zhao XC, Gao SH, Qu LW, Yu H, et al. The aryl hydrocarbon receptor mediates tobacco-induced PD-L1 expression and is associated with response to immunotherapy. *Nat Commun* (2019) 10:1125. doi: 10.1038/s41467-019-08887-7

37. Alexandrov K, Rojas M, Satarug S. The critical DNA damage by benzo(a) pyrene in lung tissues of smokers and approaches to preventing its formation. *Toxicol Lett* (2010) 198:63–8. doi: 10.1016/j.toxlet.2010.04.009

38. Saravanakumar K, Sivasantosh S, Sathiyaseelan A, Sankaranarayanan A, Naveen K, Zhang X, et al. Impact of benzo[a]pyrene with other pollutants induce the molecular alternation in the biological system: Existence, detection, and remediation methods. *Environ pollut (Barking, Essex: 1987)* (2022) 304:119207. doi: 10.1016/j.envpol.2022.119207

39. Lagoa R, Marques-da-Silva D, Diniz M, Daglia M, Bishayee A. Molecular mechanisms linking environmental toxicants to cancer development: Significance for protective interventions with polyphenols. *Semin Cancer Biol* (2022) 80:118–44. doi: 10.1016/j.semcancer.2020.02.002

40. Wang Z, Yang P, Xie J, Lin HP, Kumagai K, Harkema J, et al. Arsenic and benzo[a]pyrene co-exposure acts synergistically in inducing cancer stem cell-like property and tumorigenesis by epigenetically down-regulating SOCS3 expression. *Environ Int* (2020) 137:105560. doi: 10.1016/j.envint.2020.105560

41. Leclerc D, Staats Pires A, Guillemin G, Gilot D. Detrimental activation of AhR pathway in cancer: An overview of therapeutic strategies. *Curr Opin Immunol* (2021) 70:15–26. doi: 10.1016/j.coi.2020.12.003

42. Cirillo F, Lappano R, Bruno L, Rizzuti B, Grande F, Guzzi R, et al. AHR and GPER mediate the stimulatory effects induced by 3-methylcholanthrene in breast cancer cells and cancer-associated fibroblasts (CAFs). *J Exp Clin Cancer Res CR* (2019) 38:335. doi: 10.1186/s13046-019-1337-2

43. Trikha P, Lee D. The role of AhR in transcriptional regulation of immune cell development and function. *Biochim Biophys Acta Rev Cancer* (2020) 1873:188335. doi: 10.1016/j.bbcan.2019.188335

44. Kim M, Jee S, Kim K, Kim H, Yu K, Sung J. Quercetin and isorhamnetin attenuate benzo[a]pyrene-induced toxicity by modulating detoxification enzymes through the AhR and NRF2 signaling pathways. *Antioxid (Basel Switzerland)* (2021) 10:787(1–15). doi: 10.3390/antiox10050787

45. Martin EM, Fry RC. Environmental influences on the epigenome: Exposure-associated DNA methylation in human populations. *Annu Rev Public Health* (2018) 39:309–33. doi: 10.1146/annurev-publhealth-040617-014629

46. Hu W, Feng Z, Tang MS. Preferential carcinogen-DNA adduct formation at codons 12 and 14 in the human K-ras gene and their possible mechanisms. *Biochemistry* (2003) 42:10012–23. doi: 10.1021/bi034631s

47. Wojciechowski MF, Meehan T. Inhibition of DNA methyltransferases *in vitro* by benzo[a]pyrene diol epoxide-modified substrates. *J Biol Chem* (1984) 259:9711–6. doi: 10.1016/S0021-9258(17)42758-X

48. Sadikovic B, Rodenhiser DI. Benzopyrene exposure disrupts DNA methylation and growth dynamics in breast cancer cells. *Toxicol Appl Pharmacol* (2006) 216:458–68. doi: 10.1016/j.taap.2006.06.012

49. Sadikovic B, Haines TR, Butcher DT, Rodenhiser DI. Chemically induced DNA hypomethylation in breast carcinoma cells detected by the amplification of intermethylated sites. *Breast Cancer Res* (2004) 6:R329–337. doi: 10.1186/bcr799

50. Yoon JH, Smith LE, Feng Z, Tang M, Lee CS, Pfeifer GP. Methylated CpG dinucleotides are the preferential targets for G-to-T transversion mutations induced by benzo[a]pyrene diol epoxide in mammalian cells: Similarities with the p53 mutation spectrum in smoking-associated lung cancers. *Cancer Res* (2001) 61:7110–7.

51. Feng Z, Hu W, Chen JX, Pao A, Li H, Rom W, et al. Preferential DNA damage and poor repair determine ras gene mutational hotspot in human cancer. *J Natl Cancer Inst* (2002) 94:1527–36. doi: 10.1093/jnci/94.20.1527

52. Wilson V, Jones P. Chemical carcinogen-mediated decreases in DNA 5-methylcytosine content of BALB/3T3 cells. *Carcinogenesis* (1984) 5:1027–31. doi: 10.1093/carcin/5.8.1027

53. Baskunov V, Subach F, Kolbanovskiy A, Kolbanovskiy M, Eremin S, Johnson F, et al. Effects of benzo[a]pyrene-deoxyguanosine lesions on DNA methylation catalyzed by EcoRII DNA methyltransferase and on DNA cleavage effected by EcoRII restriction endonuclease. *Biochemistry* (2005) 44:1054–66. doi: 10.1021/bi048130y

54. Paris A, Tardif N, Galibert MD, Corre S. AhR and cancer: From gene profiling to targeted therapy. *Int J Mol Sci* (2021) 22(752):1–22. doi: 10.3390/ijms22020752

55. Li S, Bostick JW, Ye J, Qiu J, Zhang B, Urban JF Jr., et al. Aryl hydrocarbon receptor signaling cell intrinsically inhibits intestinal group 2 innate lymphoid cell function. *Immunity* (2018) 49:915–928.e915. doi: 10.1016/j.immuni.2018.09.015

56. Fu H, Wang L, Wang J, Bennett BD, Li JL, Zhao B, et al. Dioxin and AHR impairs mesoderm gene expression and cardiac differentiation in human embryonic stem cells. *Sci Total Environ* (2019) 651:1038–46. doi: 10.1016/j.scitotenv.2018.09.247

frontiers | Frontiers in Oncology

TYPE Original Research
PUBLISHED 14 February 2023
DOI 10.3389/fonc.2023.992233

OPEN ACCESS

EDITED BY
Haili Qian,
Chinese Academy of Medical Sciences and Peking Union Medical College, China

REVIEWED BY
Zhiguo Niu,
Xinxiang Medical University, China
Minglei Wang,
Shandong First Medical University and Shandong Academy of Medical Sciences, China

*CORRESPONDENCE
Xiaowei Zhang
dongfangzhizizhxw@aliyun.com
Xichun Hu
huxichun2017@163.com
Yanjing Guo
155068690@qq.com

†These authors have contributed equally to this work

SPECIALTY SECTION
This article was submitted to Molecular and Cellular Oncology, a section of the journal Frontiers in Oncology

RECEIVED 12 July 2022
ACCEPTED 27 January 2023
PUBLISHED 14 February 2023

CITATION
Guo Y, Chen X, Zhang X and Hu X (2023) UBE2S and UBE2C confer a poor prognosis to breast cancer *via* downregulation of Numb.
Front. Oncol. 13:992233.
doi: 10.3389/fonc.2023.992233

UBE2S and UBE2C confer a poor prognosis to breast cancer *via* downregulation of Numb

Yanjing Guo[1,2*†], Xinyu Chen[2,3†], Xiaowei Zhang[2,4*] and Xichun Hu[2,3*]

[1]Department of Head and Neck Tumors and Neuroendocrine Tumors, Fudan University Shanghai Cancer Center, Shanghai, China, [2]Department of Oncology, Shanghai Medical College, Fudan University, Shanghai, China, [3]Department of Breast cancer and Urological Medical Oncology, Fudan University Shanghai Cancer Center, Shanghai, China, [4]Department of Gastrointestinal Medical Oncology, Fudan University Shanghai Cancer Center, Shanghai, China

Purpose: Ubiquitin-conjugating enzymes E2S (UBE2S) and E2C (UBE2C), which mediate the biological process of ubiquitination, have been widely reported in various cancers. Numb, the cell fate determinant and tumor suppressor, was also involved in ubiquitination and proteasomal degradation. However, the interaction between UBE2S/UBE2C and Numb and their roles in the clinical outcome of breast cancer (BC) are not widely elucidated.

Methods: *Oncomine*, Cancer Cell Line Encyclopedia (CCLE), the Human Protein Atlas (HPA) database, qRT-PCR, and Western blot analyses were utilized to analyze UBE2S/UBE2C and Numb expression in various cancer types and their respective normal controls, breast cancer tissues, and breast cancer cell lines. The expression of UBE2S, UBE2C, and Numb in BC patients with different ER, PR, and HER2 status, grades, stages, and survival status was compared. By Kaplan–Meier plotter, we further evaluated the prognostic value of UBE2S, UBE2C, and Numb in BC patients. We also explored the potential regulatory mechanisms underlying UBE2S/UBE2C and Numb through overexpression and knockdown experiments in BC cell lines and performed growth and colony formation assays to assess cell malignancy.

Results: In this study, we showed that UBE2S and UBE2C were overexpressed while Numb was downregulated in BC, and in BC of higher grade, stage, and poor survival. Compared to hormone receptor negative (HR–) BC cell lines or tissues, HR + BC demonstrated lower UBE2S/UBE2C and higher Numb, corresponding to better survival. We also showed that increased UBE2S/UBE2C and reduced Numb predicted poor prognosis in BC patients, as well as in ER+ BC patients. In BC cell lines, UBE2S/UBE2C overexpression decreased the level of Numb and enhanced cell malignancy, while knocking down UBE2S/UBE2C demonstrated the opposite effects.

Conclusion: UBE2S and UBE2C downregulated Numb and enhanced BC malignancy. The combination of UBE2S/UBE2C and Numb could potentially serve as novel biomarkers for BC.

KEYWORDS

UBE2s, UBE2C, Numb, breast cancer, prognosis

1 Introduction

The latest cancer statistics have revealed that breast cancer (BC) is the most prevalent cancer of all new diagnoses threatening women's lives worldwide in 2020 (1, 2). The increasing global burden of breast cancer makes it urgent to seek effective biomarkers and intervention approaches for the advancement of BC treatment. Breast cancer is categorized into different molecular subtypes based on the expression of estrogen receptor (ER), progesterone receptor (PR), human epidermal growth factor receptor 2 (HER2), and antigen Ki-67, of which ER-positive (ER+) breast cancer is the most frequent molecular subtype (3, 4). Thus, finding differentially expressed genes between ER+ and ER-negative (ER−) breast cancer may contribute to understanding the pathogenesis of breast cancer and developing new druggable targets for breast cancer treatment (5).

The ubiquitination-proteasome pathway is a post-translational modification of the protein degradation system discovered in 2005 (6, 7). This biological process was mediated by E1, E2, and E3 enzymes, which carry out activation, conjugation, and ligation, respectively, and sequentially. According to recent studies, extensive progress has been made in the deregulation of the ubiquitination system, which has led to a variety of diseases, including cancer (8, 9). Ubiquitin-conjugating enzymes E2S (UBE2S) and E2C (UBE2C) are important members of the E2 family and were reported to play oncogenic roles in the tumorigenesis and progression of many cancers (10–15). In breast cancer, it has been reported that inhibition of UBE2S or UBE2C suppressed the malignant characteristics of breast cancer cells and sensitized cancer cells to radiation or drugs to enhance clinical effectiveness (11, 16–18). Besides, there was an interrelationship between UBE2S and UBE2C in regulating E3 ligase substrate modification, multiubiquitination, cell cycle progression, and drug resistance (19, 20). However, the prognostic effects as well as the collective regulatory mechanisms of both UBE2S and UBE2C in breast cancer remain to be elucidated.

Numb, widely known as a cell fate determinant and tumor suppressor in many cancers, was reported to regulate tumor suppressors, such as p53 and PTEN, and promote GLI1 oncogene degradation *via* ubiquitination (21–26). Regarding Numb expression regulation, LNX1 and LNX2, known as ligands of NUMB Protein X1 and X2, are E3 ubiquitin ligases that interact with Numb and promote its degradation (27). Besides, our previous work revealed an auto-regulatory model at the transcriptional level explaining the maintenance of a low Numb-expressing state, which promotes tumor aggressiveness in prostate cancer (28). It has been widely proven in breast cancer that Numb has a tumor-suppressive role (29, 30). In this study, we tend to explore the clinical outcome of differential expression of Numb in breast cancer and possible new regulatory mechanisms for different Numb-expressing statuses.

Given above, the expression and prognostic roles of UBE2S, UBE2C, and Numb were evaluated in breast cancer as well as in ER + breast cancer in this research. Besides, we explored the correlation between UBE2S/UBE2C and Numb, unraveling potential regulatory mechanisms and facilitating the development of novel therapeutic strategies.

2 Materials and methods

2.1 The cBioPortal database analysis

The cBioPortal (cBio Cancer Genomics Portal) database (https://www.cbioportal.org/), which provides visualization and analysis of large-scale cancer genomics in the TCGA database, was used for coexpression analysis. In this study, the Breast Invasive Carcinoma (TCGA, Firehose Legacy) cohort was analyzed to compare the correlation between Numb and UBE2S or UBE2C. Pearson's correlation score and Spearman score were calculated with default software parameters.

2.2 Oncomine database analysis

We analyzed the differential mRNA expression of UBE2S, UBE2C, and Numb in a variety of major cancer subtypes and their respective normal controls using the *Oncomine database* (www.oncomine.org). Besides, we also compared the overexpression or underexpression pattern of UBE2S, UBE2C, and Numb mRNA levels in nine independent datasets of breast cancer specimens and their matched normal tissues. Furthermore, the expression levels of UBE2S, UBE2C, and Numb were compared according to different clinical outcomes or survival statuses of breast cancer patients, providing evidence for potential predictors of prognosis.

2.3 Cancer Cell Line Encyclopedia analysis

The CCLE public project (https://portals.broadinstitute.org/ccle), which contains massive RNA, whole exome, and whole genome sequencing data for nearly 1,000 cancer cell lines, was applied to analyze the copy number of UBE2S, UBE2C, and Numb in certain major cancer cell lines, including breast cancer.

2.4 The Human Protein Atlas database analysis

Representative immunohistochemical staining of UBE2S, UBE2C, and Numb was retrieved from the Human Protein Atlas database (www.proteinatlas.org), which contains pathological information based on protein expression data from various forms of human cancer, including breast cancer, together with in-house generated immunohistochemically stained tissue section images.

2.5 The Kaplan-Meier plotter survival analysis

We utilized the Kaplan–Meier plotter (http://kmplot.com/analysis) web service to evaluate the correlation between prognostic values (overall survival and relapse-free survival) and investigated

genes (UBE2S, UBE2C, and Numb) mRNA expression in breast cancer and the ER+ subtype based on the hazard ratios (HR) and logrank *p*-values. The high and low groups of UBE2S, UBE2C, and Numb were defined based on a 50% cutoff or the cutoff with the most significant *p*-value.

2.6 Cell culture and reagents

All cell lines were obtained from the American Type Culture Collection (ATCC, Manassas, VA, USA). MCF10A cells were grown in DMEM/F12 (Invitrogen, Carlsbad, CA, USA) supplemented with 10% horse serum (Invitrogen), EGF (ProSpec, Rehovot, Israel), hydrocortisone (Sigma, Beijing, China), insulin (Sigma), and 1% penicillin–streptomycin (Invitrogen). MDA-MB-231, MCF7, and T47D cells were grown in DMEM (Invitrogen). MDA-MB-468 and SK-BR-3 cells were cultured with Leibovitz's L-15 (Gibco, Grand Island, USA) and McCoy's 5A (Gibco), respectively. Except for MDF10A medium, all growth media were supplemented with 10% fetal bovine serum (Invitrogen), 100 Uml^{-1} penicillin, and 100 μgml^{-1} streptomycin (Invitrogen). MDA-MB-468 cells were cultured in a humidified atmosphere of 0.03% CO_2 at 37°C while all other cell lines were cultured in the same conditions except that the CO_2 concentration was 5%.

2.7 Quantitative RT-PCR

Total RNA was extracted with TRIzol reagent following the manufacturer's instructions (Invitrogen) and proceeded to reverse transcription and real-time PCR with SYBR Premix Ex Taq (TaKaRa, Beijing, China). The expression levels of UBE2S, UBE2C, and Numb were normalized to ACTIN and calculated using the $2^{-\Delta\Delta Ct}$ method. The primer sequences (5'–3'):

UBE2S-forward: CCGACACGTACTGCTGACC;
UBE2S-reverse: GCCGCATACTCCTCGTAGTTC;
UBE2C-forward: AGTGGCTACCCTTACAATGCG;
UBE2C-reverse: TTACCCTGGGTGTCCACGTT;
NUMB-forward: TCAGCAGATGGACTCAGAGTT;
NUMB-reverse: AGGCTCTATCAAAGTTCCTGTCT;
ACTIN-forward: GCACAGAGCCTCGCCTT;
ACTIN-reverse: GTTGTCGACGACGAGCG.

2.8 Western blot analysis

MCF10A protein was extracted using M-PER containing an EDTA-free Halt Protease Inhibitor Cocktail (Thermo Fisher Scientific, Massachusetts, USA), while proteins from all other cell lines were extracted using RIPA lysis buffer. Protein transfer was performed on a nitrocellulose membrane (Bio-Rad Laboratories, California, USA). Primary antibodies include: UBE2S (11878; Cell Signaling Technology, Massachusetts, USA; 1:1,000), UBE2C (14234; Cell Signaling Technology; 1:1,000), Numb (sc-136554; Santa Cruz Biotechnology, Texas, USA; 1:200), and ACTIN (3700; Cell Signaling Technology; 1:1,000). Protein was visualized with the ECL Western Blotting Detection System (PerkinElmer, USA), and a densitometry value was determined in terms of pixel intensity by ImageJ.

2.9 Transient overexpression and knockdown

MCF7 and MDA-MB-231 cells were seeded in 6-well plates and cultured to 70%–80%. For transient overexpression (OE), cells were transfected with a constructed plasmid (pcDNA3.1, Thermo Fisher Scientific) overexpressing UBE2S/UBE2C or a negative control using Lipofectamine 3000 (Invitrogen). Gene sequences were obtained from the Ensembl human genome assembly (Genome Reference Consortium GRCh38). For transient knockdown, cells were transfected with small interfering RNAs (siRNAs) targeting UBE2S/UBE2C or a negative control (Shanghai Genechem Co., Ltd., Shanghai, China):

si-UBE2S-1: GAUCCUGCUUUGUGCUAAAGA;
si-UBE2S-2: GAAUCAGACAACCUUGUCAAA;
si-UBE2C-1: UGAAAAGGUUGUCUGAUUCAG;
si-UBE2C-2: GGAAAGACAAGGGAAGAAACC.

After 4-hour incubation, the medium was replaced with DMEM containing 10% fetal bovine serum. Transfection efficiency was determined 48 h later using RT-qPCR and Western blotting.

2.10 Colony formation assay

MCF7 and MDA-MB-231 cells were seeded in 6-well plates at a concentration of 1,000 cells per well and cultured for 10–14 days. Colonies were fixed and stained using 0.2% crystal violet.

2.11 Cell counting kit-8 assay

For the CCK-8 cell proliferation assay, MCF7 and MDA-MB-231 cells were seeded in 96-well plates at a concentration of 3,000 cells per well. The absorbance at 450 nm was determined at the indicated time points using a microplate reader two hours after adding 10 µl of CCK-8 solution (HY-K0301; MedChemExpress, China) to each well.

2.12 Statistical analysis

In this study, data obtained from the *Oncomine* database were presented using Prism GraphPad software (LaJolla) and analyzed using a Student's *t*-test. A statistical difference was determined two-sidedly with *P*-values less than 0.05, which are indicated with the following asterisks: $*P < 0.05$, $**P < 0.01$, $**P < 0.001$, $****P < 0.0001$. For the rest of the study's data, statistical analyses were calculated with default software parameters. All experiments were performed in three biological replicates.

3 Results

3.1 UBE2S and UBE2C are overexpressed while Numb is downregulated in breast cancer

To explore the expression and potential clinical significance of UBE2S, UBE2C, and Numb in breast cancer, first we analyzed the *Oncomine* microarray datasets to determine the mRNA levels of UBE2S, UBE2C, and Numb in a variety of malignant tumor types, including breast cancer. As shown in Figure 1, the expression of UBE2S and UBE2C was generally higher and Numb expression was lower in various cancer types than their respective normal controls, especially in breast cancer, although no obvious differential expression of Numb was shown in certain cancers. Besides, we resorted to the *Oncomine* datasets regarding breast cancer and found that there was evidently higher mRNA expression of UBE2S and UBE2C but lower Numb expression in breast cancer samples than their respective normal controls (Figure 2A). Next, we found that the expression of UBE2S and UBE2C was upregulated while Numb was downregulated in breast cancer tissues of higher histological grades and pathological stages (Figures 2B, C). More specifically, the comparison of UBE2S, UBE2C, and Numb mRNA expression across nine independent analyses demonstrated that UBE2S and UBE2C were markedly elevated and Numb was significantly reduced in breast cancer (Figure 3A). To identify the differential expression of UBE2S, UBE2C, and Numb in breast cancer tissues at the protein level, we resorted to the Human Protein Atlas (HPA) database. Representative images of immunohistochemical staining of UBE2S, UBE2C, and Numb in breast cancer tissues from the same patients are shown in Figure 3B. We found that breast cancer tissues with medium or high protein staining of UBE2S and UBE2C had negative or weak staining of Numb protein (Figure 3B, Cases 1–3>), whereas the lower protein levels of UBE2S and UBE2C displayed strong staining of Numb protein (Figure 3B, Case 4). Consistently, we found out that the copy numbers of UBE2S and UBE2C were significantly upregulated in breast cancer cell lines and rank relatively high among various cancer cell types through CCLE analysis, while the Numb copy number was relatively low in breast cancer cell lines (Figure S1). Taken together, these results revealed an overexpression of both UBE2S and UBE2C and a downregulation of Numb in breast cancer, indicating the oncogenic effects of UBE2S and UBE2C and the tumor suppressive role of Numb in breast cancer.

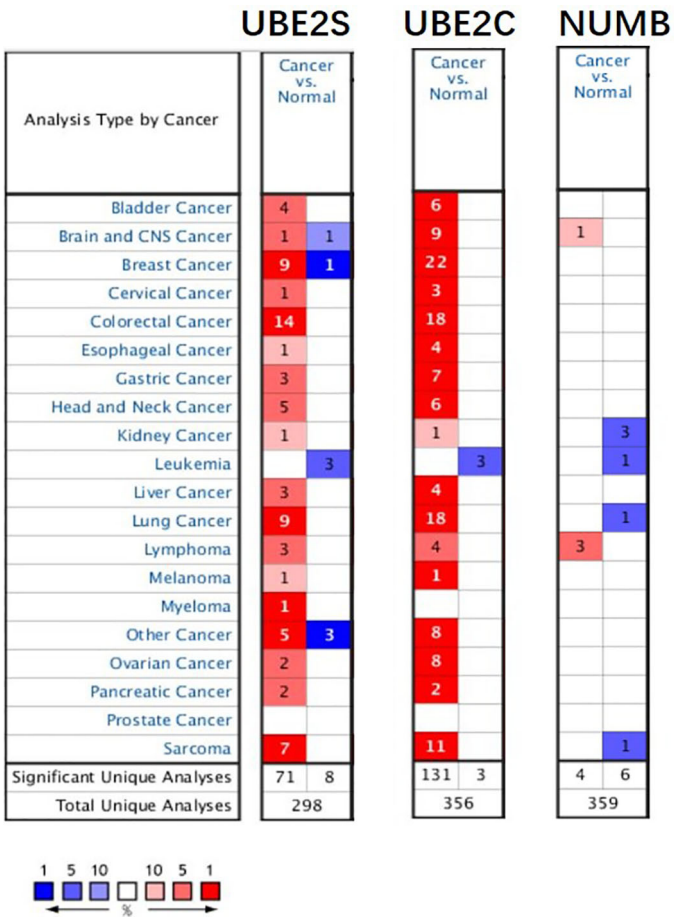

FIGURE 1
The expression of UBE2S, UBE2C, and Numb in different types of tumors (*Oncomine* database). In the diagram, the threshold parameters were set as follows: p-value of 0.01, fold change of 2, and gene rank of 10% for the cell color analysis within the cell. In each form, the number represents the number of analyses that meet the threshold across various malignancies.

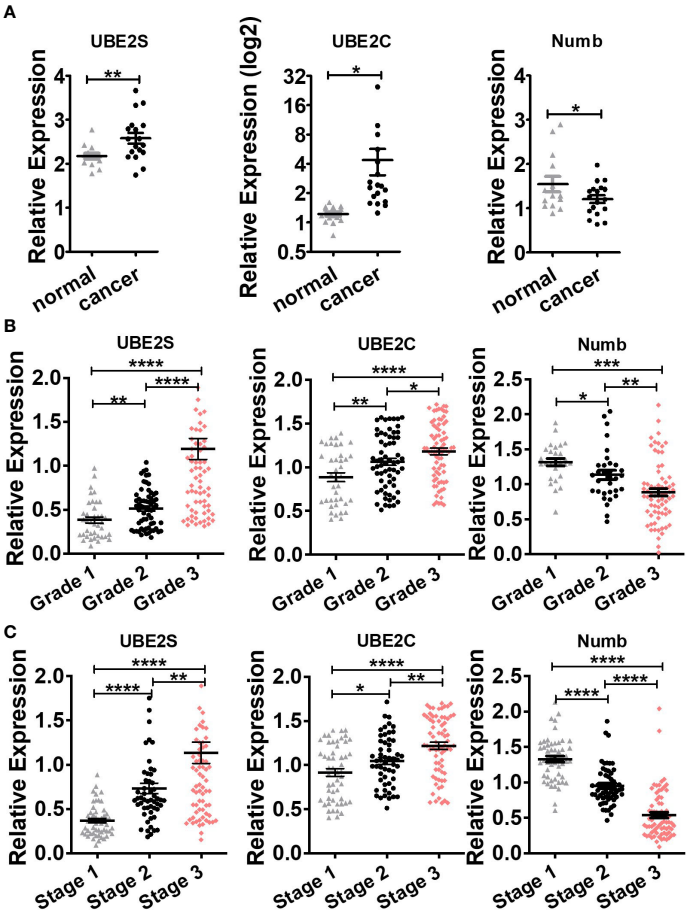

FIGURE 2
Comparison of UBE2S, UBE2C, and Numb between **(A)** normal breast tissues and breast tumors, as well as breast tumors of various **(B)** grades and **(C)** stages. **(A)** UBE2S and UBE2C are upregulated, while Numb is downregulated in breast tumors (n = 14) compared with normal breast tissues (n = 18) (*Oncomine* database of Ma breast, 2009). normal, normal breast tissues; cancer, breast cancer tissues). **(B)** With the increase in breast tumor grade (grade 1 n = 39, grade 2 n = 63, grade 3 n = 76), UBE2S and UBE2C show elevated expression while Numb exhibits decreased level. **(C)** With the increase in breast tumor stage (stage 1 n = 52, stage 2 n = 54, stage 3 n = 76), UBE2S and UBE2C show elevated expression while Numb expression decreases. A Student's t-test was used for the statistical analysis. *, P <0.05; **, P <0.01; ***, P <0.001; ****, P <0.0001.

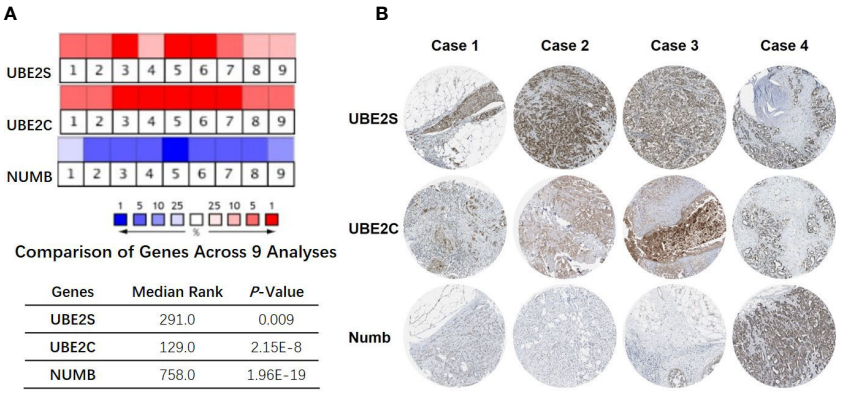

Genes	Median Rank	*P*-Value
UBE2S	291.0	0.009
UBE2C	129.0	2.15E-8
NUMB	758.0	1.96E-19

FIGURE 3
Correlation of UBE2S, UBE2C, and Numb expression. **(A)** The mRNA levels in breast cancer samples and corresponding normal controls across nine analyses (Oncomine database). The median rank and p-value for the genes across each of the analyses are shown in the graph. **(B)** Representative images of immunohistochemical staining of UBE2S, UBE2C, and Numb in four groups of breast cancer tissues, with each case from the same patients. Breast cancer tissues with medium or high protein staining of UBE2S and UBE2C have negative or weak staining of Numb protein (Cases 1–3) whereas tissues with lower levels of UBE2S and UBE2C protein expression display strong staining of Numb protein (Case 4). Data were obtained from the Human Protein Atlas (HPA) database.

3.2 UBE2S and UBE2C are downregulated while Numb is upregulated in ER+ BC compared with ER– BC

ER+ breast cancer is the most common pathological subtype and accounts for over 70% of breast cancer (31). As the most prevalent breast cancer subtype, ER+ breast cancer was correlated with lower tumor grade and lower metastatic rate of lymph nodes and better survival (32, 33). To explore the functional role of UBE2S, UBE2C, and Numb in ER+ breast cancer, we compared the mRNA levels of the three genes in ER+ and ER– breast cancer through *Oncomine* dataset analysis. As demonstrated in Figure 4A, compared with ER+ breast cancer, the mRNA levels of UBE2S and UBE2C were higher, while NUMB was reduced in ER– breast cancer. To verify the above findings in breast cell lines, we adopted one normal breast epithelial cell line (MCF10A), three ER– breast cancer cell lines (MDA-MB-231, MDA-MB-468, and SK-BR-3), and two ER+ breast cancer cell lines (MCF7 and T47D). Both qRT-PCR and western blot confirmed increased UBE2S and UBE2C, as well as decreased Numb expression, in breast cancer cell lines compared to MCF10A. Compared with ER+ breast cancer cell lines, ER– cells demonstrated higher UBE2S and UBE2C alongside lower Numb, also in line with transcriptomic results (Figures 4B, C). It is widely known that breast cancer is classified into different subtypes according to ER, PR (progesterone receptor), and HER2 (human epidermal growth factor receptor 2) status. Apart from ER+ and ER– breast cancers, we also compared the expression of UBE2S, UBE2C, and Numb in PR positive (PR+) and PR negative (PR–) breast cancers as well as in HER2 positive (HER2+) and HER2 negative (HER2–) breast cancers. As shown in Figure S2A, compared with PR+ breast cancer, the mRNA levels of UBE2S and UBE2C were higher, while NUMB was lower in PR– breast cancer. However, no statistical significance of UBE2S, UBE2C, or Numb expression was observed between HER2+ and HER2– breast cancer (Figure S2B). These data indicate that the regulation between UBE2S/UBE2C and Numb plays a more critical role in hormone receptor-positive breast cancer than in HER2+ breast cancer.

3.3 UBE2S and UBE2C are worse prognosis predictors in breast cancer and ER positive subtype patients in contrast to Numb

By using *Oncomine* data analysis and Kaplan–Meier plotter survival analysis, we further analyzed the prognostic effects of UBE2S, UBE2C, and Numb in breast cancer patients. In Figures 5A, B, it revealed that the mRNA levels of UBE2S and UBE2C were lower in breast cancer patients who had a longer lifespan than those with a shorter lifespan, grouped by overall survival status or survival status at 5 years (alive or dead). On the contrary, patients with a longer lifetime had higher Numb mRNA expression (Figure 5C). In other words, high levels of UBE2S and UBE2C and decreased Numb expression were associated with a shorter lifespan in breast cancer patients. Next, we evaluated the impact of differential mRNA expression of UBE2S, UBE2C, and Numb on the clinical survival of breast cancer patients. We found that higher levels of UBE2S and UBE2C and lower expression of

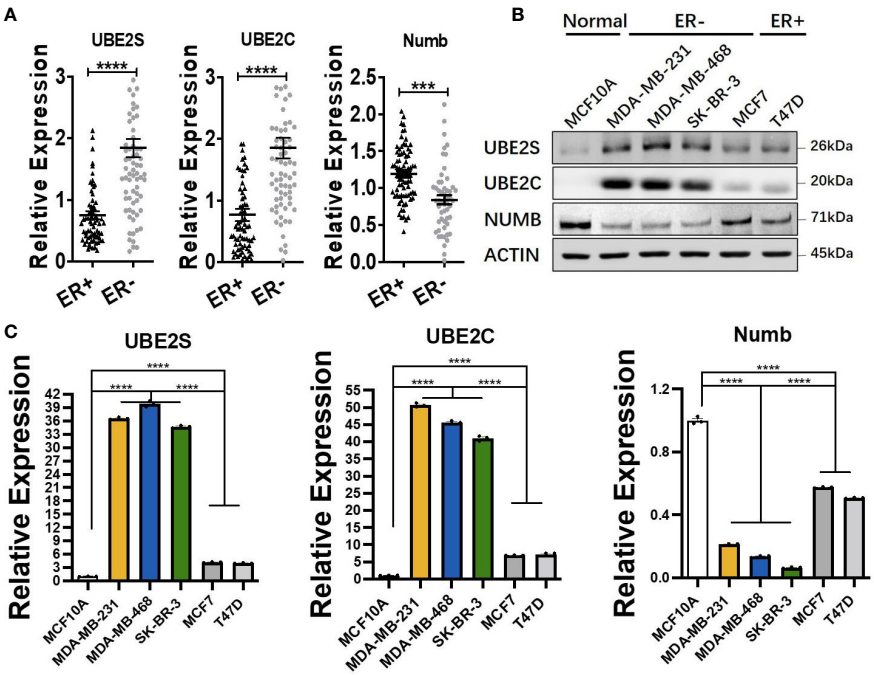

FIGURE 4
Comparison of UBE2S, UBE2C, and Numb between ER+ and ER– breast tumors. **(A)** The mRNA levels in ER+ and ER– breast tumors (ER+ *n* = 70, ER– *n* = 74). ER– breast cancer shows higher levels of UBE2S and UBE2C, as well as lower Numb expression. **(B)** Western blot for protein levels and **(C)** qRT-PCR for mRNA levels in breast cell lines. One normal breast epithelial cell line (MCF10A), three ER– breast cancer cell lines (MDA-MB-231, MDA-MB-468, and SK-BR-3), and two ER+ breast cancer cell lines (MCF7 and T47D) a re adopted. Breast cancer cell lines demonstrate higher UBE2S and UBE2C and lower Numb than normal controls. ER– breast cancer cell lines show higher UBE2S and UBE2C, as well as lower Numb expression, than ER+ breast cancer cell lines. Student's *t*-test was used for the statistical analysis. ***, $P < 0.001$; ****, $P < 0.0001$.

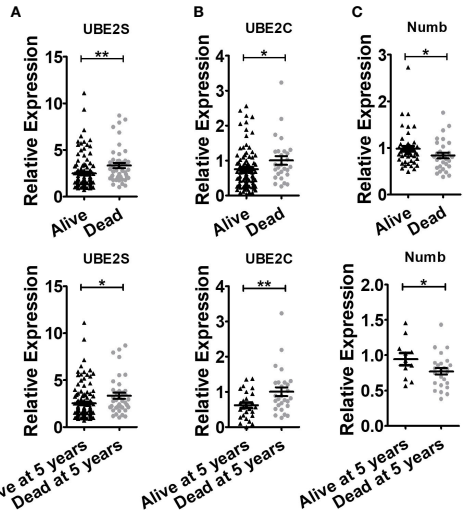

FIGURE 5
Breast cancer patients with shorter lifespans have higher levels of UBE2S and UBE2C and lower expression of Numb. **(A)** UBE2S mRNA expression in the *Oncomine* database of Pawitan Breast grouped by overall survival status (Up, Alive n = 113, Dead n = 46) and survival status at 5 years (Bottom, Alive at 5 years n = 121, Dead at 5 years n = 38). **(B)** UBE2C mRNA expression in *Oncomine* database of Esserman Breast grouped by overall survival status (Up, Alive n = 98, Dead n = 27) and survival status at 5 years (Bottom, Alive at 5 years n = 27, Dead at 5 years n = 27). **(C)** Numb mRNA expression in the *Oncomine* database of Sorlie Breast grouped by overall survival status (Up, Alive n = 46, Dead n = 30) and survival status at 5 years (Bottom, Alive at 5 years n = 11, Dead at 5 years n = 25). (*t* test was used for the statistical analysis. *, *P* <0.05; **, *P* <0.01).

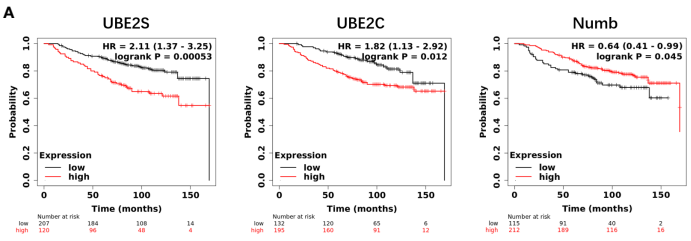

Overall survival (months)	UBE2S	UBE2C	Numb
Low expresson	136.8	136.8	79.2
High expresson	62.4	74.4	136.8
P-Value	0.0005	0.0122	0.0451

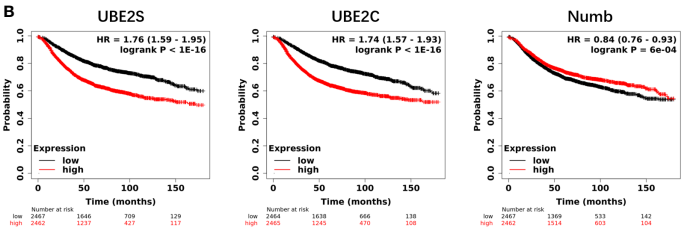

Relapse free survival (months)	UBE2S	UBE2C	Numb
Low expresson	81.6	81.6	44.4
High expresson	34.13	33	57
P-Value	<1e - 16	<1e - 16	0.0006

FIGURE 6
Higher levels of UBE2S and UBE2C and a lower level of NUMB correlate with shorter OS **(A)** and RFS **(B)** in breast cancer patients by the Kaplan–Meier plotter survival analysis. OS, Overall Survival. RFS, Relapse-Free Survival. The *p*-value and survival time were indicated in the respective graphs.

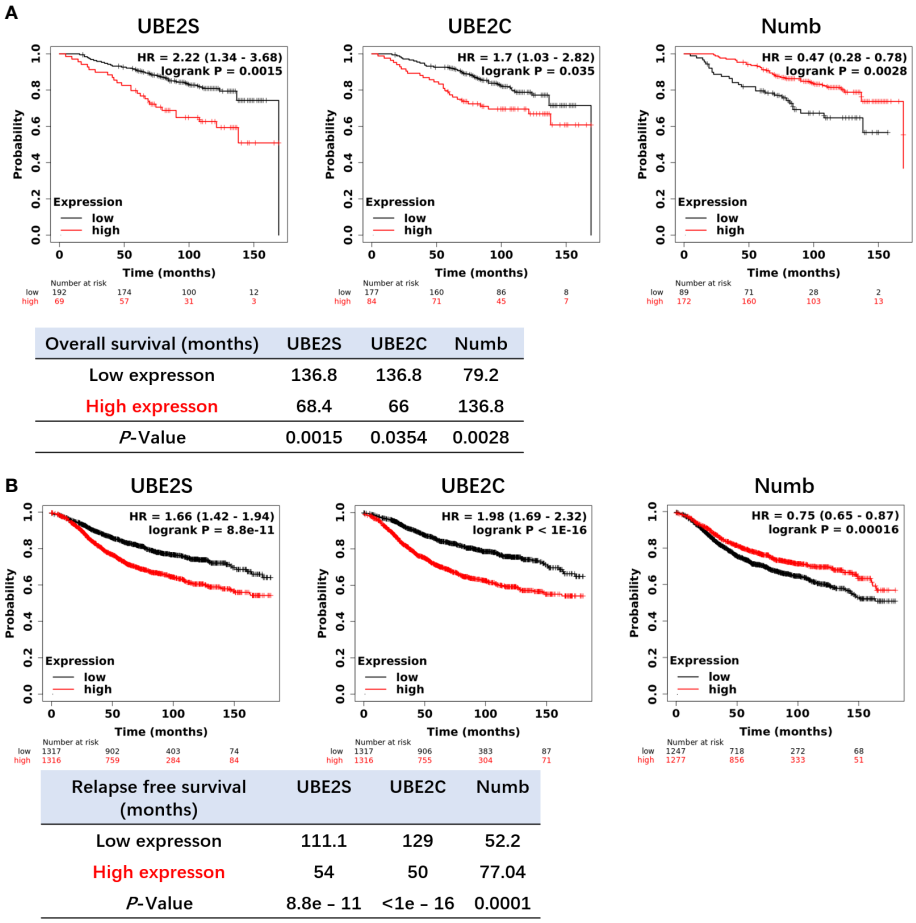

Overall survival (months)	UBE2S	UBE2C	Numb
Low expresson	136.8	136.8	79.2
High expresson	68.4	66	136.8
P-Value	0.0015	0.0354	0.0028

Relapse free survival (months)	UBE2S	UBE2C	Numb
Low expresson	111.1	129	52.2
High expresson	54	50	77.04
P-Value	8.8e - 11	<1e - 16	0.0001

FIGURE 7
Increased expression of UBE2S and UBE2C and reduced expression of Numb are related to shorter OS **(A)** and RFS **(B)** in ER+ breast cancer patients by the Kaplan–Meier plotter survival analysis. The *p*-value and survival time were indicated in the respective graphs.

Numb were correlated with shorter overall survival (OS) and relapse-free survival (RFS) in breast cancer patients (Figure 6). As mentioned above, the expression of UBE2S and UBE2C was decreased and Numb was increased in ER+ breast cancer; we thus explored the prognostic values of UBE2S, UBE2C, and Numb in ER+ breast cancer patients. As demonstrated in Figure 7, increased expression of UBE2S and UBE2C predicted worse OS and RFS, while increased Numb expression was related to a better outcome in ER+ breast cancer patients. In ER– breast cancer patients, UBE2S, UBE2C, and Numb did not show a correlation with OS or RFS (Figure S3). To further clarify the negative correlation between UBE2S/UBE2C and Numb in breast cancer prognosis, we compared the OS and RFS in breast cancer patients divided into three groups: one with higher UBE2S or UBE2C and lower Numb expression (UBE2S or UBE2C high + Numb low), one with lower UBE2S or UBE2C and higher Numb expression (UBE2S or UBE2C low + Numb high), and the rest were categorized into the third group. As indicated in Figure 8 and Supplementary Table 1, UBE2S or UBE2C high + Numb low patients had notably shorter OS and RFS compared with patients with UBE2S or UBE2C low + Numb high patients. Taken together, UBE2S and UBE2C were worse prognosis predictors in breast cancer patients as well as in ER+ patients, while Numb showed the opposite prognostic effect.

3.4 Numb is negatively correlated with UBE2S and UBE2C in breast cancer and UBE2S or UBE2C inhibit Numb expression

As indicated above, UBE2S and UBE2C predicted a poorer prognosis while Numb demonstrated opposite effects, so the correlation between Numb and UBE2S/UBE2C was further investigated in the cBioPortal database to unravel potential regulatory mechanisms. As shown in Supplementary Table 2, there were 6,431 negatively correlated genes with Numb that were statistically significant (P <0.05). Among these genes, UBE2S ranked first and UBE2C ranked 526th based on Spearman's Correlation Score. By cBioPortal regression analysis, highly negative relevant coefficients were revealed between Numb and UBE2S (Spearman's correlation = −0.52, Pearson's correlation = −0.51) and a moderately negative correlation between Numb and UBE2C (Spearman's correlation = −0.34, Pearson's correlation = −0.33) (Figure 9A). We also sought to determine the correlation between UBE2S, UBE2C, and Numb expression in three common types of breast cancer, namely ER+, HER2+, and triple-negative breast cancer (TNBC). Consistently, there was a negative correlation

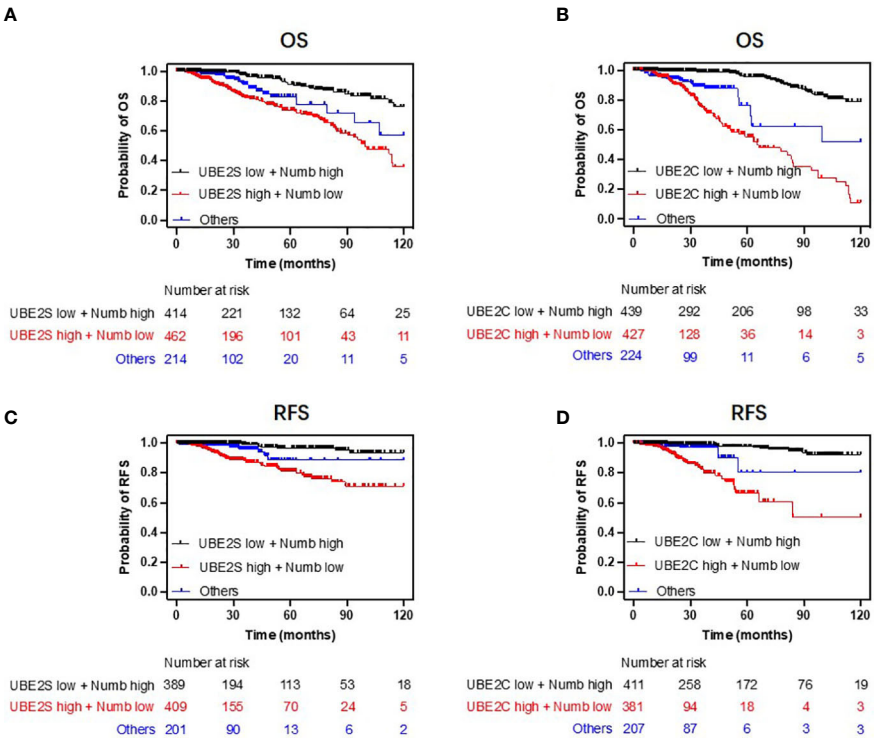

FIGURE 8
Combining UBE2S or UBE2C with Numb predicts breast cancer patients' survival. Patients with low UBE2S or UBE2C levels and high Numb expression demonstrated higher OS **(A, B)** and RFS **(C, D)** probabilities compared to those with high UBE2S or UBE2C levels and low Numb expression. Univariate regression analyses are presented in Supplementary Table 1.

between UBE2S and Numb, as well as between UBE2C and Numb, in all three subtypes, with highly negative relevant coefficients indicated in each graph, providing more evidence for the negative correlation between Numb and UBE2S, as well as between Numb and UBE2C (Figure S4). To confirm the negative regulation of Numb by UBE2S and UBE2C, we overexpressed (OE) UBE2S or UBE2C in the ER+ cell line MCF7, which exhibits higher Numb expression and lower levels of UBE2S and UBE2C and knocked down UBE2S or UBE2C with small interfering RNA (si) in the ER- cell line MDA-MB-231, which has higher levels of UBE2S and UBE2C and lower Numb expression. It turned out that OE-UBE2S and OE-UBE2C both resulted in decreased Numb expression at the protein and mRNA levels (Figures 9B, C, S5A, C), whereas a significant increase in Numb was observed by si-UBE2S and si-UBE2C (Figures 9B, C, S5B, D). To assess tumor cell malignancy, we performed colony formation and Cell Counting Kit-8 (CCK-8) assays. We found MCF7 cells with either UBE2S or UBE2C overexpression demonstrated stronger abilities to form colonies and proliferate, while MDA-MB-231 cells with either UBE2S or UBE2C knockdown showed significantly lower malignancy than control (Figures 9D, E). In conclusion, UBE2S and UBE2C both inhibited Numb expression and promoted breast tumor malignancy.

4 Discussion

With the increasing incidence of breast cancer all over the world, it is vital to explore the underlying molecular mechanism of this tumor, which jeopardizes women's lives. Different from other common cancers, breast cancer was divided into four molecular subtypes according to the status of HR, HER-2, and Ki-67, accounting for different therapeutic strategies and prognosis (34). Due to the complexity of clinical manifestations, it is urgent to explore the molecular characteristics of breast cancer, which would facilitate the development of effective clinical interventions. Great progress has been made in the development and progression of breast cancer, but inevitable treatment failure occurs due to the heterogeneity of cancer cells (35–37). The existence of cancer stem cells (CSC) or tumor initiating cells has been put forward and widely validated, accounting for progression, relapse, and treatment failure in multiple cancers (38–40). In this study, we aim to identify a breast cancer cell subpopulation as a potential clinical treatment target marked by possible prognostic markers.

Ubiquitin signaling plays an important role in protein degradation by post-translational modification, involving the multistep enzymatic actions of ubiquitin activating enzyme E1, ubiquitin conjugating enzyme E2, and ubiquitin ligase E3 (41). A growing body of research revealed that abnormalities in ubiquitin signaling were implicated in a variety of malignancies (41–43). As important members of the E2 family, it was reported that UBE2S and UBE2C were highly expressed in cancerous tissues compared with surrounding normal tissues, and aberrant expression of the genes was reported to be involved in tumorigenesis and tumor progression, including breast cancer (11, 44–49). A better understanding of the regulatory mechanisms underlying UBE2S and UBE2C function in breast cancer is expected to identify novel prognostic markers and develop new effective anticancer strategies.

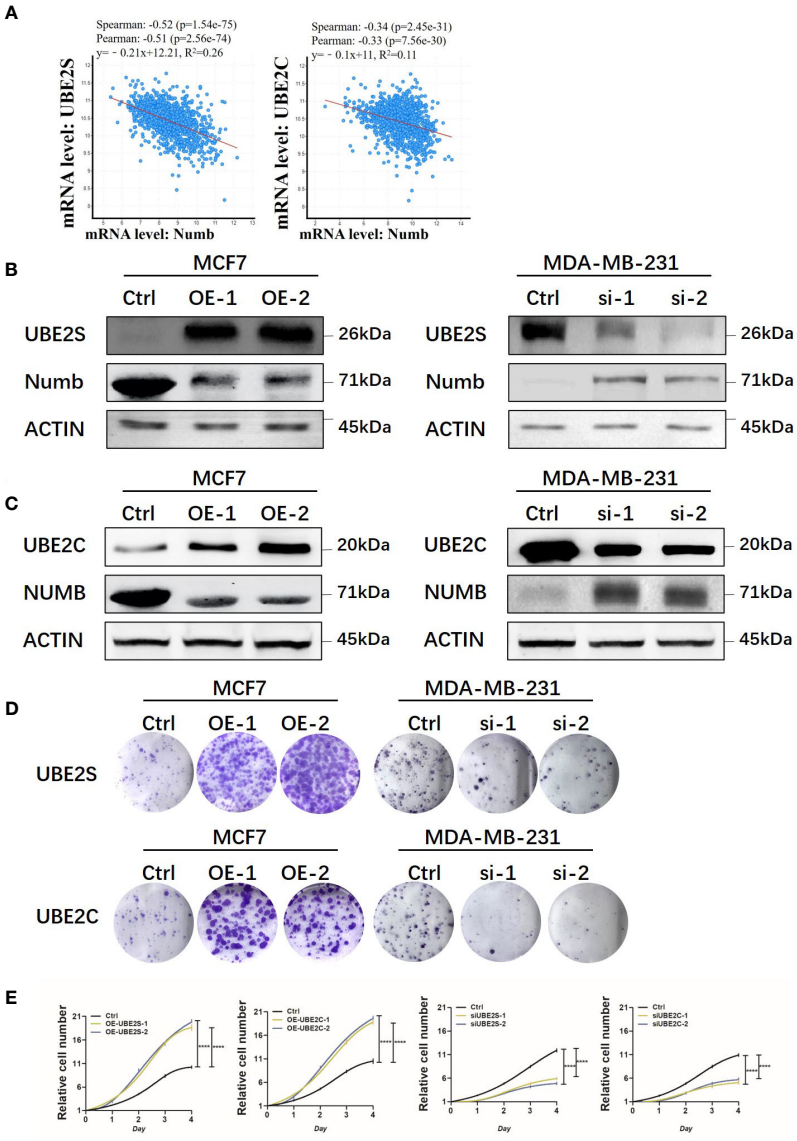

FIGURE 9
UBE2S and UBE2C inhibit Numb expression and increase colony formation and cell growth. **(A)** Numb has a negative correlation with UBE2S and UBE2C at the mRNA level in breast cancer tissues by cBioPortal database analysis. TCGA, Firehose Legacy, 1,101patients/1,108 samples. The Pearson's correlation score, Spearman score, and *p*-value were indicated in the respective graphs. UBE2S **(B)** and UBE2C **(C)** are overexpressed (OE) in MCF7 cells and knocked down with small interfering RNA (si) in MDA-MB-231 cells, and the Numb protein level is determined through western blot. β-actin was used as a loading control. Colony formation **(D)** and the CCK-8 growth assay **(E)** are performed in these cells. Each assay was repeated at least three times.

Numb was widely reported as a tumor suppressor in various cancers, and low expression of Numb was related to highly malignant tumor cells (21, 28, 50, 51). As shown in our data, there was reduced expression of Numb at the protein level, suggesting the involvement of ubiquitination and protein degradation (29, 52, 53). Since enzymes are the most attractive targets for drug development, identification of the upstream regulators of Numb downregulation is vital. This is because it has great potential for creating new efficient therapeutic targets in translational medicine. However, less is known concerning the interaction between the ubiquitin conjugating enzymes and Numb.

In the present study, we first proposed that UBE2S and UBE2C confer poor prognosis in breast cancer *via* downregulation of Numb. We reported overexpression of UBE2S and UBE2C and downregulation of Numb in breast cancer compared with normal breast tissue at both mRNA and protein levels. In a paired analysis of breast cancer and adjacent normal tissue, higher levels of UBE2S and UBE2C and lower Numb expression were found in the former. UBE2S and UBE2C also demonstrated increased expression in breast cancer with a more advanced grade and stage, while Numb showed the opposite trend. Since HR+ BC is the most common subtype with a better prognosis than HR− BC, we also found that ER or PR-negative breast cancer tissues or cells had higher levels of UBE2S and UBE2C and lower expression of Numb compared with HR+ breast cancer, providing evidence for the promoting roles of UBE2S and UBE2C and the suppressive role of Numb in breast cancer malignancy. For survival analysis, patients with a higher level of UBE2S or UBE2C had a shorter lifespan than those with a lower expression of UBE2S or UBE2C. Meanwhile, lower Numb expression was accompanied by a worse

prognosis in breast cancer patients as well as in ER+ BC patients. Specifically, by combining UBE2S or UBE2C together with Numb, we found patients with low UBE2S or UBE2C and high Numb expression demonstrated a more favorable prognosis. In contrast, patients with high UBE2S or UBE2C and low Numb levels showed a worse outcome. Therefore, we propose that combining UBE2S or UBE2C with Numb may serve as an effective predictor of breast cancer survival.

Mechanically, a notably negative correlation was found between the ubiquitin-conjugating enzymes and Numb through bioinformatic analyses. We further elucidated the underlying mechanisms through gain-and-loss-of-function studies in breast cancer cell lines. It is revealed that overexpression of UBE2S or UBE2C results in decreased Numb expression. However, a significant increase in Numb expression was observed by silencing UBE2S or UBE2C expression in breast cancer cells at both protein and mRNA levels. This confirms the downregulating roles of UBE2S and UBE2C in Numb expression. In addition, we found that overexpression of UBE2S or UBE2C led to increased capabilities of colony formation and cell proliferation while silencing of UBE2S or UBE2C displayed opposite trends in breast cancer cells, indicating the tumor-promoting effect of elevated UBE2S or UBE2C expression.

Taken together, we uncover that UBE2S and UBE2C confer a poor prognosis for breast cancer *via* downregulation of Numb. Breast cancer with higher UBE2S or UBE2C levels and lower Numb expression is correlated with a worse prognosis, providing potential biomarkers for BC therapeutics. It is speculated that UBE2S and UBE2C may work together to regulate Numb expression. However, further validation of the function and regulatory mechanism between UBE2S/UBE2C and Numb is necessary in future work to provide more effective therapeutic interventions.

Data availability statement

The original contributions presented in the study are included in the article/Supplementary Material. Further inquiries can be directed to the corresponding authors.

Author contributions

XH, XZ, and YG conceptualized and designed the study. YG and XC contributed to the data acquisition and interpretation as well as in methodology and analysis. YG, XZ, and XH were major contributors in writing, review and editing the manuscript. All authors listed have made a substantial, direct, and intellectual contribution to the work and approved it for publication.

Funding

This study is sponsored by the Shanghai Sailing Program (Grant No. 20YF1408800) and the National Natural Science Foundation of China (Grant No. 82003061) to YG.

Acknowledgments

The authors acknowledge the contributions of specific colleagues, institutions, or agencies that aided their efforts.

Conflict of interest

The authors declare that the research was conducted in the absence of any commercial or financial relationships that could be construed as a potential conflict of interest.

Publisher's note

Supplementary material

The Supplementary Material for this article can be found online at: https://www.frontiersin.org/articles/10.3389/fonc.2023.992233/full#supplementary-material

References

1. Siegel RL, Miller KD, Jemal A. Cancer statistics, 2020. *CA Cancer J Clin* (2020) 70 (1):7–30. doi: 10.3322/caac.21590

2. Cao W, Chen HD, Yu YW, Li N, Chen WQ. Changing profiles of cancer burden worldwide and in China: a secondary analysis of the global cancer statistics 2020. *Chin Med J (Engl).* (2021) 134(7):783–91. doi: 10.1097/CM9.0000000000001474

3. Hanker AB, Sudhan DR, Arteaga CL. Overcoming endocrine resistance in breast cancer. *Cancer Cell* (2020) 37(4):496–513. doi: 10.1016/j.ccell.2020.03.009

4. Provenzano E, Ulaner GA, Chin SF. Molecular classification of breast cancer. *PET Clin* (2018) 13(3):325–38. doi: 10.1016/j.cpet.2018.02.004

5. Nagini S. Breast cancer: Current molecular therapeutic targets and new players. *Anticancer Agents Med Chem* (2017) 17(2):152–63. doi: 10.2174/1871520616666160502122724

6. Wilkinson KD. The discovery of ubiquitin-dependent proteolysis. *Proc Natl Acad Sci U S A.* (2005) 102(43):15280–2. doi: 10.1073/pnas.0504842102

7. Wilkinson KD. Protein ubiquitination: A regulatory post-translational modification. *Anticancer Drug Des* (1987) 2(2):211–29.

8. Faktor J, Pjechova M, Hernychova L, Vojtesek B. Protein ubiquitination research in oncology. *Klin Onkol* (2019) 32(Supplementum 3):56–64. doi: 10.14735/amko20193S56

9. Mansour MA. Ubiquitination: Friend and foe in cancer. *Int J Biochem Cell Biol* (2018) 101:80–93. doi: 10.1016/j.biocel.2018.06.001

10. Gong Y, Wang D, Lin L, Dai J, Yu L. The expression of ubiquitin-conjugating enzyme E2C and KAI1 in ovarian carcinoma and their clinical significance. *Med (Baltimore)* (2019) 98(46):e17896. doi: 10.1097/MD.0000000000017896

11. Ayesha AK, Hyodo T, Asano E, Sato N, Mansour MA, Ito S, et al. UBE2S is associated with malignant characteristics of breast cancer cells. *Tumour Biol* (2016) 37 (1):763–72. doi: 10.1007/s13277-015-3863-7

12. Qin Y, Du J, Fan C. Ube2S regulates wnt/beta-catenin signaling and promotes the progression of non-small cell lung cancer. *Int J Med Sci* (2020) 17(2):274–9. doi: 10.7150/ijms.40243

13. Pan YH, Yang M, Liu LP, Wu DC, Li MY, Su SG. UBE2S enhances the ubiquitination of p53 and exerts oncogenic activities in hepatocellular carcinoma. *Biochem Biophys Res Commun* (2018) 503(2):895–902. doi: 10.1016/j.bbrc.2018.06.093

14. Liu Y, Zhao R, Chi S, Zhang W, Xiao C, Zhou X, et al. UBE2C is upregulated by estrogen and promotes epithelial-mesenchymal transition *via* p53 in endometrial cancer. *Mol Cancer Res* (2020) 18(2):204–15. doi: 10.1158/1541-7786.MCR-19-0561

15. Wang Y, Huang F, Liu M, Zhao Q. UBE2C mRNA expression controlled by miR-300 and HuR determines its oncogenic role in gastric cancer. *Biochem Biophys Res Commun* (2021) 534:597–603. doi: 10.1016/j.bbrc.2020.11.034

16. Tedesco D, Zhang J, Trinh L, Lalehzadeh G, Meisner R, Yamaguchi KD, et al. The ubiquitin-conjugating enzyme E2-EPF is overexpressed in primary breast cancer and modulates sensitivity to topoisomerase II inhibition. *Neoplasia.* (2007) 9(7):601–13. doi: 10.1593/neo.07385

17. Rawat A, Gopal G, Selvaluxmy G, Rajkumar T. Inhibition of ubiquitin conjugating enzyme UBE2C reduces proliferation and sensitizes breast cancer cells to radiation, doxorubicin, tamoxifen and letrozole. *Cell Oncol (Dordr).* (2013) 36(6):459–67. doi: 10.1007/s13402-013-0150-8

18. Kim YJ, Lee G, Han J, Song K, Choi JS, Choi YL, et al. UBE2C overexpression aggravates patient outcome by promoting estrogen-Dependent/Independent cell proliferation in early hormone receptor-positive and HER2-negative breast cancer. *Front Oncol* (2019) 9:1574. doi: 10.3389/fonc.2019.01574

19. Martinez-Chacin RC, Bodrug T, Bolhuis DL, Kedziora KM, Bonacci T, Ordureau A, et al. Ubiquitin chain-elongating enzyme UBE2S activates the RING E3 ligase APC/C for substrate priming. *Nat Struct Mol Biol* (2020) 27(6):550–60. doi: 10.1038/s41594-020-0424-6

20. Zhang S, Shen Y, Li H, Bi C, Sun Y, Xiong X, et al. The negative cross-talk between SAG/RBX2/ROC2 and APC/C E3 ligases in regulation of cell cycle progression and drug resistance. *Cell Rep* (2020) 32(10):108102.

21. Domingo-Domenech J, Vidal SJ, Rodriguez-Bravo V, Castillo-Martin M, Quinn SA, Rodriguez-Barrueco R, et al. Suppression of acquired docetaxel resistance in prostate cancer through depletion of notch- and hedgehog-dependent tumor-initiating cells. *Cancer Cell* (2012) 22(3):373–88. doi: 10.1016/j.ccr.2012.07.016

22. Boumahdi S, Driessens G, Lapouge G, Rorive S, Nassar D, Le Mercier M, et al. SOX2 controls tumour initiation and cancer stem-cell functions in squamous-cell carcinoma. *Nature.* (2014) 511(7508):246–50. doi: 10.1038/nature13305

23. Tosoni D, Zecchini S, Coazzoli M, Colaluca I, Mazzarol G, Rubio A, et al. The Numb/p53 circuitry couples replicative self-renewal and tumor suppression in mammary epithelial cells. *J Cell Biol* (2015) 211(4):845–62. doi: 10.1083/jcb.201505037

24. Colaluca IN, Tosoni D, Nuciforo P, Senic-Matuglia F, Galimberti V, Viale G, et al. NUMB controls p53 tumour suppressor activity. *Nature.* (2008) 451(7174):76–80. doi: 10.1038/nature06412

25. Di Marcotullio L, Greco A, Mazza D, Canettieri G, Pietrosanti L, Infante P, et al. Numb activates the E3 ligase itch to control Gli1 function through a novel degradation signal. *Oncogene.* (2011) 30(1):65–76. doi: 10.1038/onc.2010.394

26. Ye L, Lou F, Yu F, Zhang D, Wang C, Wu F, et al. NUMB maintains bone mass by promoting degradation of PTEN and GLI1 *via* ubiquitination in osteoblasts. *Bone Res* (2018) 6:32. doi: 10.1038/s41413-018-0030-y

27. Dho SE, Jacob S, Wolting CD, French MB, Rohrschneider LR, McGlade CJ. The mammalian numb phosphotyrosine-binding domain. characterization of binding specificity and identification of a novel PDZ domain-containing numb binding protein, LNX. *J Biol Chem* (1998) 273(15):9179–87. doi: 10.1074/jbc.273.15.9179

28. Guo Y, Zhang K, Cheng C, Ji Z, Wang X, Wang M, et al. Numb(-/low) enriches a castration-resistant prostate cancer cell subpopulation associated with enhanced notch and hedgehog signaling. *Clin Cancer Res* (2017) 23(21):6744–56. doi: 10.1158/1078-0432.CCR-17-0913

29. Pece S, Serresi M, Santolini E, Capra M, Hulleman E, Galimberti V, et al. Loss of negative regulation by numb over notch is relevant to human breast carcinogenesis. *J Cell Biol* (2004) 167(2):215–21. doi: 10.1083/jcb.200406140

30. Zhang J, Shao X, Sun H, Liu K, Ding Z, Chen J, et al. NUMB negatively regulates the epithelial-mesenchymal transition of triple-negative breast cancer by antagonizing notch signaling. *Oncotarget.* (2016) 7(38):61036–53. doi: 10.18632/oncotarget.11062

31. Li J, Chen Z, Su K, Zeng J. Clinicopathological classification and traditional prognostic indicators of breast cancer. *Int J Clin Exp Pathol* (2015) 8(7):8500–5.

32. El-Hawary AK, Abbas AS, Elsayed AA, Zalata KR. Molecular subtypes of breast carcinoma in Egyptian women: Clinicopathological features. *Pathol Res Pract* (2012) 208 (7):382–6. doi: 10.1016/j.prp.2012.03.011

33. Li X, Yang J, Peng L, Sahin AA, Huo L, Ward KC, et al. Triple-negative breast cancer has worse overall survival and cause-specific survival than non-triple-negative breast cancer. *Breast Cancer Res Treat* (2017) 161(2):279–87. doi: 10.1007/s10549-016-4059-6

34. Harbeck N, Gnant M. Breast cancer. *Lancet.* (2017) 389(10074):1134–50. doi: 10.1016/S0140-6736(16)31891-8

35. Ramón Y Cajal S, Sesé M, Capdevila C, Aasen T, De Mattos-Arruda L, Diaz-Cano SJ, et al. Clinical implications of intratumor heterogeneity: Challenges and opportunities. *J Mol Med (Berl).* (2020) 98(2):161–77. doi: 10.1007/s00109-020-01874-2

36. Reiter JG, Baretti M, Gerold JM, Makohon-Moore AP, Daud A, Iacobuzio-Donahue CA, et al. An analysis of genetic heterogeneity in untreated cancers. *Nat Rev Cancer.* (2019) 19(11):639–50. doi: 10.1038/s41568-019-0185-x

37. Marusyk A, Janiszewska M, Polyak K. Intratumor heterogeneity: The Rosetta stone of therapy resistance. *Cancer Cell* (2020) 37(4):471–84. doi: 10.1016/j.ccell.2020.03.007

38. Kumar VE, Nambiar R, De Souza C, Nguyen A, Chien J, Lam KS. Targeting epigenetic modifiers of tumor plasticity and cancer stem cell behavior. *Cells.* (2022) 11 (9):1403. doi: 10.3390/cells11091403

39. Walcher L, Kistenmacher A-K, Suo H, Kitte R, Dluczek S, Strauß A, et al. Cancer stem cells-origins and biomarkers: Perspectives for targeted personalized therapies. *Front Immunol* (2020) 11:1280. doi: 10.3389/fimmu.2020.01280

40. Prager BC, Xie Q, Bao S, Rich JN. Cancer stem cells: The architects of the tumor ecosystem. *Cell Stem Cell* (2019) 24(1):41–53. doi: 10.1016/j.stem.2018.12.009

41. Li X, Elmira E, Rohondia S, Wang J, Liu J, Dou QP. A patent review of the ubiquitin ligase system: 2015-2018. *Expert Opin Ther Pat.* (2018) 28(12):919–37. doi: 10.1080/13543776.2018.1549229

42. Hershko A, Ciechanover A. The ubiquitin system. *Annu Rev Biochem* (1998) 67:425–79. doi: 10.1146/annurev.biochem.67.1.425

43. Senft D, Qi J, Ronai ZA. Ubiquitin ligases in oncogenic transformation and cancer therapy. *Nat Rev Cancer.* (2018) 18(2):69–88. doi: 10.1038/nrc.2017.105

44. van Ree JH, Jeganathan KB, Malureanu L, van Deursen JM. Overexpression of the E2 ubiquitin-conjugating enzyme UbcH10 causes chromosome missegregation and tumor formation. *J Cell Biol* (2010) 188(1):83–100.

45. Okamoto Y, Ozaki T, Miyazaki K, Aoyama M, Miyazaki M, Nakagawara A. UbcH10 is the cancer-related E2 ubiquitin-conjugating enzyme. *Cancer Res* (2003) 63(14):4167–73.

46. Presta I, Novellino F, Donato A, La Torre D, Palleria C, Russo E, et al. UbcH10 a major actor in cancerogenesis and a potential tool for diagnosis and therapy. *Int J Mol Sci* (2020) 21(6). doi: 10.3390/ijms21062041

47. Li Z, Wang Y, Li Y, Yin W, Mo L, Qian X, et al. Ube2s stabilizes beta-catenin through K11-linked polyubiquitination to promote mesendoderm specification and colorectal cancer development. *Cell Death Dis* (2018) 9(5):456.

48. Hu L, Cheng X, Binder Z, Han Z, Yin Y, O'Rourke DM, et al. Molecular and clinical characterization of UBE2S in glioma as a biomarker for poor prognosis and resistance to chemo-radiotherapy. *Front Oncol* (2021) 11:640910. doi: 10.3389/fonc.2021.640910

49. Mo CH, Gao L, Zhu XF, Wei KL, Zeng JJ, Chen G, et al. The clinicopathological significance of UBE2C in breast cancer: A study based on immunohistochemistry, microarray and RNA-sequencing data. *Cancer Cell Int* (2017) 17:83. doi: 10.1186/s12935-017-0455-1

50. Garcia-Heredia JM, Lucena-Cacace A, Verdugo-Sivianes EM, Perez M, Carnero A. The cargo protein MAP17 (PDZK1IP1) regulates the cancer stem cell pool activating the notch pathway by abducting NUMB. *Clin Cancer Res* (2017) 23(14):3871–83. doi: 10.1158/1078-0432.CCR-16-2358

51. Cheng C, Huang Z, Zhou R, An H, Cao G, Ye J, et al. Numb negatively regulates the epithelial-to-mesenchymal transition in colorectal cancer through the wnt signaling pathway. *Am J Physiol Gastrointest Liver Physiol* (2020) 318(5):G841–G53. doi: 10.1152/ajpgi.00178.2019

52. Westhoff B, Colaluca IN, D'Ario G, Donzelli M, Tosoni D, Volorio S, et al. Alterations of the notch pathway in lung cancer. *Proc Natl Acad Sci U S A.* (2009) 106 (52):22293–8. doi: 10.1073/pnas.0907781106

53. Pece S, Confalonieri S, Romano PR, Di Fiore PP. NUMB-ing down cancer by more than just a NOTCH. *Biochim Biophys Acta* (2011) 1815(1):26–43. doi: 10.1016/j.bbcan.2010.10.001

frontiers | Frontiers in Oncology

TYPE Original Research
PUBLISHED 09 March 2023
DOI 10.3389/fonc.2023.1088475

OPEN ACCESS

EDITED BY
Anurag Tripathi,
Indian Institute of Toxicology Research (CSIR), India

REVIEWED BY
Yongyong Yang,
Northwestern University, United States
Pradeep Sharma,
Indian Institute of Toxicology Research (CSIR), India

*CORRESPONDENCE
Qing Zhu
zhuq@zjut.edu.cn
Dongsheng Huang
dshuang@hmc.edu.cn

†These authors have contributed equally to this work

SPECIALTY SECTION
This article was submitted to Molecular and Cellular Oncology, a section of the journal Frontiers in Oncology

RECEIVED 03 November 2022
ACCEPTED 13 February 2023
PUBLISHED 09 March 2023

CITATION
Ma Q, Lu Q, Lei X, Zhao J, Sun W, Wang J, Zhu Q and Huang D (2023) UCHL3 promotes hepatocellular carcinoma cell migration by de-ubiquitinating and stabilizing Vimentin. *Front. Oncol.* 13:1088475. doi: 10.3389/fonc.2023.1088475

UCHL3 promotes hepatocellular carcinoma cell migration by de-ubiquitinating and stabilizing Vimentin

Qiancheng Ma[1,2], Qiliang Lu[3], Xiangxiang Lei[4], Jie Zhao[1], Wen Sun[5], Jun Wang[6], Qing Zhu[1*†] and Dongsheng Huang[2*†]

[1]College of Biotechnology and Bioengineering, Zhejiang University of Technology, Hangzhou, China, [2]The Key Laboratory of Tumor Molecular Diagnosis and Individualized Medicine of Zhejiang Province, Zhejiang Provincial People's Hospital, Affiliated People's Hospital, Hangzhou Medical College, Hangzhou, China, [3]Qingdao Medical College, Qingdao University, Qingdao, China, [4]School of Basic Medical Sciences and Forensic Medicine, Hangzhou Medical College, Hangzhou, China, [5]The Second Clinical Medical College, Zhejiang Chinese Medical University, Hangzhou, China, [6]Department of Emergency and Critical Care Medicine, The First Affiliated Hospital of Xi'an Jiaotong University, Xi'an, China

Background: Hepatocellular carcinoma (HCC) is a common malignant tumor associated with a poor prognosis. Ubiquitin carboxyl-terminal hydrolase L3 (UCHL3) has been reported to promote diverse tumors, but little is known about its role in HCC.

Methods: Expression levels of UCHL3 in Huh7 and Hep3B cells were measured by qRT-PCR. UCHL3, Vimentin protein levels, and ubiquitination levels were determined by Western blot assay. co-immunoprecipitation, Immunofluorescence, and IHC were used to detect the interaction and expression association between UCHL3 and Vimentin in the cells. Wound healing and Transwell assays were used to measure cell migration. Spheroid formation assay were used to assess stem-like properties.

Results: UCHL3 expression was found to be significantly elevated in HCC and associated with poor prognosis. UCHL3 promoted migration and stem-like properties of HCC cells. Vimentin was identified as a potential de-ubiquitination substrate of UCHL3 and UCHL3 interacted with and promoted the de-ubiquitination of Vimentin, enhancing its stability. Moreover, the suppression of UCHL3 by siRNA or the inhibition by TCID upregulated ubiquitinated Vimentin. Vimentin attenuated the suppression of cell migration caused by knockdown of UCHL3.

Conclusion: UCHL3 was highly expressed in HCC and functioned as an oncogene. Vimentin is a novel substrate of UCHL3 and its stabilization and de-ubiquitination enhanced HCC cell migration.

KEYWORDS

HCC, UCHL3, Vimentin, de-ubiquitination, migration, cancer stem cells

Introduction

Liver cancer is the third most common cause of global cancer-related death (1). Over 90% of liver cancer cases are hepatocellular carcinoma (HCC), of which only 5%–15% are candidates for early-stage surgical resection. Chemotherapy and immunotherapy are used to treat advanced HCC, but metastasis leads to unsatisfactory long-term survival rates (2–4). The identification of novel therapeutic targets is thus an urgent matter.

Ubiquitin-like proteins (Ub) consist of 76 amino acids incorporating seven lysine residues, namely, K6, K11, K27, K29, K33, K48, and K63. Mono- or poly-ubiquitinated chains are involved in the regulation of processes such as DNA repair, apoptosis, transcriptional regulation, and endocytosis (5–8). Ubiquitin also play a significant role in HCC pathogenesis, raising the possibility that ubiquitinated components may be therapeutic targets (9, 10). Ubiquitination is dynamic and reversible. De-ubiquitinases (DUBs) remove ubiquitin, protecting their protein substrates from degradation (11, 12). Such enzymes include ubiquitin C-terminal hydrolases (UCHs), including UCHL1/PGP9.5 (protein gene product 9.5), ubiquitin carboxyl-terminal hydrolase L3 (UCHL3), UCHL5/UCH37, and BRCA1-associated protein-1 (BAP1) (13, 14).

Abnormal expression and a dual function of UCHL3 have been described in human cancer. UCHL3 exerts an anti-tumor activity to inhibit the epithelial-mesenchymal transition (EMT) and reduce the stem-cell-like properties of prostate cancer cells (15, 16). However, oncogenic activities have also been reported with UCHL3 being overexpressed in lung cancer (17, 18), ovarian cancer (19), pancreatic cancer (20), and melanoma (21). Aryl hydrocarbon receptor (AhR) (22, 23), FOXM1 (20), lymphoid-specific helicase (LSH) (17), COPS5 (24), and RAD51 (25) are de-ubiquitination targets of UCHL3, which indicate the possibility of UCHL3 being a therapeutic target. However, roles and mechanisms of UCHL3 in hepatocarcinogenesis remain unclear.

Epithelial cells lose polarity and acquire mesenchymal characteristics during the EMT, a process that contributes to tumor cell migration (26). The involvement of Vimentin in the initiation of the EMT has recently been demonstrated (27, 28), and Vimentin is known to be regulated by post-translational modifications, including ubiquitination, phosphorylation, O-linked glycosylation, sumoylation, and ADP-ribosylation (29–31). The ubiquitin ligases, Trim16 (32) and Trim56 (33), have been found to ubiquitinate Vimentin, but less is known about its de-ubiquitination, other than by USP14 (34).

The current study found that UCHL3 was upregulated in HCC patients, indicating a poor prognosis. UCHL3 promoted the migration and stem-like properties of HCC cells. UCHL3 was identified as a DUB, which targets Vimentin, and the consequent de-ubiquitination may be responsible for the promotion of cell migration.

Materials and methods

Clinical tissues

Clinical specimens were obtained from patients with hepatocellular carcinoma at Zhejiang Provincial People's Hospital. Freshly excised HCC tissues were fixed using formalin and embedded in paraffin for immunohistochemical (IHC) staining.

Cell culture

Hep3B, Huh7, and HepG2 cells were obtained from the Cell Bank of the Chinese Academy of Sciences (Shanghai, China) and MIHA from bnbio (Beijing, China). MIHA and Hep3B cells were grown in Minimum Essential Medium (MEM) (VivaCell, C3060-0500) containing 10% fetal bovine serum (FBS) (BI, 04001-1A) and 1% penicillin-streptomycin (Cienry, CR15140). Huh7 and HepG2 cells were grown in Dulbecco's modified Eagle's medium (DMEM) (VivaCell, C3060-0500) containing 10% FBS (BI, 04001-1A) and 1% penicillin-streptomycin (Cienry, CR15140). All cells were cultured at 37°C and 5% CO_2.

Immunofluorescence colocalization

UCHL3 plasmid (EGFP-UCHL3) (GenePharma, Shanghai, China) were transfected into HCC cells using Lipofectamine 3000 (Thermo Fisher Scientific, L3000-015). Immunofluorescence staining was performed using Vimentin antibody (Proteintech, 10366-1-AP) and Cy3-labeled Goat Anti-rabbit IgG (Beyotime, A0516). Antifade Mounting Medium with 4′,6-diamidino-2-phenylindole (DAPI) (Beyotime, P0131) was used to seal the slices and then photographed under a confocal microscope (Nikon).

Transfection of plasmids with siRNA/shRNA

Lentivirus-mediated UCHL3 shRNA and NC shRNA (Genomeditech, Shanghai, China) and Vimentin plasmid and siRNAs (100nM) (GenePharma, Shanghai, China) were transfected into HCC cells using Lipofectamine 3000 (Thermo Fisher Scientific, L3000-015).

The target sequences were as follows (5′-3′):

NC: TTCTCCGAACGTGTCACGT;

shUCHL3#1: GGTCAGACTGAGGCACCAAGT;

shUCHL3#2: GGAGGAATCTGTGTCAATGAG;

and for Vimentin (5′–3′):

NC sense: UUCUCCGAACGUGUCACGUTT; NC antisense: ACGUGACACGUUCGGAGAATT;

siVimentin#1 sense: CUGGUUGAUACCCACUCAATT; siVimentin#1 antisense: UUGAGUGGGUAUCAACCAGTT;

siVimentin#2 sense: GCAUCACGAUGACCUUGAATT; siVimentin#2 antisense: UUCAAGGUCAUCGUGAUGCTT.

Wound healing assay

Cells were cultured in six-well plates until a monolayer formed and a wound created in the middle of the well; cells were washed with 1× phosphate-buffered saline (PBS) to remove debris, and serum-free medium was added. Cell migration was assessed by

inspecting the wound area under an inverted microscope (Nikon, DS-Ri2). Images were analyzed by ImageJ software.

Transwell assay

A total of 600 μl of complete medium was added to the lower chamber of Transwell inserts (Corning), and HCC cells in serum-free medium were inoculated into the upper chamber. Cells were cultured for 24 Hours, and those in the lower chamber were fixed with 4% paraformaldehyde, stained with 0.1% crystal violet, and imaged under an inverted microscope (Nikon, DS-Ri2).

Spheroid formation assay

Oncospheres were grown in serum-free DMEM-F12 (1:1) medium containing 10 ng/ml epidermal growth factor (EGF), 10 ng/ml fibroblast growth factor (FGF), and N2 (Thermo Fisher, 17502048) for 1–2 weeks and imaged under an inverted microscope (Nikon, DS-Ri2).

Western blotting and co-immunoprecipitation analysis

Total protein was isolated in Cell lysis buffer for Western and IP (Beyotime, P0013), and concentration was determined by a BCA protein assay kit (Thermo Fisher, 23225). Proteins were separated by PAGE Gel Quick Preparation Kit(10%) (Yeasen, 20325ES62), transferred onto polyvinylidene fluoride (PVDF) membranes (Millipore, IPVH00010), and blocked with 5% skimmed milk (Yeasen, 36120ES76). Primary antibodies raised against UCHL3 (Proteintech, 12384-1-AP), β-actin (Affinity, AF7018), Vimentin (Cell Signal, D21H3), Vimentin (Proteintech, 60330-1-Ig), and Ubiquitin (Santa, P4D1) were added with incubation at 4°C overnight. Membranes were washed three times with TBST (Solarbio, T1082), incubated with horseradish peroxidase (HRP)-conjugated secondary antibody (Beyotime) for 1 h and visualized with ECL reagent (FD). Blots were imaged using the ChemiDoc™ MP Imaging System, and GoldBand 3-color Regular Range Protein Marker (10-180kDa) (Yeasen, 20351ES72) was used to indicate molecular weight.

Cell lysates were prepared in Cell lysis buffer for Western and IP (Beyotime, P0013) for co-immunoprecipitation experiments. Anti-UCHL3 (Proteintech, 12384-1-AP) or -Vimentin antibodies (Proteintech, 10366-1-AP) or IgG (negative control) were added to magnetic beads, according to the manufacturer's instructions (bimake, B23201).

Half-life and inhibitor analysis

Cells were treated with 10 μM cycloheximide (CHX; Selleck, S7418) to block protein synthesis, and proteins were extracted at various time points and protein levels assessed by Western blotting for half-life determination.

Hep3B and Huh7 cells were treated with dimethyl sulfoxide (DMSO) or 10 μM TCID (Selleck, S7140) for 24 h, and UCHL3 and Vimentin expression was determined by Western blotting. Western blotting was used to evaluate polyubiquitinated Vimentin following co-immunoprecipitation of Vimentin.

RT-qPCR

Total RNA was isolated by RNA-Quick Purification Kit (YiShan, RN001) and reverse transcribed into cDNA with PrimeScript™ RT Reagent Kit (Takara, RR037A). SYBR Green PCR Master Mix (Yeasen, 11184ES03) was used for real-time quantitative PCR (RT-qPCR) on a 7500 Real-Time PCR instrument. Relative mRNA expression was normalized by the $2^{-\Delta\Delta ct}$ calculation method. Primer sequences were as follows (5′–3′).

Vimentin:
Forward: AGG CAA AGC AGG AGT CCA CTG A;
Reverse: ATC TGG CGT TCC AGG GAC TCA T;
β-actin:
Forward: TGA CCC AGA TCA TGT TTG AG;
Reverse: CGT ACA GGG ATA GCA CAG;
UCHL3:
Forward: CTGAAGAACGAGCCAGATAC;
Reverse: GCCCATCTACATGAACTAATGC.

Statistical analysis

Means ± standard deviations for at least three replicates are presented. Statistical analyses were performed by GraphPad Prism 9 (San Diego, CA, USA), and differences were assessed by Student's t-test. A value of $p < 0.05$ was considered statistically significant.

Results

UCHL3 was upregulated in HCC and associated with poor prognosis

UCHL3 expression was analyzed by the UALCAN (35) platform and found to be upregulated in HCC by comparison with normal hepatic tissue (Figure 1A). Analysis *via* the GEPIA platform indicated that high UCHL3 expression was associated with shorter overall survival among HCC patients (Figure 1B). Kaplan–

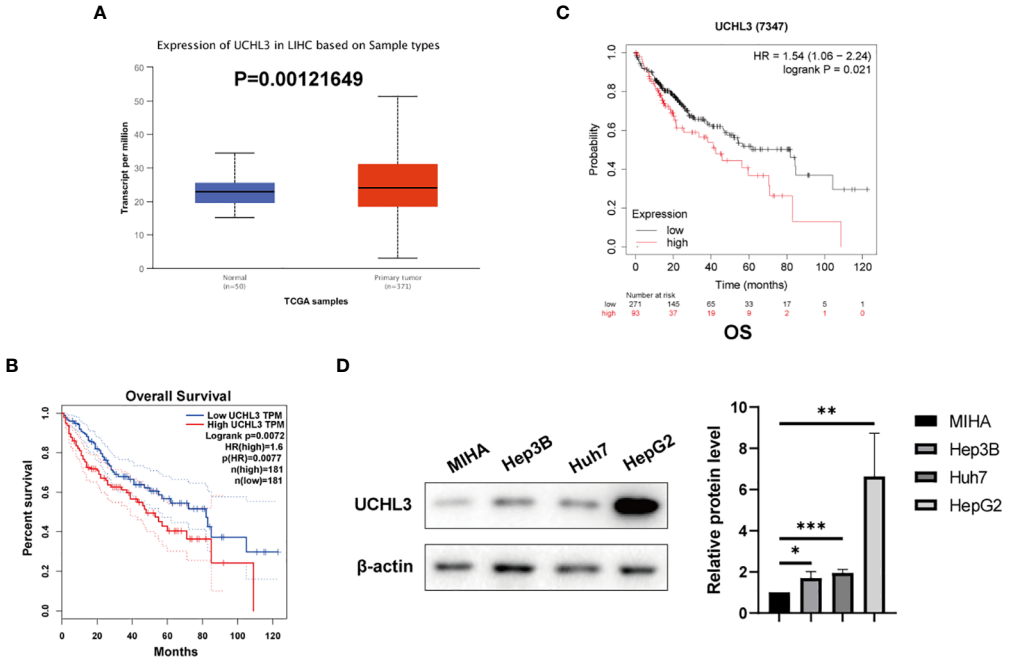

FIGURE 1
UCHL3 expression and survival analysis in HCC. **(A)** Data relating to primary liver tumors were downloaded from the TCGA database and analyzed by the UALCAN platform (http://ualcan.path.uab.edu/analysis.html) and showed higher UCHL3 expression in tumor tissue. **(B)** Kaplan–Meier analysis by the GEPIA platform (http://gepia.cancer-pku.cn) indicated that HCC patients with increased UCHL3 levels had poorer overall survival. **(C)** Kaplan–Meier analysis (https://kmplot.com/analysis/) of OS showed high UCHL3 expression to be associated with lower patient survival. **(D)** Western blots showed higher UCHL3 expression in HCC cells, Hep3B, Huh7, and HepG2, than in the normal hepatocyte cell line, MIHA. *p < 0.05, **p < 0.01, ***p < 0.001.

Meier analysis also demonstrated that high UCHL3-expressing HCC patients had reduced survival (Figure 1C). UCHL3 was also highly expressed in the HCC cell lines, namely, Hep3B, Huh7, and HepG2, by comparison with the normal hepatocyte cell line, MIHA (Figure 1D). In summary, it is suggested that UCHL3 may contribute to liver tumorigenesis and may be a useful prognostic biomarker in HCC.

UCHL3 overexpression promoted migration and stem-like properties of HCC cells

Huh7 and Hep3B cells stably overexpressing UCHL3 were generated (Figures 2A, B). UCHL3 overexpression promoted cell migration during wound healing (Figure 2C) and Transwell assays (Figure 2D). UCHL3 Overexpressing cells formed larger spheroids, indicating increased stem-like properties, compared with control cells (Figure 2E). Overall, UCHL3 may contribute to malignant progression by promoting migration and stem-like properties of HCC cells.

UCHL3 knockdown inhibited migration and reduced stem-like properties of HCC cells

Stable knockdown of UCHL3 was established in HCC cell lines (Figures 3A, B). UCHL3 knockdown inhibited cell migration and stem-like properties, as revealed by wound healing and Transwell assays (Figures 3C, D) and spheroid formation assays (Figure 3E). Loss of UCHL3 thus impaired migration and stem-like properties of HCC cells.

Identification of Vimentin as a new substrate of UCHL3

The above results demonstrate the contribution of UCHL3 to migration and stem-like properties of HCC cells, but downstream targets of this de-ubiquitinase remain unknown. Co-immunoprecipitation experiments with UCHL3 antibody followed by mass spectrometry analysis (IP-MS) were performed to identify potential substrates of UCHL3. UCHL3-binding protein complex contained peptide fragments of Vimentin, indicating a Vimentin–UCHL3 interaction (Figure 4A). Co-immunoprecipitation experiments in HCC cells confirmed the interaction of UCHL3 with Vimentin (Figure 4B). Immunofluorescence results show the colocalization of UCHL3 and Vimentin in cells (Figure 4C). The findings suggest that Vimentin is a novel protein-binding partner of UCHL3.

UCHL3 stabilized Vimentin protein *via* de-ubiquitination

We performed immunohistochemical staining for UCHL3 and Vimentin in HCC tissues. The results showed a positive correlation

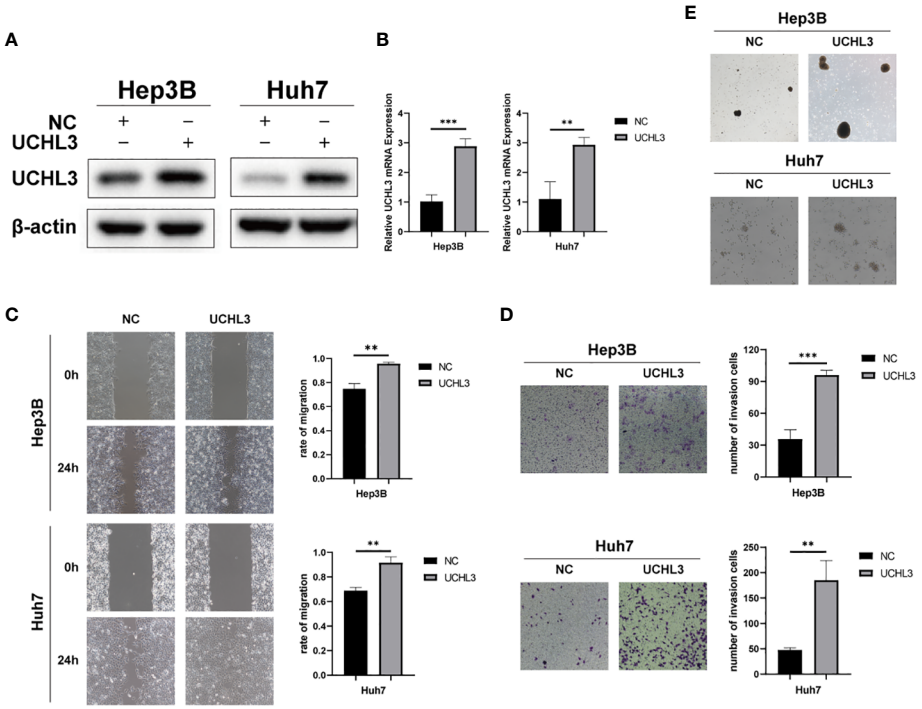

FIGURE 2
Overexpression of UCHL3 promoted HCC cell migration and stem-like properties. **(A)** UCHL3 overexpression shown by Western blots of Hep3B and Huh7 cells. **(B)** Levels of UCHL3 mRNA in Hep3B and Huh7 cells were confirmed by RT-qPCR. **(C)** UCHL3 overexpression promoted Hep3B and Huh7 migration, as shown by wound healing assay. **(D)** UCHL3 overexpression promoted Hep3B and Huh7 migration, as shown by Transwell assay. **(E)** UCHL3 overexpression promoted spheroid formation in Hep3B and Huh7 cells. **p < 0.01, ***p < 0.001.

between the expression of UCHL3 and Vimentin in HCC (Figure 4D). Next, cells in which UCHL3 was either overexpressed or knocked down were used to investigate its regulatory impact on Vimentin. UCHL3 promoted Vimentin protein expression, and UCHL3 knockdown inhibited Vimentin protein expression (Figure 4E). UCHL3 overexpression enhanced the stability of Vimentin protein, while UCHL3 inhibition suppressed its stability (Figure 4F). Consistent with the role of

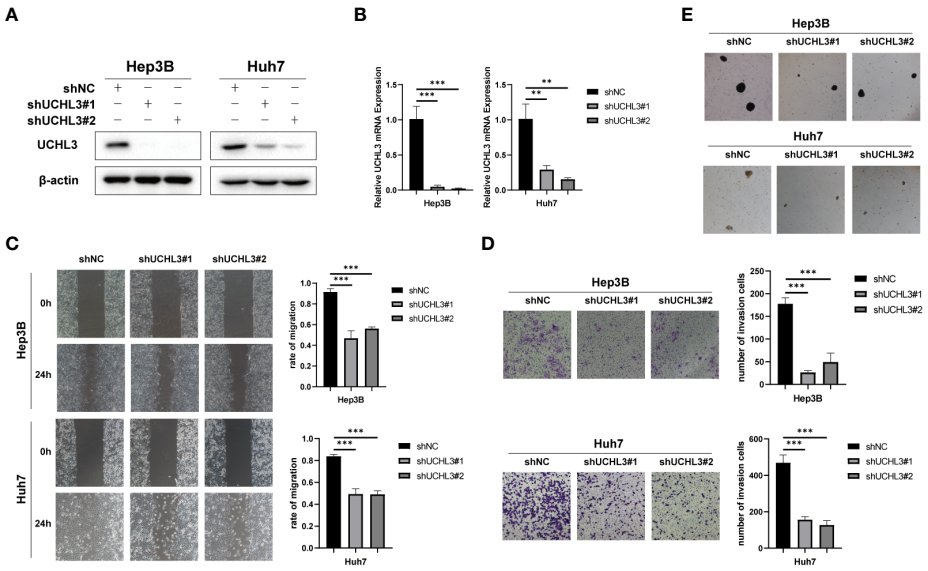

FIGURE 3
UCHL3 knockdown inhibited migration and stem-like properties of HCC cells. **(A)** Knockdown of UCHL3 in Hep3B and Huh7 cells was confirmed by Western blotting. **(B)** RT-qPCR showed reduced expression of UCHL3 mRNA in Hep3B and Huh7 cells. **(C)** UCHL3 knockdown suppressed Hep3B and Huh7 cell migration during wound healing assays. **(D)** UCHL3 knockdown suppressed Hep3B and Huh7 cell migration during Transwell assays. **(E)** UCHL3 knockdown inhibited spheroid formation in Hep3B and Huh7 cells. **p < 0.01, ***p < 0.001.

10.3389/fonc.2023.1088475

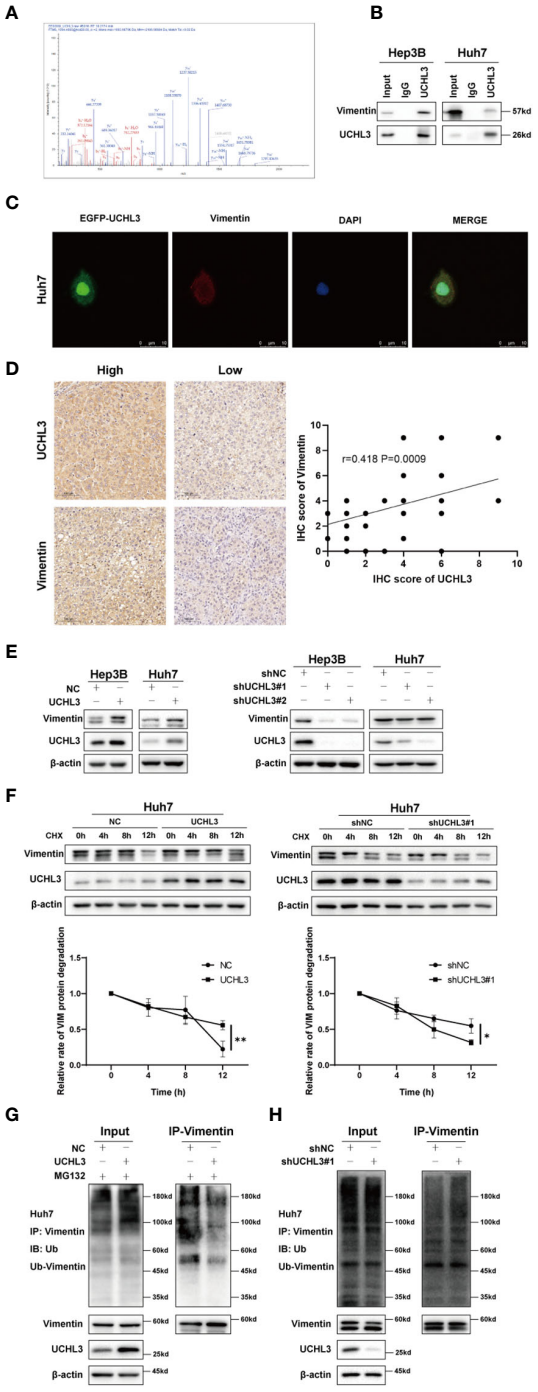

FIGURE 4
UCHL3 de-ubiquitinylated and stabilized Vimentin. **(A)** Mass spectrometry showed that the UCHL3-binding complex contained Vimentin peptide fragments. **(B)** Co-immunoprecipitation with anti-UCHL3 antibody and Western blotting showed that Vimentin interacted with UCHL3 in Hep3B and Huh7 cells. **(C)** Immunofluorescence showed the colocalization of UCHL3 and Vimentin in cells. **(D)** IHC analysis showed a positive correlation between the expression of UCHL3 and Vimentin in HCC. **(E)** UCHL3 overexpression increased Vimentin levels, and UCHL3 inhibition reduced Vimentin levels, as shown by Western blotting. **(F)** UCHL3 overexpression increased and UCHL3 knockdown decreased the stability of Vimentin protein in Huh7 cells. **(G)** The degree of Vimentin ubiquitination was significantly reduced by UCHL3 overexpression in Huh7 cells, as shown by Western blotting. **(H)** UCHL3 knockdown increased the degree of Vimentin ubiquitination in Huh7 cells, as shown by Western blotting. *p< 0.05, **p < 0.01.

UCHL3 as a DUB, UCHL3 overexpression decreased the ubiquitination level of endogenous Vimentin (Figure 4G), and Vimentin ubiquitination was increased when UCHL3 was knocked down (Figure 4H). In conclusion, the role of UCHL3 as a DUB allowed stabilization of Vimentin.

Inhibition of UCHL3 impaired HCC cell migration

TCID is an UCHL3 inhibitor (22) and was found to reduce Vimentin expression without any change in UCHL3 (Figure 5A). TCID treatment also significantly increased Vimentin ubiquitination in Hep3B and Huh7 cells (Figures 5B, C). In a similar manner to UCHL3 knockdown, TCID treatment also suppressed HCC cell migration (Figures 5D, E). In summary, inhibition of UCHL3 by TCID impaired HCC cell migration.

UCHL3 facilitated HCC cell migration through regulating Vimentin

Functional rescue experiments were performed to demonstrate actions of UCHL3 on Vimentin. Knockdown of Vimentin inhibited HCC cell migration and suppressed UCHL3-induced HCC cell migration, as illustrated by wound healing and Transwell assays (Figures 6A–C). Vimentin overexpression promoted HCC cell migration and attenuated the inhibition of cell migration due to UCHL3 knockdown (Figures 6D–F). In conclusion, the findings suggest that UCHL3 promotes HCC cell migration through stabilizing Vimentin. Together, the abovementioned results show that the DUB activity of UCHL3 stabilizes the expression of Vimentin and promotes the migration of HCC. And TCID can inhibit the DUB activity of UCHL3 (Figure 7).

Discussion

Worldwide HCC incidence is on the increase and is estimated to rank third for cancer-related deaths by 2030 (36). Indeed, liver cancers, along with pancreatic cancer, generally have low survival rates (37). Ubiquitin dysregulation, due to imbalances between ubiquitinase and de-ubiquitinase activities, is thought to affect tumor development (38–40), but UCH de-ubiquitinases have been rarely studied in HCC, by contrast with USP enzymes (41). Only UCH37 has been investigated in liver cancer cells (42), but other family members may also have an impact. The current study correlated abnormally high UCHL3 expression with the occurrence and malignant development of HCC. UCHL3 promoted HCC cell migration and stem-like properties.

Cell migration and stem-like properties contribute to the aggressiveness of tumors and poor patient prognosis (43). Many proteins involved in HCC cell migration are regulated by ubiquitination, such as β-catenin (44), snail (45, 46), and ZEB1 (47). The EMT marker, Vimentin, may also influence tumor progression. Indeed, the ubiquitination of Vimentin influenced by symmetric dimethylarginine (sDMA) is thought to be necessary for the roles of

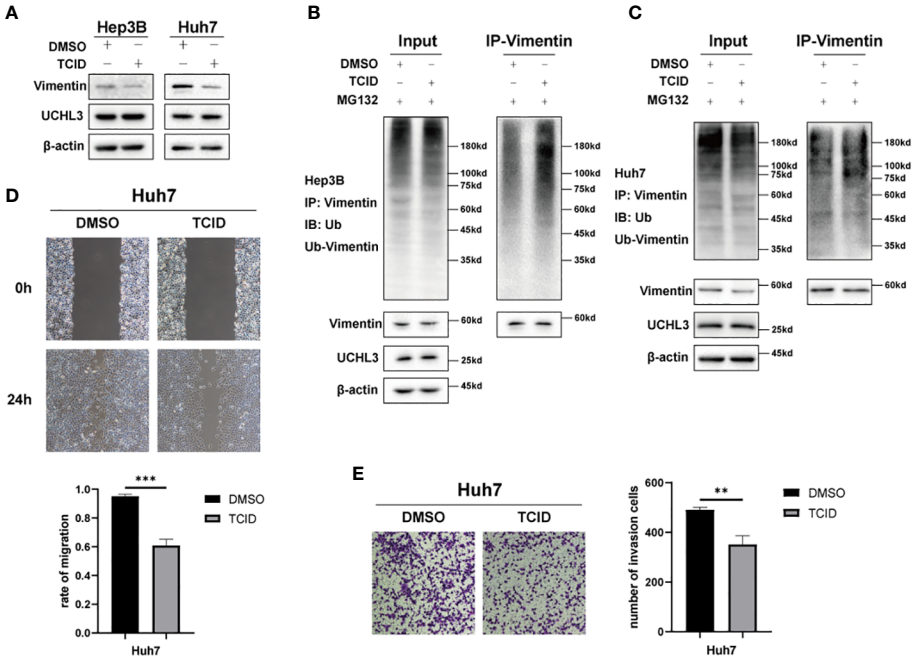

FIGURE 5
Inhibition of UCHL3 impaired HCC cell migration. **(A)** TCID treatment reduced Vimentin levels in Hep3B and Huh7 cells, as shown by Western blotting. **(B)** TCID treatment promoted Vimentin ubiquitination in Hep3B cells, as shown by Western blotting. **(C)** TCID treatment promoted Vimentin ubiquitination in Huh7 cells. **(D)** TCID inhibited Huh7 migration during wound healing assays. **(E)** TCID inhibited Huh7 migration during Transwell assays. **p < 0.01, ***p < 0.001.

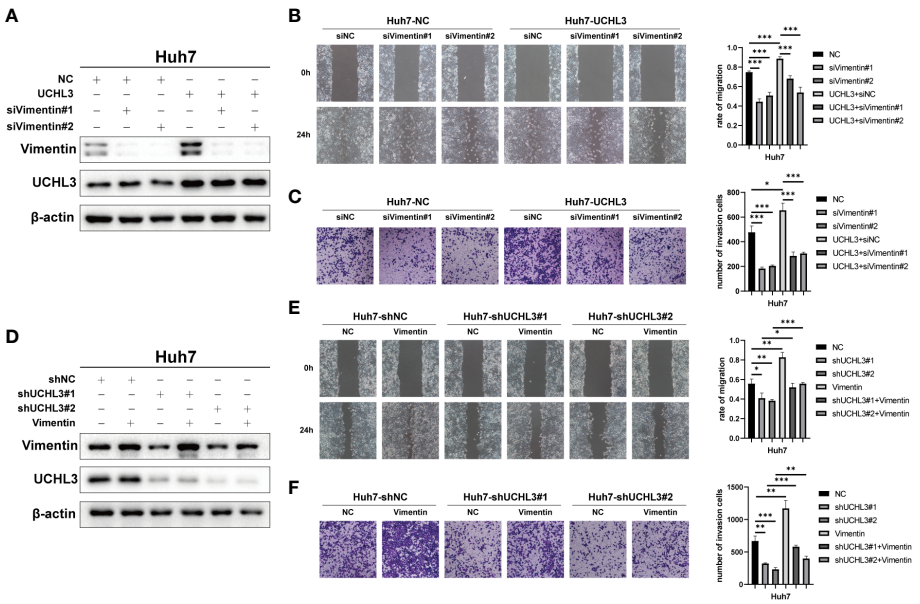

FIGURE 6
UCHL3 facilitated HCC cell migration through regulating Vimentin. **(A)** Overexpression of UCHL3 and knockdown of Vimentin in Huh7 cells shown by Western blotting. **(B)** Vimentin knockdown abolished the increased cell migration induced by UCHL3 overexpression, as shown by wound healing assays. **(C)** Vimentin knockdown abolished the increased cell migration induced by UCHL3 overexpression, as shown by Transwell assays. **(D)** Knockdown of UCHL3 and overexpression of Vimentin in Huh7 cells shown by Western blotting. **(E)** Vimentin overexpression reversed the inhibition of cell migration caused by UCHL3 knockdown, as shown by wound healing assays. **(F)** Vimentin overexpression reversed the inhibition of cell migration caused by UCHL3 knockdown, as shown by Transwell assays. *p < 0.05, **p < 0.01, ***p < 0.001.

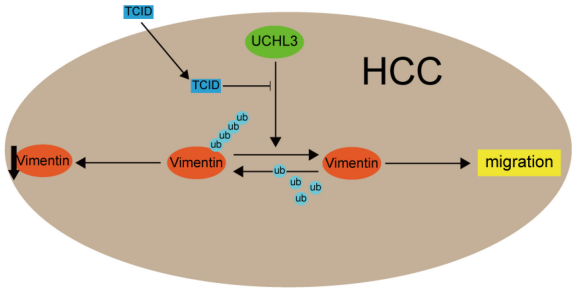

FIGURE 7
A mechanism model figure of UCHL3 facilitated HCC cell migration through regulating Vimentin.

MTAP and PRMT5 in lung cancer metastasis (48). Salvi et al. identified Vimentin as a molecular chaperone of LASP1 that participates in cancer development (49), and You et al. showed that LASP1 protects Vimentin from ubiquitination and degradation and also interacts with HBX (50). Moreover, BECN1 promoted NSCLC cell migration by regulating USP14-mediated Vimentin ubiquitination (51). AKT signaling, known to be active in cancer cells (52), has been shown to mediate lncRNA VAL binding to Vimentin to eliminate Trim16-dependent Vimentin polyubiquitination and degradation and promote LAD invasion and metastasis (32). Vimentin expression has often been linked to ubiquitination, but the influences of de-ubiquitinases have received less attention. UCHL3 was demonstrated, during the present work, to be a new DUB of Vimentin, which enhanced its stability, an effect that was inhibited by TCID treatment. Functional rescue experiments indicated the dependence of UCHL3-mediated HCC cell migration on Vimentin regulation.

Previous reports have indicated the deubiquitinating and protein-stabilizing effect of UCHL3 in several human cancer types (19, 20, 22) and demonstrated its contribution to carcinogenesis (14). UCHL3 promoted pancreatic cancer cell proliferation and migration by deubiquitinating FOXM1 (20). The Aryl hydrocarbon receptor (AhR) protein was stabilized by UCHL3 de-ubiquitination in NSCLC and promoted stem-cell-like properties (22). In addition, UCHL3 induced tumorigenesis in ovarian cancer by deubiquitinating and stabilizing TRAF2 (19). UCHL3 promoted migration of the liver cancer cells of the current study by deubiquitinating Vimentin. We acknowledge some limitations to the current *in vitro* study, and *in vivo* experiments are needed to confirm the findings.

In conclusion, UCHL3 was found to be highly expressed in HCC and indicated a poor prognosis. The DUB activity of UCHL3 stabilized Vimentin and promoted HCC malignant progression. The present findings give new insights into HCC pathogenesis, indicating that the UCHL3/Vimentin axis may provide an innovative therapeutic target.

Data availability statement

The original contributions presented in the study are included in the article/supplementary material. Further inquiries can be directed to the corresponding authors.

Ethics statement

The studies involving human participants were reviewed and approved by Medical Ethics Committee of Zhejiang Provincial People's Hospital. The patients/participants provided their written informed consent to participate in this study.

Author contributions

Conception, design, and writing by QM. Investigation, visualization, and methodology by QL, XL, JZ, WS, and JW. Administrative, supervision, or material support by QZ and DH. All authors contributed to the article and approved the submitted version.

Funding

This study was funded by the Key Research and Development Program of Shaanxi (2020KW-054).

Conflict of interest

The authors declare that the research was conducted in the absence of any commercial or financial relationships that could be construed as a potential conflict of interest.

Publisher's note

All claims expressed in this article are solely those of the authors and do not necessarily represent those of their affiliated organizations, or those of the publisher, the editors and the reviewers. Any product that may be evaluated in this article, or claim that may be made by its manufacturer, is not guaranteed or endorsed by the publisher.

References

1. Sung H, Ferlay J, Siegel RL, Laversanne M, Soerjomataram I, Jemal A, et al. Global cancer statistics 2020: GLOBOCAN estimates of incidence and mortality worldwide for 36 cancers in 185 countries. *CA Cancer J Clin* (2021) 71:209–49. doi: 10.3322/caac.21660

2. Anwanwan D, Singh SK, Singh S, Saikam V, Singh R. Challenges in liver cancer and possible treatment approaches. *Biochim Biophys Acta Rev Cancer* (2020) 1873:188314. doi: 10.1016/j.bbcan.2019.188314

3. El-Serag HB, Marrero JA, Rudolph L, Reddy KR. Diagnosis and treatment of hepatocellular carcinoma. *Gastroenterology* (2008) 134:1752–63. doi: 10.1053/j.gastro.2008.02.090

4. Maluccio M, Covey A. Recent progress in understanding, diagnosing, and treating hepatocellular carcinoma. *CA Cancer J Clin* (2012) 62:394–9. doi: 10.3322/caac.21161

5. Swatek KN, Komander D. Ubiquitin modifications. *Cell Res* (2016) 26:399–422. doi: 10.1038/cr.2016.39

6. Popovic D, Vucic D, Dikic I. Ubiquitination in disease pathogenesis and treatment. *Nat Med* (2014) 20:1242–53. doi: 10.1038/nm.3739

7. Shearer RF, Typas D, Coscia F, Schovsbo S, Kruse T, Mund A, et al. K27-linked ubiquitylation promotes p97 substrate processing and is essential for cell proliferation. *EMBO J* (2022) 41:e110145. doi: 10.15252/embj.2021110145

8. Dwane L, Gallagher WM, Ní Chonghaile T, O'Connor DP. The emerging role of non-traditional ubiquitination in oncogenic pathways. *J Biol Chem* (2017) 292:3543–51. doi: 10.1074/jbc.R116.755694

9. Han S, Wang R, Zhang Y, Li X, Gan Y, Gao F, et al. The role of ubiquitination and deubiquitination in tumor invasion and metastasis. *Int J Biol Sci* (2022) 18:2292–303. doi: 10.7150/ijbs.69411

10. Park J-S, Ma H, Roh Y-S. Ubiquitin pathways regulate the pathogenesis of chronic liver disease. *Biochem Pharmacol* (2021) 193:114764. doi: 10.1016/j.bcp.2021.114764

11. Komander D, Rape M. The ubiquitin code. *Annu Rev Biochem* (2012) 81:203–29. doi: 10.1146/annurev-biochem-060310-170328

12. Clague MJ, Urbé S, Komander D. Breaking the chains: Deubiquitylating enzyme specificity begets function. *Nat Rev Mol Cell Biol* (2019) 20:338–52. doi: 10.1038/s41580-019-0099-1

13. Fang Y, Shen X. Ubiquitin carboxyl-terminal hydrolases: Involvement in cancer progression and clinical implications. *Cancer Metastasis Rev* (2017) 36:669–82. doi: 10.1007/s10555-017-9702-0

14. Hafez N, Modather El-Awadly Z, Arafa RK. UCH-L3 structure and function: Insights about a promising drug target. *Eur J Medicinal Chem* (2022) 227:113970. doi: 10.1016/j.ejmech.2021.113970

15. Song HM, Lee JE, Kim JH. Ubiquitin c-terminal hydrolase-L3 regulates EMT process and cancer metastasis in prostate cell lines. *Biochem Biophys Res Commun* (2014) 452:722–7. doi: 10.1016/j.bbrc.2014.08.144

16. Lee JE, Lim YH, Kim JH. UCH-L1 and UCH-L3 regulate the cancer stem cell-like properties through PI3 K/Akt signaling pathway in prostate cancer cells. *Anim Cells Syst (Seoul)* (2021) 25:312–22. doi: 10.1080/19768354.2021.1987320

17. Yang R, Liu N, Chen L, Jiang Y, Shi Y, Mao C, et al. GIAT4RA functions as a tumor suppressor in non-small cell lung cancer by counteracting Uchl3-mediated deubiquitination of LSH. *Oncogene* (2019) 38:7133–45. doi: 10.1038/s41388-019-0909-0

18. Li G, Jin X, Zheng J, Jiang N, Shi W. UCH-L3 promotes non-small cell lung cancer proliferation. *via accelerating Cell Cycle inhibiting Cell apoptosis. Biotechnol Appl Biochem* (2021) 68:165–72. doi: 10.1002/bab.1909

19. Zhang M-H, Zhang H-H, Du X-H, Gao J, Li C, Shi H-R, et al. UCHL3 promotes ovarian cancer progression by stabilizing TRAF2 to activate the NF-κB pathway. *Oncogene* (2020) 39:322–33. doi: 10.1038/s41388-019-0987-z

20. Song Z, Li J, Zhang L, Deng J, Fang Z, Xiang X, et al. UCHL3 promotes pancreatic cancer progression and chemo-resistance through FOXM1 stabilization. *Am J Cancer Res* (2019) 9:1970–81.

21. He R, Zhou Y, Liu J, Zhang X, Zhao X, An L, et al. UCHL3 plays an important role in the occurrence and development of melanoma. *Oncol Lett* (2021) 22:756. doi: 10.3892/ol.2021.13017

22. Ouyang L, Yan B, Liu Y, Mao C, Wang M, Liu N, et al. The deubiquitylase UCHL3 maintains cancer stem-like properties by stabilizing the aryl hydrocarbon receptor. *Signal Transduction Targeted Ther* (2020) 5(1):78. doi:?10.1038/s41392-020-0181-3

23. Xu L-M, Yuan Y-J, Yu H, Wang S, Wang P. LINC00665 knockdown confers sensitivity in irradiated non-small cell lung cancer cells through the miR-582-5p/UCHL3/AhR axis. *J Transl Med* (2022) 20:350. doi: 10.1186/s12967-022-03516-2

24. Zhao P, Guo T, Qian L, Wang X, Yuan Y, Cheng Q, et al. Ubiquitin c-terminal hydrolase-L3 promotes interferon antiviral activity by stabilizing type I-interferon receptor. *Antiviral Res* (2017) 144:120–9. doi: 10.1016/j.antiviral.2017.06.002

25. Luo K, Li L, Li Y, Wu C, Yin Y, Chen Y, et al. A phosphorylation–deubiquitination cascade regulates the BRCA2–RAD51 axis in homologous recombination. *Genes Dev* (2016) 30:2581–95. doi: 10.1101/gad.289439.116

26. Wang R, Chen J, Yu H, Wei Z, Ma M, Ye X, et al. Downregulation of estrogen receptor-α36 expression attenuates metastasis of hepatocellular carcinoma cells. *Environ Toxicol* (2022) 37:1113–23. doi: 10.1002/tox.23469

27. Usman S, Waseem NH, Nguyen TKN, Mohsin S, Jamal A, Teh M-T, et al. Vimentin is at the heart of epithelial mesenchymal transition (EMT) mediated metastasis. *Cancers (Basel)* (2021) 13:4985. doi: 10.3390/cancers13194985

28. Pan T-L, Wang P-W, Huang C-C, Yeh C-T, Hu T-H, Yu J-S. Network analysis and proteomic identification of vimentin as a key regulator associated with invasion and metastasis in human hepatocellular carcinoma cells. *J Proteomics* (2012) 75:4676–92. doi: 10.1016/j.jprot.2012.02.017

29. Satelli A, Li S. Vimentin as a potential molecular target in cancer therapy or vimentin, an overview and its potential as a molecular target for cancer therapy. *Cell Mol Life Sci* (2011) 68:3033–46. doi: 10.1007/s00018-011-0735-1

30. Snider NT, Omary MB. Post-translational modifications of intermediate filament proteins: Mechanisms and functions. *Nat Rev Mol Cell Biol* (2014) 15:163–77. doi: 10.1038/nrm3753

31. Snider NT, Omary MB. Assays for post-translational modifications of intermediate filament proteins. *Methods Enzymol* (2016) 568:113–38. doi: 10.1016/bs.mie.2015.09.005

32. Tian H, Lian R, Li Y, Liu C, Liang S, Li W, et al. AKT-induced lncRNA VAL promotes EMT-independent metastasis through diminishing Trim16-dependent vimentin degradation. *Nat Commun* (2020) 11:5127. doi: 10.1038/s41467-020-18929-0

33. Zhao L, Zhang P, Su X-J, Zhang B. The ubiquitin ligase TRIM56 inhibits ovarian cancer progression by targeting vimentin. *J Cell Physiol* (2018) 233:2420–5. doi: 10.1002/jcp.26114

34. Zhu Y, Zhang Y, Sui Z, Zhang Y, Liu M, Tang H. USP14 de-ubiquitinates vimentin and miR-320a modulates USP14 and vimentin to contribute to malignancy in gastric cancer cells. *Oncotarget* (2016) 8:48725–36. doi: 10.18632/oncotarget.10706

35. Chandrashekar DS, Karthikeyan SK, Korla PK, Patel H, Shovon AR, Athar M, et al. UALCAN: An update to the integrated cancer data analysis platform. *Neoplasia* (2022) 25:18–27. doi: 10.1016/j.neo.2022.01.001

36. Rahib L, Smith BD, Aizenberg R, Rosenzweig AB, Fleshman JM, Matrisian LM. Projecting cancer incidence and deaths to 2030: The unexpected burden of thyroid, liver, and pancreas cancers in the united states. *Cancer Res* (2014) 74:2913–21. doi: 10.1158/0008-5472.CAN-14-0155

37. Siegel RL, Miller KD, Jemal A. Cancer statistics, 2019. *CA Cancer J Clin* (2019) 69:7–34. doi: 10.3322/caac.21551

38. Hoeller D, Dikic I. Targeting the ubiquitin system in cancer therapy. *Nature* (2009) 458:438–44. doi: 10.1038/nature07960

39. Li Q, Chao Q, Liu Y, Fang J, Xie J, Zhen J, et al. Deubiquitinase ZRANB1 drives hepatocellular carcinoma progression through SP1-LOXL2 axis. *Am J Cancer Res* (2021) 11:4807–25.

40. Mevissen TET, Komander D. Mechanisms of deubiquitinase specificity and regulation. *Annu Rev Biochem* (2017) 86:159–92. doi: 10.1146/annurev-biochem-061516-044916

41. Zhao J, Guo J, Wang Y, Ma Q, Shi Y, Cheng F, et al. Research progress of DUB enzyme in hepatocellular carcinoma. *Front Oncol* (2022) 12:920287. doi: 10.3389/fonc.2022.920287

42. Fang Y, Fu D, Tang W, Cai Y, Ma D, Wang H, et al. Ubiquitin c-terminal hydrolase 37, a novel predictor for hepatocellular carcinoma recurrence, promotes cell migration and invasion. *via interacting deubiquitinating PRP19. Biochim Biophys Acta* (2013) 1833:559–72. doi: 10.1016/j.bbamcr.2012.11.020

43. Llovet JM, Kelley RK, Villanueva A, Singal AG, Pikarsky E, Roayaie S, et al. Hepatocellular carcinoma. *Nat Rev Dis Primers* (2021) 7:1–28. doi: 10.1038/s41572-020-00240-3

44. Li B, Ge Y-Z, Yan W-W, Gong B, Cao K, Zhao R, et al. DNASE1L3 inhibits proliferation, invasion and metastasis of hepatocellular carcinoma by interacting with β-catenin to promote its ubiquitin degradation pathway. *Cell Prolif* (2022) 55:e13273. doi: 10.1111/cpr.13273

45. Wu Y, Deng J, Rychahou PG, Qiu S, Evers BM, Zhou BP. Stabilization of snail by NF-kappaB is required for inflammation-induced cell migration and invasion. *Cancer Cell* (2009) 15:416–28. doi: 10.1016/j.ccr.2009.03.016

46. Xu W, Liu H, Liu Z-G, Wang H-S, Zhang F, Wang H, et al. Histone deacetylase inhibitors upregulate snail *via* Smad2/3 phosphorylation and stabilization of snail to promote metastasis of hepatoma cells. *Cancer Lett* (2018) 420:1–13. doi: 10.1016/j.canlet.2018.01.068

47. Li X, Yuan J, Song C, Lei Y, Xu J, Zhang G, et al. Deubiquitinase USP39 and E3 ligase TRIM26 balance the level of ZEB1 ubiquitination and thereby determine the progression of hepatocellular carcinoma. *Cell Death Differ* (2021) 28:2315–32. doi: 10.1038/s41418-021-00754-7

48. Chang W, Chen Y, Hsiao Y, Chiang C, Wang C, Chang Y, et al. Reduced symmetric dimethylation stabilizes vimentin and promotes metastasis in MTAP-deficient lung cancer. *EMBO Rep* (2022) 23:e54265. doi: 10.15252/embr.202154265

49. Salvi A, Bongarzone I, Ferrari L, Abeni E, Arici B, De Bortoli M, et al. Molecular characterization of LASP-1 expression reveals vimentin as its new partner in human hepatocellular carcinoma cells. *Int J Oncol* (2015) 46:1901–12. doi: 10.3892/ijo.2015.2923

50. You H, Yuan D, Bi Y, Zhang N, Li Q, Tu T, et al. Hepatitis b virus X protein promotes vimentin expression *via* LIM and SH3 domain protein 1 to facilitate epithelial-mesenchymal transition and hepatocarcinogenesis. *Cell Commun Signal* (2021) 19:33. doi: 10.1186/s12964-021-00714-1

51. Cheng Z, Xin H, Han T. BECN1 promotes the migration of NSCLC cells through regulating the ubiquitination of vimentin. *Cell Adh Migr* (2019) 13:249–59. doi: 10.1080/19336918.2019.1638690

52. Mayer IA, Arteaga CL. The PI3K/AKT pathway as a target for cancer treatment. *Annu Rev Med* (2016) 67:11–28. doi: 10.1146/annurev-med-062913-051343

frontiers | Frontiers in Oncology

TYPE Original Research
PUBLISHED 03 May 2023
DOI 10.3389/fonc.2023.1169833

OPEN ACCESS

EDITED BY
Jixin Dong,
University of Nebraska Medical Center, United States

REVIEWED BY
Prakash Radhakrishnan,
University of Nebraska Medical Center, United States
Kamiya Mehla,
University of Oklahoma Health Sciences Center, United States

*CORRESPONDENCE
Xing Wang
foxmulder180@gmc.edu.cn
Yaozhen Pan
panyaozhen@gmc.edu.cn

†These authors have contributed equally to this work

RECEIVED 20 February 2023
ACCEPTED 20 April 2023
PUBLISHED 03 May 2023

CITATION
Liu P, Liu S, Zhu C, Li Y, Li Y, Fei X, Hou J, Wang X and Pan Y (2023) The deubiquitinating enzyme MINDY2 promotes pancreatic cancer proliferation and metastasis by stabilizing ACTN4 expression and activating the PI3K/AKT/mTOR signaling pathway. *Front. Oncol.* 13:1169833. doi: 10.3389/fonc.2023.1169833

The deubiquitinating enzyme MINDY2 promotes pancreatic cancer proliferation and metastasis by stabilizing ACTN4 expression and activating the PI3K/AKT/mTOR signaling pathway

Peng Liu[1,2†], Songbai Liu[1†], Changhao Zhu[3†], Yongning Li[2], Ying Li[3], Xiaobin Fei[1], Junyi Hou[1], Xing Wang[1,3*] and Yaozhen Pan[1,3*]

[1]College of Clinical Medicine, Guizhou Medical University, Guiyang, China, [2]Department of Hepatic-Biliary-Pancreatic Surgery, The Affiliated Hospital of Guizhou Medical University, Guiyang, China, [3]Department of Hepatic-Biliary-Pancreatic Surgery, The Affiliated Cancer Hospital of Guizhou Medical University, Guiyang, China

The pathogenic mechanisms of pancreatic cancer (PC) are still not fully understood. Ubiquitination modifications have a crucial role in tumorigenesis and progression. Yet, the role of MINDY2, a member of the motif interacting with Ub-containing novel DUB family (MINDY), as a newly identified deubiquitinating enzyme, in PC is still unclear. In this study, we found that MINDY2 expression is elevated in PC tissue (clinical samples) and was associated with poor prognosis. We also found that MINDY2 is associated with pro-carcinogenic factors such as epithelial-mesenchymal transition (EMT), inflammatory response, and angiogenesis; the ROC curve suggested that MINDY2 has a high diagnostic value in PC. Immunological correlation analysis suggested that MINDY2 is deeply involved in immune cell infiltration in PC and is associated with immune checkpoint-related genes. *In vivo* and *in vitro* experiments further suggested that elevated MINDY2 promotes PC proliferation, invasive metastasis, and EMT. Meanwhile, actinin alpha 4 (ACTN4) was identified as a MINDY2-interacting protein by mass spectrometry and other experiments, and ACTN4 protein levels were significantly correlated with MINDY2 expression. The ubiquitination assay confirmed that MINDY2 stabilizes the ACTN4 protein level by deubiquitination. The pro-oncogenic effect of MINDY2 was significantly inhibited by silencing ACTN4. Bioinformatics Analysis and Western blot experiments further confirmed that MINDY2 stabilizes ACTN4 through deubiquitination and thus activates the PI3K/AKT/mTOR signaling pathway. In conclusion, we identified the oncogenic role and mechanism of MINDY2 in PC, suggesting that MINDY2 is a viable candidate gene for PC and may be a therapeutic target and critical prognostic indicator.

KEYWORDS

pancreatic cancer, MINDY2, deubiquitinating enzyme, ACTN4, PI3K/AKT/mTOR

1 Introduction

Pancreatic cancer is a solid tumor of the gastrointestinal tract. It is the 11th most common cancer in women and the 12th most common cancer in men globally (1). Surgical techniques such as laparoscopic and robotic surgery are widely used to treat early-stage PC. Yet, patients with PC usually present with advanced-stage cancer at the time of diagnosis, thus losing their chance to undergo surgery (2–4). The lack of typical clinical symptoms and sensitive early diagnostic markers, coupled with the highly aggressive ability of PC, make its diagnosis and treatment very challenging (5). Consequently, it is necessary to investigate PC's mechanism and identify valuable targets for early diagnosis and treatment.

Ubiquitination is an essential post-translational modification (PTM) that has a significant role in various aspects of the cellular life cycle, such as cell growth, proliferation, apoptosis, and DNA repair, especially in controlling substrate degradation and regulating protein "quality" and "quantity" (6, 7). Numerous studies have indicated that the loss of control of protein homeostasis leads to the development of many diseases, including tumors. Also, abnormalities in the ubiquitin-proteasome system (UPS) have been identified as an important cause of uncontrolled protein homeostasis. Moreover, it has been found that deubiquitinating enzymes (DUBs), as an essential component of the UPS, can remove the ubiquitin chain of protein substrates, thus reversing the ubiquitination process (8, 9). DUBs are involved in almost all cellular signaling pathways, such as gene transcription, cell cycle, and receptor downregulation, and abnormal DUBs have been associated with many diseases, especially tumors (10, 11), including pancreatic, lung, breast, and bladder cancers (12–19).

There are more than 100 DUBs in the human genome (20), which can be classified into seven families based on their catalytic mechanisms and structural similarities (21, 22), including ubiquitin carboxy-terminal hydrolases (UCHs), ovarian tumor proteases (OTUs), ubiquitin-specific proteases (USPs), Machado-Josephin domain-containing proteases (MJDs), MINDYs, JAB1/MPN/MOV34 metalloenzymes (JAMMs), and Zinc finger and UFSP structural domain protein (ZUFSP). Among them, the MINDY family is a recently discovered deubiquitinase family (23, 24). In this study, we examined the effect of MINDY2 (also known as FAM63B) in PC.

2 Results

2.1 MINDY2 is a potential oncogenic target for PC

To determine the potential function of MINDY2 in PC, we performed an analysis of three datasets from the GEO database (GSE15471, GSE16515, and GSE62165) as well as the GEPIA2 database. Higher expression of MINDY2 was found in PC tissues compared to adjacent normal tissues (Figures 1A, B). The CPTAC dataset in UALCAN revealed that the total protein expression level of MINDY2 was much higher in PC tissues than in adjacent normal tissues (Figure 1C).

Next, we obtained RNAseq data of PC from the TCGA database and corresponding clinical information and found an association between MINDY2 expression and overall survival (OS), progression-free survival (PFS), and disease-specific survival (DSS) (Figure 1D). Also, MINDY2 expression correlated with T-stage, N-stage, tumor grade, and cancer stage of PC (Figures 1E–G). The receiver operating characteristic (ROC) curve further suggested that MINDY2 has a high diagnostic value in PC (Figure 1H).

The Tumor Immune Dysfunction and Exclusion (TIDE) algorithm predicted the immunotherapeutic response of MINDY2 in PC and discovered that the higher the expression of MINDY2, the better the response of PC to immune checkpoint inhibitors (Figure 1I). Then we further analyzed and found that MINDY2 was positively correlated with pro-cancer factors such as EMT, inflammatory response, ECM-related genes, angiogenesis, and tumor inflammatory features in PC, and negatively correlated with DNA repair capacity (Figures 1J, K). Also, immune correlation analysis revealed that the expression of MINDY2 in PC was positively correlated with the level of infiltration of B cells, T cells CD8+, neutrophils, macrophages, and dendritic cells (Figure 2A). Furthermore, correlation analysis between the expression of MINDY2 and the expression of immune checkpoint-related genes revealed that the expression of MINDY2 was correlated with PDCD1LG2, HAVCR2, CD274, TIGIT, and SIGLEC15 (Figure 2B). Therefore, the combined results of our bioinformatics analysis concluded that MINDY2 is a valuable oncogenic factor in PC.

2.2 MINDY2 expression is elevated in PC and is associated with poor prognosis

We investigated the expression of MINDY2 in the cancerous and adjacent normal tissues of 20 PC patients. The results demonstrated that the mRNA and protein levels of MINDY2 expression were higher in cancer tissues than in nearby normal tissues (Figures 3A, B). Subsequently, we performed an immunohistochemical analysis in tissue microarrays (TMA) containing 90 PC and corresponding adjacent normal tissue samples. We discovered that the expression of MINDY2 was higher in PC tissues than in corresponding adjacent normal tissues (Figure 3C).

To further investigate the clinical significance of MINDY2, the relationship between MINDY2 expression and clinicopathological parameters of PC patients was examined. We discovered a correlation between higher MINDY2 and TNM stage, distant metastases, vascular invasion, and neurological invasion (Table 1). Moreover, the Kaplan-Meier analysis of survival demonstrated that the overall survival of patients with high MINDY2 expression was considerably lower than that of the control group (Figure 3D).

2.3 MINDY2 promotes PC cell proliferation, invasion, and migration *in vitro*

To further investigate the biological function of MINDY2 in PC, we discovered that the expression of MINDY2 was higher in PC cell

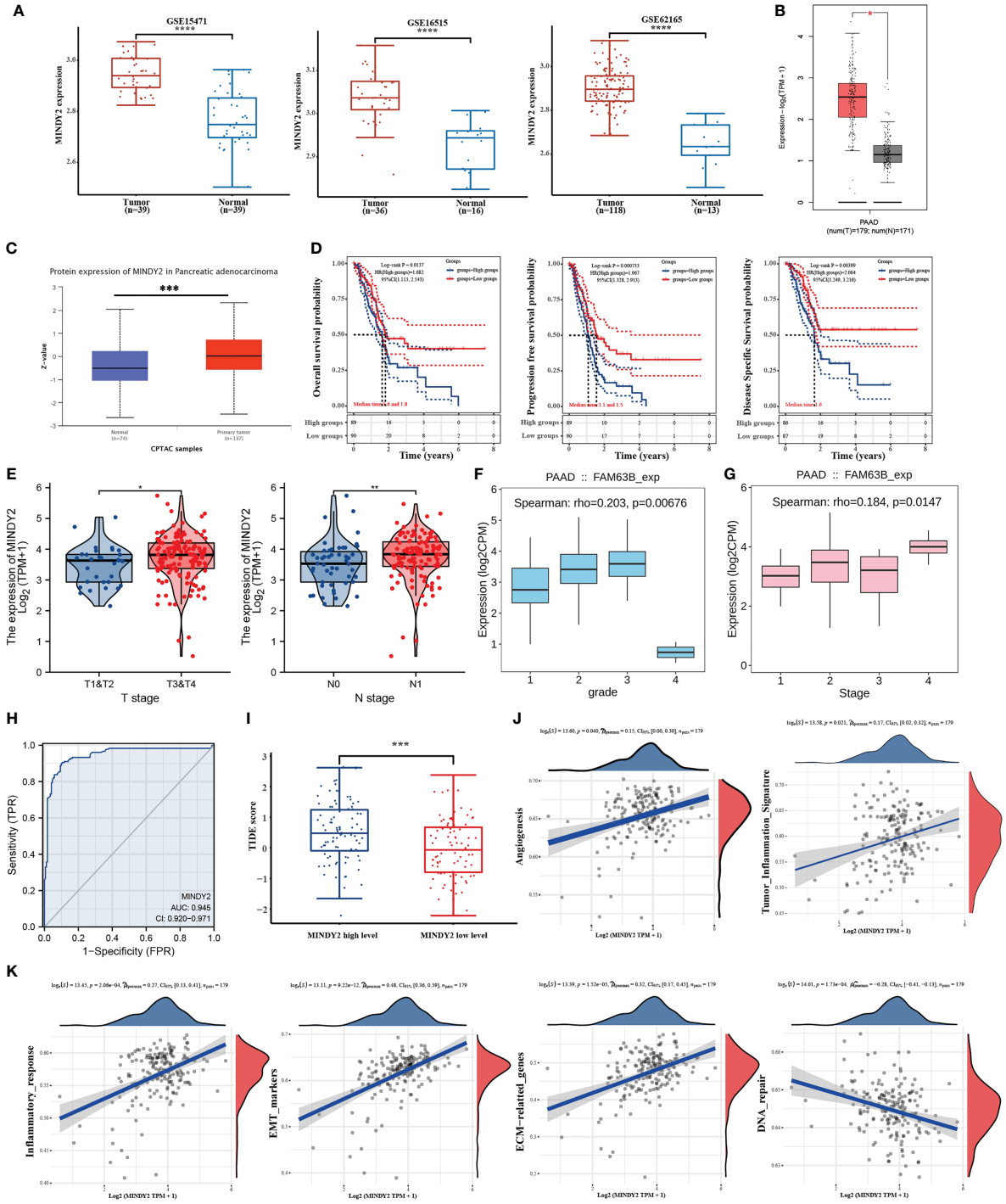

FIGURE 1
MINDY2 is a potential oncogenic target for PC. **(A, B)** Analysis of MINDY2 mRNA content in PC based on GEO and GEPIA2 datasets. **(C)** Analysis of MINDY2 expression levels of total protein in PC based on CPTAC dataset. **(D–G)** Correlation of MINDY2 with OS, PFS, DSS, T-stage, N-stage, tumor grade, and cancer stage in PC patients. **(H)** ROC curves to assess the diagnostic value of MINDY2 in PC. **(I)** TIDE algorithm to predict the relationship between MINDY2 and response to immunotherapy in PC. **(J, K)** Correlation of MINDY2 with EMT, inflammatory response, ECM-related genes, angiogenesis, tumor inflammatory features, and DNA repair. (*P < 0.05, **P < 0.01, ***P < 0.001, ****P < 0.0001).

lines (AsPC-1, BxPC-3, Capan-2, PANC-1, Mia PaCa-2, and SW1990) than in normal pancreatic ductal epithelial cells (HPDE); the lowest endogenous expression level of MINDY2 was seen in BxPC-3 cells and the highest expression in PANC-1 cells (Figure 4A). Therefore, BxPC-3 and PANC-1 were used as the target cells for this study.

Next, we designed 3 small interfering RNAs and validated their efficiency in PANC-1 cells. The results suggested that si-MINDY2#2

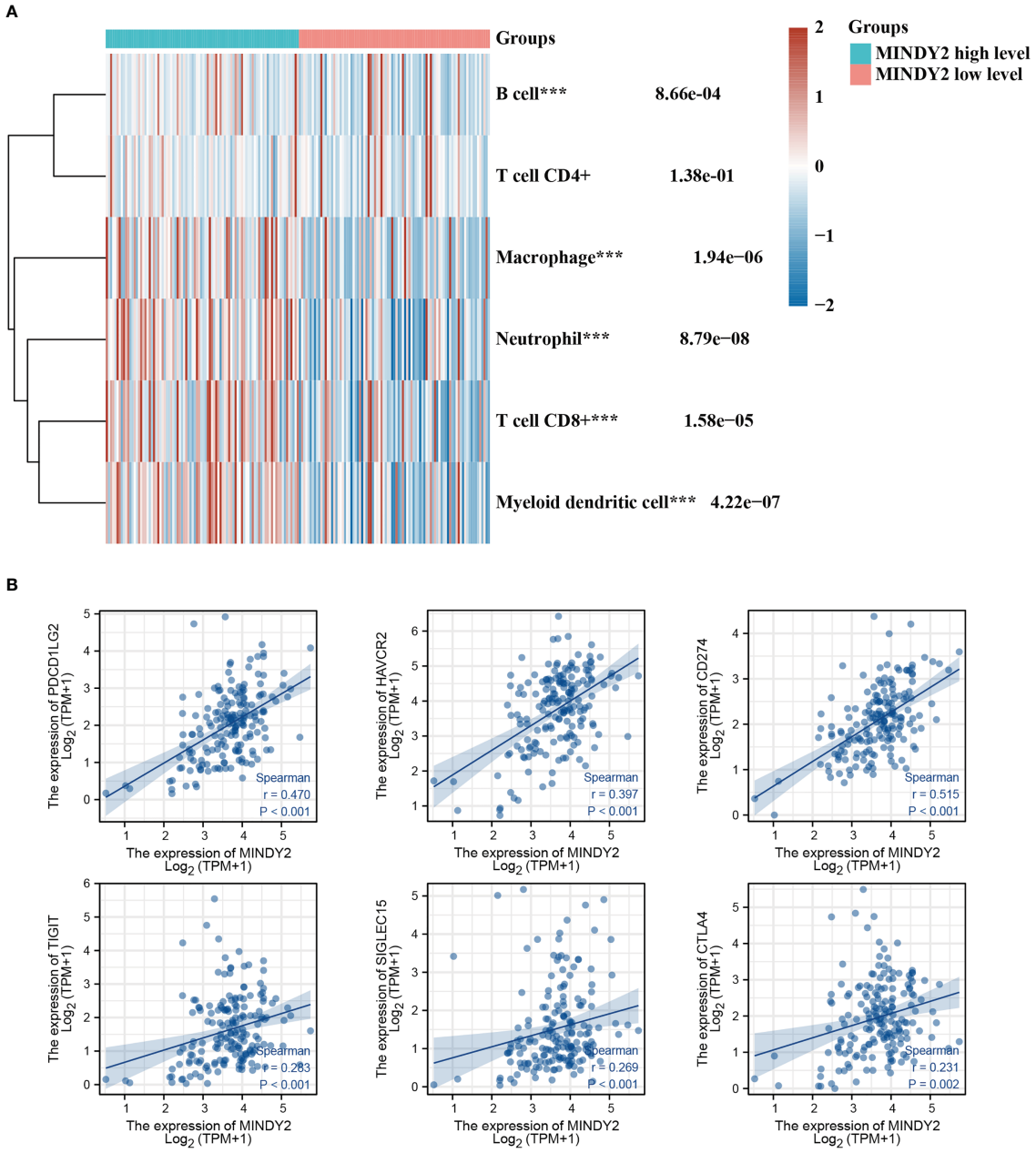

FIGURE 2
Correlation between MINDY2 and the score for tumor immune cell infiltration and immune checkpoint-related gene expression. **(A)** TIMER algorithm-based evaluation of the association between MINDY2 in PC and tumor immune cell infiltration score. **(B)** Correlation of MINDY2 in PC with immune checkpoint-related gene expression. (***P < 0.001).

and si-MINDY2#3 sequences had the best silencing effect (Figure 4B). Thus, si-MINDY2#2 and si-MINDY2#3 sequences were used to construct stable up/down-regulated lentiviral vectors for target cell infection and to verify the infection efficiency (Figure 4C). The cell viability and colony-forming ability of PC cells were significantly reduced after silencing MINDY2, and this ability was significantly enhanced after upregulating MINDY2 by CCK8 and clonogenic plate experiments (Figures 4D, E). EdU assay demonstrated that the proliferation ability of BxPC-3 cells was significantly increased after MINDY2 overexpression compared with the diminished proliferation capacity of PANC-1 cells after the down-regulation of MINDY2 (Figure 4F).

Western blot analysis revealed that the expression levels of Cyclin D1, Cyclin E1, CDK2, and CDK4 increased following MINDY2 overexpression, while these cyclins were decreased after the downregulation of MINDY2 compared with the control group (Figure 4G). In addition, flow cytometry showed that the G1 phase of BxPC-3 cells decreased significantly after overexpression of MINDY2. In contrast, the S and G2 phases significantly increased, which resulted in an accelerated G1/S phase transition

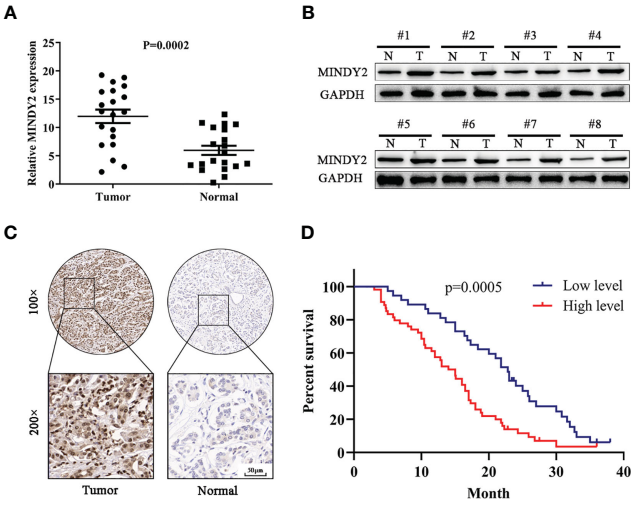

FIGURE 3
MINDY2 expression is elevated in PC and is associated with poor prognosis. **(A, B)** MINDY2 expression in PC tissues and adjacent normal tissues by Western blot and QT-PCR. **(C)** Immunohistochemical analysis of MINDY2 expression in TMA containing 90 PC and adjacent normal tissue. **(D)** Kaplan-Meier curve according to MINDY2 expression showing the survival rate of PC patients. Repre-sentative results of three biological replicates are shown.

of the cell cycle, while the results were reversed after the downregulation of MINDY2 (Figure 4H). Thus, elevated expression of MINDY2 promoted the proliferation of PC cells.

Wound healing assay and Transwell assay revealed that PC cells had greater vital invasive and migratory ability after upregulation of MINDY2. In contrast, this ability was significantly reduced after the knockdown of MINDY2 (Figures 4I, J). The identification of EMT-related proteins by Western blot revealed that the MINDY2-overexpressed group expressed higher levels of N-cadherin, Snail, and Vimentin than the control group. The levels of E-cadherin protein expression were lower than in the control group. Opposite results were obtained after the downregulation of MINDY2 (Figure 4K). In light of the preceding findings, MINDY2 may increase the invasion and metastasis of PC cells *via* EMT.

2.4 MINDY2 promotes PC growth and liver metastasis *in vivo*

To further investigate the effect of MINDY2 in tumors, we subcutaneously injected different groups of PC cells into the right axilla of nude mice to evaluate the effect of MINDY2 on tumor growth. The results showed that the volume and weight of tumor formation in nude mice were significantly higher than those in the control group after the upregulation of MINDY2; opposite result was obtained after the downregulation of MINDY2 (Figure 5A). In addition, the immunohistochemical results of tumor tissue showed that after the stable up-regulation of MINDY2, the staining intensity and positive ratio of MINDY2 in tumor tissue were higher than those in the control group. The staining of PCNA and Ki67 related to proliferation indicators was also enhanced, and the positive ratio was significantly higher than that in the control group; opposite results were seen after downregulation of MINDY2 (Figure 5B).

Meanwhile, we implanted PC cell suspensions with stable upregulation of MINDY2 in the spleen of nude mice to construct a liver metastasis model. We found that the size and number of liver metastases were significantly more substantial in the upregulated group than in the control group. In contrast, the knockdown MINDY2 group significantly inhibited PC cell liver metastasis *in vivo* (Figure 5C). HE staining of mouse liver tissue also obtained the same result (Figure 5D). Thus, MINDY2 promoted PC growth and liver metastasis *in vivo*.

2.5 MINDY2 interacts with ACTN4 and stabilizes ACTN4 by deubiquitination function

To further investigate the mechanism of MINDY2 in PC, we performed protein profiling on the samples obtained from MINDY2 immunoprecipitation experiments. ACTN4 was identified as the target protein of MINDY2. According to bioinformatics analyses, ACTN4 is significantly expressed in PC and is associated with a bad prognosis (Figure 6A, Supplementary Figure 1). Immuno-co-precipitation experiments further showed that MINDY2 interacted with ACTN4 (Figure 6B). In addition, immunofluorescence co-localization revealed that MINDY2 and ACTN4 were mainly co-localized in the cytoplasm in PC cells (Figure 6C).

Western blot assay suggested that MINDY2 could regulate the level of ACTN4 protein (Figure 6D). However, QT-PCR results indicated that MINDY2 does not impact the mRNA expression of ACTN4 (Figure 6E). We also discovered that the addition of the

TABLE 1 Clinicopathological characteristics and the relationship between MINDY2 expression in PC patients.

Features	n	MINDY2 expression		P-value
		low	high	X^2
All cases	90	37	53	
Gender				0.118	0.828
Man	53	21	32		
Female	37	16	21		
Age				0.085	0.832
<60	47	20	27		
≥60	43	17	26		
pTNM stage				7.313	**0.009**
I and II	53	28	25		
III and IV	37	9	28		
Tumor size (cm)				2.295	0.174
<4	60	28	32		
≥4	30	9	21		
Lymph node metastasis				3.884	0.075
Negative	33	18	15		
Positive	57	19	38		
Distant metastasis				5.559	**0.028**
Negative	66	32	34		
Positive	24	5	19		
Perineural invasion				7.954	**0.007**
Negative	31	19	12		
Positive	59	18	41		
Blood vessel invasion				13.986	**0.000**
Negative	52	30	22		
Positive	38	7	31		

proteasome inhibitor MG132 eliminated MINDY2's ability to regulate ACTN4 protein expression (Figure 6F). Then, we used the protein synthesis inhibitor actinomycin (CHX) to further show how MINDY2 affects the stability of the ACTN4 protein. The ACTN4 half-life was significantly shorter in cells that down-regulated MINDY2 and significantly longer in cells that overexpressed MINDY2 (Figure 6G). The results suggest that MINDY2 may regulate ACTN4 protein amount through deubiquitination modifications. To further confirm this conjecture, we performed ubiquitination experiments to analyze whether ACTN4 is a deubiquitinated substrate for MINDY2. Ubiquitination experiments showed that over-expression of MINDY2 markedly decreased the ubiquitination level of ACTN4; at the same time, the level of ACTN4 ubiquitination was significantly higher after MINDY2 downregulation (Figures 6H, I).

Moreover, the protein levels of ACTN4 and the ubiquitination level were dose-dependent for MINDY2 (Figure 6J). To further investigate the effect of MINDY2 on the type of deubiquitination modification of ACTN4, we co-expressed Flag-MINDY2 and Myc-ACTN4 as well as mutant HA-ub in BxPC-3 cells. The ubiquitination experiments showed that MINDY2 cleaved only the K48 ubiquitin chain on ACTN4 (Figures 6K, L). Thus, the above results suggested that MINDY2 stabilizes ACTN4 protein expression by cleaving the K48 chain linked to ACTN4 to avoid its degradation by ubiquitination.

2.6 MINDY2 activates the PI3K/AKT/mTOR pathway by stabilizing ACTN4

To further clarify the role of ACTN4 in the cancer-promoting process of MINDY2, after we down-regulated ACTN4 and upregulated MINDY2 co-treated BxPC-3 cells, the results of CCK-8, clonal plate, and EdU experiments suggested that the function of MINDY2 in enhancing PC cell viability and proliferation ability was reversed (Figures 7A–C). Flow cytometry demonstrated that MINDY2 inhibited the G1/S phase transition of the cell cycle (Figure 7D). Also, it was found that the knockdown of ACTN4 reduced the ability of MINDY2 to promote EMT (Figure 7E); both the Transwell test and the wound healing experiment demonstrated that MINDY2's capacity to encourage PC cell invasion and migration was significantly reduced (Figures 7F, G).

The PI3K/AKT/mTOR signaling pathway is essential for PC development (25–28), and ACTN4 performs a pro-cancer role in malignancies by activating this pathway (29, 30). Bioinformatics analysis indicted that both MINDY2 and ACTN4 in PC were associated with the PI3K/AKT/mTOR signaling pathway (Figure 7H). After MINDY2 overexpression, the total protein levels of PI3K, AKT, and mTOR did not change. In contrast, the phosphorylation level was significantly increased, and the addition of PI3K inhibitor LY294002 reversed this function of MINDY2, A similar effect was obtained after silencing ACTN4 (Figure 7I). Thus, ACTN4 is crucial in the activation of the PI3K/AKT/mTOR signaling pathway by MINDY2. According to the aforementioned findings, MINDY2 stabilizes ACTN4 expression by deubiquitinating it, which then stimulates the PI3K/AKT/mTOR pathway to encourage PC proliferation and invasive metastasis (Figure 7J).

3 Discussion

Ubiquitination is a very important PTM that has a vital role in the degradation of proteins and in maintaining intracellular environmental homeostasis (31). Three enzymes-ubiquitin activating enzymes (E1), ubiquitin-binding enzyme (E2), and ubiquitin ligase (E3)—are primarily responsible for mediating the ubiquitination process (32); yet, ubiquitination is a reversible process. For example, E3 ubiquitin ligase selectively mediates the ubiquitin-binding of substrates, while DUB negatively regulates this process so that ubiquitination and deubiquitination are maintained

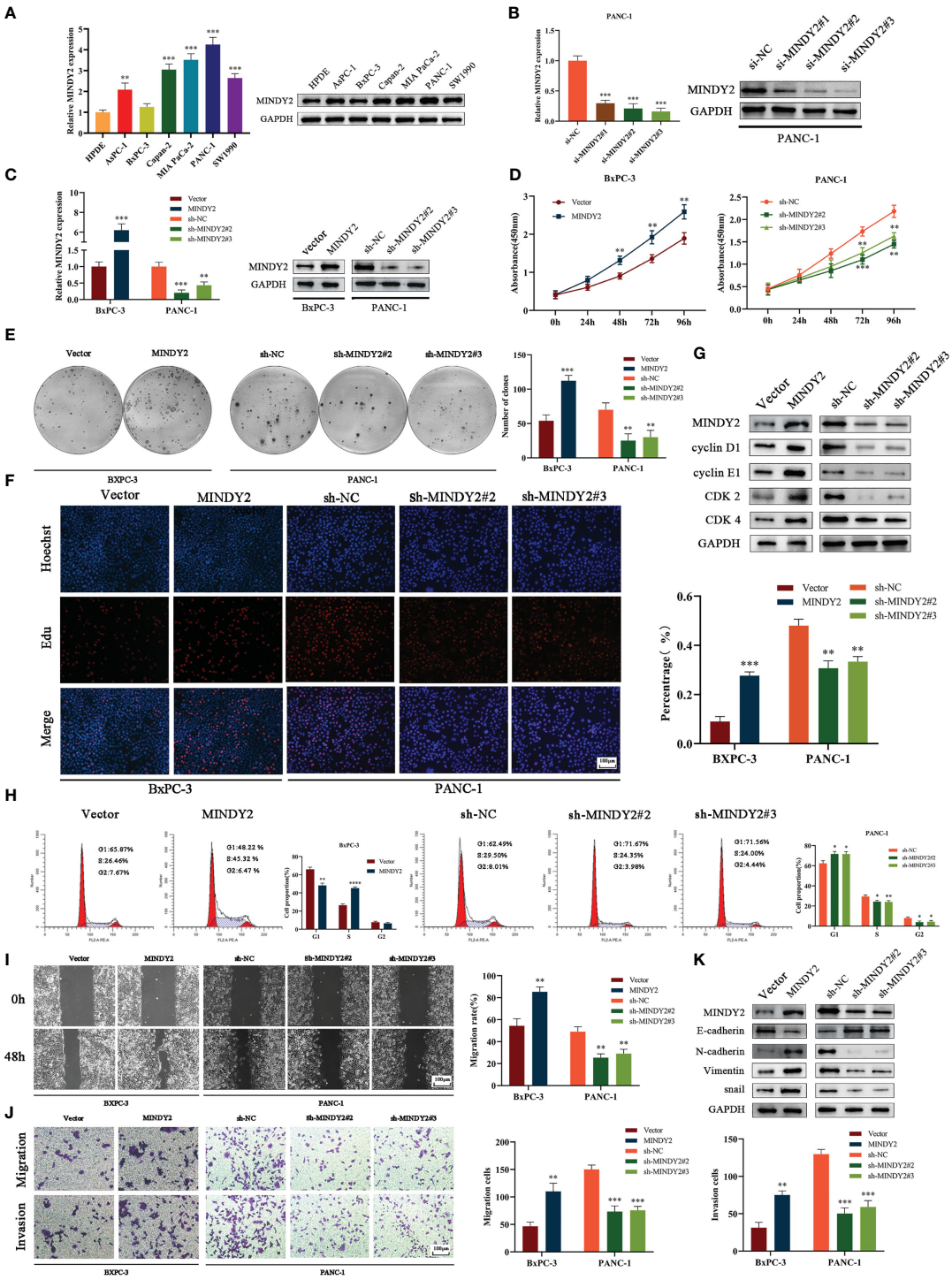

FIGURE 4
MINDY2 promotes PC cell proliferation, invasion, and migration *in vitro*. **(A)** The expression of MINDY2 in PC cell lines and HPDE detected using QT-PCR and Western blot. **(B)** QT-PCR and Western blot detected the silencing effect of three small interfering RNA sequences. **(C)** QT-PCR and Western blot assay for stable up/down-regulation of lentivirus transfection efficiency. **(D)** The effect of MINDY2 on PC cell viability assessed by CCK8 assay. **(E)** Cloning plate assay to estimate the influence of MINDY2 on the ability of PC cells to form clones. **(F)** Edu assay to evaluate the influence of MINDY2 on the proliferative capacity of PC cells. **(G)** Western blot to detect the effect of MINDY2 on cell cycle proteins. **(H)** Flow cytometry to analyze the impact of MINDY2 on the cell cycle in PC cells. **(I, J)** To evaluate the impact of MINDY2 on PC cells' capacity for invasion and migration, wound healing assays and Transwell assays were conducted. **(K)** Western blot detection of MINDY2's effect on EMT. (*P < 0.05, **P < 0.01, ***P < 0.001, ****P < 0.0001). Repre-sentative results of three biological replicates are shown.

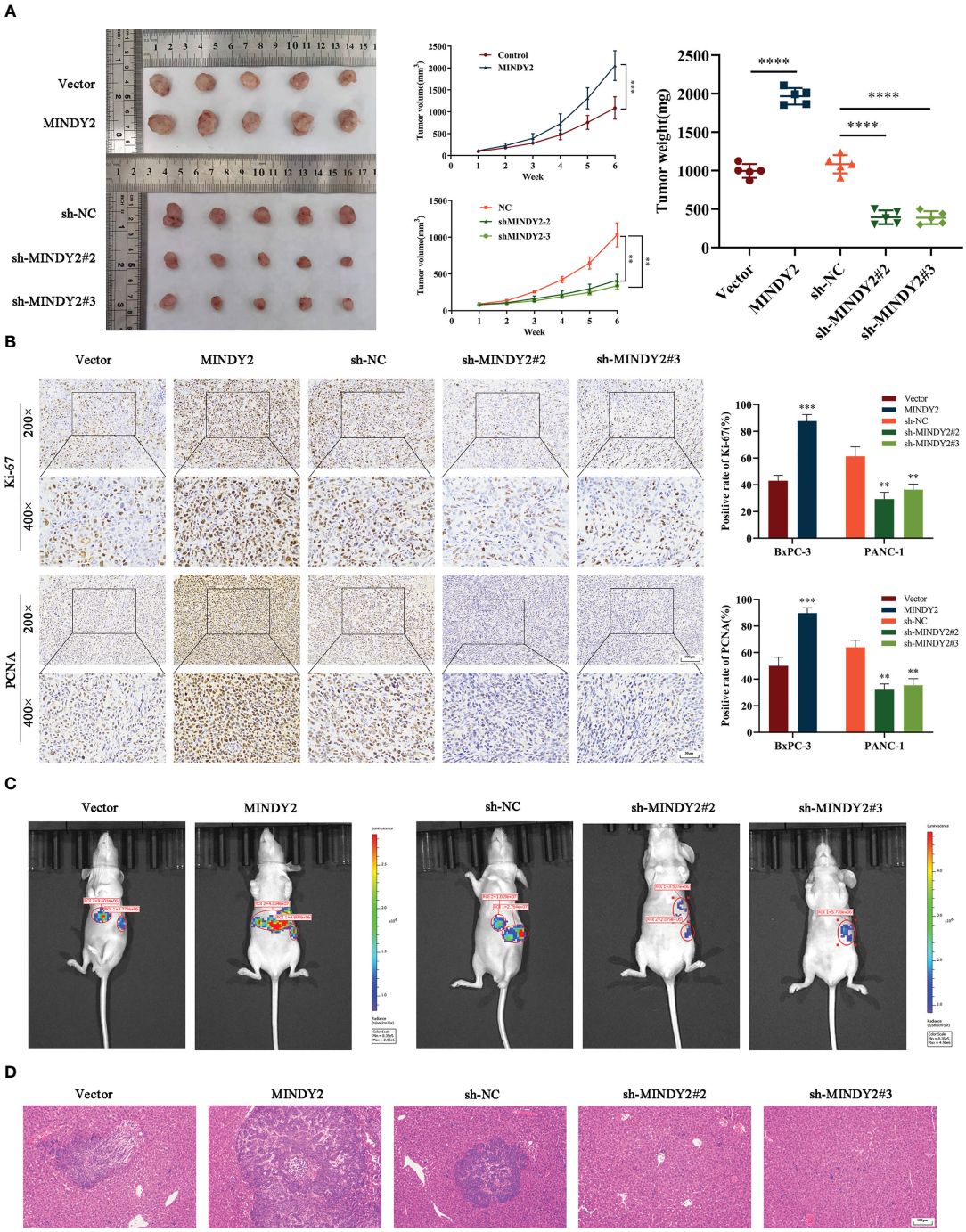

FIGURE 5
MINDY2 promotes PC growth and liver metastasis *in vivo*. **(A)** A nude mouse xenograft model was constructed to observe the effect of MINDY2 on the subcutaneous tumorigenic ability of nude mice. **(B)** IHC observed Ki67 and PCNA expression levels in tumor tissues. **(C)** Construction of a splenic envelope liver metastasis model in order to examine the effect of MIDNY2 on the ability of liver metastasis.**(D)** Representative HE stained images of liver metastases. (*P < 0.05, **P < 0.01, ***P < 0.001, ****P < 0.0001). Five repetitions were set for each group.

in dynamic balance under the coordinated action of E3 ubiquitin ligase and DUB (33). Recent investigations have demonstrated that DUB is crucial for the development of tumors, and MINDY2, a recently discovered deubiquitinating enzyme, has a unique selectivity for cleaving K48-linked polyUb (34). Nevertheless, the biological function of MINDY2 in PC has not been studied.

In this study, we first performed bioinformatics analysis by GEPIA2, GEO, and TCGA databases. We found that MINDY2 was expressed elevated in PC at mRNA and protein levels and correlated with prognostic indicators such as OS, PFS, DSS, T stage, N stage, tumor grading, and tumor stage in patients. In addition, the ROC curve indicated that MINDY2 had a high diagnostic value for PC.

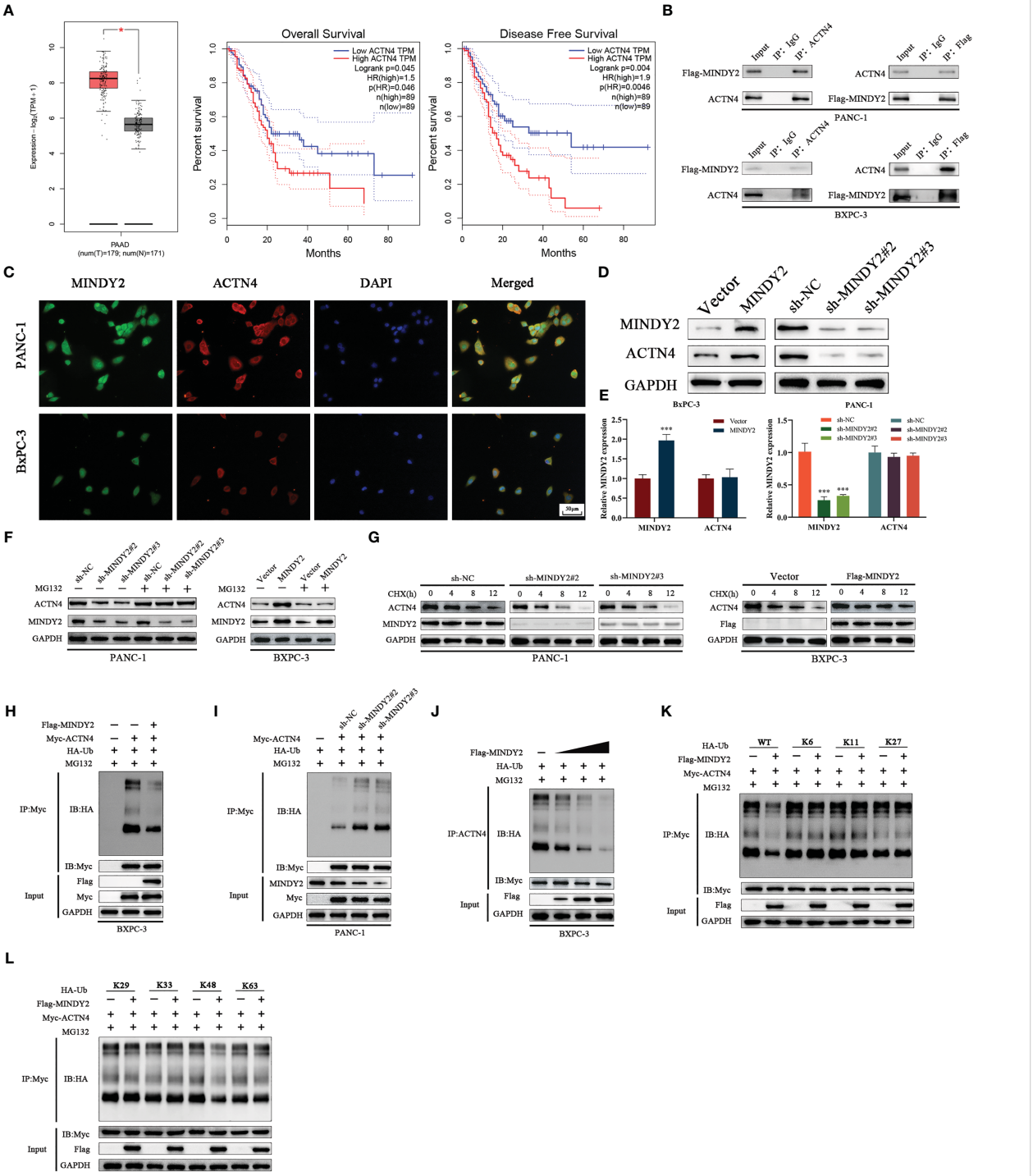

FIGURE 6
MINDY2 interacts with ACTN4 and stabilizes ACTN4 by deubiquitination function. **(A)** The expression level of ACTN4 in PC and the relationship with OS and DFS were analyzed based on the GEPIA2 database. **(B)** Immunoprecipitation experiments to detect the interaction between MINDY2 and ACTN4. **(C)** Immunolocalization assay to detect the effect of MINDY2 and ACTN4 in the cell. **(D, E)** Western blot and QT-PCR were utilized to detect the effect of MINDY2 on the protein and mRNA expression of ACTN4. **(F)** Western blot to determine the impact of MINDY2 on ACTN4 protein levels in cells treated with MG132. **(G)** CHX treatment of cells to observe the effect of MINDY2 on ACTN4 half-life. **(H, I)** Western blot examined the ubiquitination level of ACTN4 in Flag-MINDY2, HA-Ub and Myc-ACTN4 cotransfected BxPC-3 cells. **(J)** MINDY2 regulates the ubiquitination level of ACTN4 in a dose-dependent manner. **(K, L)** Western blot detection of ubiquitination of ACTN4 in Flag-MINDY2, Myc-ACTN4 and HA-Ub mutants (HA-WT, K6, K11, K27, K29, K33, K48 or K63) cotransfected BxPC-3 cells. (*P < 0.05, **P < 0.01, ***P < 0.001). Repre-sentative results of three biological replicates are shown.

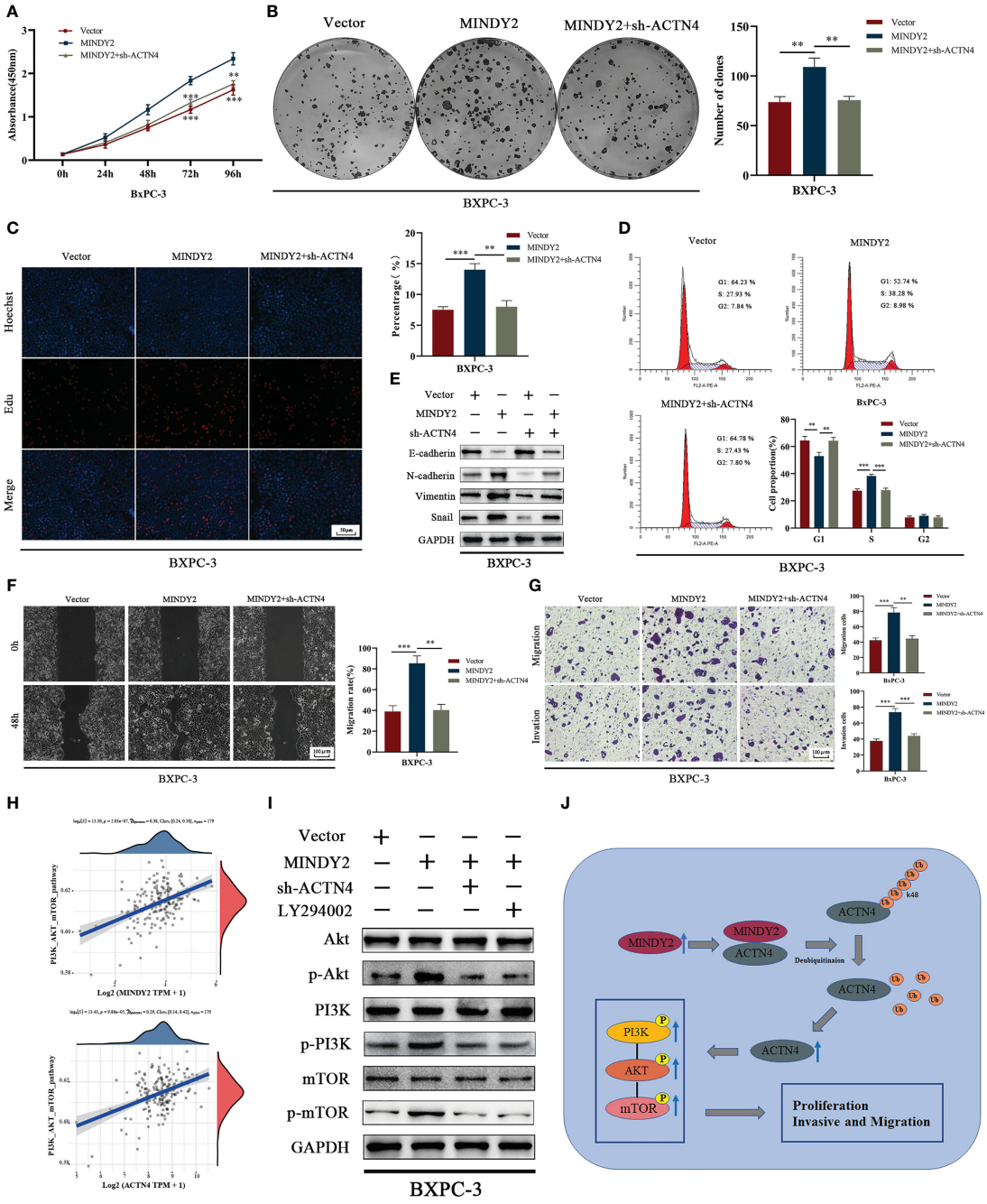

FIGURE 7
MINDY2 stabilizes ACTN4 to activate the PI3K/AKT/mTOR pathway, which promotes cancer development in PC. **(A–D)** CCK8, clonogenic plate assay, Edu, and flow cytometry to detect the effect of silencing ACTN4 on the ability of MINDY2 to promote PC cell proliferation. **(E)** Western blot to detect the effect of silencing ACTN4 on MINDY2 to promote EMT function. **(F, G)** After silencing ACTN4, a wound-healing experiment and a Transwell assay were conducted to determine the effect of MINDY2 on PC cell invasion and migration. **(H)** TCGA database-based analysis of the relationship between MINDY2, ACTN4, and PI3K/AKT/mTOR pathway. **(I)** In PC cells overexpressing MINDY2, Western blot analysis revealed alterations in the total protein levels and phosphorylation levels of PI3K, AKT, and mTOR after silencing ACTN4 or adding the PI3K inhibitor LY294002. **(J)** Mechanistic model of the MINDY2-ACTN4-PI3K/AKT/mTOR pathway axis in PC. (** P < 0.01, *** P < 0.001). Repre-sentative results of three biological replicates are shown.

In recent years, tumor immunotherapy has become a hot spot in the field of tumor treatment research and is also considered one of the most promising treatment methods. Immunotherapy has achieved great success in the treatment of many tumors (35); however, its therapeutic effect in PC is minimal (36). In this study, we analyzed the correlation between MINDY2 in PC and immunity and found that MINDY2 was significantly and positively correlated with infiltration scores of B cells, T cells CD8+, neutrophil, macrophage, and myeloid dendritic cells in PC, and although there was no statistical significance between MINDY2 and T cells CD4+, it can be concluded that the expression level of CD4+ T cells was greater in the MINDY2 high expression group than in the low expression group.

The immune checkpoint acts as an immune system suppressor, which prevents the body's immune system from producing an effective anti-tumor immune response by suppressing immune cell function, hence facilitating the immune evasion of the tumor (37). Therefore, we analyzed the relationship between MINDY2 expression and immune checkpoint-related genes in PC, finding a strong and positive correlation between MINDY2 expression and PDCD1LG2, HAVCR2, CD274, TIGIT, SIGLEC15, and CTLA. In addition, the TIDE algorithm indicated that a higher expression of MINDY2 was correlated with a better response of PC to immune checkpoint inhibitors. Then, we found that MINDY2 was associated with PC tumorigenic factors such as EMT, inflammatory response, and ECM-related genes. Therefore, based on the results of bioinformatics analysis, we have reason to believe that MINDY2 is an oncogene with significant value in PC.

To further elucidate the biological functions of MINDY2 in PC, we collected clinical samples for assay. We found that the expression level of MINDY2 was elevated in PC. *In vitro* experiments, including cloning plate, CCK-8 assay, wound healing assay, and transwell assay, revealed that MINDY2 overexpression was associated with a higher rate of PC proliferation and migration; this process was decreased after the knockdown of MINDY2. We then confirmed this ability of MINDY2 in Western blot assays to detect cell cycle-associated proteins, flow cytometry to detect cell cycle, subcutaneous tumorigenesis in nude mice, and splenic envelope liver metastasis. Activation of EMT leads to changes in cell migration and invasive functions (38, 39). Previous studies also found that the metastasis of PC is associated with EMT (40). Therefore, we detected the EMT-related protein expression and discovered that upregulation of MINDY2 was followed by upregulation of N-cadherin, Snail, and vimentin and downregulation of E-cadherin, while downregulation of MINDY2 reversed this process. Therefore, we speculate that MINDY4 in PC enhances the invasion and migration of PC by inducing EMT.

To further investigate the cancer-promoting mechanism of MINDY2 in PC, we identified ACTN4 as an interacting protein of MINDY2 by immunoprecipitation, mass spectrometry, and immunofluorescence co-localization. Notably, ACTN4 protein levels increased after overexpression of MINDY2, while mRNA levels did not significantly change, suggesting that MINDY2 is not an upstream transcription factor of ACTN4 but regulates the changes of ACTN4 through PTM. Next, we investigated whether MINDY2, a member of the deubiquitinating enzyme family, can modify ACTN4 by deubiquitination. First, we found that the half-life of ACTN4 was significantly prolonged after treating cells overexpressing MINDY2 with CHX, and the half-life of ACTN4 was shortened after silencing MINDY2.

Furthermore, the regulatory effect of MINDY2 on ACTN4 protein disappeared after the addition of MG132-treated cells. Hence, we speculate that MINDY2 stabilizes ACTN4 protein expression through deubiquitination. To further explore the regulatory mechanism, we conducted ubiquitination experiments on BxPC-3 cells after transfecting them with ubiquitin. We discovered that MINDY2 might, by explicitly deleting the K48-linked ubiquitin chain on ACTN4, lower the degree of ubiquitination of ACTN4 and block proteasome-mediated degradation of ACTN4 protein. Therefore, we concluded that MINDY2 stabilizes ACTN4 protein expression through deubiquitination. However, previous research has demonstrated that ACTN4 is crucial for carcinogenesis, metastasis, and EMT (41, 42), so it was unclear whether the pro-carcinogenic role of MINDY2 in PC is related to ACTN4. Therefore, we conducted a series of cell biology tests after silencing ACTN4 in PC cells overexpressing MINDY2 and discovered that silencing ACTN4 reversed the pro-carcinogenic role of MINDY2 in PC. Thus, ACTN4 is essential in the cancer-promoting process of MINDY2. Moreover, bioinformatics analysis found that both MINDY2 and ACTN4 were correlated with the PI3K/AKT/mTOR signaling pathway in PC. In addition, Western blot found that the phosphorylation levels of PI3K, AKT, and mTOR were increased after MINDY2 overexpression without significant changes in protein levels, and the addition of PI3K inhibitor LY294002 reversed this function of MINDY2; a similar effect was obtained after silencing ACTN4. Thus, ACTN4 is essential in the activation of the PI3K/AKT/mTOR signaling pathway by MINDY2.

4 Conclusion

we discovered that MINDY2 stabilizes ACTN4 protein expression through the deubiquitination function in PC, which activates PI3K/AKT/mTOR signaling pathway and promotes PC proliferation, invasion, and migration. Although we still have not cracked the therapeutic code of PC, targeting MINDY2 may provide new hope for the treatment of PC.

5 Materials and methods

5.1 Bioinformatics analysis

Bioinformatics analysis of three datasets (GSE15471, GSE16515, and GSE62165) was obtained in the Gene Expression Omnibus (GEO) database (https://www.ncbi.nlm.nih.gov/geo/); patients undergoing chemotherapy or radiotherapy were excluded. The data were processed using the "Limma" package in Rstudio, and box line plots were plotted by a boxplot. Gene Expression Profiling Interactive Analysis 2 (GEPIA2, https://GEPIA2.cancerpku.cn/35; general) is an analysis of gene expression in cancer and non-cancer tissues based on The Cancer Genome Atlas (TCGA, https://cancergenome.nih.gov) and Genotype-tissue Expression (GTEx). On this website, we obtained box-line plots of expression differences between PC and normal tissue in the GTEx database (43).

The CPTAC (Clinical Proteomic Tumor Analysis Consortium) dataset of UALCAN (https://UALCAN.path.uab.edu/analysisprot.html) was utilized to examine protein expression differences between PC and normal tissues, and a Box line graph was generated. The TCGA database provided the RNAseq data (level 3) for PC and the related clinical data, utilizing the "survminer" package in R software for visualization and the "survivor" package for statistical analysis of survival data. The

analysis of the T-stage and M-stage was visualized using the "ggplot2" package. An immune assessment was performed with the "immunedeconv" package of R software; a reliable R package was used for immune assessment, using the TIMER algorithm to evaluate the connection between MINDY2 expression and six immune cell infiltration scores. "ggplot2" and "pheatmap" were used to analyze and generate heat maps. The relationship between MINDY2 expression and immune checkpoint-related genes in PC was analyzed and visualized by the "ggplot2" package. The TIDE algorithm was used to predict the potential association between MINDY2 and PC response to immunotherapy, plotted and analyzed using the "ggplot2" and "ggpubr" packages of R software (44). The genes found in the associated pathways were then gathered and analyzed using the R software package "GSVA" with the parameter method= "ssgsea." The correlation between the scores of the genes and pathways was examined using Spearman's correlation.

In the TISIDB database (http://cis.hku.hk/TISIDB/), we searched for correlations between MINDY2 expression and tumor grade and cancer stage. This database combines a variety of data sources to investigate interactions between the immune system and tumors (45). Regarding ROC curves, RNAseq and relevant clinical data for PCs were obtained from the TCGA and GTEx databases. Statistical analysis and visualization were performed with R v4.2.1 software (analysis with the "pROC" package and data visualization with the "ggplot2" package) (46). The horizontal and vertical coordinates are the false positive rate (FPR) and the actual positive rate (TPR), respectively (the ROC curve's area under the curve ranges from 0.5 to 1, and diagnostic accuracy increases when the AUC is close to 1. When the AUC is between 0.5 and 0.7, accuracy is poor; when it is between 0.7 and 0.9, accuracy is moderate; and when it is beyond 0.9, accuracy is high).

5.2 Human tissue samples

Twenty cases of fresh PC tissues and adjacent normal tissues were acquired from the Affiliated Hospital of Guizhou Medical University. No patients received preoperative chemotherapy, radiotherapy, biological treatment, or Chinese medicine treatment. Also, 180-point human PC tissue microarrays were obtained from Shanghai Outdo Biotech (China).

This work was authorized by the Human Research Ethics Committee of the Affiliated Hospital of Guizhou Medical University. In addition, all patient signed an informed consent form.

5.3 Cell culture and transfection

AsPC-1, BxPC-3, Capan-2, Mia PaCa-2, PANC-1, and SW1990 cells were obtained from American Type Culture Collection (ATCC; USA), AsPC-1, BxPC-3, Capan-2, SW1990, and HPDE cell lines were cultured in RPMI 1640 (Gibco, USA), while Mia PaCa-2 and PANC-1 cell lines were grown in DMEM (Gibco, USA). Both medium were supplemented with 10%FBS and 1%Penicillin/Streptomycin. All cell lines were cultured in a humidified atmosphere containing 5%CO2/95% air at 37°C. All the cell lines had been authenticated through STR profiling and confirmed to be mycoplasma-free.

Lipofectamine3000 was purchased from Invitrogen (Invitrogen, USA); 3 small interfering RNAs (siRNA) (st-h-MINDY2-1 GCACAAGCCTCTCCATCAA, st-h-MINDY2-2 GCTGAGCAGTTTCTAAATA, and st-h-MINDY2-3 GTTCGAGTGTTTGAATATA) were provided by RiboBio (China). GeneChem (China) was responsible for designing and manufacturing lentivirus carrying negative control, MINDY2 overexpression vector (Ubi-MCS-3FLAG-SV40-puromycin), MINDY2-encoding short hairpin RNA (shRNA)(hU6-MCS-CMV-Puromycin), and shRNA targeting ACTN4(hU6-MCS-CMV-Puromycin). The directions were strictly followed during every infection or transfection step.

5.4 RNA preparation and quantitative real-time PCR

RNA was extracted from PC cell lines and PC tissue using Trizol reagent (Invitrogen, CA, USA) according to the manufacturer's instructions. cDNA was generated by reverse transcription and used in subsequent experiments. Amplification of the generated cDNA was detected using TB Green® Premix Ex TaqTM (Takara, Japan) on a CFX96TM real-time system (Bio-Rad, California, USA). The primers used in the study were: MINDY2, sense 5′- CAGGAG GCATTGCTGATGAT-3′, antisense 3′-GAAGCCTGGGGCTCA TTT-5′; ACTN4, sense 5′-CACAGTCCCATTCCTCCAC-3′, antisense 3′-GCCAACCCACAAAGAGAGA-5′. GAPDH (glyceraldehyde e-3-phosphate dehydrogenase), sense 5′-CAGGAGGCATTGCTGATGAT-3′, antisense 3′-GAAGCCTG GGGCTCATTT-5′, with GAPDH as the endogenous control, and experimental The results were calculated using the 2-ΔΔCt method.

5.5 Antibodies and chemicals

Anti-FAM63B (1:500; ThermoFisher, # 62318), Anti-ACTN4 (1:5,000; Proteintech, #66628), Anti-GHPDH (1:1,000; Proteintech, #60004), anti-E-calmodulin (1:1,000; Proteintech, #20874), anti-N-calmodulin (1:1000; Proteintech, #22018), anti-wavoprotein (1:1,000; Proteintech, #10366), anti-snail (1:1000; Proteintech, #13099), anti-cyclin D1 (1:1,000; Cell Signaling Technology [CST], #55506), anti-cyclin E1 (1:1,000; CST, #4136), anti-CDK 2 (1:1,000; CST, #2561), anti-CDK4 (1:1,000; CST, #12790), anti-AKT (1:1,000; CST, #4691), anti-p-AKT (1:2,000; CST, #4060), anti-PI3K (1:1,000; CST, #4249), anti-p-PI3K (1:1,000; CST, #17366), anti-mTOR (1:1,000; CST, #2972), anti-p-mTOR (1:1000; CST, #2971), HRP-goat anti-rabbit IgG (Boster, #BA1055), HRP-goat anti-mouse IgG (Boster, #BA1050), Anti-PCNA (1:1,000; Proteintech, # 10205), Anti-Ki67 (1:1,000; Proteintech, #28074), HA-Ubiquitin plasmid (Sangon Biotech, China), CHX (Melun Biologics, China), MG132 (MCE, USA), MINDY2 small interfering RNA (RiboBio, China), protease inhibitor (Boster

Biological Technology, China), and enhanced chemiluminescence reagent (Proteintech, #7003).

5.6 Western blot

Cells were prepared and lysed with protease inhibitor-spiked RIPA buffer (Pierce). Proteins (concentration determined using a BCA assay kit (Beyotime Biotechnology)) were denatured and separated by SDS-PAGE and transferred to polyvinylidene fluoride membranes (Millipore, USA) and incubated with primary antibody at 4°C overnight and then secondary antibody at room temperature for 2h. Enhanced chemiluminescence reagents were used to detect the immunoreactive signal.

5.7 Cell viability assay and Colony-formation assay

At the given time points, cells were tested with Cell Counting Kit-8 (Dojindo, Japan), and absorbance at 450 nm was recorded. Cells were cultivated at 5000 cells per well in 96-well plates.

Cells were inoculated in six-well plates at 1 × 103 cells/well and cultured and cultivated for 14 days. Cells were then fixed in paraformaldehyde (4%) and stained with crystal violet (0.25 percent). The colonies were tallied and photographed.

5.8 Flow cytometry

PC cells were inoculated into six-well plates for 24 hours, extracted and washed with PBS, incubated for 30 minutes at room temperature with DNA staining and permeabilization solution (Cell Cycle Staining Kit, MULTI SCIENCES, China), and then protected from light. The analysis was conducted using Summit 5.2 (Beckman Coulter, USA).

5.9 Wound healing assay

Cells were inoculated in 6-well plates. When cell confluence reached 90-100%, the cell layer was scratched using the tip of a 200μl pipette. Cells were then incubated in a medium without FBS. The remaining distance at different time points was measured.

5.10 Transwell migration and Matrigel invasion assays

The Transwell device (CoStar, USA) was prepared. Then, 1×104 cells in 200 ul of FBS-free medium were plated in the upper chamber of the transwell (with or without Matrigel gel), while 800 μl of medium (containing 10% FBS) was added to the lower chamber. Cells were then incubated at 37°C in an incubator containing 5% CO2 for 24-36 hours. Next, the upper chamber was washed with PBS, and the remaining cells from the upper chamber were removed with a cotton swab. Cells in the lower chamber were fixed, tread with methanol, stained with Giemsa, dried, and counted.

5.11 Co-immunoprecipitation

Cells were lysed with cell lysate solution (NP-40: broad-spectrum protease inhibitor: broad-spectrum phosphatase inhibitor: PMSF = 100:2:2:1) for 30 min, centrifuged, pre-purified, and slowly shaken overnight at 4°C with the corresponding antibody. Samples were then incubated with proteinA+G, recovered the magnetic bead coupling complex wash, mixed with 2× loading buffer, and boiled. Next, subsequent Western blotting experiments were carried out.

5.12 Ubiquitination assay

The ubiquitinated plasmid (purchased from Sangon Biotech) was used to transfect the cells by Lipo Lipofectamine3000 following the manufacturer's instructions. Cells were treated with the proteasome inhibitor MG132 for 9 hours and 2 days later. Then, they were removed in preparation for IP and WB assays.

5.13 Animal study

Female BALB/c nude mice, aged 6-7 weeks, were obtained from Collective Pharmachem. All the animals were housed in an environment with a temperature of 22 ± 1 °C, relative humidity of 50 ± 1%, and a light/dark cycle of 12/12 hr. All animal studies (including the mice euthanasia procedure) were done in compliance with the regulations and guidelines of Guizhou Medical University's institutional animal care and conducted according to the AAALAC and the IACUC guidelines.

Mice received a subcutaneous injection of 2x106 cells (BxPC-3 and PANC-1) into the right axilla and were then randomly divided into 5 groups (5 mice/group). Tumor volume was measured periodically using vernier calipers, computed as (length × width2)/2. After five weeks, nude mice were executed and tumors were extracted, weighed, photographed, and sectioned for additional research. Liver metastasis model construction: Nude mice were randomly divided into 5 groups (n=5), BxPC-3 and PANC-1 were adjusted to 1×106 cell density according to the corresponding groups, and then 200 μL of cell suspension was injected into the spleen of nude mice, after 6 weeks, the nude mice were observed with bioluminescence and photographed the liver metastases under the small animal in the Vivo imaging system (IVIS® Lumina III). After the photographs were taken, the nude mice were sacrificed, and the liver was taken for HE staining.

5.14 Immunohistochemistry

Fresh tumor tissue was fixed and kept at 4°C overnight, paraffin-embedded, and sectioned. It was then incubated with antibody overnight at 4°C, samples were treated with AEC chromogenic substrate, followed by hematoxylin re-staining and microscopic observation. The results were evaluated blindly by two independent pathologists.

5.15 Statistical analysis

Continuous data are expressed as mean ± standard deviation. Group pairs and multiple groups were compared using a two-tailed Student t-test and one-way ANOVA. Data analysis was carried out using GraphPad Prism 8.0. Image examination was done using ImageJ V1.46. A p-value <0.05 was considered to be statistically significant.

Data availability statement

The datasets presented in this study can be found in online repositories. The names of the repository/repositories and accession number(s) can be found in the article/ Supplementary Material.

Ethics statement

The studies involving human participants were reviewed and approved by The Ethics Committee of the Affiliated Hospital of Guizhou Medical University. The patients/participants provided their written informed consent to participate in this study. The animal study was reviewed and approved by The Animal Care Welfare Committee of Guizhou Medical University. Written informed consent was obtained from the individual(s) for the publication of any potentially identifiable images or data included in this article.

Author contributions

PL, SL, and CZ designed the experiments and performed most of the experiments; YoL , YiL analyzed data and helped with mice model construction; XF, XW, and JH revised this manuscript, XW and YP conceptualized the research and directed the study. All authors read and approved the final manuscript.

Funding

We thank the Department of Hepatobiliary Surgery, Affiliated Hospital of Guizhou Medical University (Guiyang, China) for technical support in this study. The National Natural Science Foundation of China sponsored this research (NO: 81960431; NO:81960535).

Conflict of interest

The authors declare that the research was conducted in the absence of any commercial or financial relationships that could be construed as a potential conflict of interest.

Publisher's note

All claims expressed in this article are solely those of the authors and do not necessarily represent those of their affiliated organizations, or those of the publisher, the editors and the reviewers. Any product that may be evaluated in this article, or claim that may be made by its manufacturer, is not guaranteed or endorsed by the publisher.

Supplementary material

The Supplementary Material for this article can be found online at: https://www.frontiersin.org/articles/10.3389/fonc.2023.1169833/full#supplementary-material.

References

1. Siegel RL, Miller KD, Fuchs HE, Jemal A. Cancer statistics, 2022. *CA: Cancer J Clin* (2022) 72(1):7–33. doi: 10.3322/caac.21708

2. Neoptolemos JP, Springfeld C, Hackert T. A review of pancreatic cancer. *Jama* (2021) 326(23):2436. doi: 10.1001/jama.2021.20065

3. Mizrahi JD, Surana R, Valle JW, Shroff RT. Pancreatic cancer. *Lancet (London England).* (2020) 395(10242):2008–20. doi: 10.1016/S0140-6736(20)30974-0

4. Cabasag CJ, Ferlay J, Laversanne M, Vignat J, Weber A, Soerjomataram I, et al. Pancreatic cancer: an increasing global public health concern. *Gut* (2022) 71(8):1686–7. doi: 10.1136/gutjnl-2021-326311

5. Jain T, Dudeja V. The war against pancreatic cancer in 2020 - advances on all fronts. *Nat Rev Gastroenterol Hepatol* (2021) 18(2):99–100. doi: 10.1038/s41575-020-00410-4

6. Wu X, Luo Q, Zhao P, Chang W, Wang Y, Shu T, et al. JOSD1 inhibits mitochondrial apoptotic signalling to drive acquired chemoresistance in gynaecological cancer by stabilizing MCL1. *Cell Death Differentiation* (2020) 27 (1):55–70. doi: 10.1038/s41418-019-0339-0

7. Lai KP, Chen J, Tse WKF. Role of deubiquitinases in human cancers: potential targeted therapy. *Int J Mol Sci* (2020) 21(7):2548. doi: 10.3390/ijms21072548

8. Han S, Wang R, Zhang Y, Li X, Gan Y, Gao F, et al. The role of ubiquitination and deubiquitination in tumor invasion and metastasis. *Int J Biol Sci* (2022) 18(6):2292–303. doi: 10.7150/ijbs.69411

9. Lee D, Hong JH. Physiological overview of the potential link between the UPS and Ca(2+) signaling. *Antioxidants (Basel Switzerland).* (2022) 11(5):997. doi: 10.3390/antiox11050997

10. Deng L, Meng T, Chen L, Wei W, Wang P. The role of ubiquitination in tumorigenesis and targeted drug discovery. *Signal Transduction Targeted Ther* (2020) 5 (1):11. doi: 10.1038/s41392-020-0107-0

11. Bonacci T, Emanuele MJ. Dissenting degradation: deubiquitinases in cell cycle and cancer. *Semin Cancer Biol* (2020) 67(Pt 2):145–58. doi: 10.1016/j.semcancer.2020.03.008

12. Cheng J, Guo J, North BJ, Wang B, Cui CP, Li H, et al. Functional analysis of deubiquitylating enzymes in tumorigenesis and development. *Biochim Biophys Acta Rev Cancer* (2019) 1872(2):188312. doi: 10.1016/j.bbcan.2019.188312

13. Haq S, Suresh B, Ramakrishna S. Deubiquitylating enzymes as cancer stem cell therapeutics. *Biochim Biophys Acta Rev Cancer*. (2018) 1869(1):1–10. doi: 10.1016/j.bbcan.2017.10.004

14. Li F, Hu Q, He T, Xu J, Yi Y, Xie S, et al. The deubiquitinase USP4 stabilizes Twist1 protein to promote lung cancer cell stemness. *Cancers* (2020) 12(6):1582. doi: 10.3390/cancers12061582

15. Wang Y, Zhou L, Lu J, Jiang B, Liu C, Guo J. USP4 function and multifaceted roles in cancer: a possible and potential therapeutic target. *Cancer Cell Int* (2020) 20:298. doi: 10.1186/s12935-020-01391-9

16. Tang J, Luo Y, Long G, Zhou L. MINDY1 promotes breast cancer cell proliferation by stabilizing estrogen receptor α. *Cell Death Dis* (2021) 12(10):937. doi: 10.1038/s41419-021-04244-z

17. Choi YE, Madhi H, Kim H, Lee JS, Kim MH, Kim YN, et al. FAM188B expression is critical for cell growth *via* FOXM1 regulation in lung cancer. *Biomedicines* (2020) 8(11):465. doi: 10.3390/biomedicines8110465

18. Jang EJ, Sung JY, Yoo HE, Jang H, Shim J, Oh ES, et al. FAM188B downregulation sensitizes lung cancer cells to anoikis *via* EGFR downregulation and inhibits tumor metastasis *In vivo*. *Cancers* (2021) 13(2):247. doi: 10.3390/cancers13020247

19. Luo Y, Zhou J, Tang J, Zhou F, He Z, Liu T, et al. MINDY1 promotes bladder cancer progression by stabilizing YAP. *Cancer Cell Int* (2021) 21(1):395. doi: 10.1186/s12935-021-02095-4

20. Liu B, Ruan J, Chen M, Li Z, Manjengwa G, Schlüter D, et al. Deubiquitinating enzymes (DUBs): decipher underlying basis of neurodegenerative diseases. *Mol Psychiatry* (2022) 27(1):259–68. doi: 10.1038/s41380-021-01233-8

21. Harrigan JA, Jacq X, Martin NM, Jackson SP. Deubiquitylating enzymes and drug discovery: emerging opportunities. *Nat Rev Drug Discov* (2018) 17(1):57–78. doi: 10.1038/nrd.2017.152

22. Hermanns T, Pichlo C, Woiwode I, Klopffleisch K, Witting KF, Ovaa H, et al. A family of unconventional deubiquitinases with modular chain specificity determinants. *Nat Commun* (2018) 9(1):799. doi: 10.1038/s41467-018-03148-5

23. Abdul Rehman SA, Armstrong LA, Lange SM, Kristariyanto YA, Gräwert TW, Knebel A, et al. Mechanism of activation and regulation of deubiquitinase activity in MINDY1 and MINDY2. *Mol Cell* (2021) 81(20):4176–90.e6. doi: 10.1016/j.molcel.2021.08.024

24. Abdul Rehman SA, Kristariyanto YA, Choi SY, Nkosi PJ, Weidlich S, Labib K, et al. MINDY-1 is a member of an evolutionarily conserved and structurally distinct new family of deubiquitinating enzymes. *Mol Cell* (2016) 63(1):146–55. doi: 10.1016/j.molcel.2016.05.009

25. Mortazavi M, Moosavi F, Martini M, Giovannetti E, Firuzi O. Prospects of targeting PI3K/AKT/mTOR pathway in pancreatic cancer. *Crit Rev Oncol/Hematol* (2022) 176:103749. doi: 10.1016/j.critrevonc.2022.103749

26. Mehra S, Deshpande N, Nagathihalli N. Targeting PI3K pathway in pancreatic ductal adenocarcinoma: rationale and progress. *Cancers* (2021) 13(17):4434. doi: 10.3390/cancers13174434

27. Guo X, Zhou Q, Su D, Luo Y, Fu Z, Huang L, et al. Circular RNA circBFAR promotes the progression of pancreatic ductal adenocarcinoma *via* the miR-34b-5p/MET/Akt axis. *Mol Cancer* (2020) 19(1):83. doi: 10.1186/s12943-020-01196-4

28. Singhi AD, Koay EJ, Chari ST, Maitra A. Early detection of pancreatic cancer: opportunities and challenges. *Gastroenterology* (2019) 156(7):2024–40. doi: 10.1053/j.gastro.2019.01.259

29. Zhu MX, Wei CY, Zhang PF, Gao DM, Chen J, Zhao Y, et al. Correction to: elevated TRIP13 drives the AKT/mTOR pathway to induce the progression of hepatocellular carcinoma *via* interacting with ACTN4. *J Exp Clin Cancer Res CR*. (2019) 38(1):443. doi: 10.1186/s13046-019-1454-y

30. Liao Q, Li R, Zhou R, Pan Z, Xu L, Ding Y, et al. LIM kinase 1 interacts with myosin-9 and alpha-actinin-4 and promotes colorectal cancer progression. *Br J Cancer*. (2017) 117(4):563–71. doi: 10.1038/bjc.2017.193

31. Liao TL, Wu CY, Su WC, Jeng KS, Lai MM. Ubiquitination and deubiquitination of NP protein regulates influenza a virus RNA replication. *EMBO J* (2010) 29(22):3879–90. doi: 10.1038/emboj.2010.250

32. Zhang X, Kuramitsu Y, Ma A, Zhang H, Nakamura K. Endoplasmic reticulium protein profiling of heat-stressed jurkat cells by one dimensional electrophoresis and liquid chromatography tandem mass spectrometry. *Cytotechnology* (2016) 68(4):1103–13. doi: 10.1007/s10616-015-9867-8

33. Wang B, Xie M, Li R, Owonikoko TK, Ramalingam SS, Khuri FR, et al. Role of Ku70 in deubiquitination of mcl-1 and suppression of apoptosis. *Cell Death Differentiation* (2014) 21(7):1160–9. doi: 10.1038/cdd.2014.42

34. Maurer T, Wertz IE. Length matters: MINDY is a new deubiquitinase family that preferentially cleaves long polyubiquitin chains. *Mol Cell* (2016) 63(1):4–6. doi: 10.1016/j.molcel.2016.06.027

35. Liu Z, Zhou Z, Dang Q, Xu H, Lv J, Li H, et al. Immunosuppression in tumor immune microenvironment and its optimization from CAR-T cell therapy. *Theranostics* (2022) 12(14):6273–90. doi: 10.7150/thno.76854

36. Li X, Gulati M, Larson AC, Solheim JC, Jain M, Kumar S, et al. Immune checkpoint blockade in pancreatic cancer: trudging through the immune desert. *Semin Cancer Biol* (2022) 86(Pt 2):14–27. doi: 10.1016/j.semcancer.2022.08.009

37. Pathania AS, Prathipati P, Murakonda SP, Murakonda AB, Srivastava AAvadhesh, et al. Immune checkpoint molecules in neuroblastoma: a clinical perspective. *Semin Cancer Biol* (2022) 86(Pt 2):247–58. doi: 10.1016/j.semcancer.2022.06.013

38. Yang J, Antin P, Berx G, Blanpain C, Brabletz T, Bronner M, et al. Guidelines and definitions for research on epithelial-mesenchymal transition. *Nat Rev Mol Cell Biol* (2020) 21(6):341–52. doi: 10.1038/s41580-020-0237-9

39. Derynck R, Weinberg RA. EMT and cancer: more than meets the eye. *Dev Cell* (2019) 49(3):313–6. doi: 10.1016/j.devcel.2019.04.026

40. Rodriguez-Aznar E, Wiesmüller L, Sainz BJr., Hermann PC. EMT and stemness-key players in pancreatic cancer stem cells. *Cancers* (2019) 11(8):1136. doi: 10.3390/cancers11081136

41. Tentler D, Lomert E, Novitskaya K, Barlev NA. Role of ACTN4 in tumorigenesis, metastasis, and EMT. *Cells* (2019) 8(11):1427. doi: 10.3390/cells8111427

42. Thomas DG, Robinson DN. The fifth sense: mechanosensory regulation of alpha-actinin-4 and its relevance for cancer metastasis. *Semin Cell Dev Biol* (2017) 71:68–74. doi: 10.1016/j.semcdb.2017.05.024

43. Tang Z, Kang B, Li C, Chen T, Zhang Z. GEPIA2: an enhanced web server for large-scale expression profiling and interactive analysis. *Nucleic Acids Res* (2019) 47 (W1):W556–w60. doi: 10.1093/nar/gkz430

44. Jiang P, Gu S, Pan D, Fu J, Sahu A, Hu X, et al. Signatures of T cell dysfunction and exclusion predict cancer immunotherapy response. *Nat Med* (2018) 24(10):1550–8. doi: 10.1038/s41591-018-0136-1

45. Ru B, Wong CN, Tong Y, Zhong JY, Zhong SSW, Wu WC, et al. TISIDB: an integrated repository portal for tumor-immune system interactions. *Bioinf (Oxf Eng)* (2019) 35(20):4200–2. doi: 10.1093/bioinformatics/btz210

46. Vivian J, Rao AA, Nothaft FA, Ketchum C, Armstrong J, Novak A, et al. Toil enables reproducible, open source, big biomedical data analyses. *Nat Biotechnol* (2017) 35(4):314–316. doi: 10.1038/nbt.3772

frontiers | Frontiers in Oncology

TYPE Mini Review
PUBLISHED 19 September 2023
DOI 10.3389/fonc.2023.1240115

OPEN ACCESS

EDITED BY
Arun Kumar Trivedi,
Central Drug Research Institute (CSIR), India

REVIEWED BY
Linhui Zhai,
Chinese Academy of Sciences (CAS), China

*CORRESPONDENCE
Hashnu Dutta
hashnudutta@gmail.com
Nishant Jain
nishant.iict@gov.in

RECEIVED 14 June 2023
ACCEPTED 21 August 2023
PUBLISHED 19 September 2023

CITATION
Dutta H and Jain N (2023) Post-translational modifications and their implications in cancer.
Front. Oncol. 13:1240115.
doi: 10.3389/fonc.2023.1240115

Post-translational modifications and their implications in cancer

Hashnu Dutta[1,2]* and Nishant Jain[1,2]*

[1]Department of Applied Biology, CSIR-Indian Institute of Chemical Technology, Hyderabad, India, [2]Academy of Scientific and Innovative Research (AcSIR), Ghaziabad, India

Post-translational modifications (PTMs) are crucial regulatory mechanisms that alter the properties of a protein by covalently attaching a modified chemical group to some of its amino acid residues. PTMs modulate essential physiological processes such as signal transduction, metabolism, protein localization, and turnover and have clinical relevance in cancer and age-related pathologies. Majority of proteins undergo post-translational modifications, irrespective of their occurrence in or after protein biosynthesis. Post-translational modifications link to amino acid termini or side chains, causing the protein backbone to get cleaved, spliced, or cyclized, to name a few. These chemical modifications expand the diversity of the proteome and regulate protein activity, structure, locations, functions, and protein-protein interactions (PPIs). This ability to modify the physical and chemical properties and functions of proteins render PTMs vital. To date, over 200 different protein modifications have been reported, owing to advanced detection technologies. Some of these modifications include phosphorylation, glycosylation, methylation, acetylation, and ubiquitination. Here, we discuss about the existing as well as some novel post-translational protein modifications, with their implications in aberrant states, which will help us better understand the modified sites in different proteins and the effect of PTMs on protein functions in core biological processes and progression in cancer.

KEYWORDS

post-translational modifications, protein structure, cancer, proteome diversity, protein function, covalent bond

Introduction

Post-translational modifications are typical biochemical reactions that covalently bind (poly)peptide chains, chemical moieties, lipids, or carbohydrates to amino acids of the target molecule during or after its translation (1). PTMs occur in majority of known proteins, and nearly all amino acids can be changed by one or more of these reactions. The modified proteins acquire uncommon amino acids that can have a significant impact on their structure and function (2). Akin to noncovalent binding, PTM processes may occur at the functional site (orthosteric PTMs) namely sumoylation, or at a distance (allosteric PTMs) namely, ubiquitination and phosphorylation (1).

Post-translational modifications diversify the proteome by altering protein structure, location, interactions, and function and their regulation, thus affecting all facets of cell

biology (Figure 1) (3). Currently, the UniProt database contains over 400 distinct PTMs that are covalently bonded to amino acid side chains. PTMs range in size from moderate alterations such as methylation to high-molecular-weight polyprotein chains such as polyubiquitination (4, 5).

Protein modifications are commonly catalyzed by enzymes, although a number of reports have stated that some PTMs may happen spontaneous. Non-enzymatic PTMs (that occur spontaneously) can be divided into two subclasses: irreversible and reversible non-enzymatic PTMs, based on their stability and physiological shelf-life. Non-enzymatic irreversible PTMs include stress-induced modifications, such as oxidative and metabolic stresses, that cannot be eliminated by spontaneous dissociation or enzyme-catalyzed mechanisms. These irreversible PTMs occur in a wide spectrum of amino acids, especially when basal levels of reactive oxygen species (ROS) rise and/or when metabolite concentrations approach a physiological imbalance, during aging or in diseases such as cancer, diabetes, and Alzheimer's disease (6–9). On the contrary, non-enzymatic reversible PTMs are physiologically reversible. The dissociation of these reversible PTMs can be enzyme catalyzed, or from an innate chemical instability, which is involved in various metabolic and signaling pathways.

Eukaryotes exploit post-translational modifications to modulate protein stability, function, subcellular localization, and different protein–protein interactions (10–13). PTMs control protein function of diverse physiological and pathological cellular events. Furthermore, PTMs have been reported to be linked to neurodegenerative disorders, brain tumors, breast neoplasias, and hematological disorders (14, 15). Numerous other forms of PTMs can occur due to metabolic stress. For instance, disruption of Krebs cycle enzymes might increase the fumarate levels followed by succination of cysteine residues by Michael addition reaction (16, 17). Higher succination rates can also be caused by cancer-related mutations influencing fumarate metabolizing proteins, and hence can function as a cancer biomarker (18, 19).

Despite conventional PTMs such as phosphorylation, acetylation, ubiquitination, and methylation that have been extensively studied, the emergence of numerous new

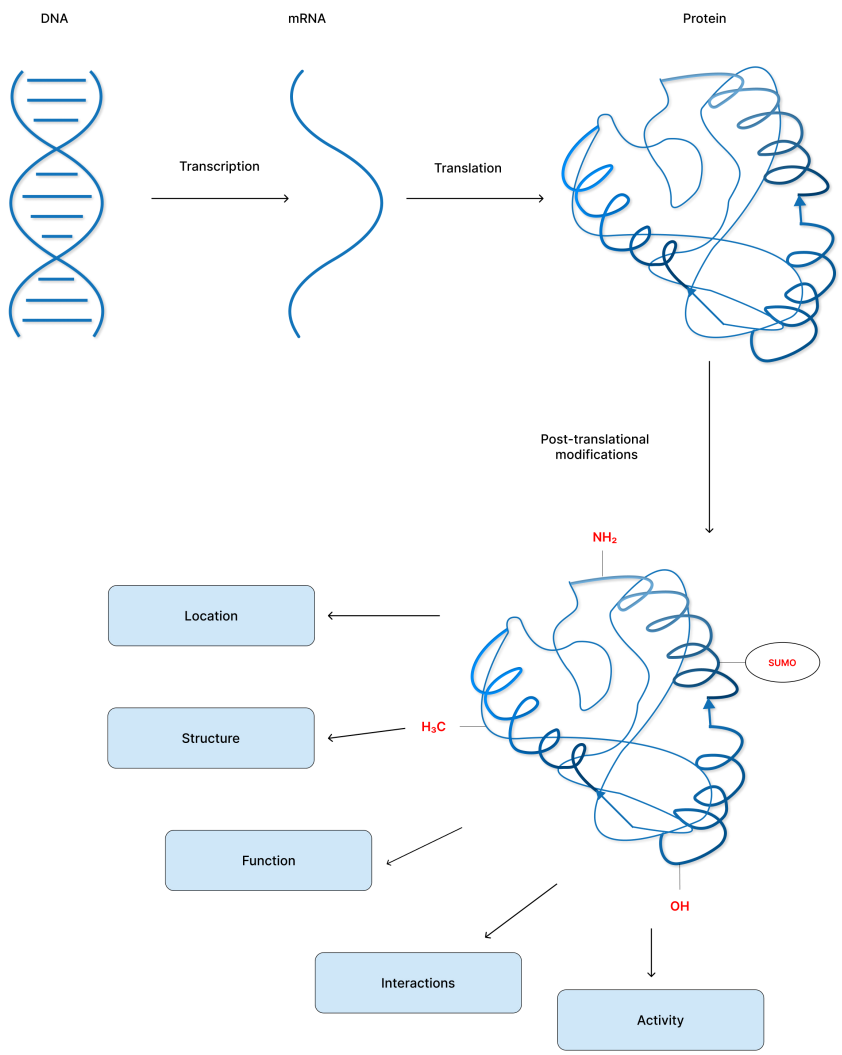

FIGURE 1
Post-translational modification of proteins increase proteome diversity to perform the core physiological processes.

modifications, such as hydroxybutyrylation, lactylation, and succinylation, add another dimension to protein regulation, shedding light to many yet-to-be-discovered modifications and their application possibilities per se (20). In this mini-review, we outline a brief overview of both classical (which have been identified within the past few decades) and the novel (newly discovered) post-translational modifications, as well as the important roles these PTMs offer in regulating human cancer hallmarks using relevant examples. Also, the different PTMs that are discussed here have been summarized highlighting the reactions involved and the enzymes catalyzing it (Table 1).

Classical post-translational modifications

Phosphorylation

Phosphorylation is the most researched and one of the essential types of PTM, which frequently occurs either in nucleus or in cytosol on target proteins in all organisms (21, 22). The kinase enzyme catalyzing the phosphorylation reaction transfers a phosphate group from adenosine triphosphate (ATP) to the receptor residues, thereby altering the protein function in either

TABLE 1 An overview of different post-translational modifications and the enzymes catalyzing these reactions.

Type of Modification	Description	Enzyme(s) involved
Phosphorylation	Addition of a phosphate group to a molecule or an ion	Kinases
Acetylation	Covalent transfer of an acetyl group from acetyl-CoA to the ε-amino group of lysine residues within the target substrates	Acetyltransferases
Glycosylation	Saccharides form glycosidic bridges with other saccharides, proteins, or lipids enzymatically	Glycosyltransferases
Methylation	Addition of a methyl group at both their N- and C-termini, as well as on side chain nitrogen atoms of lysine and arginine residues	Methyltransferases, PRMTs (Lys Methyltransferases and/or Arg Methyltransferases)
Sumoylation	Covalently attachment of small ubiquitin-like modifiers (SUMO) in the ϵ-amino group of lysine residues in the target protein	An E1 activating enzyme, an E2 conjugating enzyme and, an E3 SUMO ligase (most cases)
Ubiquitination	Covalently attachment of Ubiquitin (Ub) to protein substrates	Ub-activating (E1), Ub-conjugation (E2), and Ub-ligase (E3) enzymes
Neddylation	Reversible covalent attachment of NEDD8 to a lysine residue of the protein substrate	NEDD8-activating E1, NEDD8-conjugation E2, and substrate-specific NEDD8-E3 ligase enzymes
S-Nitrosylation	Covalent modification in which a nitric oxide (NO) molecule is coupled to the reactive thiol of an adjacent cysteine residue to generate S-nitrosothiol (SNO)	Nitric oxide (NO) synthases, S-nitrosothiol (SNO) synthases and transnitrosylases
Succination	Stable reaction between fumarate and the thiol groups on cysteine residues to produce S-(2-succino)cysteine (2SC) forming a thioether linkage	Fumarase/Fumarate hydratase (FH)
Prenylation	Attachment of either a 15-carbon farnesyl or a 20-carbon geranylgeranyl isoprenoid lipid to the cysteine residues	Farnesyltransferase (FTase) or Geranylgeranyltransferase I (GGTase I)
Palmitoylation	Reversible lipid modification by which palmitate is added via a thioester linkage to a cysteine residue	Palmitoyl acyltransferases (PATs)
Succinylation	Transfer of a succinyl group to a lysine residue via enzymatic or non-enzymatic reactions, forming an ester, thioester or amide bond	Succinate dehydrogenase (SDH)
Citrullination	Deamination of a positively charged arginine into the electrically neutral citrulline, when subjected to high Ca^{2+} concentration	Peptidyl-arginine deiminase (PAD)
Crotonylation	Evolutionary conserved, epigenetic reversible modification (short chain lysine acylations) on histone and non-histone proteins	Crotonyltransferases (writers) and Decrotonylases (erasers)
S-Glutathionylation	A reversible reaction in which cysteine residue of glutathione forms a disulphide bond with the -SH (thiol) group of a target cysteine in the protein, oxidising it	Glutaredoxins (GRX), thiol oxidoreductases
Monoaminylation	Biogenic monoamines are covalently linked to glutamine residues within certain protein substrates via transamidation reaction	Transglutaminase 2
Propionylation	Covalent attachment of the propionyl group to the lysine residues of the target protein	Propionyl-CoA Carboxylase (PCC); also, p300 and CREB-binding protein (CBP)
Butyrylation	Covalent alteration of butyryl group to the amino acid, lysine	p300 and CREB-binding protein (CBP) as butyryl-modifying enzymes (butyryl transferases) Debutyrylases (sirtuins)
Lactylation	A modification by which L-lactate (a cellular metabolite byproduct) changes lysine residues on histone proteins (Kla or Klac)	YiaC/Lactylase and CobB/Delactylase

of the two processes: via allostery or by interacting with the adjoining domains (22). Phosphorylation predominantly occurs on target sites comprising Ser, Thr, Tyr, and His residues (23). In contrast, dephosphorylation or elimination of a phosphate group is a phosphatase-mediated enzymatic reaction (24).

Cancer is one of the most abhorrent disorders in which numerous regulatory gene products are transformed (25). Recent studies have highlighted the involvement of aberrant protein phosphorylation in cancer manifestation (26–29). The primary mechanisms underlying impaired signal transduction are due to uncontrolled phosphorylation (gain- or loss-of -function mutation) (30). Yet, mutations in kinases or phosphatases which induce aberrant phosphorylation and upset the delicate equilibrium of activation or inactivation of cancer-associated proteins are regarded as both the cause and effect of cancer (31).

Acetylation

Acetylation modification is a reversible acylation process catalyzed by acetyltransferase in which an acetyl group from acetyl-CoA is covalently transferred to the ε-amino group of lysine residues (typically) within the target substrates (32, 33). Deacetylase enzymes can also reverse this biochemical process. Acetylation is critical in chromatin remodeling, gene expression, and protein function regulation (34). Many nonhistone proteins, like histones, are sensitive to acetylation and other PTMs (35). Because lysine acetylation was first discovered in histones, many KATs and KDACs are also known as histone acetyltransferases (HATs) and deacetylases (HDACs), respectively (36). Aberrant acetylation of nonhistone proteins is common in several human disorders, particularly cancer (37). Acetylation is also closely associated to active glycolysis in tumors. Phosphoglycerate kinases that include PGK1 and PGK2 are ATP producing glycolytic enzymes and few reports have showed acetylation at K323 in PGK1 increases its enzyme activity and glucose absorption, causing an increase in aberrant hepatic cell growth and carcinogenesis (38). Enolase 2 (ENO2) is another important glycolytic enzyme that is overexpressed in prostate cancer, small-cell lung cancer, metastatic neuroblastoma, and leukemia (39, 40).

Glycosylation

Glycosylation is the most common and diversified type of protein post-translational modifications that is vital for many biological processes (41). Glycosylation is an enzymatic process by which saccharides form glycosidic bridges with other saccharides, proteins, or lipids (42, 43). Protein glycosylation are of two types: N-linked glycosylation (N-glycosylation) and O-linked glycosylation (O-glycosylation), with O-linked being a more difficult modification due to its structural complexity and diversity (41). Different glycoconjugates disrupt essential cancer cell functions as well as the tumor microenvironment, resulting in carcinogenesis. Mostly, cancer cells diverge from the classical glycosylation pathway, resulting in aberrant glycan expression (44). O-GlcNAc modifications have been linked to tumor cell proliferation employing FoxM1, a transcription factor and cyclin D1, both of which are involved in cell cycle progression, cancer cell survival, and angiogenesis (45).

Methylation

Methylation is a classic post-translational modification utilized to transfer information in signal transduction pathways in the cell. Protein methylation can occur at both their N- and C-termini, as well as on side chain nitrogen atoms of lysine and arginine residues (46, 47), mediated by protein methyltransferases (PRMTs) (48). PRMTs, which are a family of enzymes that methylate both histone and nonhistone proteins (49) are of two types, namely, lysine methyltransferases (KMTs) and protein arginine methyltransferases (RMTs). Lysine residues can be mono-, di-, or trimethylated, but arginine residues can only be mono- or can remain demethylated (50). PRMT family members were identified to be overexpressed in a variety of cancers (51, 52). Elevated PRMT3 expression has been linked to poor clinical outcomes in pancreatic cancer (53), colorectal cancer (54), and hepatocellular carcinoma (55). In lung adenocarcinoma, the tumor suppressor DAL-1/4.1B interacts with PRMT3 and suppresses its methyltransferase activity, signifying a putative involvement of PRMT3 regulation in tumor progression (56).

Sumoylation

SUMOylation is an important post-translational protein modification that covalently attaches small ubiquitin-like modifiers (SUMO) in the ϵ-amino group of lysine residues in the target protein, via a multi-enzymatic reaction. SUMO is an 11 kDa protein which has a structural similarity with ubiquitin (57). SUMO is covalently linked to a lysine residue in the substrate protein via three enzymes: activating (SUMO E1), conjugating (SUMO E2), and ligase (SUMO E3) (58). Furthermore, SUMO is dissociated from the target protein by SUMO proteases (sentrin-specific protease 1, SENP1 in humans) (59). The enzymes involved in SUMO pathway are commonly increased in numerous malignancies and have been associated to carcinogenesis and poor patient prognosis. SUMOylation has been linked to chemoresistance and hormone therapy resistance in many studies. Also, the regulation of the oncogene Myc and the SUMOylation machinery has been discovered in pancreatic cancer (60).

Ubiquitination

Ubiquitin (Ub), a 76-amino acid regulatory protein, is covalently attached to protein substrates using a series of enzymatic cascade that involves Ub-activating (E1), Ub-conjugating (E2), and Ub-ligating (E3) enzymes in a highly conserved post-translational modification called as Ubiquitination (or, Ubiquitylation). Ub attaches to substrates in multiple ways,

such as a single Ub attached to an amino acid (monoubiquitination) or to many amino acids (multiple monoubiquitination), or as polymeric chains (polyubiquitination). Different Ub chains are produced via isopeptide linkage with the N-terminal methionine (M1) and seven internal lysine (K) residues (61). As a result, mono- or polyubiquitination affects the function of several proteins under healthy and/or pathological events (62, 63). Deubiquitinases (DUBs) inhibit ubiquitination by eliminating Ub modifications from their target substrates, which are crucial for cell cycle, apoptosis, and gene transcription (64, 65). Abnormal ubiquitination may contribute to tumor growth and tumorigenesis (66). Mutations in E3 ligases can rapidly degrade tumor suppressors or, conversely, loss of ubiquitination in growth-promoting oncoproteins (67). Furthermore, E3 ligases and counterbalancing Deubiquitinases are interesting prospective targets for cancer therapies because of their substrate specificity.

Neddylation

Neddylation is a reversible covalent attachment of a ubiquitin-like molecule NEDD8 (neuronal precursor cell-expressed developmentally down-regulated protein 8) to a lysine residue of the protein substrate (68, 69). The NEDD8-activating enzyme E1, the NEDD8-conjugating enzyme E2, and substrate-specific NEDD8-E3 ligases all work together to promote neddylation, similar to ubiquitination (70–72). The key family of multiunit E3 ubiquitin ligases, Cullin-RING ligases (CRLs), regulate 20% of proteasome-mediated protein degradation (73–76). Targeting cullin neddylation looks to be an appealing cancer therapeutic strategy, provided hyperactivation of CRLs support carcinogenesis (77, 78). Aberrant activation of the neddylation pathway results in increased global neddylation of substrates such as cullins, leading to subsequent degradation of tumor suppressors (e.g., p21 and p27) and facilitating carcinogenesis and progression (71, 79). Thus, utilizing the neddylation route to inactivate CRLs can be a feasible anticancer approach.

S-Nitrosylation

S-nitrosylation is a covalent post-translational modification in which a nitric oxide (NO) molecule is coupled to the reactive thiol of an adjacent cysteine residue to generate S-nitrosothiol (SNO) (80). Endogenous NO is synthesized from L-arginine in mammalian cells by three distinct gene-encoded NO synthases (NOSs): neuronal NOS (nNOS/NOS-1), inducible NOS (iNOS/NOS-2), and endothelial NOS (eNOS/NOS-3) (81). S-nitrosylation, like other post-translational modifications, regulates biological activity of a wide range of proteins *in vivo*, as well as controls transcription (82), DNA repair (83), and apoptosis (84–86). Aberrant S-nitrosylation has been associated with significant pathophysiological events, including reported studies that influence the initiation of cancer and cancer cell proliferation both directly and indirectly (83, 87). Bentz et al. demonstrated in 2000 that nitrotyrosine levels are elevated in reactive and dysplastic types of head and neck squamous cell carcinoma (HNSCC) lesions than in normal squamous mucosa (88).

Succination

Succination is a stable post-translational modification that occurs when the Krebs cycle intermediate fumarate combines with the thiol groups on cysteine residues to produce S-(2-succino)cysteine (2SC) (16). Some studies have found that 2SC is a biomarker for not only mitochondrial stress in obesity and diabetes, but also fumarate hydratase (FH) deficiency in individuals with hereditary leiomyomatosis and renal cell carcinoma (HLRCC) (16, 19, 89, 90). Interestingly, fumarate can enter other cellular and extracellular compartments, most likely because fumarate can be transported from mitochondria via specialized carriers, causing 2SC production and extra-mitochondrial protein impairment. The pool of impaired proteins is referred to as the succinated proteome, which then loses its ability to perform functional and structural activities, possibly leading to cell death (91). There is substantial evidence that shows elevated levels of protein succination in diabetes (17, 92), obesity (89), and cancer (93, 94). As a result, 2SC is identified as a mitochondrial stress biomarker, which may result in cellular dysfunction and even apoptosis in cancer and diabetes (91).

Prenylation

Prenylation is a common covalent post-translational modification that occurs in all eukaryotic cells and is mediated by the enzymes protein farnesyltransferase (FTase) or protein geranylgeranyltransferase I (GGTase I), respectively. Prenylation involves the attachment of either a 15-carbon farnesyl or a 20-carbon geranylgeranyl isoprenoid lipid to the cysteine residues (95). When the farnesyl isoprenoid is involved, this enzyme-catalyzed process is known as farnesylation and when the geranylgeranyl isoprenoid is involved, the reaction is known as geranylgeranylation (96). Prenylation is the first crucial step in membrane targeting and binding, as well as mediating protein-protein interactions for many of these proteins; heterotrimeric G-proteins also depend on prenylation for its function (97). The discovery that protein prenylation was required to maintain the malignant activity of oncogenic Ras GTPases evoked immense interest in this field, as Ras proteins have been known to drive more than 30% of human malignancies (98, 99). Preclinical trials of farnesyltransferase inhibitors (FTIs) in cancer cell lines and animal models were highly effective, which resulted in the entry of four FTIs (as monotherapy or in combination with other anti-cancer drugs) into clinical trials in 2000 (100, 101). This initial victory did not translate into significant anticancer activity in patients with advanced solid tumors or acute myeloid leukaemia (AML), despite promising phase 1 and 2 trials (102). Responses to FTIs, irrespective of cellular or tissue origin, do not appear to rely on RAS mutations, because inhibiting KRAS farnesylation directs to its geranylgeranylation (101). Thus, understanding the molecular

mechanism of farnesylated proteins and their inhibition strategies, the therapy regimen for cancer patients responsive to FTI treatment can be augmented.

Palmitoylation

Palmitoylation is an enzyme-mediated reversible lipid modification by which palmitate, a 16-carbon palmitic acid, is added via a thioester linkage to a cysteine (Cys) residue (103). The enzymes regulating both palmitoylation and depalmitoylation are the DHHC protein family named as palmitoyl acyltransferases (PATs) (104) and enzymes such as the acyl protein thioesterase (APT) and alpha beta hydrolase-domain containing protein 17 (ABHD17) protein family showing depalmitoylase activity (105, 106). Palmitoylation occurs on a number of critical cancer-related proteins. The RAS family of small GTPases is one such classic example (107, 108). A report demonstrated that palmitoylation at Cys181 site is required for oncogenic NRAS connection with the plasma membrane, and palmitoylation removal inactivated numerous signaling pathways downstream of NRAS, thereby inhibiting leukemogenesis (109).

Succinylation

Succinylation is a post-translational modification that involves the transfer of a succinyl group (-CO-CH_2-CH_2-CO_2H) to a lysine residue via enzymatic or non-enzymatic reactions (110). Succinylation PTM is predominantly mitochondrial of both prokaryotic and eukaryotic organisms (111, 112) and is involved in the production of mitochondrial energy (113, 114). Aberrant succinylation can influence cancer progression, cardiometabolic disorders, hepatometabolic disorders, and neurological disorders (115). Succinylation of a key glycolytic enzyme, pyruvate kinase muscle isotype M2 (PKM2) has been described to increase its enzymatic activity in the context of cancer, but also a different succinylated lysine residue (K498) has been reported, stating that succinylation may have contrasting effects on the same protein target depending on modified site of lysine residues (116).

Citrullination

Citrullination modification is deamination of a positively charged arginine into the electrically neutral citrulline (a non-coding amino acid), when subjected to an elevated Ca^{2+} concentration (117) catalyzed by the peptidyl-arginine deiminase (PAD). The peptidyl-arginine deiminase (PAD) enzyme family has five isoenzymes (PAD1-4 and PAD6) that target different tissues (118). Vimentin, actin, collagen, fibronectin, keratin, tubulin, and different histone proteins are amongst the proteins found in the human citrullinome (119, 120). A study found that benign tumors and non-tumor inflamed tissues were devoid of PAD4 expression (121), whereas malignant tumors had significantly higher PAD4 levels than similar primary tumors (122), implying that citrullination plays a role in the transformation from benign neoplasm to invasive malignancy.

S-Glutathionylation

S-glutathionylation is a distinct redox-driven post-translational modification in which the cysteine residue of glutathione forms a disulphide bond with the -SH (thiol) group of a target cysteine in the protein, oxidizing it. The reversible nature of this unique modification can lead to transitory alterations in the target protein's structure and/or function (123). Few proteins related to cellular metabolism and detoxification are identified to be affected by glutathionylation. One such key metabolic enzyme is pyruvate kinase M2 (PKM2), which is critical for cancer cells due to their reliance on the glycolytic pathway and its potential role in modifying antioxidant responses (124, 125). Anastasiou et al. established that S-glutathionylation of PKM2 Cys358 is important for responding to oxidative stress by permitting PKM2 deactivation (125).

Novel post-translational modifications

Monoaminylation

Monoaminylation is a biochemical process in which biogenic monoamines (serotonin, dopamine, histamine, etc.) are covalently linked to glutamine residues within certain protein substrates, by Transglutaminase 2, an enzyme that catalyzes the transamidation reaction of primary amines to glutamine-carboxamides (126). Monoaminylation is important in several aspects of cellular plasticity (in the brain and maybe elsewhere) (127). Because monoaminylation is one of numerous newly found histone PTMs, further studies are ongoing that may have biological significance in terms of carcinogenesis and cancer therapy.

Crotonylation

Protein crotonylation is one of the newly discovered post-translational modifications that occur primarily on the lysine residue, known as lysine crotonylation (Kcr). Kcr is a conserved modification that is controlled by a number of enzymes and co-enzymes, such as lysine crotonyltransferase (writer), lysine decrotonylase (eraser), specific YEATS proteins (reader), and crotonyl-coenzyme A (donor) (128). Crotonylation was first discovered as a PTM on histone lysines (129). Histone Kcr has been linked to a variety of illnesses, including depression, acute renal damage, HIV latency, and carcinogenesis (130–133). Immunohistochemical staining of tumor specimens with adjacent normal tissues reveals that lysine crotonylation occurs in both the cytoplasm and the nucleus, and that lysine crotonylation level is downregulated in liver cancer, gastric cancer, and renal carcinoma, but upregulated in thyroid, esophageal, colon, pancreatic, and lung cancers (134).

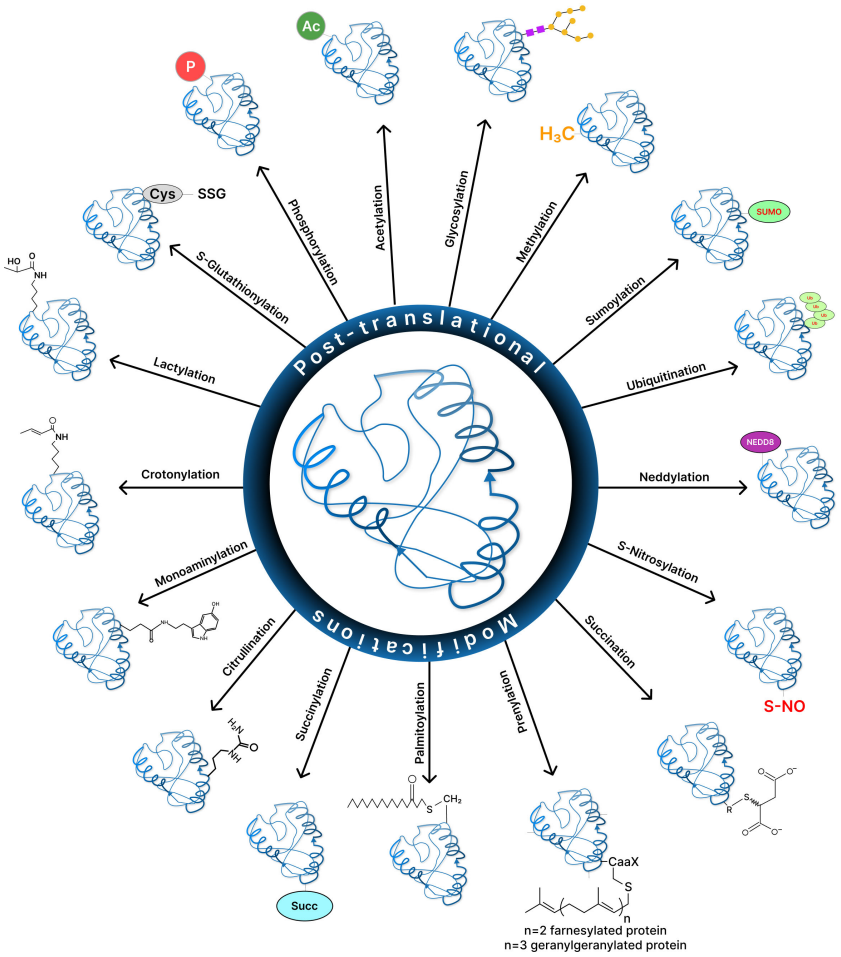

FIGURE 2
Various post-translational modificalions in cancer.

Propionylation

Propionylation (propionyl; C-3 fatty acid chain) is a novel histone acylation modification where in the propionyl group covalent attaches to the lysine residues of the target protein (Kpr). After its discovery in histone proteins, Kpr was also found to be present in nonhistones (135). Propionyl-CoA, the co-substrate for Kpr modification arises from the breakdown product of cholesterol and odd-chain fatty acid oxidation and branched-chain amino acid catabolism, which thereby provides us an insight that Kpr may have a potential role in cellular metabolism that involves chromatin architecture during fasting and catabolism (136, 137). Not much has been observed about the function of propionylation in cancer development yet but it is well-known that most of the acylation modifications act synergistically in tumor pathogenesis (138).

Butyrylation

Butyrylation is one of the newly discovered biochemical acylation modifications, observed in both plants and animals, in which the butyryl group covalently alters the amino acid, lysine (Kbu). Kbu occurs in both histone and nonhistone proteins (135). The butyryl group or butyrate (C-4 fatty acid chain) plays an important role in several human diseases, such as vascular dementia, diabetes, psychiatric disorders, and cancer whereas various plant-based substances have also been potentially associated to Kbu of histones (139–141). p300 and CBP were discovered as butyryl-modifying enzymes, that allows histone H4 to get propionylated and butyrylated. Soon after Kbu was identified, SIRT enzymes (Sirt7) with debutyrylase activities were identified that act as erasers (142). A recent study has made a comparative analysis of histone markers in two types of esophageal squamous cell carcinoma using mass spectrometry, and found that various modifications, such as lysine methylation, acetylation, as well as butyrylation on histones H3 and H4 work together in the development of cancer (143). Since these are novel acylation modifications, further studies are required to explore their roles in different disease pathologies.

Lactylation

Lactylation is another novel post-translational modification that occurs when lactate (L-lactate rather than D-lactate) changes lysine residues on histone proteins (Kla or Klac) (144, 145). Cancer cells

TABLE 2 Examples of clinically targeted oncoproteins and the associated post-translational modifications responsible for cancer therapeutics.

Oncoprotein	Description
Signal transducer and activator of transcription 3 (STAT3)	Studies have shown that knockdown of Raf Kinase Inhibitor Protein (RKIP, negative regulator of Ras-MAPK/ERK signaling pathway) in NSCLC patients, causes STAT3 phosphorylation and activation Sleading to metastasis in A549 and NCI-H1299 cell lines (1, 2).
Epidermal Growth Factor Receptor (EGFR)	In NSCLC patients, palmitoylation of EGFR oncoprotein at Cys^{797} site by ZDHHC1, ZDHHC2, and/or ZDHHC21 enzymes (Zinc finger DHHC-type containing enzymes) leads to receptor dimerization, stability, and its subsequent activation (3). When EGFR palmitoylation is inhibited using broad spectrum protein palmitoylation inhibitors such as 2-bromopalmitate (2-BP), the lethal efficacy of its targeted inhibitor, Gefitinib increases (3).
N-acetylgalactosaminyltransferases (GALNTs)	GALNTs are group of enzymes that are responsible at modulating initial mucin-type O-glycosylation, which have shown close relationship with cancer incidence and metastasis (4, 5). Previous animal studies have extensively reported that GALNT class of enzymes (GALNT1-GALNT20) act as prognostic markers for different cancers, or have been linked to alterations in cellular characteristics including cell proliferation, migration, invasion and metastasis in experimental models (6). Few of the broad range of cancers in which altered protein levels of GALNTs have been demonstrated include colorectal (7), gastric (8), breast (9), pancreatic (10), lung adenocarcinoma (11), NSCLC (12), and glioma (13). Studies showed that GALNT2 promotes tumor formation and progression in BALB/c nude mice models (14). Many transmembrane proteins are modified by N-linked glycosylation, which is responsible for tumor metastasis. This study also demonstrates that N-glycosylation of T-cell membrane protein-4 (TIM-4) at Asn^{291} site is conducive to cancer metastasis as reported *in vitro* and *in vivo* models (15).
RAS	The RAS family of GTPases are small monomeric G-proteins that regulate key biological functions like gene expression, transmembrane signaling, apoptosis, etc (16). RAS has been extensively studied and play significant roles in cancer initiation and progression. About 25-30% of human tumors harbor RAS mutations. KRAS, NRAS, HRAS are three members of this oncogene superfamily that have been reported to implicate in various malignancies; KRAS in NSCLC, pancreatic cancer; NRAS in liver cancer and in liquid tumors like AML; HRAS mutations in BCa and renal cell cancer (17–19). HRAS oncogene is only **farnesylated**, but KRAS4A, KRAS4B and NRAS are **geranylgeranylated** by GGTaseI, leading to activation of downstream signaling of MAPK/ERK pathway (20). Because many tumors rely on RAS oncogenes for their survival, a number of drugs have been developed that selectively target these oncoproteins. Earlier, researchers focused on blocking a type of **prenylation** PTM known as farnesylation on RAS which exhibited huge promise in preclinical investigations (19). Unfortunately, no therapeutic effects from farnesyl transferase inhibitors could be demonstrated, making RAS challenging to drug, but inhibitors targeting specific RAS mutations are under development (21).
MYC (*c-MYC/N-MYC/L-MYC)*	MYC family of transcription factors has several roles to play in cellular processes such as cell growth, proliferation, differentiation, and programmed cell death (22). It is deregulated in ~ 70% of human tumors, of which majority are aggressive such as in leukemias and high-grade lymphomas or in cancers which have poorer clinical outcomes like NSCLC (23). Studies have showed that the compound oridonin (a natural terpenoid) upregulates SCF^{FBXW7} causing **degradation** of MYC protein via Ub-proteasome system, and therefore leading to apoptosis in leukemia and lymphoma cell lines (24). Aurora kinase A (AURKA) blocks SCF^{FBXW7}-mediated MYC proteolysis by binding MBI motif based on a covalent association that exclusively depends on the **phosphorylation** status of T^{58} and S^{62} sites (25, 26). Overall, strategies are being made to develop small molecules that can inhibit AURKA to indirectly target MYC activity. Drugs such as MLN8237/alisertib and CD532 causes Aurora A-c-MYC/N-MYC complex non-functional and advances the tumor towards regression, as observed in neuroblastoma and human hepatocarcinoma cells (26, 27).

10.3389/fonc.2023.1240115

TABLE 3 Examples of key proteins with its corresponding post-translational modification(s) (in bold) related to cancer hallmarks/responsible for cancer pathophysiology.

Protein Name	Type of PTM(s) involved
Programmed Death-Ligand 1 (PD-L1/*CD274*)	Epigenetic modifications, such as **histone acetylation** and **methylation** of H3K3me3. - Histone acetylation helps BET domain proteins (BRD4) to associate with PD-L1. Also, HDAC inhibitors augment histone acetylation and upregulate PD-L1 expression in tumors (28–30). - Trimethylation of histone H3 on lysine 4 increases PD-L1 expression in cancer cells. For example, Histone methyltransferase (HMTase) MLL1 associate with *CD274* promoter and catalyzes H3K4me3, thereby upregulating its expression, which in turn boosts PD-L1 mRNA levels in tumors (31).
N-acetylgalactosaminyltransferases (GALNTs)	GALNTs are group of enzymes that are responsible at modulating initial mucin-type O-**glycosylation**, which have shown close relationship with cancer incidence and metastasis (4, 5). Previous animal studies have extensively reported that GALNT class of enzymes (GALNT1-GALNT20) act as prognostic markers for different cancers, or have been linked to alterations in cellular characteristics including cell proliferation, migration, invasion and metastasis in experimental models (6). Few of the broad range of cancers in which altered protein levels of GALNTs have been demonstrated include colorectal (7), gastric (8), breast (9), pancreatic (10), lung adenocarcinoma (11), NSCLC (12), and glioma (13). Studies showed that GALNT2 promotes tumor formation and progression in BALB/c nude mice models (14). Many transmembrane proteins are modified by N-linked glycosylation, which is responsible for tumor metastasis. This study also demonstrates that N-glycosylation of T-cell membrane protein-4 (TIM-4) at Asn^{291} site is conducive to cancer metastasis as reported *in vitro* and *in vivo* models (15).
Prohibitin (PHB)	PHBs (PHB1 and PHB2) are evolutionary conserved scaffold proteins that are ubiquitously expressed in mitochondria, plasma membrane and nucleus. They exhibit diverse compartment-specific regulatory roles such as cell proliferation, metabolism, lipid scaffolding in cell membrane, mitochondrial remodeling, and apoptosis (32–35). PHBs play an important role in carcinogenesis by regulating vital cellular signaling pathways (such as the Ras-Raf-MEK-ERK signaling axis) that leads to cell proliferation, and metastasis and these proteins are tightly controlled by **phosphorylation** (36, 37). In bladder cancer (BCa), the expression levels of PHB1 were found to be higher (in 141 out of 167 patients), indicating that PHB1 is required for BCa cell proliferation (38). Another report demonstrated that mitochondrial localization of PHB is regulated by Protein Kinase B (PKB)/Akt-mediated phosphorylation of Prohibitin at Thr^{258} site (in the cytoplasm) in BCa patients. Thus, phosphorylated-PHB is a suitable therapeutic target in BCa (39). Besides, phosphorylation of PHB1 at Ser^{121}, Tyr^{259}, and Tyr^{114} regions is also responsible for tumor formation (40, 41).
MYC (*c-MYC/N-MYC/L-MYC)*	The oncoprotein MYC is a pleiotropic transcription factor that affects essential cellular functions such as proliferation, differentiation, cell cycle, metabolism, and apoptosis (23). Strong evidence defines both aberrant MYC expression as an oncogenic driver of malignancies as well as its association to all of cancer 'hallmarks' (42, 43). Surprisingly, MYC allows tumor cells to escape immune-surveillance either by downregulating MHCI expression or by upregulating inhibitory cytokines and immune-checkpoint proteins such as PD-L1 and CD47, thereby shedding light on associating MYC inhibition and escape of immune-checkpoints to target MYC (44–46).
Fructose-1,6-bisphosphatase (FBP-1)	Fructose-1,6-bisphosphatase (FBP-1 or FBPase) is a rate-limiting enzyme catalyzing the conversion of fructose 1,6-bisphosphate to fructose 6-phosphate and inorganic phosphate, which is an important step in gluconeogenesis, required for the regulation of energy metabolism and maintenance of glucose homeostasis (47). Evidences support that FBP-1 downregulation is considered to be as a prognostic cancer marker for different tumor types such as gastric cancer, lung cancer and breast cancer, increasing the glycolytic rate and cancer stem cells in number (48–50). Recent reports demonstrated that TRIM28, which is an E3 Ubiquitin ligase, helps in regulation of FBP-1 expression levels by some post-translational changes in hepatic cancer. Furthermore, it was observed that TRIM28 directly associate with and recruits to **ubiquitination** by degrading FBP1 protein. Direct interacting partners of TRIM28 such as MAGE-A3 and MAGE-C2 (51, 52), can augment TRIM28-specific degradation of FBP1 by forming a ternary ubiquitin ligase complexes with TRIM28 (53).
Heat shock protein 90 (HSP90)	HSP90 is an evolutionarily conserved molecular chaperone that participates in cellular homeostasis and is an important mediator of oncogene addiction (54, 55). Studies showed that NO-dependent **nitrosylation** at Cys^{597} position in C domain of HSP90 blocks chaperone function in endothelial cell lines (56). Existing findings about anti-cancerous activity of externally administered NO may have been caused from its blockade of HSP90 in tumors (57), which is consistent with the observations that HSP90 in regulation of telomeric activity (58).

10.3389/fonc.2023.1240115

rely on aerobic glycolysis to produce energy and metabolites, forming lactate, which supports lysine lactylation (Kla) (145). The role of histone Kla has been investigated in mouse embryo fibroblasts (MEFs), ocular melanoma cells (146), and non-small cell lung cancer (NSCLC) cells (147), suggesting that Kla is important in controlling pluripotency and oncogenesis. Recently it was found that Kla levels were considerably greater in 51 tumor tissues as compared to its corresponding para-cancerous tissues, when pan-Kla levels in gastric tumors and adjacent tissues were evaluated (148). Furthermore, higher Kla levels were associated with poorly differentiated tumors, lymph node metastases, and poorer prognostic rates of patients, thus implying that Kla has prognostic significance in gastric tumors (148).

Discussion

Post-translational modifications (PTMs) affect many essential biological processes by reversibly altering the conformation, function, and/or interaction regions of a protein. Aberrant changes are signs of cellular stress or malfunction, and they have been linked to cancer and a variety of other diseases. Understanding which proteins has changed, at which locations, and the associated biological consequences are therefore critical (Figure 2). Therefore, identification of a multitude of post-translationally modified protein sites has become an important and promising endeavor with the advent of mass spectrometry (MS)-based proteomics, chemical biology tools, fluorescence-based, and bioinformatic techniques (149, 150). However, these cutting-edge approaches present a number of complex challenges. Few of the difficulties may be to determine which proteins are altered, at what locations, and what biological relevance it has. Also, whether cells are biased on non-enzymatic over enzymatic pathway of modification and what is the reason behind that preference can be some of the intriguing questions to consider.

Exciting breakthroughs in identifying PTMs on a proteome-wide and cellular levels show a growing impact in understanding the proteome's diversity. Once PTM analysis at the proteome level becomes regular, the role of PTMs in disease can be explored considerably more systematically than before and will promote in the discovery of novel drugs and cancer therapeutic strategies. Few key proteins whose post-translational modifications are clinical targets for cancer therapeutics as well as associated with the hallmarks of cancer or its pathophysiology have been enlisted (Tables 2, 3).

A number of small molecule drugs that target PTM regulators, such as kinase, deacetylase, and methyltransferase inhibitors, have been approved for cancer treatment. However, in addition to the therapeutic target, each upstream regulator often has several substrates. Therefore, unbiased inhibition of PTM regulators may result in off-target effects, limiting their therapeutic usage. As a result, 'small' molecules with profound selectivity that can modulate a particular PTM of a protein are in huge demand. Many chemical proximity-induced PTM methods, such as proteolysis-targeting chimera (PROTAC), have arrived in the last two decades as having immense potential for targeting 'undruggable' proteins and for clinical translation in the treatment of cancer (151, 152).

Author contributions

HD and NJ wrote and drafted the manuscript. All authors contributed to the article and approved the submitted version.

Funding

This work was supported by grants from the Department of Biotechnology (6242-P69/RGCB/PMD/DBT/NDJN/2015), and the Council of Scientific and Industrial Research (CSIR-IICT/MLP0068), India to NJ. HD is supported by a senior research fellowship from Department of Science and Technology-INSPIRE, India.

Acknowledgments

We thank the Director, CSIR-IICT (Ms. No. IICT/Pubs./2023/215) for providing all the required facilities to carry out the work. To whom correspondence may be addressed: Department of Applied Biology, CSIR-Indian Institute of Chemical Technology, Uppal Road, Tarnaka, Hyderabad 500007, Telangana State, India. Tel.: 91-40-27191857; Fax: 91-40-27191812; E-mail: H.D, hashnudutta@gmail.com and N.J, nishant.iict@gov.in.

Conflict of interest

The authors declare that the research was conducted in the absence of any commercial or financial relationships that could be construed as a potential conflict of interest.

Publisher's note

References

1. T.U. Consortium. The universal protein resource (UniProt) 2009. *Nucleic Acids Res* (2008) 37:D169–74.

2. Fearon WR. The carbamido diacetyl reaction: a test for citrulline. *Biochem J* (1939) 33:902–7. doi: 10.1042/bj0330902

3. Walsh CT, Garneau-Tsodikova S, Gatto GJ Jr. Protein posttranslational modifications: the chemistry of proteome diversifications *Angewandte Chemie Int Edition* (2005) 44:7342–72 doi: 10.1002/anie.200501023

4. Barski A, Cuddapah S, Cui K, Roh T-Y, Schones DE, Wang Z, et al. High-resolution profiling of histone methylations in the human genome. *Cell* (2007) 129:823–37. doi: 10.1016/j.cell.2007.05.009

5. Meierhofer D, Wang X, Huang L, Kaiser P. Quantitative analysis of global ubiquitination in heLa cells by mass spectrometry. *J Proteome Res* (2008) 7:4566–76. doi: 10.1021/pr800468j

6. Singh R, Barden A, Mori T, Beilin L. Advanced glycation end-products: a review. *Diabetologia* (2001) 44:129–46. doi: 10.1007/s001250051591

7. Verbrugge FH, Tang WHW, Hazen SL. Protein carbamylation and cardiovascular disease. *Kidney Int* (2015) 88:474–8. doi: 10.1038/ki.2015.166

8. Dalle-Donne I, Giustarini D, Colombo R, Rossi R, Milzani A. Protein carbonylation in human diseases. *Trends Mol Med* (2003) 9:169–76. doi: 10.1016/S1471-4914(03)00031-5

9. Kalim S, Karumanchi SA, Thadhani RI, Berg AH. Protein carbamylation in kidney disease: pathogenesis and clinical implications. *Am J Kidney Dis* (2014) 64:793–803. doi: 10.1053/j.ajkd.2014.04.034

10. Beltrao P, Albanèse V, Kenner LR, Swaney DL, Burlingame A, Villén J, et al. Systematic functional prioritization of protein posttranslational modifications. *Cell* (2012) 150:413–25. doi: 10.1016/j.cell.2012.05.036

11. Walsh G, Jefferis R. Post-translational modifications in the context of therapeutic proteins. *Nat Biotechnol* (2006) 24:1241–52. doi: 10.1038/nbt1252

12. Deribe YL, Pawson T, Dikic I. Post-translational modifications in signal integration. *Nat Struct Mol Biol* (2010) 17:666–72. doi: 10.1038/nsmb.1842

13. Peng Y, Liu H, Liu J, Long J. Post-translational modifications on mitochondrial metabolic enzymes in cancer. *Free Radical Biol Med* (2022) 179:11–23. doi: 10.1016/j.freeradbiomed.2021.12.264

14. Karve TM, Cheema AK. Small changes huge impact: the role of protein posttranslational modifications in cellular homeostasis and disease. *J Amino Acids* (2011) 2011:207691. doi: 10.4061/2011/207691

15. Xu H, Wang Y, Lin S, Deng W, Peng D, Cui Q, et al. PTMD: A database of human disease-associated post-translational modifications. *Genomics Proteomics Bioinf* (2018) 16:244–51. doi: 10.1016/j.gpb.2018.06.004

16. Alderson NL, Wang Y, Blatnik M, Frizzell N, Walla MD, Lyons TJ, et al. S-(2-Succinyl)cysteine: A novel chemical modification of tissue proteins by a Krebs cycle intermediate. *Arch Biochem Biophysics* (2006) 450:1–8. doi: 10.1016/j.abb.2006.03.005

17. Blatnik M, Thorpe SR, Baynes JW. Succination of proteins by fumarate. *Ann New York Acad Sci* (2008) 1126:272–5. doi: 10.1196/annals.1433.047

18. Adam J, Yang M, Soga T, Pollard PJ. Rare insights into cancer biology. *Oncogene* (2014) 33:2547–56. doi: 10.1038/onc.2013.222

19. Bardella C, El-Bahrawy M, Frizzell N, Adam J, Ternette N, Hatipoglu E, et al. Aberrant succination of proteins in fumarate hydratase-deficient mice and HLRCC patients is a robust biomarker of mutation status. *J Pathol* (2011) 225:4–11. doi: 10.1002/path.2932

20. Wang H, Yang L, Liu M, Luo J. Protein post-translational modifications in the regulation of cancer hallmarks. *Cancer Gene Ther* (2023) 30:529–47. doi: 10.1038/s41417-022-00464-3

21. Edwards AS, Scott JD. A-kinase anchoring proteins: protein kinase A and beyond. *Curr Opin Cell Biol* (2000) 12:217–21. doi: 10.1016/S0955-0674(99)00085-X

22. Duan G, Walther D. The roles of post-translational modifications in the context of protein interaction networks. *PloS Comput Biol* (2015) 11:e1004049. doi: 10.1371/journal.pcbi.1004049

23. Panni S. Phospho-peptide binding domains in S. cerevisiae model organism. *Biochimie* (2019) 163:117–27. doi: 10.1016/j.biochi.2019.06.005

24. Skamnaki VT, Owen DJ, Noble MEM, Lowe ED, Lowe G, Oikonomakos NG, et al. Catalytic mechanism of phosphorylase kinase probed by mutational studies. *Biochemistry* (1999) 38:14718–30. doi: 10.1021/bi991454f

25. Jin J, Pawson T. Modular evolution of phosphorylation-based signalling systems. *Philos Trans R Soc B: Biol Sci* (2012) 367:2540–55. doi: 10.1098/rstb.2012.0106

26. Hanahan D, Weinberg RA. The hallmarks of cancer. *Cell* (2000) 100:57–70. doi: 10.1016/S0092-8674(00)81683-9

27. Appella E, Anderson CW. Post-translational modifications and activation of p53 by genotoxic stresses. *Eur J Biochem* (2001) 268:2764–72. doi: 10.1046/j.1432-1327.2001.02225.x

28. Santarpia L, Lippman SM, El-Naggar AK. Targeting the MAPK–RAS–RAF signaling pathway in cancer therapy. *Expert Opin Ther Targets* (2012) 16:103–19. doi: 10.1517/14728222.2011.645805

29. Jaggi M, Rao PS, Smith DJ, Hemstreet GP, Balaji KC. Protein kinase C μ is down-regulated in androgen-independent prostate cancer. *Biochem Biophys Res Commun* (2003) 307:254–60. doi: 10.1016/S0006-291X(03)01161-6

30. Radivojac P, Baenziger PH, Kann MG, Mort ME, Hahn MW, Mooney SD. Gain and loss of phosphorylation sites in human cancer. *Bioinformatics* (2008) 24:i241–7. doi: 10.1093/bioinformatics/btn267

31. Lim YP. Mining the tumor phosphoproteome for cancer markers. *Clin Cancer Res* (2005) 11:3163–9. doi: 10.1158/1078-0432.CCR-04-2243

32. Hu M, He F, Thompson EW, Ostrikov K, Dai X. Lysine acetylation, cancer hallmarks and emerging onco-therapeutic opportunities. *Cancers* (2022) 14:346. doi: 10.3390/cancers14020346

33. Wellen KE, Hatzivassiliou G, Sachdeva UM, Bui TV, Cross JR, Thompson CB. ATP-citrate lyase links cellular metabolism to histone acetylation. *Science* (2009) 324:1076–80. doi: 10.1126/science.1164097

34. Harachi M, Masui K, Cavenee WK, Mischel PS, Shibata N. Protein acetylation at the interface of genetics. *Epigenet Environ Cancer Metabolites* (2021) 11:216. doi: 10.3390/metabo11040216

35. Latham JA, Dent SYR. Cross-regulation of histone modifications. *Nat Struct Mol Biol* (2007) 14:1017–24. doi: 10.1038/nsmb1307

36. Allis CD, Berger SL, Cote J, Dent S, Jenuwien T, Kouzarides T, et al. New nomenclature for chromatin-modifying enzymes. *Cell* (2007) 131:633–6. doi: 10.1016/j.cell.2007.10.039

37. Shang S, Liu J, Hua F. Protein acylation: mechanisms, biological functions and therapeutic targets. *Signal Transduction Targeted Ther* (2022) 7:396. doi: 10.1038/s41392-022-01245-y

38. Hu H, Zhu W, Qin J, Chen M, Gong L, Li L, et al. Acetylation of PGK1 promotes liver cancer cell proliferation and tumorigenesis. *Hepatology* (2017) 65:515–28. doi: 10.1002/hep.28887

39. Gu L, Zhu Y, Lin X, Li Y, Cui K, Prochownik EV, et al. Amplification of glyceronephosphate O-acyltransferase and recruitment of USP30 stabilize DRP1 to promote hepatocarcinogenesis. *Cancer Res* (2018) 78:5808–19. doi: 10.1158/0008-5472.CAN-18-0340

40. Carney D, Ihde D, Cohen M, Marangos P, Bunn P, Minna J, et al. SERUM NEURON-SPECIFIC ENOLASE: A MARKER FOR DISEASE EXTENT AND RESPONSE TO THERAPY OF SMALL-CELL LUNG CANCER. *Lancet* (1982) 319:583–5. doi: 10.1016/S0140-6736(82)91748-2

41. Behren S, Schorlemer M, Schmidt G, Aktories K, Westerlind U. Antibodies directed against galNAc- and glcNAc-O-tyrosine posttranslational modifications – a new tool for glycoproteomic detection. *Chem – A Eur J* (2023) 29:e202300392. doi: 10.1002/chem.202300392

42. Fuster MM, Esko JD. The sweet and sour of cancer: glycans as novel therapeutic targets. *Nat Rev Cancer* (2005) 5:526–42. doi: 10.1038/nrc1649

43. Moremen KW, Tiemeyer M, Nairn AV. Vertebrate protein glycosylation: diversity, synthesis and function. *Nat Rev Mol Cell Biol* (2012) 13:448–62. doi: 10.1038/nrm3383

44. Kakugawa Y, Wada T, Yamaguchi K, Yamanami H, Ouchi K, Sato I, et al. Up-regulation of plasma membrane-associated ganglioside sialidase (Neu3) in human colon cancer and its involvement in apoptosis suppression. *Proc Natl Acad Sci* (2002) 99:10718–23. doi: 10.1073/pnas.152597199

45. Ma Z, Vosseller K. Cancer metabolism and elevated O-glcNAc in oncogenic signaling*. *J Biol Chem* (2014) 289:34457–65. doi: 10.1074/jbc.R114.577718

46. Anderson JL, Henriksen BS, Gibbs RA, Hrycyna CA. The isoprenoid substrate specificity of isoprenylcysteine carboxylmethyltransferase: DEVELOPMENT OF NOVEL INHIBITORS*. *J Biol Chem* (2005) 280:29454–61. doi: 10.1074/jbc.M504982200

47. Aletta JM, Cimato TR, Ettinger MJ. Protein methylation: a signal event in post-translational modification. *Trends Biochem Sci* (1998) 23:89–91. doi: 10.1016/S0968-0004(98)01185-2

48. Stanevich V, Jiang L, Satyshur KA, Li Y, Jeffrey PD, Li Z, et al. The structural basis for tight control of PP2A methylation and function by LCMT-1. *Mol Cell* (2011) 41:331–42. doi: 10.1016/j.molcel.2010.12.030

49. Bedford MT, Clarke SG. Protein arginine methylation in mammals: who, what, and why. *Mol Cell* (2009) 33:1–13. doi: 10.1016/j.molcel.2008.12.013

50. Wesche J, Kühn S, Kessler BM, Salton M, Wolf A. Protein arginine methylation: a prominent modification and its demethylation. *Cell Mol Life Sci* (2017) 74:3305–15. doi: 10.1007/s00018-017-2515-z

51. Hwang JW, Cho Y, Bae G-U, Kim S-N, Kim YK. Protein arginine methyltransferases: promising targets for cancer therapy. *Exp Mol Med* (2021) 53:788–808. doi: 10.1038/s12276-021-00613-y

52. Baldwin RM, Morettin A, Côté J. Role of PRMTs in cancer: Could minor isoforms be leaving a mark? *World J Biol Chem* (2014) 5:115–29. doi: 10.4331/wjbc.v5.i2.115

53. Hsu M-C, Tsai Y-L, Lin C-H, Pan M-R, Shan Y-S, Cheng T-Y, et al. Protein arginine methyltransferase 3-induced metabolic reprogramming is a vulnerable target of pancreatic cancer. *J Hematol Oncol* (2019) 12:79. doi: 10.1186/s13045-019-0769-7

54. Zhang X, Wang K, Feng X, Wang J, Chu Y, Jia C, et al. PRMT3 promotes tumorigenesis by methylating and stabilizing HIF1α in colorectal cancer. *Cell Death Dis* (2021) 12:1066. doi: 10.1038/s41419-021-04352-w

55. Lei Y, Han P, Chen Y, Wang H, Wang S, Wang M, et al. Protein arginine methyltransferase 3 promotes glycolysis and hepatocellular carcinoma growth by enhancing arginine methylation of lactate dehydrogenase A. *Clin Trans Med* (2022) 12:e686. doi: 10.1002/ctm2.686

56. Singh V, MIranda TB, Jiang W, Frankel A, Roemer ME, Robb VA, et al. DAL-1/4.1B tumor suppressor interacts with protein arginine N-methyltransferase 3 (PRMT3) and inhibits its ability to methylate substrates in *vitro* and in *vivo*. *Oncogene* (2004) 23:7761–71. doi: 10.1038/sj.onc.1208057

57. Mustfa SA, Singh M, Suhail A, Mohapatra G, Verma S, Chakravorty D, et al. SUMOylation pathway alteration coupled with downregulation of SUMO E2 enzyme at mucosal epithelium modulates inflammation in inflammatory bowel disease. *Open Biol* (2017) 7:170024. doi: 10.1098/rsob.170024

58. Desterro JMP, Rodriguez MS, Kemp GD, Hay RT. Identification of the enzyme required for activation of the small ubiquitin-like protein SUMO-1*. *J Biol Chem* (1999) 274:10618–24. doi: 10.1074/jbc.274.15.10618

59. Hickey CM, Wilson NR, Hochstrasser M. Function and regulation of SUMO proteases. *Nat Rev Mol Cell Biol* (2012) 13:755–66. doi: 10.1038/nrm3478

60. Du L, Liu W, Rosen ST. Targeting SUMOylation in cancer. *Curr Opin Oncol* (2021) 33:520–5. doi: 10.1097/CCO.0000000000000765

61. Husnjak K, Dikic I. Ubiquitin-binding proteins: decoders of ubiquitin-mediated cellular functions. *Annu Rev Biochem* (2012) 81:291–322. doi: 10.1146/annurev-biochem-051810-094654

62. Shmueli A, Oren M. Life, death, and ubiquitin: taming the mule. *Cell* (2005) 121:963–5. doi: 10.1016/j.cell.2005.06.018

63. López-Otín C, Hunter T. The regulatory crosstalk between kinases and proteases in cancer. *Nat Rev Cancer* (2010) 10:278–92. doi: 10.1038/nrc2823

64. Ikeda F, Dikic I. Atypical ubiquitin chains: new molecular signals. *EMBO Rep* (2008) 9:536–42. doi: 10.1038/embor.2008.93

65. Rajalingam K, Dikic I. Expanding the ubiquitin code. *Cell* (2016) 164:1074–1074.e1071. doi: 10.1016/j.cell.2016.02.019

66. Morrow JK, Lin H-K, Sun S-C, Zhang S. Targeting ubiquitination for cancer therapies. *Future Medicinal Chem* (2015) 7:2333–50. doi: 10.4155/fmc.15.148

67. Mansour MA. Ubiquitination: Friend and foe in cancer. *Int J Biochem Cell Biol* (2018) 101:80–93. doi: 10.1016/j.biocel.2018.06.001

68. Kamitani T, Kito K, Nguyen HP, Yeh ETH. Characterization of NEDD8, a developmentally down-regulated ubiquitin-like protein*. *J Biol Chem* (1997) 272:28557–62. doi: 10.1074/jbc.272.45.28557

69. Dimitris P. Xirodimas, Novel substrates and functions for the ubiquitin-like molecule NEDD8. *Biochem Soc Trans* (2008) 36:802–6. doi: 10.1042/BST0360802

70. Enchev RI, Schulman BA, Peter M. Protein neddylation: beyond cullin–RING ligases. *Nat Rev Mol Cell Biol* (2015) 16:30–44. doi: 10.1038/nrm3919

71. Zhou L, Zhang W, Sun Y, Jia L. Protein neddylation and its alterations in human cancers for targeted therapy. *Cell signalling* (2018) 44:92–102. doi: 10.1016/j.cellsig.2018.01.009

72. Zhao Y, Morgan MA, Sun Y. Targeting Neddylation pathways to inactivate cullin-RING ligases for anticancer therapy. *Antioxid Redox Signal* (2014) 21:2383–400. doi: 10.1089/ars.2013.5795

73. Petroski MD, Deshaies RJ. Function and regulation of cullin–RING ubiquitin ligases. *Nat Rev Mol Cell Biol* (2005) 6:9–20. doi: 10.1038/nrm1547

74. Deshaies RJ, Joazeiro CAP. RING domain E3 ubiquitin ligases. *Annu Rev Biochem* (2009) 78:399–434. doi: 10.1146/annurev.biochem.78.101807.093809

75. Nakayama KI, Nakayama K. Ubiquitin ligases: cell-cycle control and cancer. *Nat Rev Cancer* (2006) 6:369–81. doi: 10.1038/nrc1881

76. Soucy TA, Smith PG, Milhollen MA, Berger AJ, Gavin JM, Adhikari S, et al. An inhibitor of NEDD8-activating enzyme as a new approach to treat cancer. *Nature* (2009) 458:732–6. doi: 10.1038/nature07884

77. Zhao Y, Sun Y. Cullin-RING ligases as attractive anti-cancer targets. *Curr Pharm Design* (2013) 19:3215–25. doi: 10.2174/1381612811319990300

78. Jia L, Sun Y. SCF E3 ubiquitin ligases as anticancer targets. *Curr Cancer Drug Targets* (2011) 11:347–56. doi: 10.2174/156800911794519734

79. Zhao Y, Morgan MA, Sun Y. Targeting neddylation pathways to inactivate cullin-RING ligases for anticancer therapy. *Antioxidants Redox Signaling* (2014) 21:2383–400. doi: 10.1089/ars.2013.5795

80. Stamler JS, Lamas S, Fang FC. Nitrosylation: the prototypic redox-based signaling mechanism. *Cell* (2001) 106:675–83. doi: 10.1016/S0092-8674(01)00495-0

81. Nathan C, Xie Q-w. Nitric oxide synthases: Roles, tolls, and controls. *Cell* (1994) 78:915–8. doi: 10.1016/0092-8674(94)90266-6

82. Marshall HE, Merchant K, Stamler JS. Nitrosation and oxidation in the regulation of gene expression. *FASEB J* (2000) 14:1889–900. doi: 10.1096/fj.00.011rev

83. Foster MW, Hess DT, Stamler JS. Protein S-nitrosylation in health and disease: a current perspective. *Trends Mol Med* (2009) 15:391–404. doi: 10.1016/j.molmed.2009.06.007

84. Mannick JB. Regulation of apoptosis by protein S-nitrosylation. *Amino Acids* (2007) 32:523–6. doi: 10.1007/s00726-006-0427-6

85. Benhar M, Stamler JS. A central role for S-nitrosylation in apoptosis. *Nat Cell Biol* (2005) 7:645–6. doi: 10.1038/ncb0705-645

86. Melino G, Bernassola F, Knight RA, Corasaniti MT, Nistic G, Finazzi-Agr A. S-nitrosylation regulates apoptosis. *Nature* (1997) 388:432–3. doi: 10.1038/41237

87. Hess DT, Matsumoto A, Kim S-O, Marshall HE, Stamler JS. Protein S-nitrosylation: purview and parameters. *Nat Rev Mol Cell Biol* (2005) 6:150–66. doi: 10.1038/nrm1569

88. Bentz BG, Haines GKIII, Radosevich JA. Increased protein nitrosylation in head and neck squamous cell carcinogenesis. *Head Neck* (2000) 22:64–70. doi: 10.1002/(SICI)1097-0347(200001)22:1<64::AID-HED10>3.0.CO;2-J

89. Thomas SA, Storey KB, Baynes JW, Frizzell N. Tissue distribution of S-(2-succino)cysteine (2SC), a biomarker of mitochondrial stress in obesity and diabetes. *Obesity* (2012) 20:263–9. doi: 10.1038/oby.2011.340

90. Frizzell N, Lima M, Baynes JW. Succination of proteins in diabetes. *Free Radical Res* (2011) 45:101–9. doi: 10.3109/10715762.2010.524643

91. Merkley ED, Metz TO, Smith RD, Baynes JW, Frizzell N. The succinated proteome. *Mass Spectrometry Rev* (2014) 33:98–109. doi: 10.1002/mas.21382

92. Frizzell N, Thomas SA, Carson JA, Baynes JW. Mitochondrial stress causes increased succination of proteins in adipocytes in response to glucotoxicity. *Biochem J* (2012) 445:247–54. doi: 10.1042/BJ20112142

93. Pollard PJ, Brière JJ, Alam NA, Barwell J, Barclay E, Wortham NC, et al. Accumulation of Krebs cycle intermediates and over-expression of HIF1α in tumours which result from germline FH and SDH mutations. *Hum Mol Genet* (2005) 14:2231–9. doi: 10.1093/hmg/ddi227

94. Yang M, Soga T, Pollard P, Adam J. The emerging role of fumarate as an oncometabolite. *Front Oncol* (2012) 2. doi: 10.3389/fonc.2012.00085

95. Zhang FL, Casey PJ. PROTEIN PRENYLATION: molecular mechanisms and functional consequences. *Annu Rev Biochem* (1996) 65:241–69. doi: 10.1146/annurev.bi.65.070196.001325

96. Ashby MN. CaaX converting enzymes. *Curr Opin Lipidology* (1998) 9:99–102. doi: 10.1097/00041433-199804000-00004

97. Placzek AT, Krzysiak AJ, Gibbs RA. Chemical probes of protein prenylation. In: *The enzymes*, vol. 30. Cambridge, MA: Academic Press Inc (2011). p. 91–127.

98. Jackson JH, Cochrane CG, Bourne JR, Solski PA, Buss JE, Der CJ. Farnesol modification of Kirsten-ras exon 4B protein is essential for transformation. *Proc Natl Acad Sci United States America* (1990) 87:3042–6. doi: 10.1073/pnas.87.8.3042

99. Cox AD, Fesik SW, Kimmelman AC, Luo J, Der CJ. Drugging the undruggable RAS: mission possible? *Nat Rev Drug Discovery* (2014) 13:828–51. doi: 10.1038/nrd4389

100. Cutsem EV, v.d. Velde H, Karasek P, Oettle H, Vervenne WL, Szawlowski A, et al. Phase III trial of gemcitabine plus tipifarnib compared with gemcitabine plus placebo in advanced pancreatic cancer. *J Clin Oncol* (2004) 22:1430–8. doi: 10.1200/JCO.2004.10.112

101. Rao S, Cunningham D, d. Gramont A, Scheithauer W, Smakal M, Humblet Y, et al. Phase III double-blind placebo-controlled study of farnesyl transferase inhibitor R115777 in patients with refractory advanced colorectal cancer. *J Clin Oncol* (2004) 22:3950–7. doi: 10.1200/JCO.2004.10.037

102. Harousseau J-L, Martinelli G, Jedrzejczak WW, Brandwein JM, Bordessoule D, Masszi T, et al. f.t.F.-A.-. Investigators, A randomized phase 3 study of tipifarnib compared with best supportive care, including hydroxyurea, in the treatment of newly diagnosed acute myeloid leukemia in patients 70 years or older. *Blood* (2009) 114:1166–73. doi: 10.1182/blood-2009-01-198093

103. Linder ME, Deschenes RJ. Palmitoylation: policing protein stability and traffic. *Nat Rev Mol Cell Biol* (2007) 8:74–84. doi: 10.1038/nrm2084

104. Korycka J, Łach A, Heger E, Bogusławska DM, Wolny M, Toporkiewicz M, et al. Human DHHC proteins: A spotlight on the hidden player of palmitoylation. *Eur J Cell Biol* (2012) 91:107–17. doi: 10.1016/j.ejcb.2011.09.013

105. Duncan JA, Gilman AG. A cytoplasmic acyl-protein thioesterase that removes palmitate from G protein α Subunits and p21RAS*. *J Biol Chem* (1998) 273:15830–7. doi: 10.1074/jbc.273.25.15830

106. Lin DTS, Conibear E. ABHD17 proteins are novel protein depalmitoylases that regulate N-Ras palmitate turnover and subcellular localization. *eLife* (2015) 4:e11306. doi: 10.7554/eLife.11306.017

107. Schmick M, Kraemer A, Bastiaens PIH. Ras moves to stay in place. *Trends Cell Biol* (2015) 25:190–7. doi: 10.1016/j.tcb.2015.02.004

108. Dekker FJ, Rocks O, Vartak N, Menninger S, Hedberg C, Balamurugan R, et al. Small-molecule inhibition of APT1 affects Ras localization and signaling. *Nat Chem Biol* (2010) 6:449–56. doi: 10.1038/nchembio.362

109. Cuiffo B, Ren R. Palmitoylation of oncogenic NRAS is essential for leukemogenesis. *Blood* (2010) 115:3598–605. doi: 10.1182/blood-2009-03-213876

110. Zhang Z, Tan M, Xie Z, Dai L, Chen Y, Zhao Y. Identification of lysine succinylation as a new post-translational modification. *Nat Chem Biol* (2011) 7:58–63. doi: 10.1038/nchembio.495

111. Chen H, Xu H, Potash S, Starkov A, Belousov VV, Bilan DS, et al. Mild metabolic perturbations alter succinylation of mitochondrial proteins. *J Neurosci Res* (2017) 95:2244–52. doi: 10.1002/jnr.24103

112. Gibson GE, Xu H, Chen H-L, Chen W, Denton TT, Zhang S. Alpha-ketoglutarate dehydrogenase complex-dependent succinylation of proteins in neurons and neuronal cell lines. *J Neurochemistry* (2015) 134:86–96. doi: 10.1111/jnc.13096

113. Smestad J, Erber L, Chen Y, Maher LJ. Chromatin succinylation correlates with active gene expression and is perturbed by defective TCA cycle metabolism. *iScience* (2018) 2:63–75. doi: 10.1016/j.isci.2018.03.012

114. Wang G, Meyer JG, Cai W, Softic S, Li ME, Verdin E, et al. Regulation of UCP1 and mitochondrial metabolism in brown adipose tissue by reversible succinylation. *Mol Cell* (2019) 74:844–857.e847. doi: 10.1016/j.molcel.2019.03.021

115. Alleyn M, Breitzig M, Lockey R, Kolliputi N. The dawn of succinylation: a posttranslational modification. *Am J Physiology-Cell Physiol* (2018) 314:C228–32. doi: 10.1152/ajpcell.00148.2017

116. Xiangyun Y, Xiaomin N, linping G, Yunhua X, Ziming L, Yongfeng Y, et al. Desuccinylation of pyruvate kinase M2 by SIRT5 contributes to antioxidant response and tumor growth. *Oncotarget* (2016) 8(4):6984-93. doi: 10.18632/oncotarget.14346

117. Fujisaki M, Sugawara K. Properties of peptidylarginine deiminase from the epidermis of newborn rats1. *J Biochem* (1981) 89:257–63. doi: 10.1093/oxfordjournals.jbchem.a133189

118. Rogers GE, Simmonds DH. Content of citrulline and other amino-acids in a protein of hair follicles. *Nature* (1958) 182:186–7. doi: 10.1038/182186a0

119. Tilvawala R, Nguyen SH, Maurais AJ, Nemmara VV, Nagar M, Salinger AJ, et al. The rheumatoid arthritis-associated citrullinome. *Cell Chem Biol* (2018) 25:691–704.e696. doi: 10.1016/j.chembiol.2018.03.002

120. Lee CY, Wang D, Wilhelm M. Mining the human tissue proteome for protein citrullination. *Mol Cell Proteomics* (2018) 17:1378–91. doi: 10.1074/mcp.RA118.000696

121. Chang X, Han J, Pang L, Zhao Y, Yang Y, Shen Z. Increased PADI4 expression in blood and tissues of patients with Malignant tumors. *BMC Cancer* (2009) 9:40. doi: 10.1186/1471-2407-9-40

122. Yuzhalin AE, Gordon-Weeks AN, Tognoli ML, Jones K, Markelc B, Konietzny R, et al. Colorectal cancer liver metastatic growth depends on PAD4-driven citrullination of the extracellular matrix. *Nat Commun* (2018) 9:4783. doi: 10.1038/s41467-018-07306-7

123. Dalle-Donne I, Rossi R, Colombo G, Giustarini D, Milzani A. Protein S-glutathionylation: a regulatory device from bacteria to humans. *Trends Biochem Sci* (2009) 34:85–96. doi: 10.1016/j.tibs.2008.11.002

124. Dong G, Mao Q, Xia W, Xu Y, Wang J, Xu L, et al. PKM2 and cancer: The function of PKM2 beyond glycolysis. *Oncol Lett* (2016) 11:1980–6. doi: 10.3892/ol.2016.4168

125. Anastasiou D, Poulogiannis G, Asara JM, Boxer MB, Jiang J-k, Shen M, et al. Inhibition of pyruvate kinase M2 by reactive oxygen species contributes to cellular antioxidant responses. *Science* (2011) 334:1278–83. doi: 10.1126/science.1211485

126. Bader M. Serotonylation: serotonin signaling and epigenetics. *Front Mol Neurosci* (2019) 12. doi: 10.3389/fnmol.2019.00288

127. Al-Kachak A, Maze I. Post-translational modifications of histone proteins by monoamine neurotransmitters. *Curr Opin Chem Biol* (2023) 74:102302. doi: 10.1016/j.cbpa.2023.102302

128. Wang ZA, Kurra Y, Wang X, Zeng Y, Lee Y-J, Sharma V, et al. A versatile approach for site-specific lysine acylation in proteins. *Angewandte Chemie Int Edition* (2017) 56:1643–7. doi: 10.1002/anie.201611415

129. Tan M, Luo H, Lee S, Jin F, Yang JS, Montellier E, et al. Identification of 67 histone marks and histone lysine crotonylation as a new type of histone modification. *Cell* (2011) 146:1016–28. doi: 10.1016/j.cell.2011.08.008

130. Ruiz-Andres O, Sanchez-Niño MD, Cannata-Ortiz P, Ruiz-Ortega M, Egido J, Ortiz A, et al. Histone lysine crotonylation during acute kidney injury in mice. *Dis Models Mech* (2016) 9:633–45. doi: 10.1242/dmm.024455

131. Liu Y, Li M, Fan M, Song Y, Yu H, Zhi X, et al. Chromodomain Y-like protein–mediated histone crotonylation regulates stress-induced depressive behaviors. *Biol Psychiatry* (2019) 85:635–49. doi: 10.1016/j.biopsych.2018.11.025

132. Jiang G, Nguyen D, Archin NM, Yukl SA, Méndez-Lagares G, Tang Y, et al. HIV latency is reversed by ACSS2-driven histone crotonylation. *J Clin Invest* (2018) 128:1190–8. doi: 10.1172/JCI98071

133. Berger K, Moeller MJ. Mechanisms of epithelial repair and regeneration after acute kidney injury. *Semin Nephrol* (2014) 34:394–403. doi: 10.1016/j.semnephrol.2014.06.006

134. Wan J, Liu H, Ming L. Lysine crotonylation is involved in hepatocellular carcinoma progression. *Biomedicine Pharmacotherapy* (2019) 111:976–82. doi: 10.1016/j.biopha.2018.12.148

135. Chen Y, Sprung R, Tang Y, Ball H, Sangras B, Kim SC, et al. Lysine propionylation and butyrylation are novel post-translational modifications in histones*. *Mol Cell Proteomics* (2007) 6:812–9. doi: 10.1074/mcp.M700021-MCP200

136. William G, Kaelin S, McKnight L. Influence of metabolism on epigenetics and disease. *Cell* (2013) 153:56–69. doi: 10.1016/j.cell.2013.03.004

137. Garrity J, Gardner JG, Hawse W, Wolberger C, Escalante-Semerena JC. N-lysine propionylation controls the activity of propionyl-coA synthetase*. *J Biol Chem* (2007) 282:30239–45. doi: 10.1074/jbc.M704409200

138. Rousseaux S, Khochbin S. Histone acylation beyond acetylation: terra incognita in chromatin biology. *Cell J (Yakhteh)* (2015) 17:1–6. doi: 10.22074/cellj.2015.506

139. Chen X-F, Chen X, Tang X. Short-chain fatty acid, acylation and cardiovascular diseases. *Clin Sci* (2020) 134:657–76. doi: 10.1042/CS20200128

140. Xu H, Wu M, Ma X, Huang W, Xu Y. Function and mechanism of novel histone posttranslational modifications in health and disease. *BioMed Res Int* (2021) 2021:6635225. doi: 10.1155/2021/6635225

141. Li X, Yang Y, Zhang B, Lin X, Fu X, An Y, et al. Lactate metabolism in human health and disease. *Signal Transduction Targeted Ther* (2022) 7:305. doi: 10.1038/s41392-022-01151-3

142. Aksnes H, Drazic A, Marie M, Arnesen T. First things first: vital protein marks by N-terminal acetyltransferases. *Trends Biochem Sci* (2016) 41:746–60. doi: 10.1016/j.tibs.2016.07.005

143. Zhang K, Li L, Zhu M, Wang G, Xie J, Zhao Y, et al. Comparative analysis of histone H3 and H4 post-translational modifications of esophageal squamous cell carcinoma with different invasive capabilities. *J Proteomics* (2015) 112:180–9. doi: 10.1016/j.jprot.2014.09.004

144. Zhang D, Tang Z, Huang H, Zhou G, Cui C, Weng Y, et al. Metabolic regulation of gene expression by histone lactylation. *Nature* (2019) 574:575–80. doi: 10.1038/s41586-019-1678-1

145. Moreno-Yruela C, Zhang D, Wei W, Bæk M, Liu W, Gao J, et al. Class I histone deacetylases (HDAC1–3) are histone lysine delactylases. *Sci Adv* (2022) 8:eabi6696. doi: 10.1126/sciadv.abi6696

146. Yu J, Chai P, Xie M, Ge S, Ruan J, Fan X, et al. Histone lactylation drives oncogenesis by facilitating m6A reader protein YTHDF2 expression in ocular melanoma. *Genome Biol* (2021) 22:85. doi: 10.1186/s13059-021-02308-z

147. Jiang J, Huang D, Jiang Y, Hou J, Tian M, Li J, et al. Lactate modulates cellular metabolism through histone lactylation-mediated gene expression in non-small cell lung cancer. *Front Oncol* (2021) 11. doi: 10.3389/fonc.2021.647559

148. Yang D, Yin J, Shan L, Yi X, Zhang W, Ding Y. Identification of lysine-lactylated substrates in gastric cancer cells. *iScience* (2022) 25:104630. doi: 10.1016/j.isci.2022.104630

149. Farley AR, Link AJ. Chapter 40 Identification and Quantification of Protein Posttranslational Modifications. In: Burgess RR, Deutscher MP, editors. *Methods in Enzymology*, vol. 463. Cambridge, MA: Academic Press Inc (2009). p. 725–63.

150. Chuh KN, Pratt MR. Chemical methods for the proteome-wide identification of posttranslationally modified proteins. *Curr Opin Chem Biol* (2015) 24:27–37. doi: 10.1016/j.cbpa.2014.10.020

151. Stanton BZ, Chory EJ, Crabtree GR. Chemically induced proximity in biology and medicine. *Science* (2018) 359:eaao5902. doi: 10.1126/science.aao5902

152. Sakamoto KM, Kim KB, Verma R, Ransick A, Stein B, Crews CM, et al. Development of protacs to target cancer-promoting proteins for ubiquitination and degradation*. *Mol Cell Proteomics* (2003) 2:1350–8. doi: 10.1074/mcp.T300009-MCP200

frontiers | Frontiers in Oncology

TYPE Original Research
PUBLISHED 19 May 2025
DOI 10.3389/fonc.2025.1252544

OPEN ACCESS

EDITED BY
Anurag Tripathi,
Indian Institute of Toxicology Research (CSIR), India

REVIEWED BY
João Pessoa,
University of Aveiro, Portugal
Stefan Riwaldt,
Otto von Guericke University Magdeburg, Germany

*CORRESPONDENCE
Rebecca E. Schweppe
Rebecca.Schweppe@cuanschutz.edu

RECEIVED 03 July 2023
ACCEPTED 14 April 2025
PUBLISHED 19 May 2025

CITATION
Kellett MD, Sharma V, Sherlock ME, Pugazhenthi U, Rose MM, Joshi MU, Dzieciatkowska M, Nguyen V, Reigan P, Hansen KC, Kieft JS and Schweppe RE (2025) Focal adhesion kinase promotes ribosome biogenesis to drive advanced thyroid cancer cell growth and survival. *Front. Oncol.* 15:1252544. doi: 10.3389/fonc.2025.1252544

Focal adhesion kinase promotes ribosome biogenesis to drive advanced thyroid cancer cell growth and survival

Meghan D. Kellett[1], Vibha Sharma[1], Madeline E. Sherlock[2], Umarani Pugazhenthi[1], Madison M. Rose[1], Molishree U. Joshi[3,4], Monika Dzieciatkowska[5], Vu Nguyen[6], Philip Reigan[6], Kirk C. Hansen[5], Jeffrey S. Kieft[2] and Rebecca E. Schweppe[1,4]*

[1]Division of Endocrinology, Metabolism, and Diabetes, Department of Medicine, University of Colorado, Aurora, CO, United States, [2]Department of Biochemistry and Molecular Genetics, University of Colorado, Aurora, CO, United States, [3]Department of Pharmacology, University of Colorado, Aurora, CO, United States, [4]University of Colorado Cancer Center, University of Colorado, Aurora, CO, United States, [5]Division of Structural Biology and Biophysics, Department of Medicine, University of Colorado, Aurora, CO, United States, [6]Department of Pharmaceutical Sciences, Skaggs School of Pharmacy and Pharmaceutical Sciences, University of Colorado, Aurora, CO, United States

Introduction: Advanced thyroid cancer, including papillary (PTC) and anaplastic thyroid cancer (ATC), are the leading causes of endocrine cancer deaths. Thus, there is a critical need to identify novel therapeutic targets to improve standard of care. Focal Adhesion Kinase (FAK) is overexpressed and phosphorylated in thyroid cancer and drives thyroid cancer growth, invasion, and metastasis. FAK is a nonreceptor tyrosine kinase that is autophosphorylated at tyrosine 397 (Y397) in response to integrin or growth factor receptor signaling, resulting in the recruitment of SRC proto-oncogene and downstream signaling pathways. FAK is predominately localized at the plasma membrane but has recently been shown to accumulate in the nucleus as well as the nucleolus to drive tumor growth. The nucleolus is a membraneless subnuclear organelle that is involved in ribosomal biogenesis through the transcription, processing, and assembly of ribosomal RNA (rRNA). The role of FAK in ribosome biogenesis is currently unknown.

Methods: Nuclear/nucleolar FAK localization and function were studied using genetic and pharmacological approaches. High resolution microscopy was used to study the subcellular localization of FAK. Functional and biochemical assays including transformation and clonogenic assays, polysome profiling, and nascent protein synthesis assays were utilized to assess cell growth and survival. Protein-protein interactions of FAK were determined using a proximity dependent biotinylation (BioID) proteomics approach.

Results: We have found that pY397 FAK accumulates in the nucleolus of advanced thyroid cancer cells and that autophosphorylation of FAK at pY397 and FAK kinase activity are important for nucleolar accumulation of FAK. Furthermore, knockdown of nucleophosmin 1 (NPM1), an important structural component of the nucleolus, reduced pY397 FAK nucleolar accumulation. Functionally, we showed that nuclear FAK and FAK kinase activity are necessary

for anchorage independent growth. We demonstrated that targeted degradation of FAK results in decreased protein synthesis with a specific decrease in the 60S ribosomal subunit. Using a BioID proteomics approach, we showed that autophosphorylated FAK interacts with a network of nucleolar proteins including nucleolar protein 56 (NOP56) which is a core small ribonucleoprotein (snoRNP) important for 60S ribosome biogenesis. Finally, we found that pY397 FAK co-localizes with NOP56 and that knockdown of NOP56 phenocopies FAK depletion.

Conclusions: Overall, these findings highlight a novel function for FAK in promoting ribosome biogenesis and suggest that nucleolar FAK represents a promising therapeutic target.

KEYWORDS

thyroid cancer, focal adhesion kinase, nucleolus, ribosomal biogenesis, NOP56

Introduction

Thyroid cancer is the most common endocrine malignancy with 43,800 new cases reported in the United States in 2022 (1). Patients with unresectable, advanced thyroid cancer have only a 10-year survival of approximately 40-42% (2). Therefore, there is a critical need to identify novel therapeutic targets in the treatment of thyroid cancer as well as biomarkers to determine who will develop more advanced disease.

Focal Adhesion Kinase (FAK) is a promising therapeutic target that is overexpressed and phosphorylated in a variety of cancers including thyroid cancer to drive growth, survival, migration, and metastasis (3–13). FAK is a nonreceptor tyrosine kinase that interacts with growth factor receptors and integrins to promote the autophosphorylation of tyrosine 397 (pY397) FAK which recruits SRC proto-oncogene (SRC) and leads to the activation of downstream signaling pathways (14). FAK possesses a nuclear localization sequence (NLS) and has been shown to accumulate in the nucleus to drive survival, regulate inflammation, and promote immune evasion (15–17). Nuclear pY397 FAK has been correlated with decreased survival and poor prognosis in colorectal cancer and in breast cancer (18, 19). Interestingly, pY397 FAK has recently been shown to accumulate in the nucleolus in breast cancer to regulate cell growth through the nucleolar protein, nucleostemin (20). However, it remains to be determined whether FAK regulates ribosomal biogenesis which is the primary function of the nucleolus.

The nucleolus is the largest membrane-less organelle in the nucleus and is responsible for the transcription, processing, and assembly of ribosomal RNA (rRNA) to synthesize ribosomes (21). Cancer cells possess an increased number and size of nucleoli to promote rRNA transcription and protein synthesis, which are necessary to support the increased demands of tumor growth. The eukaryotic ribosome is comprised of the small subunit (40S) and large subunit (60S). The 40S subunit is formed by the 18S rRNA and 33 ribosomal proteins while the 60S subunit is formed by the 5S, 5.8S, and 28S rRNAs and 46 ribosomal proteins (22). The nucleolus is highly structured and is composed of three regions: the fibrillarin center (FC), the dense fibrillarin compartment (DFC), and the granular component (GC) (23). In the FC, ribosomal DNA (rDNA) is transcribed by RNA Polymerase I (POLI) to produce a long primary transcript, 47S pre-rRNA (21). In the DFC, the primary transcript undergoes processing and cleavage of the internal transcribed spacer 1 and 2 (ITS1 and ITS2) and 5' and 3' external transcribed spacers (5'- ETS1 and 3'-ETS2) to form the 18S, 5.8S, and 28S rRNAs (21, 22). Furthermore, core box c/d small ribonucleoproteins (snoRNPs), including fibrillarin (FBL), nucleolar protein 56 (NOP56), and nucleolar protein 58 (NOP58), promote the 2'-O-methylation of pre-rRNAs to influence assembly and function of the 60S ribosome (24). In the GC, rRNA in combination with ribosomal proteins forms pre-ribosomal subunits to be exported to the cytoplasm.

This study defines the localization and function of FAK in the nucleolus in advanced thyroid cancer. First, we identified that nuclear and phosphorylated FAK are required for anchorage independent growth. We discovered that pY397 FAK is localized to the nucleolus in thyroid cancer cells and that phosphorylation of Y397 FAK and NPM1 are important for FAK nucleolar accumulation. We found that targeted degradation of FAK decreases clonogenic growth as well as decreases global protein synthesis, actively translating ribosomes, and 60S large ribosomal subunits. Furthermore, we identified that pY397 FAK co-localizes with NOP56, a core snoRNP involved in 60S ribosome biogenesis, as a potential mediator to regulate clonogenic growth. Together, our data demonstrate that nucleolar FAK promotes ribosome biogenesis and protein synthesis to drive thyroid cancer growth and survival, and thus presents a promising therapeutic target to treat thyroid and other FAK-driven cancers.

Materials and methods

Cell lines and culture conditions

All cell lines were authenticated by Short Tandem Repeat DNA profiling using the Applied Biosystems Identifier kit (#4322288) or Globalfiler® System (#4476135) at the University of Colorado Barbara Davis Center (BDC) Bioresources Core and tested for mycoplasma using the Mycoalert system (Lonza Bioscience). STR genotypes were compared to previously published data by our lab (25, 26). Cells were not used past passage 20. BCPAP (RRID: CVCL_0153) cells were kindly provided by Dr. M. Santoro, respectively, in 2007. Dr. J. Fagin kindly provided 8505C (RRID: CVCL_1054) cell lines in 2007. KTC1 (RRID: CVCL6300) and KTC2 (RRID: CVCL_6476) cells were generously provided by Dr. Kurebayashi in 2008. HCT116 TP53 isogenic cell lines including HCT116 TP53 (+/+), HCT116 TP53 (-/-), HCT116 TP53 (R248W/+), and HCT116 TP53 (R248W/-) (RRID: CVCL_0291, CVCL_HD97, CVCL_RJ69, and CVCL_RJ68 respectively) were generously provided by Dr. N. Papadopoulas in 2024 through the Johns Hopkins Biorepository & Cell Center. Human thyroid cancer cells (BCPAP, 8505C, KTC1, KTC2, C643 (RRID: CVCL_5969), ACT1 (RRID: CVCL_6291), CUTC5 (RRID: CVCL_W916), and CUTC60 (RRID: CVCL_VM61) were grown in RPMI1640 (Invitrogen) with 5% Fetal Bovine Serum (FBS). HEK293T cells (RRID: CVCL_0063) were grown in DMEM (Invitrogen) with 10% FBS (Invitrogen). Human colorectal HCT116 TP53 isogenic cell lines were grown in McCoy's 5A Medium (Invitrogen) with 10% FBS (Invitrogen). All cells were grown in 5% CO_2 at 37° C. KTC1 and CUTC5 were derived from pleural effusions of PTC patients. BCPAP cells were derived from a lymph node metastasis from a PTC patient. 8505C, KTC2, and CUTC60 were derived from ATC human tissue.

Generation of FAK CRISPR/Cas9 cell lines

FAK (*PTK2*) was knocked out in the BCPAP cells using the Horizon Discovery system (Cambridge, UK). Small guide RNAs (sgRNAs) were designed using the MIT CRISPR selection tool (http://crispr.mit.edu/) and are listed in Supplementary Table 1. Cells were transfected with pD1301-AD:156638, which expresses Cas9, GFP, and the indicated sgRNAs targeting FAK, using Turbofect (Invitrogen, R0531) according to manufacturer's directions. Transfection efficiency was measured by GFP visualization. 72 hours after transfection, genomic DNA was harvested using a Quick guide DNA miniprep kit (ZYMO, D3025), and mutations were screened using the SURVEYOR Mutation Detection assay (IDT, 706025). FAK-KO was confirmed by SANGER sequencing, Western blot, and qPCR analysis. The gRNA sequence used in this study is 5'-ATAATACTGGCCCAGGTGGT-3'. The identity was confirmed by STR genotyping, as above.

pLentiV5-FAK cloning

pBabe-puro-FAK constructs expressing WT-avian-FAK, the Y397F and K454R mutants were generously provided by Dr. Filippo G. Giancotti (27). WT-, Y397F-, or K454R-FAK sequences were amplified by PCR and cloned into pLenti6/V5-D-TOPO according to manufacturer's directions (Invitrogen, K4955). The primers are listed in Supplementary Table 1. The 3' PCR primer was designed to correct a missing G at 3' end. The FAK-nuclear localization mutant (NLM) in which the R177A, R178A, K190A, K191A, K216A, K218A sites were mutated and cloned into pLenti6/V5-D-TOPO, as above. Sequences were confirmed by SANGER sequencing in the University of Colorado BDC core. Lentivirus were packaged using Effectene Transfection Reagent (Qiagen) according to the manufacturer's instructions. FAK-KO cells were transduced with lentivirus in presence of 8μg/mL of polybrene and selected with 10μg/mL blasticidin. Stable cell lines were validated by STR genotyping, as above.

Lentiviral transduction and knockdowns using mission shRNA

Lentiviruses were packaged using Effectene Transfection Reagent (Qiagen) according to the manufacturer's instructions. Cells were transduced with lentivirus in presence of 8μg/mL of polybrene and selected with 2mg/ml puromycin for 8505C or 1μg/ml puromycin for KTC2 cells. The shRNA TRC IDs are listed in Supplementary Table 2. Confirmation of lentiviral transductions and knockdowns were validated by immunoblotting to indicate presence of transgene or absence of protein respectively.

Reagents

FAK PROTAC I (CAS 2301916-69-6) was obtained from MedChem Express. All antibodies used for immunoblotting and immunofluorescence are listed in Supplementary Table 3.

Immunoblotting

Total protein was harvested in CHAPS lysis buffer (10 mM CHAPS, 50 mM Tris (pH 8.0), 150 nM NaCl, and 2 mM EDTA) with phosphatase and protease inhibitor cocktail (Roche). Protein was separated on an SDS polyacrylamide gel electrophoresis and transferred to Immobilon-FL polyvinylidene fluoride (PVDF) membrane (Millipore). Primary antibody incubation was performed overnight at 4°C with indicated antibodies in 5% bovine serum albumin (BSA) in TBST. Antibodies used in western blotting include pY397 FAK (Invitrogen), total FAK (BD Biosciences), NPM1 (Abcam), NOP56 (Abcam), TAMRA (Invitrogen), p53 (Cell Signaling), pY402 PYK2 (Invitrogen), total PYK2 (Cell Signaling), α-tubulin (Sigma), and vinculin (Cell Signaling). Secondary antibodies of goat anti-rabbit or goat anti-mouse IRDye (LI-COR) were applied for one hour at room temperature. Blots were imaged using the LI-COR Odyssey Imaging System and ImageStudiov4.1 software. Immunoblotting was performed in at least 2 independent biological replicates for each experiment. All antibodies used for immunoblotting are listed in Supplementary Table 3.

Immunofluorescence

15,000-40,000 cells were grown on 8-well chamber slides for 48 hours prior to fixation with 4% paraformaldehyde (PFA) (Invitrogen) for 15 minutes, permeabilization with 0.5% Triton-X (Sigma) for 10 minutes, blocking with 5% normal goat serum (NGS) (Invitrogen), and incubation with primary antibodies against V5 (Cell Signaling), HA (Cell Signaling), Total FAK (BD Biosciences), pY397 FAK (Invitrogen), and fibrillarin (Invitrogen) overnight at 4° C. Slides were then incubated for one hour with Alexa Fluorophores 488 Goat Anti-Rabbit (Invitrogen) at 1:500 and Alexa Fluor 555 Goat Anti-Mouse (Invitrogen) at 1:500 dilution followed by staining with DAPI (3 µg/mL) (Invitrogen) for 30 minutes. Chambers were then removed, and samples were cured with Prolong Diamond Anti-Fade Mounting Media (Invitrogen). Images were acquired using the FV1000 Olympus Confocal Microscope with 60X or 100X objectives at the University of Colorado Advanced Light Microscopy Core (ALMC). For high resolution microscopy, thyroid cancer cells were plated on 1.5H coverslips (MatTek), and fixed, permeabilized, and blocked as stated above. Secondary antibodies of Star Red and Star Orange (Abberior) were utilized at 1:200 dilution. Images were acquired on STED Abberior Stedycon Instrument in the ALMC. In all experiments, at least 30 cells were imaged from at least two independent biological replicates. All antibodies used for immunofluorescence are listed in Supplementary Table 3.

Structural modeling of FAK

A homology model of human FAK kinase and FERM domain was constructed from the human FAK sequence using the avian (*gallus gallus)* Protein Data Bank of [2J0J] and [6CB0], using the Prime module of Schrodinger release 2022-4 (19, 28–31). The resulting model was subjected to an energy minimization, referred to as the "parent" homology model. The parent homology model was separately altered with mutations in the nuclear localization sequence of FAK (comprising of R177A/R178A, K190A/K191A, K204A/K205A, and K216A/K218A), referred to as the "NLM FAK mutant". The NLM FAK mutant was subjected to energy minimizations and overlaid onto the parent model to evaluate secondary structural changes that arise from the mutations. Structures, domains, regions, and residues of interest were labelled (32, 33).

Proximity-dependent biotin identification mass spectrometry

WT FAK and Y397F FAK were cloned to the C-terminus of BioID2 in myc-BioID2-MCS (kindly provided by Kyle Roux; RRID: Addgene plasmid #74223). FAK was amplified using primers listed in Supplementary Table 1 and cloned using Gibson Assembly (NEB E5510S) into the BioID2 vector cut with EcoRI and BamHI. SANGER sequencing was performed to verify sequence identity. Lentiviruses were packaged using Effectene Transfection Reagent (Qiagen) according to the manufacturer's instructions, and virus was transduced into BCPAP thyroid cancer cells. Cells were selected with 0.5mg/ml G418 to create stable clones. 4.0 x 10^6 BCPAP cells were plated and treated with 16 hours of 50 mM of EZ-Link Biotin (Invitrogen) prior to harvesting in BioID lysis buffer (50mM Tris, 500mM NaCl, 0.2% SDS, 1mM DTT, and 1X protease/phosphatase inhibitor). Lysates were pulled down with streptavidin-magnetic beads (Dynabeads MyOne Streptavidin T1, Invitrogen). Mass Spectrometry was performed in the University of Colorado Cancer Center Mass Spectrometry Proteomics Shared Resource (RRID: SCR_021988) using the Qexactive HF Orbitrap coupled to the nanoEasy 1000 chromatography system as described (34). Two independent experiments were performed. Data analysis included spectral processing and identification using the Mascot search program. Subtraction of proteins identified in the vector control samples along with CRAPome database was used to identify common nonspecific interactors. Data analysis included spectral processing and subtraction of proteins identified in the vector control samples with CRAPome database to identify common nonspecific interactors. Gene Ontology and String Analysis were performed on proteins that were identified in both datasets with a spectral count greater than two-fold of the WT versus EV.

RNA isolation and quantitative RT-PCR

1.2x10^6 KTC1 cells and 1.0x10^6 KTC2 cells were plated in 10 cm dishes and treated with 0, 4, 8, or 16 hours of FAK PROTAC. RNA was isolated with the RNeasy Mini Kit followed by on-column DNase digest (Qiagen). cDNA was synthesized using the High-Capacity c-DNA Reverse Transcription kit (ABI-P/N 4368814). Real time PCR reactions were carried out in MicroAmp optical 96-well reaction plates (PE ABI-N8010560) in a 20 µl mix containing 1X-Power SYBR™ Green PCR master mix (Life Technologies 4367659), 250 nM forward primer, 250 nM reverse primer and 5 µl template cDNA. The mRNA for 28S, 18S, and 5.8S were measured by real-time quantitative RT-PCR using ABI QuantStudio 7 flex Sequence detector in the University of Colorado PCR core. Thermal cycling conditions were as follows: Initiation was performed at 50°C for 2 min followed by activation of TaqGold at 95°C for 10 min. Subsequently 40 cycles of amplification were performed at 95°C for 30 secs followed by 60°C for 30 secs and 72°C for 30 secs. Melt curve analysis was performed to confirm the specificity of the amplicons for each target. Quantities of targets in test samples were normalized to the corresponding h*GAPDH* (Life Technologies-4448489). All primer sequences are provided in Supplementary Table 1. Three independent biological replicates were performed for each experiment.

Polysome profiling

3 x 10^6 BCPAP, 1.5 x 10^6 8505C, 3 x 10^6 KTC1, or 2.5 x 10^6 KTC2 cells were plated in 6 x 15 cm dishes and treated with

DMSO or 1 µM FAK PROTAC for 24 or 48 hours. Cell confluency was approximately 70% at the time of harvest. The culture media was supplemented with 100 µg/mL cycloheximide (CHX) (Sigma) for 10 minutes prior to lysis with polysome preparation lysis buffer (20 mM HEPES pH 7.4, 15 mM $MgCl_2$, 200 mM NaCl, 1% Triton X-100, 100 µg/ml CHX, 2 mM DTT, and 100 U RNasin) to halt translation. Supernatants were collected after centrifugation at 16,000 x *g*, 4°C for 15 minutes and 400 µl were loaded on 10–60% sucrose gradients in SW41 tubes in lysis buffer lacking Triton-X-100. Samples were ultracentrifuged at 160,000 × *g* for 3 hours at 4 °C and then fractionated using a BioComp system at 4°C, monitoring absorbance at 260 nm. Three independent biological replicates were performed in KTC2 cells and at least two replicates were performed in BCPAP, 8505C, and KTC1 cells.

Nascent protein synthesis assays

1.2 x 10^6 BCPAP, 0.8 x 10^6 8505C, 1.2 x 10^6 KTC1, 1.0 x 10^6 KTC2 cells, and 2.5 x 10^6 HCT116 TP53 isogenic cell lines were plated in 10 cm dishes and treated with DMSO or 1 µM FAK PROTAC for 24, 48, or 72 hours. At the end of the time point, cells were washed twice with PBS and incubated with methionine-free RPMI media (Invitrogen) for one hour. Cells were pre-treated with water or 10 µg/ul of Cyclohexamide (CHX) (Sigma) for 30 minutes prior to a one-hour incubation with 50 µM of L-Homopropargylglycine (HPG) (Invitrogen). Lysates were incubated with 4 mM of tetramethylrhodamine (TAMRA) using the Protein Synthesis Click-it Kit (Invitrogen). Immunoblotting of lysates with antibodies against TAMRA and vinculin were utilized to assess nascent protein synthesis and loading. Three independent biological experiments were performed for each experiment.

Colony formation assay

100–1000 cells were seeded in 6-well plates. Cell medium was changed every 3–4 days for 10–14 days. Colonies were fixed (10% methanol/10% acetic acid) and stained with 0.4% crystal violet. Crystal violet was dissolved in fixative and absorbance was measured at 570 nm using Odyssey CLx imager (Image Studio Acquisition Software Version 5.2.5, LICOR). Three independent biological replicates were performed for each experiment.

Statistical consideration

Statistical analyses and P value calculations were performed using Graphpad Prism v8. Quantitative data are expressed as mean +/- standard error of the mean unless otherwise noted. Analysis of variance (ANOVA) was used to identify significant differences in multiple comparisons. Paired *t*-tests were used to compare two groups. All experiments were completed in at least two independent experiments with statistical tests calculated on at least 3 independent biological replicates. For all statistical analyses, the level of significance was set at 0.05. Unless otherwise noted, ns=not significant, * = $p < 0.05$, ** = $p < 0.01$, *** = $p < 0.001$, **** = $p < 0.0001$.

Results

Nuclear FAK and FAK kinase activity are required for anchorage independent growth

Given that nuclear pY397 FAK has been correlated with poor survival in colorectal and breast cancer, we aimed to determine the role of nuclear FAK in thyroid cancer. To specifically study nuclear FAK in cells devoid of endogenous FAK, we generated a FAK knockout (FAK-KO) model in the *BRAF*-mutant BCPAP thyroid cancer cell line using CRISPR/Cas9. As expected, these cells successfully knocked out FAK protein ($p<0.0001$) and well-characterized phosphorylation sites, including the Y397 autophosphorylation site, the Src-dependent Y925 site, and S910, which is a MAPK-dependent site (Figure 1A; Supplementary Figure 1A**).** Consistent with our previously published data using shRNA to knockdown FAK, FAK-KO decreased thyroid cancer adherent growth by 55% (Figure 1B, not significant) and nearly ablated anchorage independent growth by 25-fold ($p < 0.01$) (35) (Figure 1C). To determine the specific role of nuclear FAK in growth and survival, we rescued the FAK-KO cells by transducing with empty vector (EV), wild type FAK (WT), a nuclear localization mutant of FAK to exclude FAK from the nucleus (NLM), in which the NLS was mutated, a non-phosphorylatable FAK mutant (Y397F), and a kinase dead FAK (KD). We confirmed similar levels of WT FAK expression among the rescues and confirmed significantly decreased pY397 FAK expression levels in the Y397F FAK and KD FAK rescues compared to the WT ($p<0.05$) (Figure 1D; Supplementary Figure 1B). Finally, we confirmed that the FAK-NLM successfully excluded pY397 FAK from the nucleus by immunofluorescence (Figure 1E). To determine the functional role of nuclear FAK, we performed soft agar transformation assays and found that WT FAK is sufficient to rescue soft agar in the FAK-KO cells. However, excluding FAK from the nucleus (FAK-NLM), expression of a Y397F autophosphorylation mutant, or kinase dead FAK, failed to rescue soft agar ($p<0.001$) (Figure 1F). Together, these data indicate that nuclear FAK, along with FAK autophosphorylation and kinase activity are necessary for anchorage independent growth, which is phenocopied by loss of FAK autophosphorylation and kinase activity.

In Figure 1, we observed that pY397 FAK exhibited punctate nuclear staining in the FAK-WT rescue cells but not in the nuclear-localization mutant (FAK-NLM) cells. NLS sequences can serve as nuclear as well as nucleolar localization sequences for proteins (36–38). To further delineate the importance of the NLS on FAK structure, we performed structural modeling of the avian-based FAK model. We found that modeling global mutations in the NLS (R177/178A, K190/191A, K204/205A, and K216/218A) promote β-sheet disordering around the regions of 399–402 compared with the

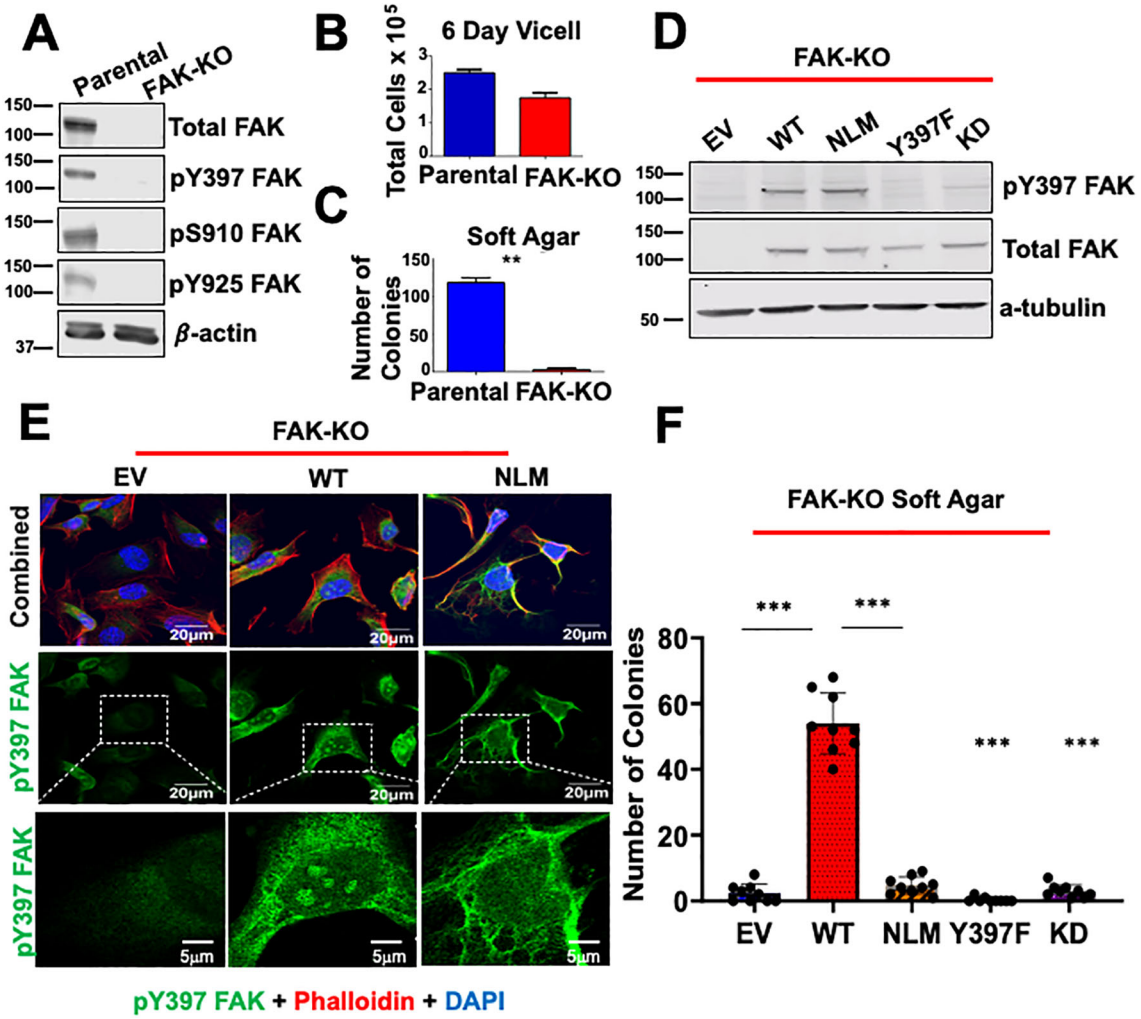

FIGURE 1
Excluding FAK from the nucleus decreases anchorage independent growth. **(A)** Parental and FAK Knockout CRISPR cells (FAK-KO) were immunoblotted with antibodies against pY397 FAK, pS910, pY925, total FAK, and β-actin. Molecular weight (MW) marker is shown on the left of each blot in kiloDaltons (kDa). **(B)** Parental and FAK-KO cells were plated for a 6 Day Vi-cell and total number of cells per mL was recorded. **(C)** Soft agar transformation assays were performed for parental and FAK-KO cells with the number of colonies counted after three weeks. **(D)** FAK-KO cells transduced with EV, WT FAK, NLM FAK, Y397F FAK, and KD FAK were immunoblotted with antibodies against pY397 FAK, total FAK, and α-tubulin. MW marker is shown on the left of each blot in kDa. **(E)** FAK-KO cells transduced with EV, WT FAK, and NLM FAK were stained with antibodies against pY397 FAK, Phalloidin, and DAPI prior to imaging at 60X with scale bar at 20μm. Inserts of zoomed in images have a scale bar of 5μm. At least 50 cells were imaged in three independent experiments. **(F)** FAK-KO CRISPR cells transduced with EV, WT FAK, NLM FAK, Y397F, and K454R were grown in soft agar assays, and the number of colonies were counted after three weeks. Experiments were performed in biological triplicates. Results are displayed as mean +/- SEM. **p < 0.01; ***p < 0.001.

parental structure (Supplementary Figure 2). Thus, these data suggest that the NLS of FAK is important for the structure around the pY397 FAK residue, which could regulate nuclear and/or nucleolar accumulation.

pY397 FAK is present in the nucleolus of thyroid cancer cells and is important for nucleolar accumulation of FAK

Given the subnuclear punctate accumulation of pY397 FAK, we next aimed to investigate the accumulation of pY397 FAK in a panel of thyroid cancer cells with BRAF V600E and RAS mutations. BRAF V600E mutations occur in approximately 50-70% of PTC, and mutations in RAS occur in approximately 40-50% in FTC (39). We found that a fraction of pY397 FAK co-localizes with the nucleolar marker, FBL, in the panel of *BRAF*- and *RAS*-mutant thyroid cancer cell lines derived from PTC or ATC tumors (Figure 2A; Supplementary Figure 3). We next evaluated the accumulation of total FAK in thyroid cancer cell lines expressing BRAF V600E mutations due to their association with recurrence, extrathyroidal extension, advanced stage, and distant metastases in thyroid cancer (26, 39). While we found pY397 FAK specifically localizes in the nucleolus, we found that total FAK is distributed throughout the nucleus (Figure 2B). Thus, these data suggest that pY397-FAK is enriched in the nucleolus in advanced thyroid cancer

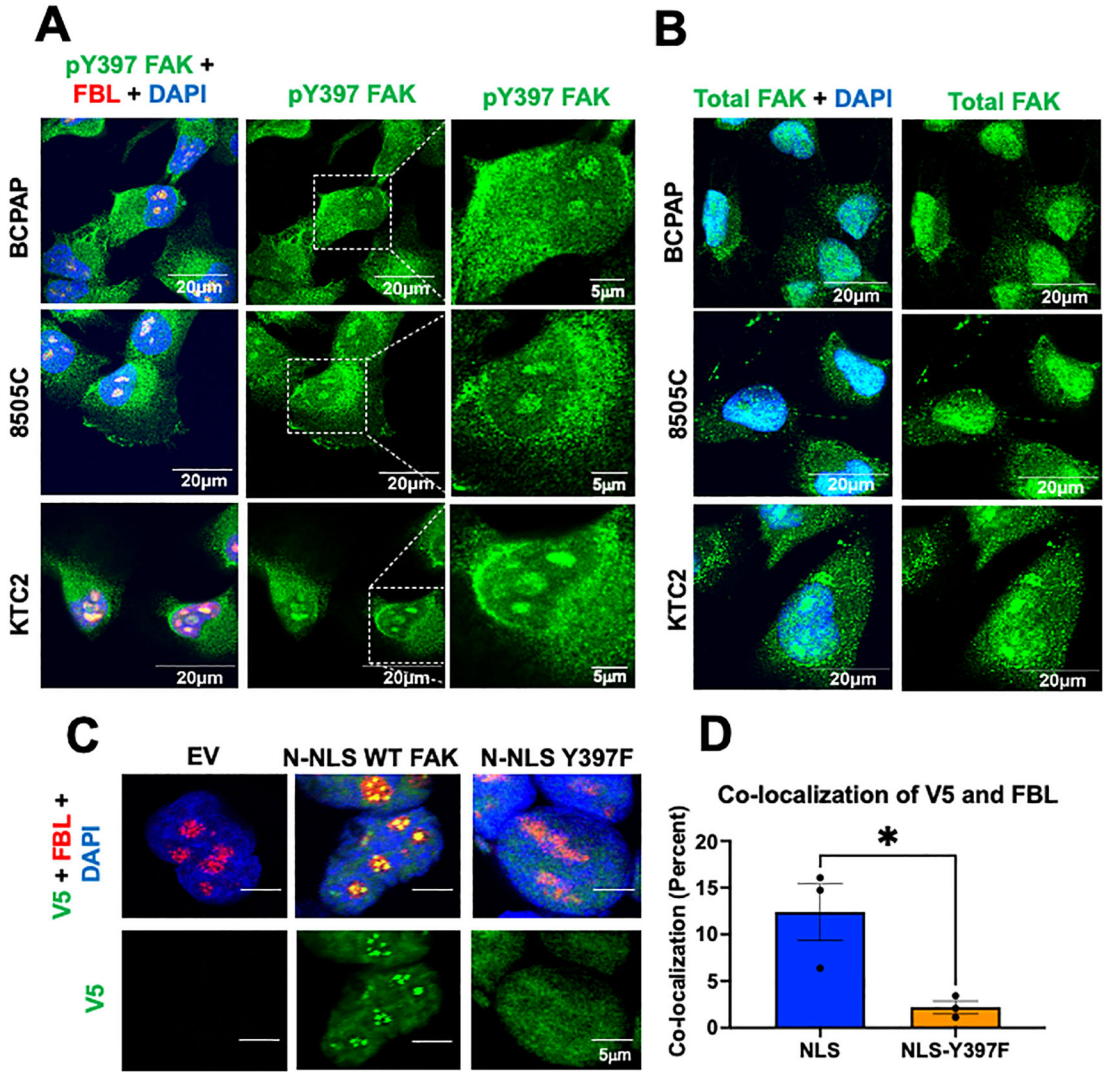

FIGURE 2
pY397 FAK localizes to the nucleolus and influences nucleolar FAK accumulation **(A)** BCPAP, 8505C, and KTC2 cells were stained with antibodies against pY397 FAK, FBL, and DAPI prior to confocal imaging at 100X. **(B)** BCPAP, 8505C cells, and KTC2 cells were probed with antibodies against total FAK and DAPI prior to imaging at 100X confocal. Results shown are representative images from 20–30 images taken in at least two independent experiments. Scale bar represents 20μM. **(C)** FAK-KO cells transduced with EV, N-terminal NLS FAK, and N-terminal NLS-Y397F were probed with antibodies against V5, Fibrillarin, and DAPI prior to imaging at 100X on Olympus Confocal. At least 50 cells were imaged in three independent experiments. Scale bars represent 5μm. **(D)** Percent of co-localization between V5 and FBL in NLS versus NLS-Y397F KO-FAK transduced cells using Integrated Density Analysis by Image J. Results displayed as mean +/- SEM. *, $p<0.05$.

cells, while total FAK is localized throughout the nucleus, as previously observed (15, 17) suggesting that pY397-FAK plays a specific role in the nucleolus.

The phosphorylation of proteins has been shown to facilitate nucleolar accumulation (40, 41). Therefore, we asked if pY397 FAK is important for nucleolar accumulation of FAK. Given that NLS sequences can serve as nuclear as well as nucleolar localization sequences for proteins, we fused 3 NLS sequences (PKKKRKV) from an SV40 NLS onto the N-terminus of WT FAK (NLS-FAK) or a non-phosphorylatable FAK mutant (NLS-Y397F-FAK) plasmid which possess a V5 tag and transduced these constructs into the FAK-KO CRISPR BCPAP cell line. We confirmed that these constructs are sufficient to induce nuclear FAK accumulation (Supplementary Figure 4A). Notably, we found that expression of NLS-WT-FAK results in discrete punctate localization of FAK that specifically co-localizes with the nucleolar marker, fibrillarin (FBL) (Figure 2C). Thus, 3x NLS is sufficient to induce nucleolar FAK accumulation. Next, we targeted FAK into the nucleus with a non-phosphorylatable Y397F-FAK mutant. Interestingly, we found that the NLS-Y397F-FAK resulted in significantly decreased nucleolar FAK accumulation (3- fold decrease) ($p<0.05$) (Figure 2C, D), indicating that pY397 FAK is important for nucleolar accumulation. To corroborate our results, we utilized an additional model with NLS fused to the C-terminus of the WT FAK or NLS-Y397 FAK and similarly found that targeting FAK to the nucleus increases nucleolar FAK which is reduced in the NLS-Y397F-FAK (Supplementary Figure 4B). Overall, these data indicate that pY397 is localized in the nucleolus of advanced

thyroid cancer cells and pY397 FAK is important for FAK nucleolar accumulation.

NPM1, a key protein of the granular component, contributes to pY397 FAK accumulation in the nucleolus

The nucleolus is a highly compartmentalized organelle with each layer representing a different nucleolar function. To better define the localization and subsequent function of nucleolar pY397 FAK, we performed high resolution 2D stimulated emission depletion (STED) microscopy with antibodies against nucleophosmin 1 (NPM1), fibrillarin (FBL), and upstream binding transcription factor (UBTF) as markers for the granular component, dense fibrillarin component, and fibrillarin center respectively. We found that pY397 FAK accumulates in all three nucleolar layers and is potentially enriched in the granular component, with a >10% co-localization with NPM1 in this representative cell line (Figure 3A, B, 2.5-fold enrichment, not statistically significant). pY397 FAK also co-localizes with FBL (fibrillarin center marker) and UBTF (dense fibrillarin layer marker) at <5% (Figure 3A, B). Given the potential enrichment of pY397 FAK in the granular component, we focused on the role of FAK in the granular component. To assess if the granular component is necessary for FAK accumulation, we knocked down *NPM1* with three different shRNAs and confirmed expression by western blot. The protein expression of pY397 FAK and total FAK was not affected by *NPM1* knockdown (Figure 3C). Upon *NPM1* knockdown, we observed a notable decrease in pY397 FAK nucleolar accumulation (Figure 3D, E). Thus, NPM1 which is the critical component of the granular compartment contributes to pY397 nucleolar accumulation.

Targeted FAK degradation decreases protein synthesis, translation, and clonogenic growth

We next evaluated the regulation of ribosome biogenesis and protein synthesis by FAK. To quickly and selectively target FAK, we used a proteolysis targeting chimera (PROTAC) approach, which utilizes the ubiquitin proteasome system, to degrade a protein of interest. Furthermore, PROTACs are emerging as a new therapeutic approach in precision medicine (42). The FAK PROTAC consists of the FAK kinase inhibitor, defactinib, fused via a linker to the von Hippel-Lindau (VHL) E3 Ligase to specifically target and degrade FAK. With targeted degradation of FAK, we found an effective decrease in total FAK protein within 4 hours of FAK PROTAC treatment and a corresponding decrease in pY397 FAK expression in 24 hours in *BRAF*-mutant, KTC1 and KTC2, thyroid cancer cells (Figure 4A). Residual pY397 FAK expression upon treatment with FAK PROTAC may be due to cross-reactivity of this antibody with the highly related kinase, PYK2 (*PTK2B*) (43). We also found that degradation of FAK did not significantly alter the transcription of the mature 18S, 28S, or 5.8S rRNAs which is expected given the long half-life of rRNAs of 3 to 7 days (44) (Supplementary Figure 5A). To assess if the targeted degradation of FAK impacts the association of mRNA and ribosomes, we then performed polysome profiling with sucrose gradients. At baseline, the polysome traces of the KTC2 and KTC1 cells show an imbalance in subunit abundance with a higher 40S/60S ratio, along with the presence of polysomes, indicating active translation (Figure 4B). Upon targeted FAK degradation, we identified a significant reduction of the 60S large ribosomal subunit ($p<0.05$) and loading of mRNA on polysomes ($p<0.001$), indicating a decrease in active translation in KTC2 cells and similar trend in KTC1 cells (Figure 4B; Supplementary Figure 5B). Accordingly, we found a >50% decrease in global nascent protein synthesis upon FAK degradation in the presence of the methionine analog, HPG, in KTC2 and KTC1 cells (Figure 4C). This decrease in protein synthesis is likely not due to a global decrease in cell growth, as we only observed a ~20% reduction in cell number at 24 hours (Supplementary Figure 5C). However, loss of FAK leads to a decrease in cell growth at later time points with a 40-60% inhibition of cell number at 3 and 6 days (Supplementary Figure 5C). Finally, we observed a 4-fold decrease and 2.5-fold decrease in clonogenic growth in KTC2 and KTC1 cells, respectively, upon 14 days of 1 μM FAK-PROTAC treatment compared to DMSO ($p<0.01$) (Figure 4D). Together, our data indicate that FAK regulates 60S ribosomal biogenesis, impacting loading of mRNA on polysomes, nascent protein synthesis, and ultimately thyroid cancer growth.

Next, we addressed the role of FAK degradation in the *BRAF*-mutant thyroid cancer cells, BCPAP and 8505C. While we identified that FAK PROTAC successfully degraded FAK within 24 hours of treatment, we found no effect on polysome profiling, nascent protein synthesis, or clonogenic growth in these cell lines (Supplementary Figure 6). Of note, KTC1 and KTC2 cells express *TP53-WT* while BCPAP and 8505C cells express mutant-*TP53* (26). We hypothesized that this difference in ribosome biogenesis may be due to *TP53*-status as *TP53* actively regulates various stages of ribosome biogenesis, and *TP53*-mutant cells promote increased ribosome biogenesis compared to *TP53*-WT cells (45, 46). However, there was no difference in nascent protein synthesis in isogenic colorectal *TP53* HCT116 cell lines upon degradation with a FAK PROTAC at 24 and 48 hours (Supplementary Figure 7). Thus, further investigation is warranted to investigate the underlying differences between these cell lines.

pY397 FAK co-localizes with NOP56 as a potential mediator to regulate 60S biogenesis and thyroid cancer growth

To investigate how FAK regulates 60S active translation, we utilized proximity-based biotinylation mass spectrometry to identify interacting partners of FAK. Through this approach, we fused a promiscuous biotin ligase (BioID2) to wild type FAK (WT) or a non-phosphorylatable FAK mutant (Y397F) (Figure 5A) (47). Upon addition of biotin, proteins that come within approximately 10 nm of FAK are biotinylated, pulled down, and identified by mass spectrometry. First, we confirmed expression of the 27kDa BioID2 construct fused to WT or Y397 FAK by immunoblotting

10.3389/fonc.2025.1252544

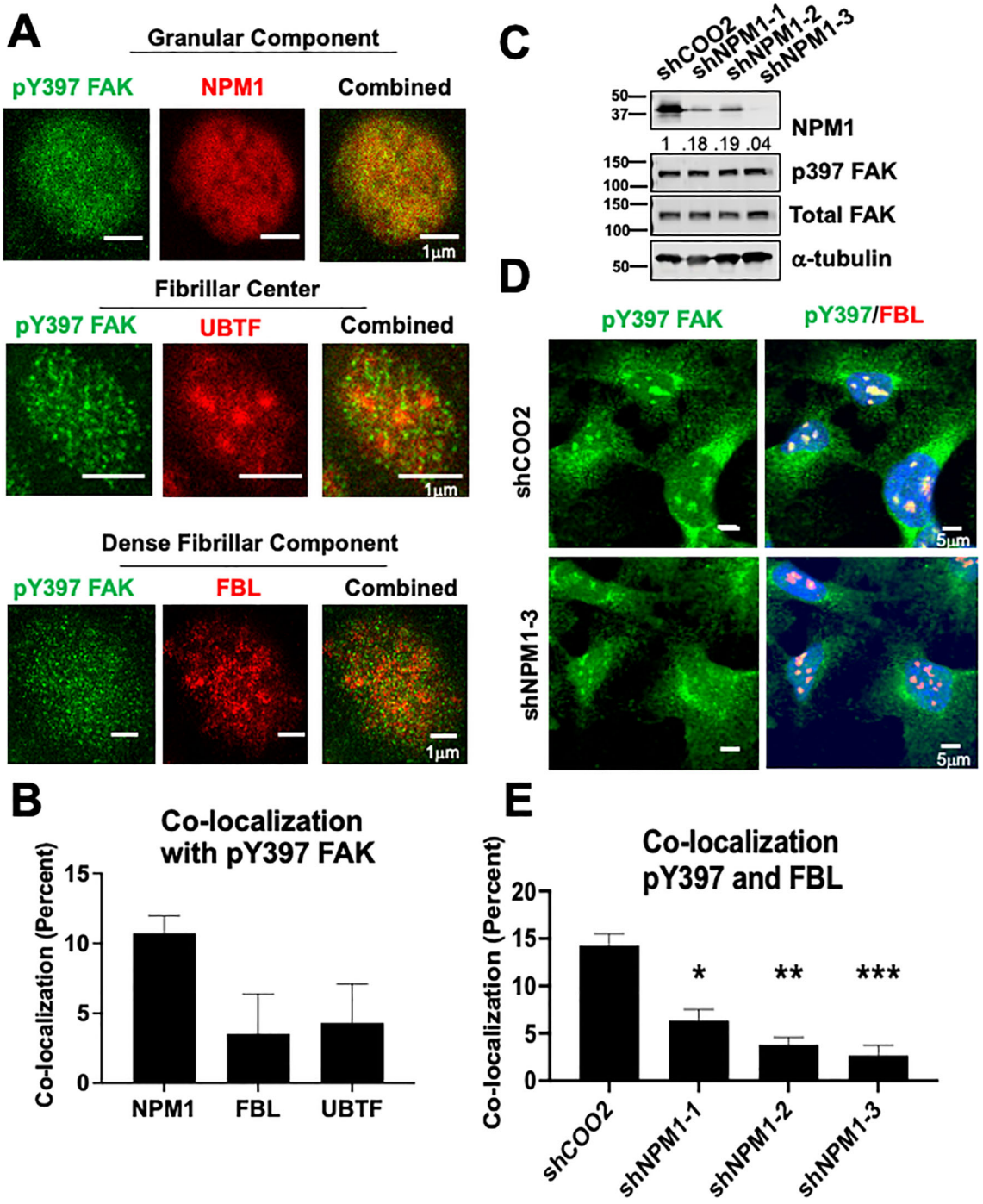

FIGURE 3
NPM1 is necessary for pY397 FAK localization to the nucleolus in adherent cells **(A)** BCPAP cells were probed with antibodies against NPM1, FBL, and UBTF and imaged using STED microscopy. At least 50 cells were visualized in three independent experiments. Scale bar represent 1µm. **(B)** Percent of co-localization between pY397 FAK and NPM1, UBTF, and FBL respectively using Integrated Density Analysis by Image J.**(C)** 8505C cells were knocked down with either a non-targeting control or three shRNAs targeting NPM1 prior to immunoblotting with antibodies against NPM1, pY397 FAK, total FAK, or α-tubulin. Quantification of NPM1 expression is normalized to α-tubulin and sh-COO2 control and is listed under the NPM1 blot. MW marker is shown on the left of each blot in kDa. Two independent experiments were performed. **(D)** Immunofluorescence was performed in 8505C shCOO2 or shNPM1 cells probed with antibodies against pY397 FAK, FBL, and DAPI. Cells were imaged at 60X confocal imaging in three independent experiments with visualization of at least 50 cells. Scale bar represent 5 µm. **(E)** Percent of co-localization between pY397 FAK and FBL in our non-targeting controls and shNPM1 knockdown cells using Integrated Density Analysis by Image J. Results displayed as mean +/- SEM. *, $p<0.05$; **$p < 0.01$; ***$p < 0.001$.

10.3389/fonc.2025.1252544

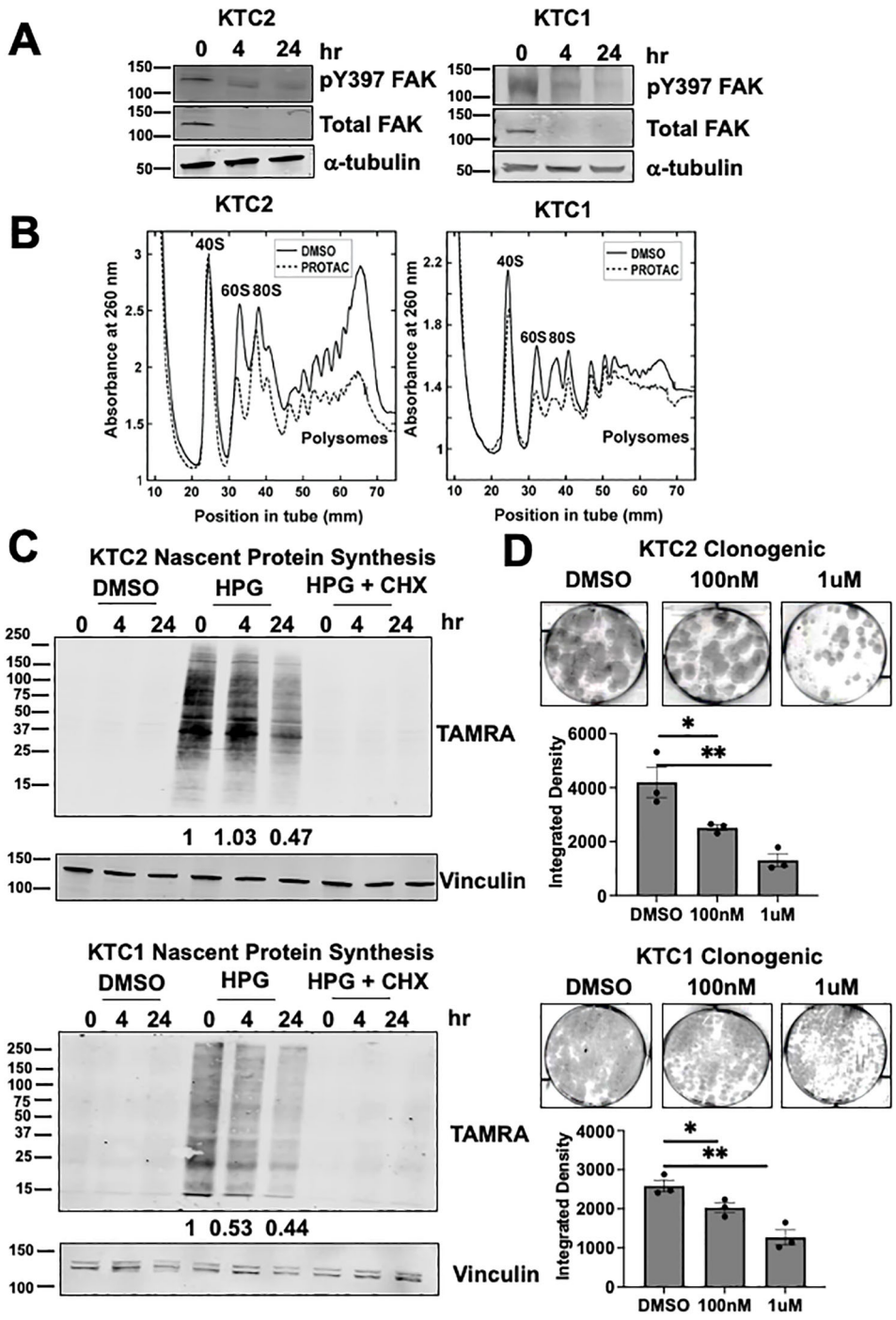

FIGURE 4
FAK regulates 60S biogenesis, nascent protein synthesis, and thyroid cancer growth **(A)** KTC1 and KTC2 cells were treated with 0, 4, or 24 hours of 1 μM PROTAC and immunoblotted with antibodies against pY397 FAK, total FAK, or α-tubulin. MW marker is shown on the left of each blot in kDa. **(B)** Polysome profiling of KTC1 and KTC2 cells treated with DMSO or 1 μM PROTAC for 24 hours was performed with absorbance measured at 260nm. Polysome profiling of KTC2 cells were performed in biological triplicate and KTC1 cells were performed in two biological replicates. **(C)** KTC1 and KTC2 cells were treated with DMSO or 1 μM PROTAC for 24 hours prior to methionine starvation, pre-treatment with water or CHX, and 1 hour treatment with methionine analog HPG. Lysates were immunoblotted with antibodies against TAMRA and vinculin. MW marker is shown on the left of each blot in kDa. At least two independent replicates were performed for all cell lines. **(D)** KTC1 and KTC2 cells were grown in clonogenic assays, treated with DMSO, 100 nM, or 1μM PROTAC, and stained with crystal violet after 14 days. Quantification of clongenic growth was performed by integrated density analysis using LICOR Odyssey. Experiments were performed in biological triplicate. Results are displayed as mean +/- SEM. *, $p < 0.05$; **, $p < 0.01$.

(Figure 5B). To assess interacting partners of FAK, we analyzed proteins that were identified in both of our BioID biological replicates and bound WT FAK with greater than 2-fold change compared to EV. As expected, WT FAK interacts with itself as well as known interacting partners including paxillin (PXN) and ezrin (EZR) (Figure 5C). Next, we identified significantly enriched pathways that are FAK-dependent. Interestingly, we found that "RNA binding" as well as the "fibrillar center" and the "nucleolus" are significantly enriched pathways (FDR < 0.05) (Figure 5D, E). Despite the mass spectrometry being performed in whole cell lysates and the nucleolus only comprising ~7% of the entire proteome, these data indicate that regulation of nucleolar processes is a key function for pY397-FAK. The nucleolar proteins that we identified by mass spectrometry include NOP56, TOP1, PRKDC, EZR, ARL6IP4, and RBL36, all of which have functions in ribosome biogenesis (Figure 5F). Of these proteins, NOP56 passed stringent criteria to interact with WT FAK and not EV or Y397F FAK in both of our BioID replicates (Supplementary Tables 4–6). NOP56 is a core box C/D snoRNP that is involved in the 2'-O-methylation of pre-rRNA necessary for 28S rRNA maturation and thus 60S ribosome biogenesis. These novel findings suggest that pY397 FAK is important for 60S ribosome biogenesis and protein synthesis via NOP56. First, we confirmed that pY397 FAK and NOP56 are co-localized in the nucleolus of our thyroid cancer cells by microscopy (12% co-localization) (Figure 5G; Supplementary Figure 8). To confirm the functional role of NOP56, we transduced the KTC2 cells with 3 shRNAs targeting NOP56 and observed the greatest knockdown of NOP56 (approximately 50%) with shNOP56-500 (Figure 5H). Thus, we assessed the role of NOP56 on clonogenic growth using shNOP56-500. We found that knocking down NOP56 results in a 3-fold decrease in clonogenic growth compared to the non-targeting control ($p<0.05$) (Figure 5I). Overall, these data suggest that pY397 FAK functionally interacts with NOP56 as a potential mediator to regulate 60S biogenesis and thyroid cancer growth.

Discussion

FAK is overexpressed and phosphorylated in a multitude of cancers including thyroid cancer and represents a promising therapeutic target to halt FAK mediated tumorigenic processes including growth, drug resistance, invasion, cell survival, and metastasis (3–13, 48–51). However, FAK inhibitors have largely been ineffective in the clinic. Therefore, it is essential to understand the biology of FAK to target FAK more efficiently and to identify the correct patient population. We have shown that pY397 FAK is localized in the nucleolus in aggressive thyroid cancer cells where it interacts with nucleolar proteins involved in ribosomal biogenesis including NOP56, TOP1, RPL36, and PRKDC. We identified that autophosphorylation of pY397 FAK is important for FAK nucleolar accumulation. We further observed a potential enrichment of pY397 FAK with NPM1 in the granular component and that NPM1 contributes to FAK nucleolar accumulation. Upon FAK degradation, we observed a decrease in the 60S large ribosomal subunit, a global reduction in actively translating ribosomes, and corresponding decrease in growth and survival. Finally, we showed that a fraction of pY397 FAK co-localizes with NOP56, a key regulator of 60S ribosome biogenesis, and that NOP56 is important for thyroid cancer growth and survival. Overall, our studies highlight that FAK regulates 60S ribosome biogenesis and global protein synthesis to drive thyroid cancer growth and survival, providing a novel therapeutic vulnerability.

In this study, we found that nuclear FAK and FAK kinase activity are necessary for anchorage independent growth using advanced thyroid cancer as a model in Figure 1. FAK has been shown to accumulate in the nucleus in several cancers, and elevated levels of Y397 nuclear FAK in breast cancer and colorectal cancer patient tissues are associated with a poor prognosis (18, 19). The kinase activity of nuclear FAK has also been shown to play a role in immune evasion. Specifically, nuclear FAK promotes immune evasion through increased CCL5 expression to drive exhaustion of CD8+ T cells and recruit regulatory T cells (Tregs) in the tumor microenvironment (16). While our work corroborates existing literature that nuclear FAK and FAK kinase activity promote increased thyroid cancer growth and survival, the role of nucleolar FAK in these previous studies would be of interest to evaluate.

Furthermore, our nuclear FAK model provides instrumental insight into the localization of nucleolar FAK. We found that excluding FAK from the nucleus reduces nucleolar p397 FAK accumulation in Figure 1. Conversely, we found that forcing FAK into the nucleus with 3x SV40 NLS results in nuclear and nucleolar accumulation in Figure 2. Our data suggests that a NLS (endogenous and SV40) are important for FAK nucleolar accumulation, supporting existing literature that NLS sequences can serve as nuclear as well as nucleolar localization sequences for proteins (36–38). Furthermore, we found that mutating the NLS of FAK affects the structure around pY397 FAK through structural modeling. The function of a protein may be highly influenced by its sequence, structure, and flexibility. Thus, our data highlights that the nucleolar accumulation of FAK is influenced by its NLS and that pY397 likely plays a key role in FAK nucleolar accumulation.

In further investigation of pY397 FAK, we identified that a fraction of pY397 FAK accumulates in the nucleolus of cell lines derived from advanced thyroid cancer patients and that pY397 FAK is important for FAK nucleolar localization in Figure 2. The nucleolus which is a membraneless organelle forms through liquid liquid phase separation (LLPS). Interestingly, phosphorylation of proteins has been shown to facilitate nucleolar accumulation. Of relevance to FAK, tyrosine phosphorylation specifically promotes liquid phase condensates through recruitment of SH domains promoting multi-valent protein-protein interactions (40, 41). Indeed, FAK has recently been shown to undergo LLPS with p130Cas (BCAR1) at the plasma membrane (52). Thus, it will be interesting to determine whether LLPS regulates FAK nucleolar accumulation in the future. Our data

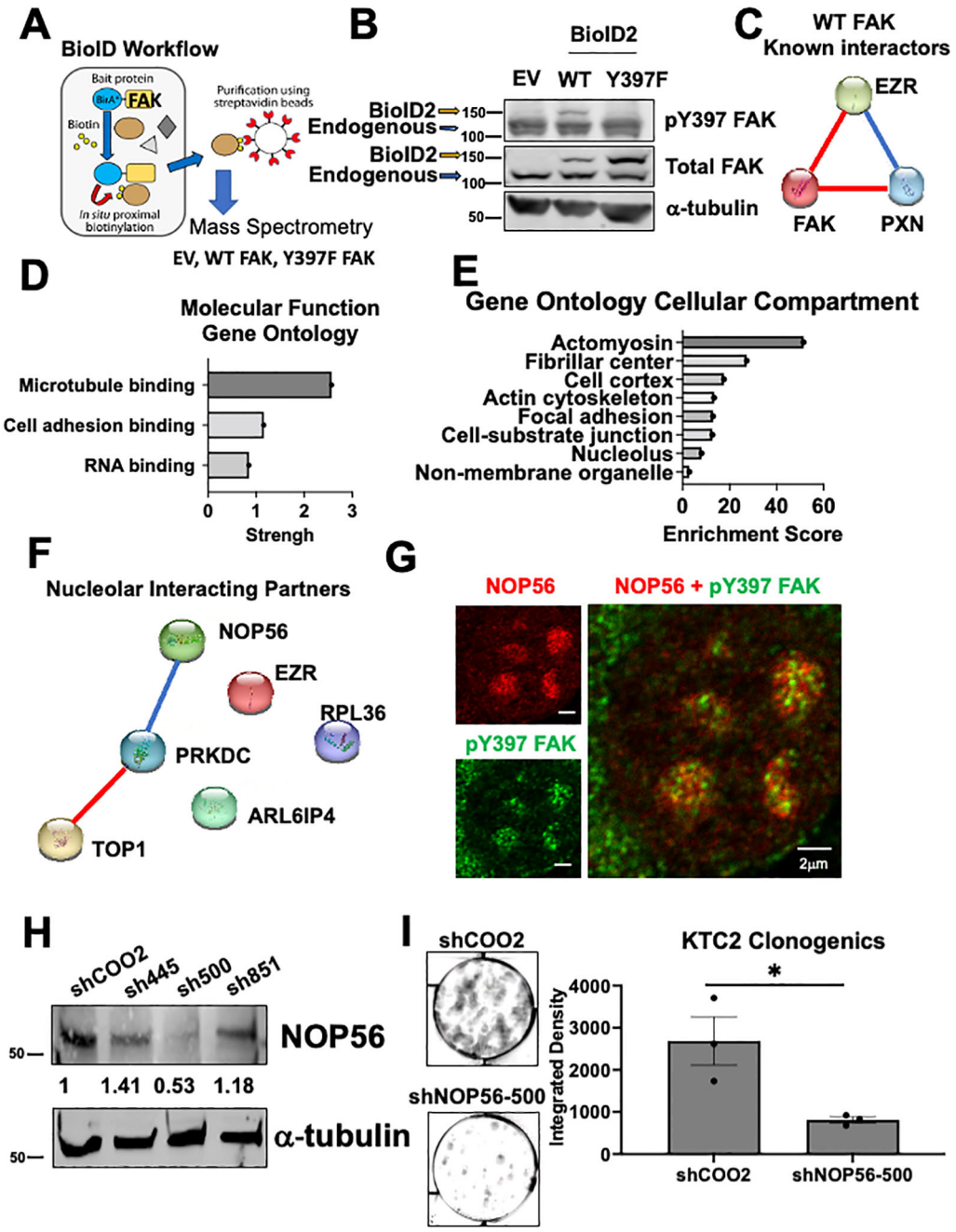

FIGURE 5
NOP56 co-localizes with pY397 FAK and promotes thyroid cancer growth **(A)** BioID workflow representing FAK fused to a promiscuous biotin ligase and interacting partners of FAK being biotinylated, pulled down, and identified by mass spectrometry.**(B)** Immunoblotting of BCPAP cells transduced with EV, WT, and Y397F FAK BioID2 and probed with antibodies against pY397 FAK, total FAK, and α-tubulin. The higher MW band represents the 27kDA BioID2 construct fused to WT or Y397 FAK and lower MW band is the endogenous FAK band. **(C)** STRING analysis of significantly enriched proteins reveals known interacting partners of FAK. Blue connections signify known interactions from database. Red connections signify experimentally determined known interactions. **(D)** FAK interacting partners were identified by analyzing proteins that bind to WT FAK in both datasets and enriched at least 2-fold change compared to EV. Gene Ontology Pathway Analysis was conducted for molecular function pathways with a false discovery rate (FDR) <0.05. **(E)** Gene Ontology Pathway Analysis was conducted for cellular compartment pathways with FDR < 0.05. **(F)** STRING analysis of nucleolar proteins identified by Gene Ontology Pathway Analysis. Blue connections signify known interactions from database. Red connections signify experimentally determined known interactions. **(G)** Confocal microscopy of KTC2 cells was performed with antibodies against pY397 FAK and NOP56. At least 50 cells were imaged at 100X with the Abberior Stedycon microscope in two independent experiments. Scale bar represent 2 μm. **(H)** Immunoblotting of KTC2 cells transduced with a non-targeting control or three NOP56 shRNAs was performed with antibodies against NOP56 and α-tubulin. MW marker is shown on the left of each blot in kDa .**(I)** Clonogenic assays of KTC2 cells transduced with non-targeting control or NOP56 shRNA were performed. Colonies were stained with crystal violet and imaged after 10 days. Integrated Density was utilized to quantify clonogenic growth using LICOR Odyssey software. Experiments were performed in biological triplicate experiments. Results are displayed as mean +/- SEM. *, $p < 0.05$.

also supports the findings from Tancioni et al. that identified pY397 FAK accumulates in the nucleolus of breast cancer cells to drive stabilization of nucleostemin through NPM1 and AKT (20). Together, these data suggest a role for nucleolar FAK in human cancer. Overall, our data highlight that a fraction of pY397 FAK accumulates in the nucleolus of thyroid cancer cells and that pY397 FAK is important for nucleolar accumulation as well as growth and survival.

Using STED imaging, we observed that pY397 FAK may localize in all layers of the nucleolus, with a potential enrichment with NPM1 in the granular component in Figure 3. Using shRNA knockdown of NPM1, the main component of the granular component, we showed that NPM1 contributes to pY397 FAK nucleolar accumulation in Figure 3. The granular component is vital for final rRNA processing steps, rRNA assembly, and rRNA export. We identified that FAK is important for 60S subunit levels, mRNA loading, and nascent protein synthesis in Figure 4. Using a protein-protein interaction proteomics approach, we identified a network of nucleolar proteins that specifically interact with pY397 FAK. Of these, NOP56 plays a role in 60S ribosome biogenesis. We further showed that a fraction of pY397 FAK co-localizes with NOP56. While NOP56 is predominately found in the dense fibrillarin component, it also partitions to the granular component (53). Thus, our data offer novel insights into the role of FAK in ribosome biogenesis through influence of the 60S ribosome, mRNA loading, and nascent protein synthesis.

NOP56 is a core c/d box snoRNP that is involved in the 2'-O-methylation of pre-rRNA and assembly of the 60S ribosome (54). 2'-O-Methylation of rRNA occurs in functionally important regions of the ribosome such as the peptidyl transferase center to influence ribosome assembly and function (55). Furthermore, NOP56 is highly regulated by SUMOylation to alter its function. NOP56 has been found to be SUMOylated by USP36 which is a nucleolar deubiquitinating enzyme (56). It remains to be determined whether pY397 FAK regulates the SUMOylation and subsequent methylation activity of NOP56 in future studies.

In this study, we utilized a panel of thyroid cancer cell lines derived from advanced PTC and ATC tumors. Given the limited treatment options for ATC and unresectable, advanced PTC, identification of therapeutic targets including FAK holds substantial clinical significance (2). An important future direction includes histological evaluation of FAK localization in low risk versus high-risk PTC as well as highly aggressive ATC patient tissue.

Finally, this study offers innovative approaches to elucidate the localization and function of nucleolar FAK. We are the first group to successfully target FAK to the nucleus using 3x SV40 NLS in which we observed the importance of pY397 FAK in FAK nucleolar accumulation. This model will offer novel insight into the biochemical importance of p397 FAK in nucleolar accumulation in future studies. Of note, the NLS constructs exhibited some instability and therefore expression will need to be optimized for future experimental assays. In addition, we utilized a FAK PROTAC which is an emerging tool in precision medicine to degrade FAK (42). It enabled the efficient degradation of FAK to investigate the regulation of protein synthesis. This model provided novel insights that FAK regulates actively translating ribosomes, 60S subunit levels, and nascent protein synthesis. These findings highlight nucleolar FAK as a novel therapeutic target in cancer.

Data availability statement

The datasets presented in this study can be found in the article/Supplementary Material.

Ethics statement

Ethical approval was not required for the studies on humans in accordance with the local legislation and institutional requirements because only previously published cell lines available in repositories were used. The study was conducted in accordance with the local legislation and institutional requirements. No potentially identifiable images or data are presented in this study.

Author contributions

MDK: Conception and design, Acquisition of data, Analysis and interpretation of data, Writing – original draft, Writing – review & editing. VS: Acquisition of data, Analysis and interpretation of data, Writing – review & editing. MES: Acquisition of data, Analysis and interpretation of data, Writing – review & editing. UP: Acquisition of data, Writing – review & editing. MMR: Acquisition of data, Writing – review & editing. MUJ: Acquisition of data, Writing – review & editing. MD: Acquisition of data, Analysis and interpretation of data, Writing – review & editing. VN: Acquisition of data, Analysis and interpretation of data, Writing – review & editing. PR: Conception and design, Acquisition of data, Analysis and interpretation of data, Writing – review & editing. KCH: Conception and design, Writing – review & editing. JSK: Conception and design, Analysis and interpretation of data, Writing – review & editing. RES: Conception and design, Analysis and interpretation of data, Writing – original draft, Writing – review & editing, Study supervision.

Funding

The author(s) declare that financial support was received for the research and/or publication of this article. This work was supported by the National Institutes of Health National Cancer Institute (MDK, F30CA250194 and T32CA17468; MMR, F31CA247211-01 and T32CA190216; RES, 1R01CA222299 and 1R01CA164193), the University of Colorado Cancer Center (MDK, P30CA046934), the Cancer League of Colorado (RES, AWD-203511-RS and AWD-240631-RS), Colorado HNC Spore grant (RES, P50CA261605) and

University of Colorado School of Medicine (RES, Across the Finish Line Grant).

Acknowledgments

We thank the Barbara Davis Center at the Anschutz Medical Campus for assistance with STR genotyping and DNA sequencing. We also acknowledge the Functional Genomics Shared Resource (RRID: SCR_021987), the Mass Spectrometry Proteomics Shared Resource Facility (RRID: SCR_021988), and the Research Histology Shared Resource (RRID: SCR_021994), all within the University of Colorado Cancer Center (P30CA046934) for their technical assistance. We thank Dr. Radu Moldovan and Dr. Dominik Stich in the Advanced Light Imaging Core for guidance and training in microscopy. Thank you to Dr. Vikram Paralkar for expertise, reagents, and guidance related to the fields of rRNA biology. We appreciate Dr. Chris Thorne from Horizon Discovery Group for advice and helpful discussions on CRISPR/Cas9 knockout of FAK. Finally, we thank Dr. Arthur Gutierrez Hartmann, Dr. Christopher Korch, Dr. Hannah Hicks, Dr. Veronica Nassar, Dr. Aaron Knox, and Dr. Rebecca Tucker for technical support and/or input on experimental design.

Conflict of interest

The authors declare that the research was conducted in the absence of any commercial or financial relationships that could be construed as a potential conflict of interest.

Publisher's note

Supplementary material

The Supplementary Material for this article can be found online at: https://www.frontiersin.org/articles/10.3389/fonc.2025.1252544/full#supplementary-material

References

1. Program NCIS. *Cancer stat facts: thyroid cancer* (2023). Available online at: https://seer.cancer.gov/statfacts/html/thyro.html (Accessed February 10, 2023).

2. Cabanillas ME, McFadden DG, Durante C. Thyroid cancer. *Lancet.* (2016) 388:2783–95. doi: 10.1016/S0140-6736(16)30172-6

3. Beierle EA, Massoll NA, Hartwich J, Kurenova EV, Golubovskaya VM, Cance WG, et al. Focal adhesion kinase expression in human neuroblastoma: immunohistochemical and real-time PCR analyses. *Clin Cancer Res.* (2008) 14:3299–305. doi: 10.1158/1078-0432.CCR-07-1511

4. Cance WG, Harris JE, Iacocca MV, Roche E, Yang X, Chang J, et al. Immunohistochemical analyses of focal adhesion kinase expression in benign and Malignant human breast and colon tissues: correlation with preinvasive and invasive phenotypes. *Clin Cancer Res.* (2000) 6:2417–23.

5. Lark AL, Livasy CA, Dressler L, Moore DT, Millikan RC, Geradts J, et al. High focal adhesion kinase expression in invasive breast carcinomas is associated with an aggressive phenotype. *Mod Pathol.* (2005) 18:1289–94. doi: 10.1038/modpathol.3800424

6. Theocharis SE, Kouraklis GP, Kakisis JD, Kanelli HG, Apostolakou FE, Karatzas GM, et al. Focal adhesion kinase expression is not a prognostic predictor in colon adenocarcinoma patients. *Eur J Surg Oncol.* (2003) 29:571–4. doi: 10.1016/S0748-7983(03)00120-3

7. Furuyama K, Doi R, Mori T, Toyoda E, Ito D, Kami K, et al. Clinical significance of focal adhesion kinase in resectable pancreatic cancer. *World J Surg.* (2006) 30:219–26. doi: 10.1007/s00268-005-0165-z

8. Miyazaki T, Kato H, Nakajima M, Sohda M, Fukai Y, Masuda N, et al. FAK overexpression is correlated with tumour invasiveness and lymph node metastasis in oesophageal squamous cell carcinoma. *Br J Cancer.* (2003) 89:140–5. doi: 10.1038/sj.bjc.6601050

9. Wang XY, Liu T, Zhu CZ, Li Y, Sun R, Sun CY, et al. Expression of KAI1, MRP-1, and FAK proteins in lung cancer detected by high-density tissue microarray. *Ai Zheng.* (2005) 24:1091–5.

10. Ocak S, Chen H, Callison C, Gonzalez AL, Massion PP. Expression of focal adhesion kinase in small-cell lung carcinoma. *Cancer.* (2012) 118:1293–301. doi: 10.1002/cncr.26382

11. Sood AK, Coffin JE, Schneider GB, Fletcher MS, DeYoung BR, Gruman LM, et al. Biological significance of focal adhesion kinase in ovarian cancer: role in migration and invasion. *Am J Pathol.* (2004) 165:1087–95. doi: 10.1016/S0002-9440(10)63370-6

12. Kim SJ, Park JW, Yoon JS, Mok JO, Kim YJ, Park HK, et al. Increased expression of focal adhesion kinase in thyroid cancer: immunohistochemical study. *J Korean Med Sci.* (2004) 19:710–5. doi: 10.3346/jkms.2004.19.5.710

13. Schweppe RE, Kerege AA, French JD, Sharma V, Grzywa RL, Haugen BR. Inhibition of Src with AZD0530 reveals the Src-Focal Adhesion kinase complex as a novel therapeutic target in papillary and anaplastic thyroid cancer. *J Clin Endocrinol Metab.* (2009) 94:2199–203. doi: 10.1210/jc.2008-2511

14. Schaller MD, Borgman CA, Cobb BS, Vines RR, Reynolds AB, Parsons JT. pp125FAK a structurally distinctive protein-tyrosine kinase associated with focal adhesions. *Proc Natl Acad Sci U S A.* (1992) 89:5192–6. doi: 10.1073/pnas.89.11.5192

15. Lim ST, Chen XL, Lim Y, Hanson DA, Vo TT, Howerton K, et al. Nuclear FAK promotes cell proliferation and survival through FERM-enhanced p53 degradation. *Mol Cell.* (2008) 29:9–22. doi: 10.1016/j.molcel.2007.11.031

16. Serrels A, Lund T, Serrels B, Byron A, McPherson RC, von Kriegsheim A, et al. Nuclear FAK controls chemokine transcription, Tregs, and evasion of anti-tumor immunity. *Cell.* (2015) 163:160–73. doi: 10.1016/j.cell.2015.09.001

17. Lim ST, Miller NL, Chen XL, Tancioni I, Walsh CT, Lawson C, et al. Nuclear-localized focal adhesion kinase regulates inflammatory VCAM-1 expression. *J Cell Biol.* (2012) 197:907–19. doi: 10.1083/jcb.201109067

18. Albasri A, Fadhil W, Scholefield JH, Durrant LG, Ilyas M. Nuclear expression of phosphorylated focal adhesion kinase is associated with poor prognosis in human colorectal cancer. *Anticancer Res.* (2014) 34:3969–74.

19. Andisha NM, McMillan DC, Gujam FJA, Roseweir A, Edwards J. The relationship between phosphorylation status of focal adhesion kinases, molecular subtypes, tumour microenvironment and survival in patients with primary operable ductal breast cancer. *Cell Signal.* (2019) 60:91–9. doi: 10.1016/j.cellsig.2019.04.006

20. Tancioni I, Miller NL, Uryu S, Lawson C, Jean C, Chen XL, et al. FAK activity protects nucleostemin in facilitating breast cancer spheroid and tumor growth. *Breast Cancer Res.* (2015) 17:47. doi: 10.1186/s13058-015-0551-x

21. Gallagher JE, Dunbar DA, Granneman S, Mitchell BM, Osheim Y, Beyer AL, et al. RNA polymerase I transcription and pre-rRNA processing are linked by specific SSU processome components. *Genes Dev.* (2004) 18:2506–17. doi: 10.1101/gad.1226604

22. Henras AK, Plisson-Chastang C, O'Donohue MF, Chakraborty A, Gleizes PE. An overview of pre-ribosomal RNA processing in eukaryotes. *Wiley Interdiscip Rev RNA.* (2015) 6:225–42. doi: 10.1002/wrna.1269

23. Schwarzacher HG, Wachtler F. The nucleolus. *Anat Embryol (Berl).* (1993) 188:515–36. doi: 10.1007/BF00187008

24. Falaleeva M, Welden JR, Duncan MJ, Stamm S. C/D-box snoRNAs form methylating and non-methylating ribonucleoprotein complexes: Old dogs show new tricks. *Bioessays.* (2017) 39:1600264. doi: 10.1002/bies.201600264

25. Schweppe RE, Klopper JP, Korch C, Pugazhenthi U, Benezra M, Knauf JA, et al. Deoxyribonucleic acid profiling analysis of 40 human thyroid cancer cell lines reveals cross-contamination resulting in cell line redundancy and misidentification. *J Clin Endocrinol Metab*. (2008) 93:4331–41. doi: 10.1210/jc.2008-1102

26. Landa I, Pozdeyev N, Korch C, Marlow LA, Smallridge RC, Copland JA, et al. Comprehensive genetic characterization of human thyroid cancer cell lines: A validated panel for preclinical studies. *Clin Cancer Res*. (2019) 25:3141–51. doi: 10.1158/1078-0432.CCR-18-2953

27. Pylayeva Y, Gillen KM, Gerald W, Beggs HE, Reichardt LF, Giancotti FG. Ras- and PI3K-dependent breast tumorigenesis in mice and humans requires focal adhesion kinase signaling. *J Clin Invest*. (2009) 119:252–66. doi: 10.1172/JCI37160

28. Marlowe T, Dementiev A, Rivera A, Flavin M, Cance W. High resolution crystal structure of the FAK FERM domain reveals new insights on the Druggability of tyrosine 397 and the Src SH3 binding site. *BMC Mol Cell Biol*. (2019) 20:10. doi: 10.1186/s12860-019-0193-4

29. Lietha D, Cai X, Ceccarelli DF, Li Y, Schaller MD, Eck MJ. Structural basis for the autoinhibition of focal adhesion kinase. *Cell*. (2007) 129:1177–87. doi: 10.1016/j.cell.2007.05.041

30. Jacobson MP, Pincus DL, Rapp CS, Day TJ, Honig B, Shaw DE, et al. A hierarchical approach to all-atom protein loop prediction. *Proteins*. (2004) 55:351–67. doi: 10.1002/prot.10613

31. Schrödinger. *Schrödinger release*. New York, NY (2022). 42023.

32. Zhou J, Yi Q, Tang L. The roles of nuclear focal adhesion kinase (FAK) on Cancer: a focused review. *J Exp Clin Cancer Res*. (2019) 38:250. doi: 10.1186/s13046-019-1265-1

33. Ossovskaya V, Lim ST, Ota N, Schlaepfer DD, Ilic D. FAK nuclear export signal sequences. *FEBS Lett*. (2008) 582:2402–6. doi: 10.1016/j.febslet.2008.06.004

34. Carlson P, Dasgupta A, Grzelak CA, Kim J, Barrett A, Coleman IM, et al. Targeting the perivascular niche sensitizes disseminated tumour cells to chemotherapy. *Nat Cell Biol*. (2019) 21:238–50. doi: 10.1038/s41556-018-0267-0

35. Kessler BE, Sharma V, Zhou Q, Jing X, Pike LA, Kerege AA, et al. FAK expression, not kinase activity, is a key mediator of thyroid tumorigenesis and protumorigenic processes. *Mol Cancer Res*. (2016) 14:869–82. doi: 10.1158/1541-7786.MCR-16-0007

36. Kurnaeva MA, Zalevsky AO, Arifulin EA, Lisitsyna OM, Tvorogova AV, Shubina MY, et al. Molecular coevolution of nuclear and nucleolar localization signals inside the basic domain of HIV-1 tat. *J Virol*. (2022) 96:e0150521. doi: 10.1128/JVI.01505-21

37. Yang CP, Chiang CW, Chen CH, Lee YC, Wu MH, Tsou YH, et al. Identification and characterization of nuclear and nucleolar localization signals in 58-kDa microspherule protein (MSP58). *J BioMed Sci*. (2015) 22:33. doi: 10.1186/s12929-015-0136-0

38. Martin RM, Ter-Avetisyan G, Herce HD, Ludwig AK, Lattig-Tunnemann G, Cardoso MC. Principles of protein targeting to the nucleolus. *Nucleus*. (2015) 6:314–25. doi: 10.1080/19491034.2015.1079680

39. Cancer Genome Atlas Research N. Integrated genomic characterization of papillary thyroid carcinoma. *Cell*. (2014) 159:676–90. doi: 10.1016/j.cell.2014.09.050

40. Cohen GB, Ren R, Baltimore D. Modular binding domains in signal transduction proteins. *Cell*. (1995) 80:237–48. doi: 10.1016/0092-8674(95)90406-9

41. Lopez-Palacios TP, Andersen JL. Kinase regulation by liquid-liquid phase separation. *Trends Cell Biol*. (2023) 33:649–66. doi: 10.1016/j.tcb.2022.11.009

42. Bekes M, Langley DR, Crews CM. PROTAC targeted protein degraders: the past is prologue. *Nat Rev Drug Discov*. (2022) 21:181–200. doi: 10.1038/s41573-021-00371-6

43. Zhu X, Bao Y, Guo Y, Yang W. Proline-rich protein tyrosine kinase 2 in inflammation and cancer. *Cancers (Basel)*. (2018) 10:139. doi: 10.3390/cancers10050139

44. Johnson LF, Levis R, Abelson HT, Green H, Penman S. Changes in RNA in relation to growth of the fibroblast. IV. Alterations in theproduction and processing of mRNA and rRNA in resting and growing cells. *J Cell Biol*. (1976) 71:933–8. doi: 10.1083/jcb.71.3.933

45. Liu K, Lin FT, Graves JD, Lee YJ, Lin WC. Mutant p53 perturbs DNA replication checkpoint control through TopBP1 and Treslin. *Proc Natl Acad Sci U S A*. (2017) 114:E3766–E75. doi: 10.1073/pnas.1619832114

46. Lindstrom MS, Bartek J, Maya-Mendoza A. p53 at the crossroad of DNA replication and ribosome biogenesis stress pathways. *Cell Death Differ*. (2022) 29:972–82. doi: 10.1038/s41418-022-00999-w

47. Kim DI, Jensen SC, Noble KA, Kc B, Roux KH, Motamedchaboki K, et al. An improved smaller biotin ligase for BioID proximity labeling. *Mol Biol Cell*. (2016) 27:1188–96. doi: 10.1091/mbc.E15-12-0844

48. Cary LA, Chang JF, Guan JL. Stimulation of cell migration by overexpression of focal adhesion kinase and its association with Src and Fyn. *J Cell Sci*. (1996) 109:1787–94. doi: 10.1242/jcs.109.7.1787

49. Wu X, Gan B, Yoo Y, Guan JL. FAK-mediated src phosphorylation of endophilin A2 inhibits endocytosis of MT1-MMP and promotes ECM degradation. *Dev Cell*. (2005) 9:185–96. doi: 10.1016/j.devcel.2005.06.006

50. Lim ST, Chen XL, Tomar A, Miller NL, Yoo J, Schlaepfer DD. Knock-in mutation reveals an essential role for focal adhesion kinase activity in blood vessel morphogenesis and cell motility-polarity but not cell proliferation. *J Biol Chem*. (2010) 285:21526–36. doi: 10.1074/jbc.M110.129999

51. Diaz Osterman CJ, Ozmadenci D, Kleinschmidt EG, Taylor KN, Barrie AM, Jiang S, et al. FAK activity sustains intrinsic and acquired ovarian cancer resistance to platinum chemotherapy. *Elife*. (2019) 8:e47327. doi: 10.7554/eLife.47327

52. Case LB, De Pasquale M, Henry L, Rosen MK. Synergistic phase separation of two pathways promotes integrin clustering and nascent adhesion formation. *Elife*. (2022) 11:e72588. doi: 10.7554/eLife.72588

53. Lavering ED, Petros IN, Weeks DL. Component analysis of nucleolar protein compartments using Xenopus laevis oocytes. *Dev Growth Differ*. (2022) 64:306–17. doi: 10.1111/dgd.12794

54. Baldini L, Charpentier B, Labialle S. Emerging data on the diversity of molecular mechanisms involving C/D snoRNAs. *Noncoding RNA*. (2021) 7:30. doi: 10.3390/ncrna7020030

55. Decatur WA, Fournier MJ. rRNA modifications and ribosome function. *Trends Biochem Sci*. (2002) 27:344–51. doi: 10.1016/S0968-0004(02)02109-6

56. Ryu H, Sun XX, Chen Y, Li Y, Wang X, Dai RS, et al. The deubiquitinase USP36 promotes snoRNP group SUMOylation and is essential for ribosome biogenesis. *EMBO Rep*. (2021) 22:e50684. doi: 10.15252/embr.202050684

Frontiers in Oncology

Advances knowledge of carcinogenesis and tumor progression for better treatment and management

The third most-cited oncology journal, which highlights research in carcinogenesis and tumor progression, bridging the gap between basic research and applications to imrpove diagnosis, therapeutics and management strategies.

Discover the latest Research Topics

See more →

Frontiers

Avenue du Tribunal-Fédéral 34
1005 Lausanne, Switzerland
frontiersin.org

Contact us

+41 (0)21 510 17 00
frontiersin.org/about/contact